ЖУРНАЛ
ПРИКЛАДНОЙ ХИМИИ

Volume 31 No. 9

September 1958

JOURNAL OF
APPLIED CHEMISTRY
OF THE USSR

(ZHURNAL PRIKLADNOI KHIMII)

IN ENGLISH TRANSLATION

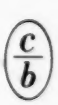

CONSULTANTS BUREAU, INC.

DENDRITIC CRYSTALLIZATION

by **D. D. SARATOVKIN**

2nd Edition,
Revised and Enlarged

Translated from Russian

THIS SIGNIFICANT volume has been extensively revised by the author from the 1953 edition; in particular with *fresh material derived from observations under the stereoscopic microscope.*

The first section deals briefly with some general concepts on crystallization, drawing an important distinction between *genetic* and *structural* types of crystals, including some aspects of the *defect crystal state.* The second section covers at length the illuminating ideas and observations of the 19th-century Russian metallurgist D. K. Chernov, who proposed many of the basic ideas of dendritic crystallization. The third section is an extended survey of current views on dendritic crystallization, in which the ideas of many Soviet and other scientists are briefly summarized and criticized. Section four presents the growth forms of real crystals; all types are reviewed, but only dendritic or closely related forms are selected for subsequent investigation.

Following sections discuss the causes and forms of crystal growth, with *detailed applications* to certain substances that have been extensively studied *(particularly the ammonium halides),* and to eutectics in metal and organic systems; an extensively revised presentation on steel castings which provides a lucid explanation of how the various structures found in real castings can be fitted into the author's theory of dendritic crystallization. Nearly all the concepts developed earlier in the book are utilized in this final section.

The main bulk of the volume contains many *original* and *unpublished* ideas and observations, and is an excellent example of the modern macroscopic approach to the crystalline state by an experienced worker concerned with the infinite variety of real crystals—all of which is enhanced by a *profusion of explanatory line diagrams and sets of stereoscopic photographs.*

CB translations are by bilingual scientists, and include all photographic, diagrammatic and tabular material integral with the text.

CONTENTS

Cloth-bound; 126 pp., illustrated; $6.00

CONSULTANTS BUREAU, INC.
227 WEST 17TH STREET, NEW YORK 11, N. Y

Volume 31 No. 9

September 1958

JOURNAL OF
APPLIED CHEMISTRY
OF THE USSR

(ZHURNAL PRIKLADNOI KHIMII)

A publication of the Academy of Sciences of the USSR

IN ENGLISH TRANSLATION

Year and issue of first translation:
Vol. 23, No. 1 January 1950

	U. S. and Canada	*Foreign*
Annual subscription	*$60.00*	*$65.00*
Annual subscription for libraries of non-profit academic institutions	*20.00*	*25.00*
Single issue	*7.50*	*7.50*

CONSULTANTS BUREAU INC.
227 W. 17th ST., NEW YORK 11, N. Y.

Printed in the United States of America

JOURNAL OF APPLIED CHEMISTRY OF THE USSR

Volume 31, Number 9 September, 1958

CONTENTS

(continued)

CONTENTS (continued)

COMPARATIVE REDUCTION OF TRICALCIUM PHOSPHATE BY GASEOUS REDUCING AGENTS – HYDROGEN, CARBON MONOXIDE, AND METHANE – AND BY SOLID CARBON

N. N. Postnikov

Although solid carbon – coke or anthracite – is used at present as a reducing agent in industrial furnaces, investigation of the reduction of tricalcium phosphate by gaseous reducing agents – hydrogen, carbon monoxide, and methane – is of both theoretical and practical interest, as gaseous reducing agents may be more economic in some cases. The reduction of tricalcium phosphate by hydrogen has been reported by Lassier [1], Nielsen [2], Jansen [3], and Liuban [4], who showed that hydrogen reduces tricalcium phosphate at temperatures of 1100° and over. Lassier and Jansen report that up to 1300° carbon monoxide does not reduce tricalcium phosphate. According to Liuban, reduction occurs only at 1250°, and according to Nielsen, at 1175°.

The difference between the temperatures at which these workers observed the reduction of tricalcium phosphate by carbon monoxide is probably due to differences in the composition of the original tricalcium phosphate [5].

Padovani and Nardella [6] showed that methane reduces tricalcium phosphate at 1100° and over. It should be remembered that solid carbon also reduces tricalcium phosphate at 1100° and over, i. e., the temperature ranges of the reduction reaction are very similar for such reducing agents as carbon, hydrogen, and methane. Reduction by carbon monoxide takes place at higher temperatures.

EXPERIMENTAL*

In order to obtain comparative data on the reducing activities of hydrogen, carbon monoxide, methane, and solid carbon, we carried out experiments on the reduction of tricalcium phosphate and apatite concentrate by these substances.

Starting materials. Tricalcium phosphate (the β-modification) was prepared by the method developed by the author [5]. The apatite concentrate was of works origin, and contained 96.5% of fluorapatite. Silica was prepared from very pure quartz sand by treatment with boiling aqua regia. The carbon, metallurgical coke, contained 86.5% C. Technical compressed hydrogen and methane were used.

The experiments were performed in a furnace with a tubular carbon heater. A porcelain tube was inserted into the carbon heating tube. A weighed quantity of the material was placed in a boat and introduced into the porcelain tube heated to the required temperature. The mixtures containing carbon were briquetted, and the briquets, 1.0 cm in diameter and 0.8-1.0 cm long, were also heated in boats.

Hydrogen, carbon monoxide, and methane were passed through the furnace at a rate of 2.7 liters/minute. In the experiments with solid carbon, nitrogen freed from oxygen was blown through the furnace at a rate of 200 ml/minute.

The degree of reduction was estimated from the P_2O_5 contents of the solid reaction products, which were analyzed for P_2O_5 and CaO. The amount of phosphorus distilled off was estimated from the P_2O_5/CaO ratios before and after the experiment. P_2O_5 was determined photocolorimetrically, and CaO by the oxalate method.

* With the assistance of O. V. Vasil'eva.

TABLE 1

Comparative Reducibility of Tricalcium Phosphate and Fluorapatite in Presence of Silica, by the Action of Solid Carbon, and of Gaseous Reducing Agents – Carbon Monoxide, Hydrogen, and Methane (duration of experiment 30 minutes)

Original phosphate	temperature (in °)	Reducing agent	Rate (liters/minute)	P_2O_5 content of residue (%)	Distillation of phosphorus (%)
β-Tricalcium phosphate	1300	CO	2.7	35.97	0
		H_2	2.7	27.55	22.74
		CH_4	2.7	27.47	22.84
		C	0.2	10.9	70.5
Fluorapatite . . .	1300	CO	2.7	31.02	0
		H_2	2.7	24.05	22.82
		CH_4	2.7	24.12	22.92
		C	0.2	12.52	59.20
β-Tricalcium phosphate	1400	CO	2.7	27.5	23.33
		H_2	2.7	17.42	51.14
		CH_4	2.7	17.74	53.41
		C	0.2	0.63	98.75
Fluorapatite . . .	1400	CO	2.7	19.31	24.57
		H_2	2.7	16.49	46.15
		CH_4	2.7	14.62	55.50
		C	0.2	2.07	93.54

TABLE 2

Reduction of Tricalcium Phosphate by Carbon, Hydrogen, and Carbon Monoxide (carbon ratio 300%)

Temperature (°C)	Reducing agent	Gas rate (liters/minute)	Distillation of phosphorus (%)
1300	C (coke)	0.2	41.2
	H_2	2.7	9.7
	CO	2.7	0.0
1400	C (coke)	0.2	83.8
	H_2	2.7	20.1
	CO	2.7	2.7

The results of the experiments are given in Tables 1 and 2.

The first series of experiments was performed with phosphate – silica mixtures, the composition of which was such as to give a molecular ratio of 2:3 between SiO_2 and CaO in the slags. The amount of reducing gas passed through the furnace during the experiment was at least 30 times the theoretical. Solid carbon was taken in 10% excess.

It follows from Table 1 that carbon monoxide reduces tricalcium phosphate and fluorapatite only at temperatures above 1300°. Further, it may be considered that the reducing powers of hydrogen and methane are almost equal. The cause probably lies in previous thermal dissociation of methane into carbon and hydrogen, so that not methane but its dissociation products react with the phosphate. Comparison of the degree of reduction of phosphates by solid carbon and gaseous reducing agents shows that under the conditions used solid carbon is a more active reducing agent than hydrogen or methane, and even more so than carbon monoxide.

Similar results were obtained in experiments carried out without addition of silica to the charge (Table 2).

It also follows from Table 2 that a higher degree of reduction is reached with solid carbon than with gaseous reducing agents.

It must be noted that calcium phosphide was not detected in the reaction products.

The following conclusions may be drawn from these results.

1. Solid carbon is a more active reducing agent for tricalcium phosphate and fluorapatite than methane, hydrogen, or carbon monoxide, despite the fact that the gaseous reducing agents were used in enormous excess. The low reduction rates suggest that in the experimental conditions used, even if physical adsorption or chemisorption took place at all, their effects were extremely small and could be ignored. Evidently the reduction of tricalcium phosphate by hydrogen and carbon monoxide is associated only with impacts of the gas molecules with the phosphate surface, although comparison of the reduction rates of tricalcium phosphate by hydrogen and carbon monoxide shows that the ratio of these rates is not strictly consistent with the kinetic theory. This inconsistency is readily explained; first, not every impact results in reaction; and second, diffusion in the phosphate must be taken into account. It may prove possible to draw final conclusions after kinetic studies of the reduction of tricalcium phosphate by gaseous reducing agents.

2. The absence of calcium phosphide in the products of the reaction between hydrogen or carbon monoxide and tricalcium phosphate is very important in determination of the mechanism of reduction of tricalcium phosphate by carbon. According to the theory of Frank and Füldner [7], when tricalcium phosphate is reduced by carbon, calcium phosphide is formed as an intermediate product of the first-stage reaction (analogously to the reduction of calcium sulfate).

$$\begin{array}{ll} \text{Stage I:} & 5Ca_3(PO_4)_2 + 40C = 5Ca_3P_2 + 40CO \\ \text{Stage II:} & 5Ca_3P_2 + 3Ca_3(PO_4)_2 = 24CaO + 8P_2 \\ \hline \text{Aggregate}^*\text{:} & Ca_3(PO_2)_2 + 5C = 3CaO + 5CO + P_2 \end{array}$$

However, whereas in the reduction of calcium sulfate calcium sulfide is formed in almost theoretical quantity, irrespective of whether carbon, hydrogen, or carbon monoxide is used for the reduction [8], phosphide is not formed when phosphate is reduced by hydrogen and by carbon monoxide. Therefore the reduction of calcium phosphate and sulfate, respectively, proceeds by different mechanisms.

3. The fact that phosphates are not reduced by carbon monoxide at temperatures below 1250-1300°, as found by us and also by Lassier, Jansen, and Liuban, casts doubt on the views put forward by Gel'd, Vlasov, and Serebrennikov on the mechanism of reduction of tricalcium phosphate by carbon [9]. According to these authors, the first stage of the reduction reaction consists of interaction of tricalcium phosphate with carbon monoxide, which is oxidized to carbon dioxide. The latter is reduced by carbon to the monoxide.

$$\begin{array}{l} Ca_3(PO_4)_2 + 5CO = 3CaO + 5CO_2 + P_2 \\ 5CO_2 + 5C = 10CO \\ \hline Ca_3(PO_4)_2 + 5C = 3CaO + 5CO + P_2 \end{array}$$

If this is true, then the carbon monoxide formed in the reduction of phosphates must have different properties from those of carbon monoxide made by the decomposition of formic acid. However, such an assumption cannot be justified.

It is reasonable to suppose that, in practice, reduction of phosphates by carbon monoxide must take place, but this process is of subordinate significance.

The small role of carbon monoxide in the reduction of phosphates probably accounts for the high contents of carbon monoxide in the waste gases from phosphorus blast furnaces.

The CO_2 and CO contents in waste gases from metallurgical and phosphorus blast furnaces are given below.

*The aggregate equation is divided through by 8.

Blast furnace	Type of iron	CO	CO_2	CO_2+CO
Makeevka [10]	Martin	30.1	9.2	39.3
Kuznetsk [10]	Cast	27.6	12.2	39.8
Phosphorus	——	33.4	0.0	33.4
		36.0	0.6	36.6

SUMMARY

1. Solid carbon is a more active reducing agent for tricalcium phosphate and fluorapatite than hydrogen, carbon monoxide, and methane; carbon monoxide does not reduce tricalcium phosphate or fluorapatite at temperatures below 1300°.

2. Calcium phosphide was not detected in the reaction products when tricalcium phosphate was reduced by carbon monoxide or hydrogen.

3. It is suggested that the results do not confirm the theory of Frank and Fūldner, according to whom the reduction of tricalcium phosphate by carbon proceeds with formation of calcium phosphide as an intermediate product; and that the reduction of tricalcium phosphate by carbon monoxide is of subordinate significance and cannot provide a basis for an explanation of the mechanism of reduction of tricalcium phosphate by carbon.

LITERATURE CITED

[1] A. Lassier, Origin. Comm. 8 Internat. Congr. appliq chem., II, 175 (1912).

[2] R. Nielsen, Ferrum, 10, 97 (1913).

[3] W. Jansen, Z. anorg. allg. Ch., 210, 113 (1933).

[4] A. P. Liuban, Metallurgist, 11, 2, 54 (1936).

[5] N. N. Postnikov, J. Appl. Chem. 1, 8 (1951).*

[6] C. Padovanie and A. Nardella, Ann. Chim. Appliq, 21, 109 (1931).

[7] H. Frank u. H. Fūldner, Z. anorg. allg. Ch., B, 204, 97 (1932).

[8] P. P. Budnikov, Gypsum (1943). [In Russian]

[9] P. V. Gel'd, V. G. Vlasov, and N. N. Serebrennikov, J. Appl. Chem. 25, 2, 121 (1952).*

[10] M. A. Pavlov, Metallurgy of Cast Iron 2 (1945). [In Russian]

Received December 29, 1956.

*Original Russian pagination. See C. B. Translation.

DIRECT REDUCTION OF CHROMIC OXIDE

Iu. O. Esin and P. V. Gel'd

Studies of the kinetics and mechanism of the direct reduction of oxides (mainly those which are easily reducible) showed that carbon monoxide, continuously regenerated by the carbon, is the direct reducing agent of the oxide. In a number of cases the last reaction stage determines the rate of the whole process. It is difficult to say how far these views are applicable to high-temperature reduction processes. Individual preliminary experiments [1] on the direct reduction of Cr_2O_3 and MnO appear to confirm this hypothesis. However, the results obtained in that investigation required amplification, and the present study was therefore carried out.

Starting materials and method of investigation. Chemically pure chromic oxide, graphite (ash content ~ 0.5%), metallurgical coke (ash content about 10%), and pitch coke were used for the experiments. All the materials were previously degasified in a vacuum unit at about 1000°.

The charges were prepared from the thoroughly ground materials, mixed in the ratio Cr_2O_3:C = 1:4.5, and briquetted under a pressure of 300 kg/ cm^2. Pieces 2-3 mm in size were used for the experiments.

Investigations of the direct-reduction kinetics were carried out in a vacuum unit; the design and procedure were described in the preceding paper [2].

EXPERIMENTAL

The results obtained in the present investigation are presented mainly in the form of isothermal kinetic curves representing the weight loss of the samples (in mg/ g Cr_2O_3) as a function of time.

Investigations of the composition of the gas phase obtained in numerous experiments showed that it consists almost entirely of carbon monoxide. The very small quantities of CO_2 which were occasionally detected at the early reaction stages are formed in side processes which inevitably take place because of incomplete degasification of the charge and the consequent presence of various C_xO_g complexes on the surface of the reducing agent.

The results obtained in a study of the reduction of chromic oxide by graphite in vacuum are presented in Fig. 1. It should be noted that as the reaction developed the pressure generally increased, the increase being greater at higher temperatures. Thus, when the pressure in the system before the experiment was 10^{-4}–10^{-5} mm Hg, in the initial period of intensive action it sometimes rose to 10^{-2} mm, and fell again to 10^{-3}–10^{-4} mm only when the gas evolution slowed down. Thus, the results are characteristic of a process taking place in not entirely isobaric conditions.

Examination of the graphs in Fig. 1. immediately reveals the existence of a fairly distinct induction period, which increases regularly with decrease of temperature. This shows that direct reduction is autocatalytic in character, as is seen more clearly in an examination of the relationship between the rate and degree of reduction. It follows from Fig. 2. that the reduction rate increases rapidly in the initial period, reaches a maximum, and then decreases slowly. It is clear that this form of relationship cannot be accounted for by lack of thermal equilibrium in the system and, in particular, by slowness in the heating of the charge. Indeed, at 1000-1400° the induction period is 20-60 minutes, which is very much longer than the time required to heat the charge through (3-4 minutes). Despite this, the character of the low-temperature isotherms does not differ in any way from that of the high-temperature isotherms (Fig. 2). Further, the abscissas of the maxima of all the isotherms are very close together (within about 1.5%). This shows that coalescence of the individual reaction zones arising

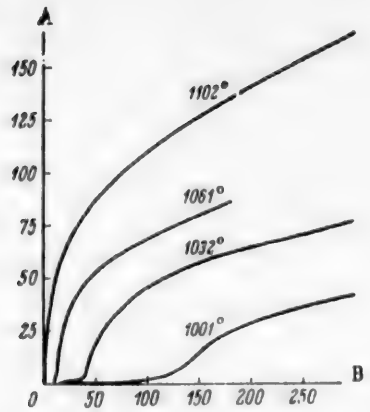

Fig. 1. Kinetics of the reduction of Cr_2O_3 by graphite in vacuum. A) Weight loss of sample (mg/ g Cr_2O_3; B) time (minutes).

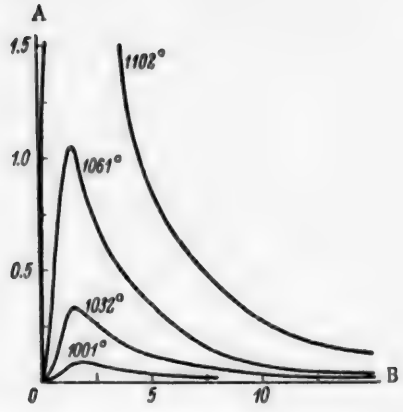

Fig. 2. Variation of the reduction rate of Cr_2O_3 by graphite with the degree of reduction. A) Reduction rate (%/minute); B) degree of reduction (%).

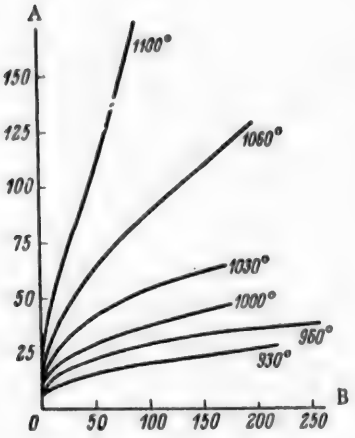

Fig. 3. Reduction kinetics of chromic oxide in a charge made by baking of the reaction mixture with benzene and pitch (Cr_2O_3 + 4.5 C_{pitch} + benzene). A) Weight loss of sample (mg/ g Cr_2O_3), B) time (minutes).

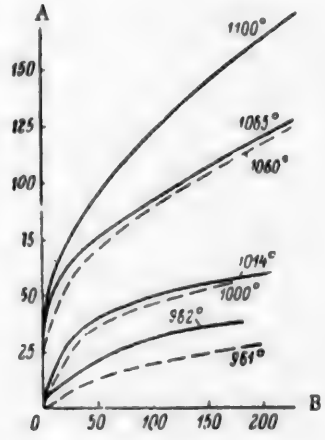

Fig. 4. Reduction of chromic oxide by graphite, with additions of 3% of dry Na_2CO_3 (continuous line) and K_2CO_3 (dash line), under moderate vacuum. A) Weight loss of sample (mg/ g Cr_2O_3), B) time (minutes).

near individual nuclei of the new phase occurs under the same conditions both at 1000 and at 1100°. In other words, the number and distribution of the initial reaction centers depends little on the temperature under the conditions in question. Finally, the rapid increase of the reaction rate with increasing degree of reduction in the initial period, followed by the slow decrease, indicates the presence of a relatively large number of active centers on the surface of the Cr_2O_3 particles.

Analogous results were obtained in a study of the reduction of chromic oxide by graphite without removal of the gaseous reaction products, i. e., in conditions in which the carbon monoxide pressure in the confined reaction space increased as the reaction developed. In these conditions there was again an induction period which increased with fall of temperature. Direct comparison of these results with the results of vacuum experiments is

complicated by the fact that in the former case the CO pressure in the system increased continuously and reached almost 140 mm Hg in some instances. Despite this, it may be stated that at lower temperatures (~1000°) increase of pressure retards the interaction somewhat, whereas at higher temperatures it accelerates it appreciably.

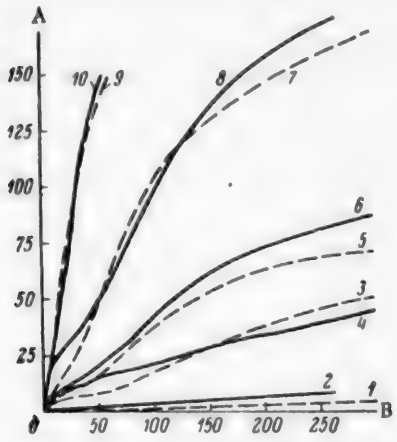

Fig. 5. Reduction of chromic oxide (with accumulation of gaseous reaction products) in a charge containing graphite with additions of 3% of dry Na_2CO_3 (continuous line) and K_2CO_3 (dash line).
A) Weight loss of sample (mg/ g Cr_2O_3), B) time (minutes).
Temperature (in °C) and pressure (mm Hg) respectively: 1) 960 and 8.5; 2) 960 and 9; 3) 1010 and 72; 4) 1001 and 45; 5) 1032 and 97; 6) 1032 and 123; 7) 1062 and 186; 8) 1061 and 138; 9) 1101 and 210; 10) 1104 and 211.

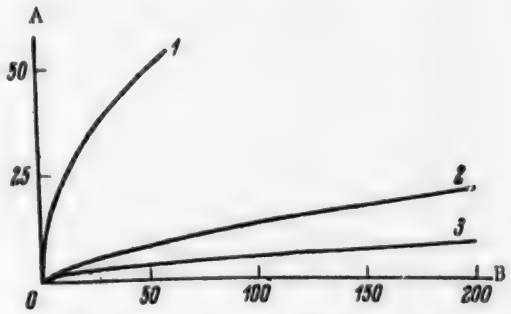

Fig. 6. Kinetics of the gasification of carbon dioxide at 1000°.
A) Degree of gasification (%), B) time (minutes).
1) Graphite impregnated with 3% Na_2CO_3; 2) graphite powder briquetted under 300 kg/ cm^2 pressure; 3) graphite lump.

For clarification of the influence of the kind of carbon on the reaction kinetics, metallurgical coke, pitch, and pitch coke were used in addition to graphite. It was found that the reduction rate fell sharply if graphite was replaced by metallurgical coke. Under these conditions the reaction at 1000° could not be reliably studied even in experiments lasting 3-4 hours. The reaction at 1100° proceeded at a rate similar to that observed in experiments with graphite at 1040°.

It should be noted that accumulation of CO in the system had a greater effect on the process kinetics in this series of experiments than in experiments with graphite. In this case the rate of the process was almost doubled, although it was still below the rate with graphite. The change in the form of the isotherms, caused by accumulation of carbon monoxide, is also noteworthy. As in the experiments with graphite during a definite time interval the isotherms become convex rather than concave toward the abscissa axis, i. e., the reaction rates begin to increase with time. In contrast to the initial regions of the isotherms, the shape of which is determined by autocatalysis, the regions in question undoubtedly reflect the specific action of carbon monoxide, the pressure of which increases continuously during the reaction. Although replacement of metallurgical by pitch coke increases the rate somewhat, it remains lower than in the experiments with graphite.

The process is accelerated sharply with the use of charges prepared* by the following method. The required amounts of chromic oxide and pitch were put into a ball mill and mixed thoroughly in presence of benzene for 3 hours. The mixture was dried by means of a stream of warm air, briquetted, and the briquets were coked. With this method of charge preparation not only was good contact between the pitch coke and oxide particles ensured, but highly active carbon formed by pyrolysis of hydrocarbons was liberated in the pores of the material. Fig. 3 shows that the reaction rate was particularly high in experiments with this material, and interaction could be detected even at temperatures of about 900-930°. It should be noted that this acceleration

* With the kind cooperation of G. P. Shveikin (UF Acad. Sci. USSR), to whom the authors offer their gratitude.

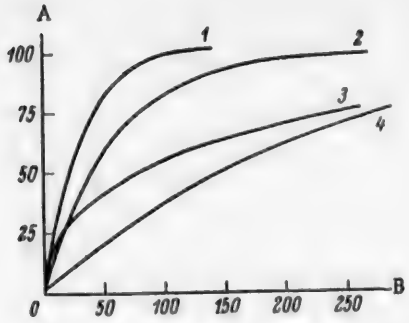

Fig. 7. Kinetics of the gasification of carbon present in charge briquets (made at 300 kg/ cm^2) by carbon dioxide at 1000°.
A) Degree of gasification (%), B) time (minutes). 1) (Cr_2O_3 + 4.5 C_{pitch} + benzene), coked, 2) Cr_2O_3 + 4.5 C_{gr}, 3) Cr_2O_3 + 4.5 C_{pitch}, 4) Cr_2O_3 + 4.5 C_{coke}.

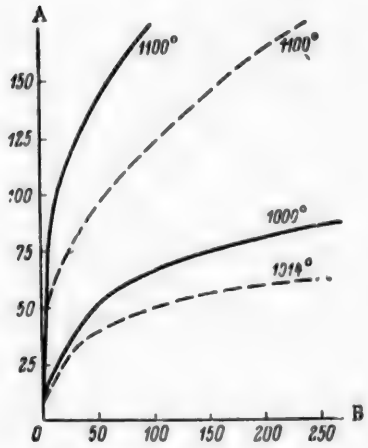

Fig. 8. Effect of the amount of carbon on the reduction kinetics of chromic oxide by graphite under moderate vacuum.
A) Weight loss of sample (mg/ g Cr_2O_3), B) time (minutes). Cr_2O_3 + 9.0 C_{gr} (continuous line), Cr_2O_3 + 4.5 C_{gr} (dash line).

extended over a considerable period, and was especially pronounced after a unified reaction zone had been formed, rather than during the initial period. The reduction rate of chromic oxide under these conditions exceeded the rate observed with the use of graphite. As was shown earlier, the reduction rate of chromic oxide varies appreciably with different reducing agents. This is possibly because of differences in their reactivity on the one hand, and of different contact conditions between the oxide and reducing agent particles on the other. In order to obtain more definite data on the role of the activity of the reducing agent, experiments were performed with the use of graphite activated by additions of 3% of sodium and potassium carbonates.

The first series of experiments was carried out with a charge into which the activators were introduced as the dry salts. Fig. 4 shows that the effects produced by sodium and potassium carbonates differ little. However, as comparison of Figs. 1 and 4 shows, the reaction is accelerated substantially in their presence, and can be clearly detected from about 900°. This shows that the reactivity of the reducing agent has an appreciable effect on the reaction kinetics.

Similar results were obtained in experiments with accumulation of carbon monoxide in the system. In this series of experiments, the results of which are presented in Fig. 5, it was again found that sodium and potassium carbonates have almost the same effect. It was further found that accumulation of carbon monoxide accelerates reduction only in the region of relatively high temperatures. For example, the reaction rate at 1060 and 1100° in a closed system is approximately 1.5-2.0 times the rate with continuous removal of the gaseous reaction products. On the other hand, as in the experiments with nonactivated graphite, accumulation of carbon monoxide at 960° somewhat retards direct reduction.

Finally, as in the vacuum experiments, in experiments with accumulation of carbon monoxide the reaction is accelerated if the reducing agent is activated by alkali-metal salts.

The next series of experiments was carried out with materials into which the activators were introduced by impregnation of graphite with their aqueous solutions. The results of vacuum experiments showed that the expected acceleration of the reduction process was not obtained. This evidently suggests that at high temperatures the reducing agent becomes impregnated by the vapors of the dry salts, which activate it to the same degree as the aqueous solutions.

Similar results were also obtained in experiments with a closed system. Under these conditions the kinetic characteristics of the process differ little from those described previously for the "dry" charge (Fig. 5).

The foregoing results thus confirm the significant influence of activation of the reducing agent on the rate of the reduction process. This result is usually associated with the known accelerating effect of alkali-metal

salts on the gasification rate of carbon by carbon dioxide. To test this hypothesis, a kinetic study was carried out of the gasification of graphite by carbon dioxide. For this, a weighed sample of the reducing agent was suspended in a wire basket from the spring of the apparatus, and the experiment was carried out in a current of CO_2 (under 1 atmos pressure). The results obtained at 1000° are plotted in Fig. 6. It is seen that gasification of lump graphite proceeds at the lowest rate. The rate of reaction of CO_2 with a briquet made from ground graphite is somewhat higher. The process is greatly accelerated with the use of graphite impregnated with alkali-metal salts.

It is clear that the conditions for the reaction of CO_2 with the reducing agent in these experiments are not equivalent to those for the reduction of oxides, but nevertheless some analogy between the kinetic characteristics of the two processes is to be expected. Further confirmation of this is provided by studies of the kinetics of the interaction of carbon dioxide with briquets containing oxide mixed with reducing agents. Fig. 7 shows that the reduction of CO_2 by metallurgical coke present in briquets mixed with chromic oxide proceeds at the lowest rate. The reaction with a material made with pitch coke is somewhat more rapid. The reaction of briquets containing graphite, and especially the pyrolysis products of pitch, develops much more rapidly. These differences in the rates of carbon dioxide reduction correspond to those found earlier in the direct reduction of chromic oxide. This fact once again emphasizes the importance of the reactivity of the reducing agent and probably also the significance of the gasification of carbon. In particular, the fact that the reduction rate of chromic oxide depends appreciably on the amount of reducing agent present in the charge suggests that carbon gasification is significant. It follows from Fig. 8 that if the amount of reducing agent is doubled, the reaction rate is increased approximately 1.5-fold (if the initial period of interaction is disregarded).

Thus, all measures which accelerate reduction of CO_2 also intensify direct reduction.

DISCUSSION OF RESULTS

Attempts to explain the above results on the hypothesis that the process of direct reduction consists, throughout its development, of a rapid stage of indirect reduction and a slow stage of carbon monoxide regeneration [1] encounter a number of difficulties. Most prominent among these is the extremal character of the process, due to its autocatalytic nature.

This feature of the interaction of carbon with a number of oxides has been described before. For example, Tatievskaia, Chufarov, and Stafeeva [3] reported the autocatalytic nature of the direct reduction of copper oxides; Arkharov, Bogoslovskii, Zhuravleva, and Chufarov [4], and Vlasov and Lisniak [5] obtained similar results for ferrous oxide, and Eliutin, Pavlov, and Merkulova [6], for nickel oxide. These studies, and a number of others, indicate that such reaction characteristics are fairly common.

It is known that the autocatalytic characteristics of a process become especially distinct if, in a complex reaction consisting of a number of stages, the slow step is rearrangement of the oxide lattice to the lattice of the metal (or a lower oxide).

This leads to the suggestion that in the early stages of the reduction of Cr_2O_3 by carbon the determining step is reconstruction of the oxide to the metal (or carbide) lattice, while the regeneration of carbon monoxide is a relatively more rapid step. This hypothesis is supported by the fact that the activation energy at that stage of the interaction is very high (above 100,000 cal/ mole), and decreases rapidly with increasing degree of reduction. Unfortunately, there are no reliable data on the activation energy of self-diffusion, not only of oxygen but also of chromium ions, which largely determines the rate of lattice reconstruction. However, the available data on chromic oxide lend some measure of support for the above hypothesis. According to Lindner's approximate determinations [7], the activation energy of self-diffusion of chromium into Cr_2O_3 is very high, close to 100,000 cal/ mole.

It should be pointed out, however, that the determining step in reconstruction of the Cr_2O_3 lattice is migration of oxygen rather than of chromium ions, i. e., of larger and less mobile particles. The activation energy of their migration should be even higher, and possibly close to the value found for the initial stage of the reduction process.

Thus, the initial stage of the reduction of chromic oxide is slowed down by a stage of lattice reconstruction. This probably applies to the course of reduction of other stable oxides under vacuum conditions, when the number

of collisions between the molecules of the reducing agent and the oxide surface is not large, and the new phase can originate only in particularly active centers of the lattice.

It should be noted that formation of a reaction zone considerably reduces the energy difficulties in the reduction process, and as a result the activation energy of the process is greatly reduced (by almost one half).

Further, if the period of formation of the reaction zone, which is very brief under normal pressure, is excluded from consideration, the role of the carbon-gasification stage becomes quite distinct.

Indeed, as was noted earlier, the reduction rate of chromic oxide is highly sensitive to the reactivity of the carbon. The kinds of carbon which react more rapidly with CO_2 under equal conditions are also more active reducing agents toward chromic oxide. This is in complete harmony with the results obtained by numerous workers in studies of the direct reduction of other compounds [8-10]. Moreover, activation of carbon by alkali-metal salts also accelerates the reaction.

The following facts are also indicative of the importance of the carbon-gasification stage.

Acceleration of reduction processes with accumulation of gaseous reaction products is most prominent in the reduction of easily-reducible oxides [3,4]. In the reduction of chromic oxide, the process is accelerated only at fairly high temperatures (1050-1100°), at which the system is far from equilibrium with the gas phase. Conversely, at low temperatures (<1030°) accumulation of the reaction products retards the reaction. This is convincing evidence of the important role of the carbon-gasification stage. This is also supported by the presence of inflections on the isotherms with accumulation of carbon monoxide in the system (Fig. 5). The explanation for these inflections is that at definite degrees of reduction the kinetic complications associated with lattice reconstruction are reduced, and the rate of direct reduction is largely determined by the stage of carbon gasification. The rate of this last process is known to increase with increasing pressure of the gas phase.

The hypothesis is also supported by the fact that the reduction of chromic oxide is accelerated with increase of the amount of reducing agent in the charge.

Thus, the direct reduction of chromic oxide is a fairly complex process, and the roles of its constituent reactions vary at different stages of the process.

At the initial period of the reduction, the slow step consists of generation and formation of the reaction zone. Subsequently the role of carbon gasification increases. The activation energy of the process therefore decreases, and the reaction becomes sensitive to the pressure of the gas phase and other parameters which influence the regeneration rate of carbon monoxide. Evidently the significance of this stage of the process diminishes substantially toward the end of the reaction, when the surface of the reaction zone decreases considerably. Under such conditions (in presence of excess carbon) the rate of the process is again governed by the crystal-lattice stage.

The following facts [11] account for the relatively high activation energies (70,000-80,000 cal/ mole). When carbon gasification is the slow step, the reduction rate is represented by the expression

$$v = v_{C,\,CO_2} = k_{C,\,CO_2} \cdot p^n_{CO_2},$$

while the gas phase is virtually in equilibrium with respect to the indirect-reduction reaction

$$K_{CO} = \frac{p_{CO_2}}{p_{CO}}.$$

Therefore

$$p_{CO_2} = \frac{K_{CO} \cdot P}{1 + K_{CO}} \quad \text{and} \quad v = k_{C,\,CO_2}\left(\frac{K_{CO} \cdot P}{1 + K_{CO}}\right)^n.$$

In the reduction of chromic oxide $K_{CO} \ll 1$, and therefore

$$v = k_{C,CO_2} \cdot K_{CO}^n \cdot P^n.$$

Since, for the indirect-reduction reaction

$$\Delta F_{CO}^0 = A + BT = -RT \ln K_{CO},$$

$$K_{CO} = C' \cdot e^{-\frac{A}{RT}} \text{ and } k_{C,CO_2} = C'' \cdot e^{-\frac{E_{C,CO_2}}{RT}},$$

Therefore

$$v = C' \cdot e^{-\frac{E_{C,CO_2}+nA}{RT}} \cdot P^n = C \cdot e^{-\frac{E}{RT}} \cdot P^n,$$

where n is a coefficient close to unity [12].

It follows from this last equation that the activation energy of direct reduction increases linearly with increase of A (and therefore with stability of the oxide); this is in good agreement with the results of a number of workers [5, 13]. In particular, for the reaction in question $A_{Cr_2O_3} \simeq 12{,}000$. This accounts for the relatively high activation energy of the process.

SUMMARY

1. The direct reduction of chromic oxide is shown to be autocatalytic in character.

2. The rate of direct reduction of Cr_2O_3 depends to a considerable extent on the kind of reducing agent. The rate of the process increases with increase of its reactivity (toward CO_2) and of the amount present. Activation of carbon by salts of alkali metals has a similar effect.

3. Accumulation of gaseous reaction products in the system, under conditions in which the pressure is far from equilibrium, appreciably accelerates the reduction process.

LITERATURE CITED

[1] P. V. Gel'd, V. G. Vlasov, and N. N. Serebrennikov, J. Appl. Chem. 25, 2, 121 (1952).*

[2] Iu. O. Esin and P. V. Gel'd, J. Appl. Chem. 31, 7, 986 (1958).*

[3] E. P. Tatievskaia, G. I. Chufarov, and N. M. Stafeeva, J. Phys. Chem. 28, 843 (1954).

[4] V. I. Arkharov, V. N. Bogoslovskii, M. G. Zhuravleva, and G. I. Chufarov, Proc. Acad. Sci. USSR 98, 803 (1954); J. Phys. Chem. 29, 272 (1955).

[5] S. S. Lisniak, Kinetics of the Reduction of Iron Oxides by Solid Carbon [in Russian] (Sverdlovsk, Urals Polytech Inst., 1956).

[6] V. P. Elutin, Iu. A. Pavlov, and R. F. Merkulova, in the book: Use of Radioactive Isotopes in Metallurgy [in Russian] (Metallurgy Press, 1955), p. 48.

[7] R. Linder, Z. Naturforsch, 10a, 1027 (1955).

[8] H. L. Saunders and H. I. Tress, J. Iron and Steel Inst. 157, 215 (1947).

[9] G. I. Chufarov, Bull. Acad. Sci. USSR 6, 883 (1946).

[10] D. Ia. Markovskii, Trans. State Inst. Appl. Chem. 34, 36 (1940).

[11] P. V. Gel'd, Trans. Urals Polytech. Inst. (Metallurgy Press, 1957), p. 72.

[12] O. A. Esin and P. V. Gel'd, Physical Chemistry of Pyrometallurgical Processes, 1 [In Russian] (Metallurgy Press, 1950).

[13] V. A. Kozlov, Kinetics of the Reduction of Manganese Oxides by Solid Carbon [In Russian] (Sverdlovsk, Urals Polytech. Inst., 1956).

Received June 7, 1957.

*Original Russian pagination. See C.B. translation.

PRODUCTION OF BORIDES OF ALKALINE-EARTH METALS BY REDUCTION OF THE OXIDES BY CARBON

L. Ia. Markovskii and V. N. Vekshina

(State Institute of Applied Chemistry)

Alkaline-earth borides, especially calcium boride, are of considerable interest and are used in various branches of technology. In a number of patents the use of these substances in heat-resisting and nonscaling compositions and hard-alloys is described [1]. The peculiar thermoemissive properties of these borides may also be of great importance [2-4]. All these properties are the consequence of the structural characteristics of alkaline-earth borides, which crystallize with a cubic lattice of the CsCl type, composed of metal atoms and octahedral complexes of 6 boron atoms. The metal atoms are enclosed in a dense framework of boron atoms, which confers high thermal and chemical stability on borides.

Several methods for the production of alkaline-earth borides are described in the literature. Apparently these substances can be synthesized most simply by interaction of the elements in vacuum or an inert atmosphere [5], or in hydrogen at high temperatures [3]. Considerable heat is evolved in the reaction. Stock and Holle [6] and Dürr [7] prepared calcium boride by reduction of B_2O_3 with metallic calcium. Moissan [8] described the preparation of calcium boride by the aluminothermic method. Finally, in recent years fairly wide use has been made in laboratory practice of the electrochemical method of Andrieux [9], based on the electrolysis of fused borates. This method yields pure and well-crystallized boride powders, but is complicated and rather unproductive, as it involves laborious separation of the powders from the solidified electrolytes [10].

It is known that borides of the transition metals can be successfully prepared by the reduction of mixtures of metal oxides and boron by means of carbon:

$$MeO + B_2O_3 + 4C \rightarrow MeB_2 + 4CO.$$

This method, first proposed by McKenna [11], can be used for the production of relatively pure borides of titanium, zirconium, and chromium [12, 13]. The literature contains no information on the use of this "carbothermic" method for the production of alkaline-earth borides.

The formation of alkaline-earth borides by the carbothermic method is represented by the following theoretical equation:

$$MeO + 3B_2O_3 + 10C \rightarrow MeB_6 + 10CO.$$

The aims of the present investigation were a study and development of the carbothermic method for the synthesis of alkaline-earth borides. In the case of the alkaline-earth metals the main reaction of boride formation is complicated by the occurrence of side processes. In the consideration of possible side reactions, the first point to be taken into account is the formation of the corresponding carbides. Because of the high chemical activity of the carbides of the metals in the 2nd group of the periodic system and the known inertness of borides, it was thought that the latter could be isolated completely by treatment of the reaction mixtures with acids.

However, it was found that such treatment results in the formation of organic compounds which contaminate the borides and hinder the preparation of pure, carbon-free products. These reactions form the main obstacle to the carbothermic synthesis of the required compounds.

TABLE 1

Results of Experiments on the Removal of Carbides from Boride Sinters by Fusion with B_2O_3

Borides	C content before calcination (in %)	Chemical composition of borides after calcination (in %)					Results of x-ray phase analysis*
		Me	B	C	N	total	
CaB_6	26.5	38.2	60.4	0.2	1.9	100.7	Pure CaB_6
	22.0	33.7	61.7	2.4	5.6	103.4	CaB_6. Weak additional line present
	13.2	33.0	59.5	1.6	5.8	99.9	CaB_6. Additional line present
	10.6	33.8	62.2	1.6	4 0	101.6	Pure CaB_6
SrB_6	14.7	53.4	42.5	1.0	3.4	100.3	Pure SrB_6
BaB_6	24.1	51.7	39.4	4.8	1.0	96.9	Pure BaB_6

* Iu. D. Kondrashev took the x-ray photographs.

TABLE 2

Purification of Ca and Sr Borides by Alkali Treatment

Borides	C content before treatment	Chemical composition of purified boride (in %)				Results of x-ray phase analysis
		Me	B	C	total	
CaB_6	20.6	38.6	59.5	2.5	100.6	Pure CaB_6
SrB_6	18.0	56.2	40.5	2.7	99.4	Pure SrB_6

EXPERIMENTAL

Methods. The borides were synthesized from chemically pure oxides of calcium, barium, and strontium, and powdered boric anhydride. The reducing agent was powdered electrode graphite containing less than 0.1% ash. The reaction mixture was thoroughly mixed in the required proportions and briquetted under 500-800 kg/ cm^2 pressure. The briquets were calcined in cylindrical graphite beakers in a Tammann furnace without the use of a protective atmosphere. The reaction temperature was measured by means of a Siemens optical pyrometer sighted onto the hot cover of the graphite crucible.

Formation of organic compounds in the hydrolysis of boride sinters. The very first experiments showed that the primary products of the reduction of oxide mixtures contain considerable amounts of carbon, evidently present mainly in the form of carbides. However, only traces of acetylene were detected in the gas phase as the result of decomposition by water or dilute acids. Analysis of the substance left after acid treatment showed that the carbon content was virtually unchanged, and in some experiments even increased owing to extraction of excess metal oxide. The following question therefore arose: is the carbon in the product after acid treatment present in the free state, or in the form of compounds?

Experiments showed that when the sinters, formed in the reduction of oxide mixtures, are treated with water or acids, solid and liquid organic compounds are formed; if these are removed by the methods described below, Ca and Sr borides can be made almost entirely free from carbon, and the carbon content of barium boride can be reduced considerably. The formation of these organic compounds in the acid treatment of boride sinters is revealed by the external appearance of the solid residue and the solution, and by the sharp unpleasant odor. The residue becomes dark brown and is amorphous in appearance (extensive amorphous background appears in the x-ray patterns, especially in the case of barium). When heated above 100° the product begins to liberate greenish-brown vapor with a sharp odor; on further heating the vapor inflames in air, while all the solid portion becomes red-hot.

The amount of organic substances formed is particularly large if the reaction mixture contains excess metal. However, they are formed, although in considerably smaller amounts, if the original components are

TABLE 3

Results of Experiments on the Preparation of Calcium Boride

Reaction mixture	Temperature of experiment (in °C)	Chemical composition of original product (%)				C content after acid treatment (%)	Chemical composition of product purified by calcination (%)				Results of x-ray phase analysis
		Ca	B	C	total		Ca	B	C	total	
$CaO + 3B_2O_3 + 10C$	1900	—	—	28	—	22	—	—	17.8	—	CaB_6 and C lines
$2CaO + 3B_2O_3 + 10C$	1600	—	—	15.9	—	—	—	—	—	—	No CaB_6 lines
	1700	41.2	32.6	14.2	88	12.6	—	—	2.6	—	CaB_6 lines, no impurities
	1800	—	—	17	—	20.3	38.8	59	3.2	101	
	1900	—	—	6.7	—	4.0	38.6	61.7	0.8	101.1	
	1900	—	—	16.5	—	14	39.2	58.1	1.6	98.9	
	1900	—	—	15.4	—	17	36.4	56.3	1.4	94.1	
	1900	—	—	10.7	—	11	41.1	58.7	Нет	99.8	
	2000	39.2	41.8	13.7	94.7	11.6	38.8	61.2	1.7	101.7	
	2100	—	—	22.7	—	20.0	—	—	9	—	CaB_6, C, and additional lines
$CaO + 6B_2O_3 + 10C$	1900	—	—	10.8	—	—	—	—	11.1	—	CaB_6 and C lines
	1900	—	—	11.9	—	—	—	—	12.3	—	
	1800	—	—	17.9	—	—	—	—	13.2	—	CaB_6, C, and CB_4 lines
	2000	—	—	9.8	—	—	—	—	11.2	—	

TABLE 4

Results of Experiments on the Preparation of Barium and Strontium Borides

Reaction mixture	Temperature of experiment (in °C)	Chemical composition of original product (%)				C content after acid treatment (%)	Chemical composition of product purified by calcination (%)				Results of x-ray phase analysis
		Me	B	C	total		Me	B	C	total	
$BaO + 3B_2O_3 + 10C$	1700	44.2	27.9	21.4	93.5	—	—	—	15.1	—	No BaB_6 lines, unknown phase
	2250	—	—	17.9	—	19.0	40.6	50.7	9.8	101.1	BaB_6 and additional lines
$2BaO + 3B_2O_3 + 10C$	1900	—	—	20	—	—	—	—	8.3	—	No BaB_6 lines
	2050	56.4	16.6	17.2	90.2	21.3	—	—	18.7	—	BaB_6 and C lines, additional lines present
	2200	59.7	20.5	15.1	95.3	19.4	—	—	8.1	—	
	2200	—	—	18.5	—	18.0	66.7	30.8	3.2	100.7	BaB_6 lines
	2250	—	—	18.1	—	22.	58.6	27.8	12.5	98.9	
	2200	59.6	19.5	19	98.1	20.0	59	28	7.9	94.9	
$2SrO + 3B_2O_3 + 10C$	1700	—	—	14.5	—	15.2	59.7	34.6	2.7	97.0	SrB_6 lines
	1900	—	—	17.6	—	18.7	54.7	39.1	4	97.8	
	2000	—	—	10.8	—	11.0	54.7	40.9	3.0	98.6	

TABLE 5

Results of Carbothermic Synthesis of Titanium and Zirconium Borides

Borides	Reaction temperature (in °C)	Chemical composition (in %)				Results of x-ray phase analysis
		Me	B	C	total	
TiB_2	1700	69.1	30.4	0.7	100.2	Pure TiB_2
ZrB_2	1900	80.9	18.1	0.3	99.3	Pure ZrB_2

present in stoichiometric proportions, or if excess B_2O_3 is present. It proved impossible to prevent completely the formation of organic compounds by variations of the reagent ratio.

Two hypotheses may be considered in relation to the possible causes of the formation of organic compounds in the hydrolysis of the primary products formed in the reduction of oxides by carbon.

On the one hand, in thermal reduction of alkaline-earth metal oxides and boric oxide by carbon there may by formed, in addition to borides, carbides different from known carbides of the MeC_2 type, which yield acetylene on hydrolysis. Erlwein [14] and Bredig [15] noted the possibility of formation of such carbides, for example CaC or Ca_2C_3, although the existence of these carbides has not been proved experimentally in any way. The hydrolysis of such carbides may be presumed to yield more complex organic compounds, rather than acetylene. However, this hypothesis was not confirmed by special experiments on the synthesis of calcium carbides from the elements with an excess of Ca to correspond to the compositions CaC and Ca_2C_3. These experiments were carried out in a hydrogen atmosphere at 1100°. The product yielded only acetylene on hydrolysis. No liquid products were formed, at least in measurable quantities. A similar result was obtained in experiments in which calcium boride was added to the mixture of calcium and carbon.

On the other hand, the result of these experiments tends to favor another hypothesis concerning the formation of these organic compound; namely, that they are formed as the result of polymerization of acetylene liberated when water acts on the carbides present in the borides as impurities.

Polymerization of acetylene may be catalyzed by unreacted boric anhydride or the alkaline-earth boride itself. It is known from the literature that polymerization of acetylene under the influence of a number of catalysts may occur even at room temperature [16, 17]. It is interesting, however, that if an attempt is made to reproduce these reactions artificially by treatment of powdered mixtures of CaB_6, CaC_2 and CaB_6, B_2O_3, CaC_2 with acids, the formation of organic polymerized compounds cannot be detected in practice. Evidently the polymerization of acetylene formed by decomposition of carbides is favored by close contact between the carbide and boride molecules, such as is found in the fusion products of oxide – carbon mixtures.

Experiments on the sintering of synthetic CaB_6 and BaB_6 with carbon(1700-2000°) confirmed the thermodynamic stability of the alkaline-earth borides [18]. No changes of phase composition could be detected in the sintered products by x-ray or chemical analysis, and organic compounds or acetylene were not formed as the result of acid treatment. If the boride powders obtained after acid treatment are extracted with solvents for many hours, some of the organic substances can be extracted from them. However, the borides could not be completely freed from the organic compounds by means of benzene, acetone, toluene, or even tetrahydrofuran, which was found to be the best solvent for these compounds. After evaporation of the solvents, liquid oily products, the nature of which has not been precisely determined as yet, can be obtained from the extracts. (C – H lines were detected by means of L. D. Shcherba's infrared spectroscopic method). However, most of the organic matter remains as an impurity in the boride.

It should be noted that the cyanamides of Ca, Sr, and Ba are not formed in the production of alkaline-earth borides; this was confirmed by chemical analysis, which showed that the total nitrogen content of the boride sinters did not exceed 1%, and cyanamide nitrogen was entirely absent.

Removal of organic impurities and carbon from borides (Table 1-4). In the development of a method for production of pure borides, free from organic impurities and carbon, two possible courses were investigated: 1) decomposition of the carbides initially formed, and 2) decomposition of the organic compounds formed by hydrolysis of carbides.

The first method consisted of calcination of the boride sinters with boric anhydride at 1800-1900° for 5-10 minutes, until evolution of glowing vapor ceased. Boric anhydride reacted with the alkaline-earth carbides in the process to yield hexaborides. The products were free from carbides and did not form organic compounds when treated with acid.

Table 1 shows that the carbon content of borides falls sharply as the result of calcination with B_2O_3, to 1-1.5% for Ca and Sr, and 5% for Ba. It was found, however, that in these calcination conditions and in absence of a protective atmosphere the borides absorb appreciable amounts of nitrogen from the air, forming nitrides. Contamination of borides by nitrides may be avoided if the calcination is carried out in an inert atmosphere such as argon.

In purification by the second method, it proved most convenient to burn out the organic substances in air at 500-600°, the solid residue then being treated with acid to remove oxides formed by the partial oxidation of borides. This operation may be performed in porcelain boats or crucibles.

In this way it was possible to prepare calcium and strontium borides containing 1-2% of carbon, with a nearly theoretical ratio of metal to boron (Tables 3 and 4).

Removal of carbon from boron boride by this method is much less successful (Table 4).

Its carbon content could not be lowered by an increase of the calcination time, as this results in considerable oxidation of the boride itself, and the amount of carbon in the boride does not decrease.

Organic impurities may be removed from borides by another method, in which the products are leached with strong alkali solution to hydrolyze the boride sinters before the acid treatment. Most of the organic matter is dissolved, while boride remains in the residue. The alkaline solution is decanted, the residual boride is washed several times with alkali by decantation, then with acid to dissolve metal oxides, and finally with hot water.

According to the results of x-ray phase analysis, this purification method gives pure calcium and strontium borides. Chemical analysis (Table 2) shows that the metal – boron ratio in the calcium and strontium borides is close to the theoretical. However, barium boride contains large amounts of carbon even after the alkali treatment, so that it cannot be freed from carbon by that method. This is probably due to the presence of large amounts of elemental carbon, possibly in the form of solid solution.

Study of the process conditions in the reduction of oxide mixtures by carbon. The experimental results obtained in the synthesis of Ca, Sr, and Ba borides by the carbothermic method are given in Table 3 (for Ca boride) and Table 4 (for Ba and Sr borides). Analytical data both for the primary and for the purified products are given in these tables. The results of these experiments were used to determine the optimum conditions for the preparation of each boride, and to find the effects of the composition of the reaction mixture, temperature, and process conditions on the reaction of boride formation. It follows from these results that calcium boride should be made at temperatures about 1900-2000°, with a 2-fold excess of CaO over the stoichiometric amount*. These are also the optimum conditions for preparation of strontium boride. The temperature of barium boride formation is considerably higher. Thus, barium boride is not formed at 1700-2000°. The optimum temperature for its formation is 2200-2300°, when a 2-fold excess of BaO should be used. The reaction of boride formation should be intensified as much as possible, i. e., the temperature should be raised rapidly, and the exposure at the required maximum temperature should be short (~10 minutes). Otherwise the carbon content of the borides increases considerably, probably because of an increase in the amount of it present in elemental form.

For comparison with data on the alkaline-earth borides, Table 5 contains results obtained in carbothermic synthesis of the borides of certain transition metals.

It is clear from these results that the carbothermic method gives good results in the production of zirconium and titanium borides, without additional purification, the carbon contents of the borides being in the range of a few tenths of one per cent.

SUMMARY

1. The borides of calcium, strontium, and barium, containing a certain admixture of carbon, can be pre-

* If excess boric anhydride is present in the reaction mixture, the primary product always contains considerable amounts of elemental C and B_4C, which cannot be completely removed by any of the methods used.

pared by the reduction of mixtures of metal and boron oxides with carbon (graphite). The optimum conditions were found, and the influence of temperature and composition of the initial mixtures on the reaction of boride formation was determined.

2. The formation of alkaline-earth borides is considerably complicated by side reactions, primarily the formation of carbides, which on further treatment with water and acids yield organic substances the nature of which was not finally established. It is suggested that these organic products are formed by the catalytic polymerization of the acetylene which is initially liberated. They contaminate the borides with carbon and make the preparation of quite pure products impossible.

3. Three methods for removal of carbon from boride sinters have been worked out. They all give satisfactory results with calcium and strontium borides, but not with barium boride. The latter fact is probably due to the presence of considerable amounts of elemental carbon in the form of solid solution in barium boride.

In conclusion, we thank A. G. Petrova, Iu. D. Kondrasheva, and L. D. Shcherba for help in this work.

LITERATURE CITED

[1] E. Lowe, U. S. Patent 2,647,061 28, VII (1953).

[2] B. M. Tsarev, Contact Potential Difference [in Russian] (Moscow, GTTI, 1956).

[3] J. Lafferty, J. Appl. Phys., 22, 299 (1951).

[4] I. D. Morgulis, Progr. Phys. Sci. 58, 534 (1954).

[5] M. Stackelberg and F. Neumann, Z. Phys. Chem. B, 19, 314 (1932).

[6] A. Stock and W. Holle, Ber. 23, 772 (1908).

[7] L. Dürr, Ch. Ztg. 36, 657 (1912).

[8] H. Moissan, Le four électrique, Paris (1897).

[9] L. Andrieux, Ann. Chim. Phys. 12, 423 (1929).

[10] G. V. Samsonov and L. Ia. Markovskii, Progr. Chem. 25, 190 (1956).

[11] P. McKenna, Ind. Eng. Chem. 28, 767 (1936).

[12] R. Kieffer and P. Schwarzkopf. Hartstoffe und Hartmetalle. Vienna (1953).

[13] P. Schwarzkopf and R. Kieffer, Refractory Hard Metals, N. Y. (1955).

[14] G. Erlwein, Z. Elektroch. 17, 177 (1911).

[15] M. Bredig. J. Phys. Chem. 46, 801 (1942).

[16] S. Berkman, J. Morrell, and G. Egloff, Catalysis, Organic and Inorganic (Moscow, State Fuel Tech. Press, 1949), 482 [Russian translation].

[17] Ia. M. Paushkin, Catalytic Polymerization of Olefins to Motor Fuel (Izd. AN SSSR, 1955) [In Russian].

[18] L. Brewer and H. Haraldsen, J. Electroch. Soc. 102, 399 (1955).

Received February 22, 1957.

PHASE DIAGRAM OF THE SYSTEM: IRON COMPOUND – AQUEOUS MEDIUM, IN REDOX POTENTIAL – pH COORDINATES

O. N. Lapteva

(The A. I. Gertsen Pedagogic Institute, Leningrad)

Both thermodynamic and kinetic methods are used in studies of metal corrosion and development of effective methods for its prevention. In kinetic studies of corrosion processes use is generally made of polarization curves which characterize the rates of electrochemical processes at the metal surface under consideration. Thermodynamic studies of corrosion processes are very often based on investigations of the oxidation – reduction potentials of systems: metal or its compound – aqueous medium. It is known that hydrogen-ion activity has a special influence on the character and rate of corrosion processes. Therefore studies of the variations of the redox potential of a system with pH often make it possible to investigate the nature of the processes taking place in the system, and of the compounds formed, and to determine their thermodynamic characteristics. Clark [1] plotted the potentials of hydrogen and oxygen electrodes against pH in order to determine the thermodynamic stability of water. His graph proved useful in studies of many oxidation – reduction processes in aqueous media. Pourbaix [2-5] developed Clark's idea in relation to metal – water systems. His diagrams were based on theoretical calculations with the use of standard thermodynamic data for different metal compounds, and on assumptions relating to their stability in aqueous media at different pH values. Similar diagrams were obtained by Shultin [6,7] for the systems iron – water and copper – water.

Such diagrams can be used to give an indication of the pH and redox potential at which a given metal is thermodynamically stable and therefore not subject to corrosion, and also of the values at which the metal is thermodynamically unstable, i. e., is attacked, with the formation of compounds more stable under the given conditions, such as oxides or hydroxides. It is thus possible to characterize the possible processes in the metal – water system with variations of pH at a given temperature. In the case of the system iron – water, the diagram for the redox potential as a function of pH is somewhat complex. The diagram plotted for this system by Pourbaix [3, 8] contains 8 regions, bounded by 26 lines; each region corresponds to a definite thermodynamically – stable compound of iron, and each line separating the regions corresponds to equilibrium between two such compounds.

In view of the fact that the thermodynamic data necessary for calculation of various equilibria in the system iron compound – aqueous medium differ considerably in different sources [9-19], Pourbaix had to put forward two versions of the diagram. The important difference between them lay in the positions of the regions for the stable existence of ferric hydroxide and magnetic oxide.

In the first version (version "a") it is assumed that the change of isobaric potential $\Delta Z^0_{Fe(OH)_3}$ for ferric hydroxide is – 167.64 kcal/ mole, while in the second (version "b") this is taken to be – 172.74 kcal/ mole.

Because of this discrepancy, we thought it useful to plot the phase diagram for the system iron compounds – aqueous medium at various pH values (t=25°) on the basis of our own experimental data [19].

Table 1 contains the equilibria studied, used as the basis for the diagram, and the thermodynamic equations for their potentials in relation to the pH of the medium and the concentrations of ferric and ferrous ions.

These data were used to plot the phase diagram in redox potential – pH coordinates, shown in Fig. 1, where each line represents one of the equilibria, the regions represent the equilibrium existence of various iron compounds, and the intersections represent replacement of one equilibrium by another.

TABLE 1

Equilibrium	Equation for calculation of the redox potential φ_{redox}
1) $Fe^{\cdot\cdot} \rightleftarrows Fe^{\cdot\cdot\cdot} + e$	$\varphi = 0.738 + 0.058 \log \frac{a_{Fe^{\cdot\cdot\cdot}}}{a_{Fe^{\cdot\cdot}}}$
2) $Fe^{\cdot\cdot} + 3H_2O \rightleftarrows Fe(OH)_3 + 3H^{\cdot} + e$	$\varphi = 0.908 - 0.175pH - 0.058 \log a_{Fe^{\cdot\cdot}}$
3) $3Fe^{\cdot\cdot} + 4H_2O \rightleftarrows Fe_3O_4 + 8H^{\cdot} + 2e$	$\varphi = 1.206 - 0.234pH - 0.087 \log a_{Fe^{\cdot\cdot}}$
4) $Fe_3O_4 + OH^{\prime} + 4H_2O \rightleftarrows 3Fe(OH)_3 + e$	$\varphi = 0.330 - 0.058pH$
5) $3Fe + 8OH^{\prime} \rightleftarrows Fe_3O_4 + 4H_2O + 8e$	$\varphi = 0.043 - 0.058pH$

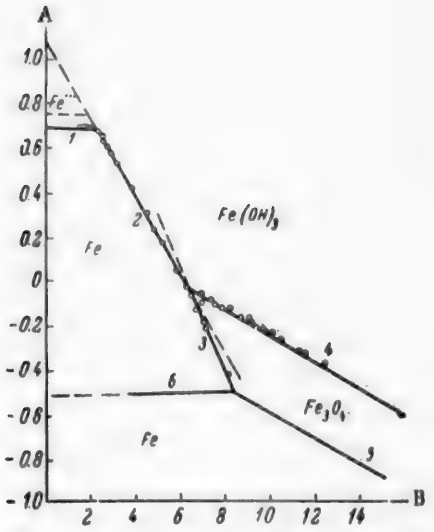

Fig. 1. Phase diagram for the system iron – water.

Solution characteristics: $\frac{C_{Fe^{\cdot\cdot\cdot}}}{C_{Fe^{\cdot\cdot}}} = \frac{0.01}{0.01}$, $\frac{a_{Fe^{\cdot\cdot\cdot}}}{a_{Fe^{\cdot\cdot}}} = 0.103$, $\log \frac{a_{Fe^{\cdot\cdot\cdot}}}{a_{Fe^{\cdot\cdot}}} = -0.98$, $\log a_{Fe^{\cdot\cdot}} = -2.68$. A) Redox potential (v), B) pH.

Examination of the diagram in Fig. 1 shows that Equilibrium (1) exists in strongly acid media up to pH = 2.2. This is followed by the new Equilibrium (2), when ferric hydroxide is precipitated. This equilibrium directly involves $H^{\cdot}$ and $Fe^{\cdot\cdot}$ ions. When pH of about 6.3-6.5 was reached, a new regular change of potential was observed, indicative of a new equilibrium in the system. It was found that in this pH region a black precipitate was formed; when dried, it was attracted by a magnet [10]. This indicates that magnetic iron oxide Fe_3O_4 is involved in the new equilibrium. The slope of the line based on experimental data corresponds to Equilibrium (3). If a mixture is made of magnetic iron oxide and ferric hydroxide, freshly precipitated in an aqueous medium, and alkali solution is gradually added in absence of oxygen (in a nitrogen atmosphere), the variation of the oxidation potential with pH is represented by Line 4. Its slope corresponds to the law represented by the equation for Equilibrium (4), as is clear from the positions of the points on the experimental diagram. This equilibrium, as far as can be judged from the experimental data in the diagram, may exist under the specified conditions in the system at pH = 6.3-6.5 and in the alkaline region. The experimental data show that the region in which Equilibrium (3) exists, like the regions of Equilibria (1) and (2), is restricted. It terminates at pH of about 8.5, i. e., in a weakly alkaline medium. In media of higher alkalinity $Fe^{\cdot\cdot}$ ions cannot exist in equilibrium in the solution. It may further be assumed that Equilibrium (5) exists only in the alkaline region. Line 5, which corresponds to this equilibrium, is also indicated on the diagram. This equilibrium exists at negative potentials of the platinum electrode ($\varphi_{ox} \approx 0.5$ v and less). Finally, in the same potential region, but in weakly alkaline and weakly acid regions (pH approximately 4.0-8.5), the equilibrium $Fe \rightleftharpoons Fe^{\cdot\cdot} + 2e$ (6) should exist; like Equilibrium (1), this is independent of pH.

Thus, the region of thermodynamic stability of the $Fe^{\cdot\cdot}$ ion is contained by the Lines 1, 2, 3, and 6, and that of magnetic oxide of iron, by the Lines 3, 4, and 5; the region above this corresponds to the stable state of ferric hydroxide.

Comparison of our diagram with the versions of the Pourbaix diagram (Fig. 2) leads to the conclusion that the general character of the distribution of the stability regions of different compounds in our diagram is closer to the second version ("b") of Pourbaix. However, the line for Equilibrium (2) is closer to version "a". The

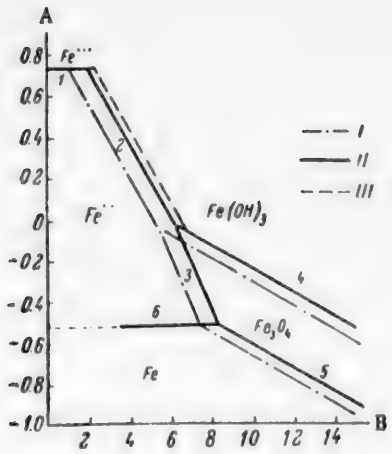

Fig. 2. Phase diagram for the system iron – water.

A) Redox potential (v), B) pH.

I) Version "b" of Pourbaix, II) experimental data, III) line 2 from version "a" of Pourbaix.

Equilibrium	Standard potentials (v)		
	Experimental results	Values given by Pourbaix	
		<<a>>	<<b>>
1	0.738	0.745	
2	0.908	0.969	0.748
3	1.206	0.983	0.982
4	—0.490	0.112	—0.551
5	—0.863	—0.913	

main cause of the differences between our diagram and the Pourbaix versions is that our values of $\Delta Z^0_{Fe(OH)_3}$ and $\Delta Z_{Fe_3O_4}$, based on experimental data, differ from the values used by Pourbaix. The standard potentials of Equilibria (1), (2), (3), (4), and (5) also differ in the two cases. The values are compared in Table 2.

It should be noted that, according to our data (Fig. 1), magnetic iron oxide is stable in an alkaline medium at ordinary temperatures. Many still consider that this compound is formed only at high temperatures, and cannot exist in an equilibrium state in aqueous media at ordinary temperatures [20, 21].

As the result of a large number of experiments, we established that when the pH is raised to 7.0 the precipitate formed is not ferrous hydroxide but a black substance which is attracted by a magnet. This substance is undoubtedly magnetic iron oxide. Therefore magnetic iron oxide (Fe_3O_4) is stable at ordinary temperatures in aqueous media at pH above 7. This result is confirmed by another series of our experiments, on the stability of ferrous hydroxide and magnetic oxide in aqueous solutions without access of air. It was shown in these experiments that the precipitate of magnetic oxide, placed in a sealed bulb in a nitrogen or hydrogen atmosphere, remains unchanged even in presence of a catalyst (platinum). However, ferrous hydroxide precipitate, under the same conditions, was instantaneously converted into a black precipitate of the magnetic oxide after very brief contact with smooth platinum. The same took place, but more slowly, in presence of excess ferrous ions in solution. Our conclusion concerning the stability of Fe_3O_4 at ordinary temperatures is in agreement with the results of other authors [22-26].

SUMMARY

1. Experimental data were used to plot the phase diagram for the system 2- and 3-valent iron compounds – aqueous medium at 25°, in oxidation potential – pH coordinates. The following equilibria are represented in the diagram: $Fe^{++} - Fe^{+++} + e$ (1), $Fe^{++} + 3H_2O \rightleftharpoons Fe(OH)_3 + 3H^+ + e$ (2), $3Fe^{++} + 4H_2O \rightleftharpoons Fe_3O_4 + 8H^+ + 2e$ (3) $Fe_3O_4 + OH^+ + 4H_2O^- \rightleftharpoons 3Fe(OH)_3 + e$ (4) and $3Fe + 8OH^+ \rightleftharpoons Fe_3O_4 + 4H_2O + 8e$ (5). In addition, it shows stability regions for soluble compounds of 2- and 3-valent iron, ferric hydroxide, and magnetic iron oxide.

2. It is shown that magnetic iron oxide is thermodynamically stable at ordinary temperatures in absence of oxygen in an alkaline medium. Ferrous hydroxide is thermodynamically unstable under the same conditions, and is converted into the magnetic oxide.

3. The experimental phase diagram is compared with the two versions of the Pourbaix diagram, and it is shown that the experimental diagram is generally closer to version "b" of the Pourbaix diagram. Some modifications are introduced in relation to the boundaries of the equilibrium $Fe^{++} + 3H_2O \rightleftharpoons Fe(OH)_3 + 3H^+ + e$ (2).

LITERATURE CITED

[1] W. M. Clark, Determination of Hydrogen Ions (Baltimore, 1928).

[2] M. Pourbaix, Metaux et Corrosion 13, 189 (1938).

[3] M. Pourbaix, Thermodinamique des Solutions Aqueuses Diluées (Delft, 1945).

[4] M. Pourbaix, Metaux et Corrosion 21, 121 (1946).

[5] M. Pourbaix, Corrosion 5, 121 (1949).

[6] A. I. Shultin, J. Phys. Chem. 15, 3, 367 (1941).

[7] A. I. Shultin, J. Appl. Chem. 20, 8, 739 (1947).

[8] M. Pourbaix, Thermodynamics of Dilute Aqueous Solutions (London, 1950).

[9] D. Bezier, Ann. Chim. 20, 161 (1945).

[10] W. Schumb and S. Sweetser, J. Am. Chem. Soc. 57, 871 (1935).

[11] K. Jellinek and H. Gordon, Z. Phys. Ch. 112, 236 (1924).

[12] H. Britton, J. Chem. Soc. 127, 2148 (1925).

[13] P. A. Kriukov and G. P. Avseevich, Trans. Leningrad Div. All-Union Sci. Res. Inst. 17, 135 (1933).

[14] L. Cooper, Pr. Roy. Soc. B, 124, 299 (1937).

[15] I. E. Flis, Candidate's Dissertation, A. I. Gertsen Pedagogic Inst. (1939).

[16] D. Bezier, C. r. 216, 798 (1943).

[17] M. Quintin, C. r. 232, 1303 (1951).

[18] K. Boock and M. Hermann, Z. Anorg. Ch. 273, 1 (1953).

[19] O. N. Lapteva, J. Appl. Chem. 31, 8, 1210 (1958).

[20] W. M. Latimer, Oxidation States of the Elements and their Potentials in Aqueous Solutions (IL, 1954) [Russian translation].

[21] P. Dalahay, M. Pourbaix and P. Rosselberghe, J. Chem. Education 27, 683 (1950).

[22] W. Traube and W. Lange, Ber. 58, 2776 (1925).

[23] G. Schikorr, Z. Elektroch. 35, 60 (1929).

[24] K. Murata, J. Soc. Chem. Ind. Japan 35, 523 (1932).

[25] G. Schikorr, Z. Anorg. Ch. 212, 33 (1933).

[26] U. Evans and J. Wanklin, Nature 162, 27 (1948).

Received April 20, 1957

REDUCTION OF A LAYER OF COPPER OXIDE UNDER HIGH PRESSURE OF THE GASEOUS PHASE

A. S. Tumarev and L. A. Paniushin

(Laboratory of High-Pressure Electrothermics, the A. A. Baikov Institute of Metallurgy, Acad. Sci. USSR)

Many papers have been published in the periodicals of various countries on the influence of pressure on the course of reduction of oxides and ores.

Without critical analysis of the published data, we may refer to certain papers [1-5], which contain attempts at theoretical generalization of the known experimental data, and mention the most important researches in this field.

It must be pointed out, however, that despite the large amount of work done, many problems still remain unsolved in relation both to the course of reduction processes at high pressures, and to the theoretical interpretation of the observed effects. Continued research in this field is therefore necessary.

The reduction of oxides by gaseous reducing agents is a complex heterogeneous process, which develops in the form of interconnected physical effects and chemical conversions, dependent on numerous factors.

The most important stages of the process are: diffusion of the reacting substances into the reaction zone (and also diffusion of the gaseous reaction products out of the reaction zone), adsorption of the reacting gas on the oxide surface, and changes involving the crystal chemistry of the reacting substances.

It is believed that the rate of a heterogeneous process is determined by the rate of the slowest transformation. However, this is more or less valid only in certain limiting cases. In reality, all these factors influence the rate of the process simultaneously, although to different extents. Physical adsorption, characteristic of low temperatures, occurs very rapidly and cannot retard the process, especially at high pressures of the gas phase. With regard to chemisorption, it is difficult to separate this from chemical reaction, and to determine its influence on the rate of the process. However, it can be regarded fairly reliably as a stage in the development of crystallochemical conversion.

Thus, two principal factors are seen to influence the rate of a heterogeneous process: diffusion, and chemical reaction. The action of each of these factors is also rather complex. In particular, the nature of the diffusion and the laws governing it may change during the course of a heterogeneous process. With regard to the effect of pressure on diffusion rate it may be said that the rate of external diffusion (mass transfer from the core of the gas stream to the solid surface), and of gas diffusion through the layer of solid along channels of diameter greater than the mean free path of the gaseous molecules, which conform to Fick's law, are unchanged by pressure owing to the fact that the diffusion coefficient and the velocity gradient undergo equal changes in opposite directions on increase of pressure.

If the diameter of the channels is of the same order of magnitude as the mean free path of the gas molecules, diffusion conforms to the Knudsen equations; its rate then increases with increase of pressure. In real bodies, the channels may vary greatly in diameter, and therefore diffusion conforming to different laws may take place simultaneously. In such cases increase of pressure in the diffusion region may accelerate the process in accordance with the proportion of Knudsen diffusion. The rate of chemical interaction increases with increase of pressure owing to increased concentration of the reducing gas. It follows that in the diffusion region (in absence of Knudsen diffusion) increase of pressure cannot accelerate reduction, while in the kinetic region the rate of the process should increase with increase of pressure.

The purpose of the present investigation was to verify the foregoing hypothesis with the aid of a method in which the experimental conditions could be defined most strictly and made most reproducible.

Oxide in the form of a powder of 200 mesh, spread in an even layer, was used for the reduction. Carbon monoxide was passed through the layer at different rates and under different pressures. Because of the small dimensions of the individual grains, diffusion from their surfaces to the centers cannot have a significant influence on the course of the process, and there is a simple relationship between the gas flow into the reaction zone and the reaction rate.

Let the height of the oxide layer be h, and the velocity of the gas stream, v. The carbon-monoxide concentration in the layer varies from $C_0 = 100\%$ on the lower surface, where it enters the layer, to a certain value C at the top surface of the layer.

The gas passes through a layer height dh in time dt.

On the assumption that the reaction is of the first order, the change of carbon-monoxide concentration in this layer in time dt may be represented as $\frac{dC}{dt} = -kC$, but $dh = vdt$, and hence $v\frac{dC}{dh} = -kC$.

Rearrangement and integration along the layer height between O and h gives the equation

$$2.3\log\frac{C_0}{C} = \frac{kh}{v},$$

where $C_0 = 100\%$; C is the CO content of the exit gas (%); K is a constant; h may be regarded as constant if its small decrease before the maximum content of carbon dioxide is reached is ignored.

If we replace the liner velocity v by the volume of the gas passing per unit time through the section S, and express this volume in terms of the ideal gas equation, then at pressure P = n we find the following expression, after simple mathematical transformations:

$$\left(2.3\log\frac{C_0}{C}\right)_{P=1} : \left(2.3\log\frac{C_0}{C}\right)_{P=n} = 1 : n.$$

It follows from this expression that the rate of reduction in the kinetic region should increase with increase of pressure.

To verify these conclusions and to determine the deviations of the rates of real processes of oxide reduction from those derived above, it is necessary to carry out investigations which cover both the kinetic and the diffusion regions of the process.

EXPERIMENTAL

Apparatus and method of investigation. Chemically pure copper oxide, calcined at 1000°, was used for the reduction. The oxide samples taken weighed 5.0g. In order that the kinetic region of the process could be reached more easily, the experiments were performed at 100°. Measures were taken to prevent formation of channels in the oxide layer, and to elinimate dead spaces in the reaction volume, which would distort the results of experiments at high pressures of the gas phase.

The reduction was performed in a reaction bomb, the volume of which was so designed as to exceed only slightly the volume of the material being reduced. The reaction bomb was heated in a liquid thermostat. Carbon monoxide was preheated to the experimental temperature before being introduced into the reaction zone.

The composition of the gas mixture formed was automatically recorded by means of Kurnakov's apparatus during the experiment.

The experimental results were obtained in the form of diagrams (Fig. 1) showing the carbon dioxide content at any instant during the process. The nature of the curves not only gives a qualitative indication of the influence of pressure and gas flow rate on the course of reduction, but makes it possible to evaluate the effects of these factors quantitatively.

The reduction rate, which is expressed in terms of the amount of carbon dioxide formed in one minute, is

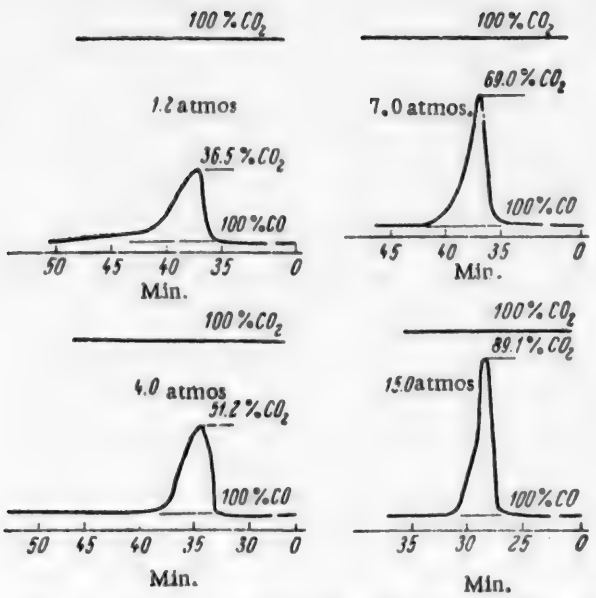

Fig. 1. Reduction of chemically pure copper oxide with carbon monoxide fed at 50.0 liters/hour.

calculated from the maximum contents of carbon dioxide observed in the reaction products during the reduction. This makes the values obtained under different conditions comparable.

Results of reduction under different pressures, and discussion. The experiments were performed at pressures of 1.2, 4.0, 7.0, and 15.0 atmos (absolute), with carbon monoxide rates from 5.0 to 50.0 liters/hour inclusive.

TABLE 1

CO rate (liters/hour)	Pressure (atmos)	Maximum CO_2 content (%)	Reduction rate (liters of CO_2/minute)	Length of induction period (minutes)	CO rate (liters/hour)	Pressure (atmos)	Maximum CO_2 content (%)	Reduction rate (liters of CO_2/minute)	Length of induction period (minutes)
10.0	1.20	81.3	0.135	27.5	30.0	7.00	88.4	0.442	31.3
10.0	4.00	91.1	0.152	18.4	30.0	15.00	91.8	0.458	26.5
10.0	7.00	91.5	0.153	16.5	40.0	1.20	46.3	0.309	30.1
10.0	15.00	94.4	0.157	11.8	40.0	4.00	59.1	0.395	20.3
20.0	1.20	75.6	0.252	35.5	40.0	7.00	83.2	0.555	26.8
20.0	4.00	80.6	0.268	28.5	40.0	15.00	91.2	0.608	26.6
20.0	7.00	82.1	0.274	27.0	50.0	1.20	36.5	0.305	36.9
20.0	15.00	91.2	0.304	18.0	50.0	4.00	51.2	0.427	32.5
30.0	1.20	56.6	0.282	29.0	50.0	7.00	69.0	0.575	36.4
30.0	4.00	73.6	0.368	25.6	50.0	15.00	89.1	0.742	27.0

The results calculated from the experimental curves are given in Table 1.

Effect of the carbon-monoxide rate. The effect of the carbon-monoxide rate on the reduction rate is plotted in Fig. 2.

This relationship between the reduction rate and the carbon-monoxide rate may be explained as follows. Until the limiting gas rate is reached, reduction occurs in the diffusion region. Here at low carbon-monoxide rates, when the reducing power of the carbon monoxide is utilized almost completely, the rate of the process is directly proportional to the gas rate. After the limiting gas velocity has been reached, reduction occurs either

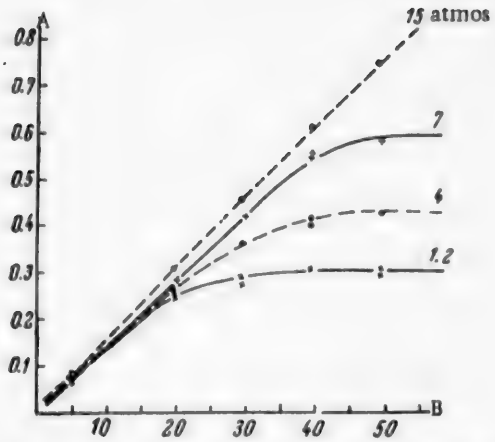

Fig. 2. Effect of carbon-monoxide rate on the reduction rate.

A) Reduction rate (liters of CO_2/ minute), B) CO rate (liters/ hour).

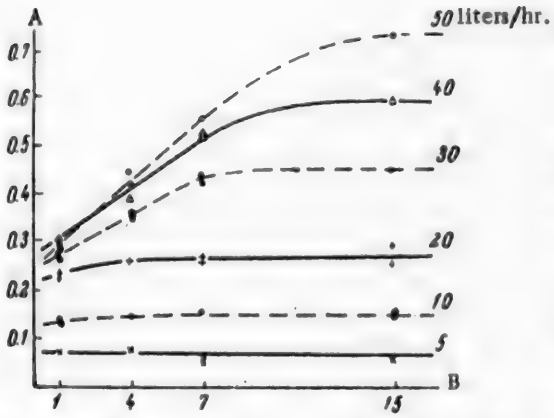

Fig. 3. Effect of carbon-monoxide pressure on the reduction rate.

A) Reduction rate (liters of CO_2/ minute), B) CO pressure (atmos).

in the internal-diffusion or in the kinetic region. In view of the state of subdivision of the oxide (200 mesh) it is to be expected that the influence of internal diffusion is insignificant, and the process takes place in the kinetic region. This is confirmed by the influence of the gas rate on the duration of the induction period.

Increase of pressure at the same volumetric flow rates lowers the linear gas velocity. Therefore, the higher the pressure, the higher are the volumetric flow rates at which the limiting velocities are reached.

Effect of pressure. The effects of pressure on the reduction rate are different under different reduction conditions. This is illustrated by the curves in Fig. 3.

It follows from the data given earlier that at a carbon-monoxide rate of 5.0 liters/ hour the carbon dioxide content of the gaseous reaction products is about 90% even under normal pressure. In view of such high utilization of the reducing power of carbon monoxide, increase of pressure cannot appreciably accelerate reduction. Increase of the carbon-monoxide rate lowers the carbon dioxide content in the gaseous reaction products under normal pressure, and the possibility of an acceleration of the reduction rate increases with increase of pressure.

If the compositions of the gaseous mixtures formed under different pressures are fairly far from the equilibrium values, the relationship between reduction rate and pressure is close to linear. Thus, at a rate of 50.0 liters/ hour a relationship of this type holds up to a pressure of 10.0 atmos.

The above experimental data show convincingly that the influence of pressure on the reduction rate is slight in the diffusion region. As the process is displaced into the kinetic region, the influence of pressure increases, and becomes greater as kinetic conditions become increasingly predominant.

A quantitative relationship between the pressure and the reduction rate was derived earlier in this paper.

The corresponding calculations for different carbon-monoxide rates are given in Table 2.

The differences between the values at different pressures increase rather rapidly with increase of the carbon-monoxide rate.

At 50.0 liters/ hour, they are in the following proportions:

$$\beta_{P=1.0} : \beta_{P=4.0} : \beta_{P=7.0} : \beta_{P=15.0} =$$
$$= 0.43 : 0.72 : 1.17 : 2.22 = 1.00 : 1.71 : 2.76 : 5.23.$$

TABLE 2

Calculated Data for the Effect of Pressure on Reduction Rate

CO rate (liters/ hour)	Values of $\beta = 2.3 \log \frac{C_0}{C}$ at pressure P (atmos)			
	1.2	4.0	7.0	15.0
10.0	1.96	2.42	2.42	2.98
20.0	1.41	1.64	1.72	2.43
30.0	0.84	1.33	2.15	2.50
40.0	0.62	0.89	1.78	2.43
50.0	0.43	0.72	1.17	2.22

TABLE 3

Calculated Values of β

CO rate (liters/ hour)	Values of $\beta = 2.3 \lg \frac{C_0}{C}$ at pressure P (atmos)			
	1.20	4.0	7.0	15.0
60.0	0.32	0.62	1.19	2.16
70.0	0.22	0.53	1.12	2.12
80.0	0.15	0.50	1.09	2.08

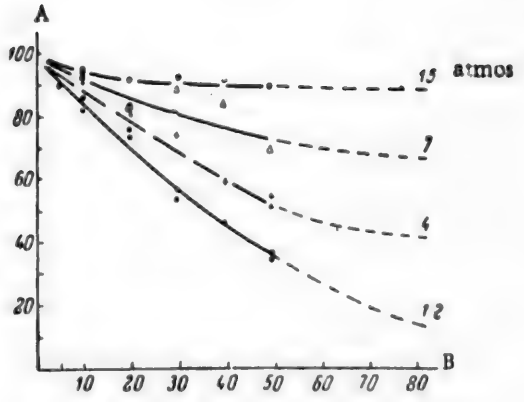

Fig. 4. Extrapolation of experimental data to higher carbon-monoxide rates.

A) CO_2 content of reaction products (%), B) CO rate (liters/hour).

However, this is rather far from the proportions 1 : 4 : 7 : 15.

With the variation of the maximum carbon dioxide content with the carbon-monoxide rate found in the 10.0-50.0 liter/hour range taken into account, it is possible to find approximately, by extrapolation, the carbon-monoxide rates at which agreement between the calculated and the experimental proportions is to be expected.

The corresponding experimental data and the extrapolated results are plotted in Fig. 4. Calculations based on these graphical data are presented in Table 3.

For a carbon monoxide rate of 80.0 liters/hour the data in Table 3 may presented in the following form:

$$\beta_{P=1.0} : \beta_{P=4.0} : \beta_{P=7.0} : \beta_{P=15.0} = 1.0 : 3.34 : 7.25 : 13.85.$$

This is very close to the proportions 1 : 4 : 7 : 15.

It follows that, under the real conditions under consideration, the true kinetics of the heterogeneous reduction process can be determined directly only at carbon monoxide rates above 80.0 liters/hour.

Influence of different factors in the induction period. It follows from the data in Table 1 that the length of

the induction period increases with the carbon monoxide rate, while at constant carbon monoxide rate it decreases with increase of pressure. Sometimes the induction period could be shortened by slight changes of the reduction conditions, or by means of a blow on the reaction bomb.

Increase of the carbon-monoxide rate above 50.0 liters/hour greatly lengthened the induction period. Thus, at a carbon-monoxide rate of 70-80 liters/hour the duration of the induction period increased 3 to 4-fold and more over the corresponding value at 50.0 liters/hour. After the start of reduction the process was slow, and generally died down, so that reduction could not be completed at these rates.

SUMMARY

1. In the region in which the process is governed by external diffusion, the reduction rate is directly proportional to the carbon monoxide rate. The range of gas rates in which this relationship holds widens with increase of pressure.

2. Pressure has no significant influence on the rate of heterogeneous reduction in the diffusion region. In the kinetic region, increase of pressure increases the reduction rate considerably.

3. The influence of pressure on the rate of heterogeneous reduction in the kinetic region increases with the gas velocity, i. e., with the predominance of the kinetic factor.

4. In the kinetic region, in conditions far from the equilibrium state, the relationship between heterogeneous-reduction rate and pressure is almost linear.

5. The results obtained are in good agreement with the conclusions drawn on theoretical grounds.

LITERATURE CITED

[1] S. T. Rostovtsev, Trans. Dnepropetrovsk Metallurgical Inst. 29 (1952).

[2] A. S. Tumarev and L. A. Paniushin, Proc. Conf. on the Physicochemical Principles of the Blast-Furnace Process (Metallurgy Press, 1956) [In Russian].

[3] A. N. Ramm and Iu. P. Svintsov, Trans. Leningrad Polytech. Inst. 179 (1955).

Received December 28, 1956.

SOLUBILITY IN THE SYSTEM CALCIUM CHLORIDE – POTASSIUM DICHROMATE – WATER

Z. I. Konopkina

Solubility studies of the system calcium chloride – potassium dichromate – water are not only of theoretical interest (as this system has not been studied previously), but are also of definite practical importance in relation to the use of aqueous salt solutions as cooling liquids of low melting points (antifreezes) in internal-combustion engines in aircraft, automobile transport, and refrigeration systems.

Aqueous calcium chloride solution has a cryohydric point at – 55°; it may be used as a coolant, but only if its strong corrosive action on metals is reduced. One method for reducing the corrosive action of a medium is the introduction of substances retarding corrosion, such as oxidizing agents – chromates or dichromates – into the solution [1].

The purpose of the present investigation was to study solubility in the reciprocal 4-component system consisting of calcium chloride, potassium dichromate, and water, $(CaCl_2 + K_2Cr_2O_7 \rightleftharpoons CaCr_2O_7 + 2KCl) - H_2O$, at various temperatures, in order to determine the nature of the changes taking place in the system and to establish the component ratios.

Of the binary and ternary systems constituting the 4-component system in question, the ternary system $CaCr_2O_7 - CaCl_2 - H_2O$ has not been studied as yet. Solubility in this system was also studied in this investigation.

EXPERIMENTAL

Chemically pure dichromates and chlorides of potassium and calcium were required for the experiments. Potassium dichromate was synthesized from chromic anhydride and calcium oxide [2]; the other salts were made by recrystallization of chemically pure reagents from the Main Administration of Chemical Reagents [3].

The solubilities of the components in the ternary and quaternary systems were determined by the isothermal method. The solution compositions were determined from the quantitative contents of the following ions: $Cr_2O_7^{=}$, Cl^{-}, Ca^{++} and K^{+} (the last was found by difference).

Changes in the solid phase were observed by examination of the external form of the crystals under the microscope.

The time required for equilibrium to be reached was found by means of consecutive analyses at definite time intervals until the composition of the solution became constant.

The ternary system $CaCr_2O_7 - CaCl_2 - H_2O$. Experiments were performed at 0, 25, and 50°. In order to obtain saturated calcium chloride solutions at 50°, it was necessary to dehydrate calcium chloride hexahydrate. In studies of the equilibrium it was found that, owing to the presence of calcium chloride in solution, a high concentration of Ca^{++} ions is established in the system $CaCr_2O_7 - CaCl_2 - H_2O$; as a result, even at 25° the equilibrium between dichromate and chromate ions ($Cr_2O_7^{=} + H_2O \rightleftharpoons 2H^{+} + 2CrO_4^{=}$) is shifted in the direction of the chromate ion, with formation of the sparingly soluble calcium chromate: $Ca^{++} + CrO_4^{=} \rightarrow CaCrO_4\downarrow$.

This effect is especially prominent with saturated solutions of calcium chloride containing any amounts of added calcium dichromate, and saturated solutions of calcium dichromate to which large amounts of calcium chloride are added; under these conditions the solubility product of calcium chromate is reached more rapidly and the total solubility of this salt decreases.

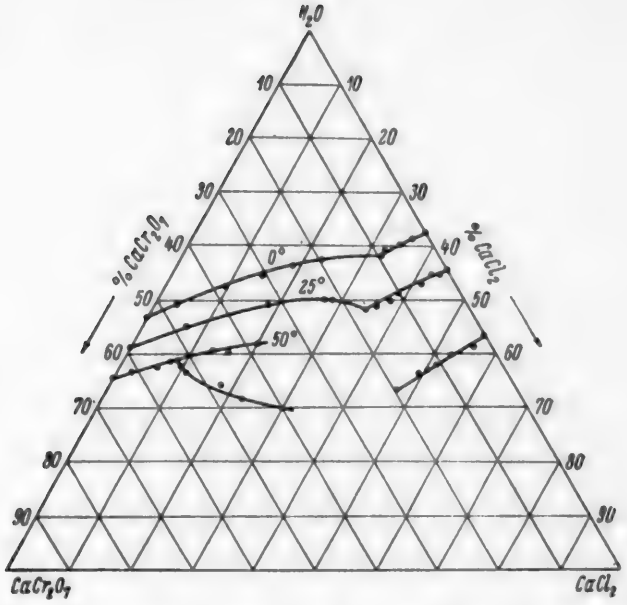

Fig. 1. Solubility isotherms for the system $CaCr_2O_7$–$CaCl_2$ – H_2O at 0, 25, and 50°.

TABLE 1

Solubilities of the Components in the System $CaCr_2O_7 - CaCl_2 - H_2O$ at 0°

Point No.	Solution composition, wt. %			Solution composition, molar %			Solid phase
	$CaCr_2O_7$	$CaCl_2$	H_2O	$CaCr_2O_7$	$CaCl_2$	H_2O	
1	53.47	—	46.53	7.47	—	92.53	$CaCr_2O_7 \cdot 6H_2O$
2	47.27	3.94	48.79	6.30	1.21	92.49	
3	37.69	10.10	52.21	4.69	2.90	92.41	
4	31.10	14.68	54.22	3.72	4.05	92.23	
5	24.87	19.05	56.08	2.87	5.07	92.06	
6	19.33	23.27	57.40	2.17	6.04	91.79	
7	9.63	32.65	57.72	1.06	8.31	90.63	$CaCr_2O_7 \cdot 6H_2O$ + $+ CaCl_2 \cdot 6H_2O$
8	9.41	32.45	58.14	1.03	8.22	90.75	$CaCl_2 \cdot 6H_2O$
9	8.45	32.71	58.84	0.92	8.19	90.89	
10	5.66	34.92	59.42	0.61	8.65	90.74	
11	2.62	36.22	61.16	0.27	8.74	90.99	
12	—	37.16	62.84	—	8.75	91.25	

Increase of the solution temperature also accelerates this process. Therefore, owing to experimental difficulties (thickening of the solutions due to the presence of $CaCrO_4$), the compositions of the solutions in equilibrium with solid phases at the eutonic•point at 50°, and at the points close to it in the solubility curve, were not determined. The precipitated calcium chromate is deposited in the solid phase, while part remains suspended in the solution; the solutions are turbid and difficult to settle out.

When samples of the solution are taken for analysis, $CaCrO_4$ must first be removed from it. This was done by filtration through a fine glass filter in an electrical thermostat by means of a pump. The precipitate separated from the solution was analyzed to confirm its composition. The analytical results corresponded to the formula of calcium chromate. Equilibrium became established in the system after 5 hours.

• Transliteration of Russian – Publisher's note.

TABLE 2

Solubilities of the Components in the System $CaCr_2O_7 - CaCl_2 - H_2O$ at 25°

Point No.	Solution composition wt. %			Solution composition molar %			Solid phase
	$CaCr_2O_7$	$CaCl_2$	H_2O	$CaCr_2O_7$	$CaCl_2$	H_2O	
1	59.00	—	41.00	9.19	—	90.81	$CaCr_2O_7 \cdot 5H_2O$
2	47.86	7.33	44.81	6.82	2.41	90.77	
3	32.47	18.77	48.76	4.22	5.63	90.15	
4	22.80	27.31	49.89	2.86	7.92	89.22	
5	21.64	28.36	50.00	2.71	8.20	89.09	
6	16.88	34.81	48.31	2.15	10.24	87.61	$CaCr_2O_7 \cdot 5H_2O +$ $+ (CaCrO_4)$
7	17.01	35.04	47.95	2.18	10.36	87.46	$CaCr_2O_7 \cdot 5H_2O +$ $+ CaCl_2 \cdot 6H_2O + (CaCrO_4)$
8	14.94	36.47	48.59	1.89	10.64	87.47	$CaCl_2 \cdot 6H_2O + (CaCrO_4)$
9	12.92	37.52	49.56	1.61	10.76	87.63	
10	12.33	38.43	49.24	1.54	11.06	87.40	
11	10.05	38.93	51.02	1.22	10.88	87.90	
12	5.87	41.82	52.31	0.69	11.40	87.91	
13	2.95	42.73	54.32	0.34	11.27	88.39	
14	1.77	43.93	54.30	0 20	11.58	88.22	
15	—	44.44	55.56	—	11.48	88.52	$CaCl_2 \cdot 6H_2O$

TABLE 3

Solubilities of the Components in the System $CaCr_2O_7 - CaCl_2 - H_2O$ at 50°

Point No.	Solution composition wt. %			Solution composition molar %			Solid phase
	$CaCr_2O_7$	$CaCl_2$	H_2O	$CaCr_2O_7$	$CaCl_2$	H_2O	
1	64.35	—	35.65	11.26	—	88.74	$CaCr_2O_7 \cdot 4H_2O$
2	61.02	2.63	36.35	10.45	1.04	88.51	
3	60.14	2.89	36.27	10.32	1.14	88.54	
4	56.25	6.16	37.59	9.29	2.35	88.36	
5	53.62	7.97	38.41	8.67	2.97	88.36	
6	52.57	8.84	38.59	8.45	3.28	88.27	
7	52.88	9.84	37.28	8.73	3.75	87.52	$CaCr_2O_7 \cdot 4H_2O + (CaCrO_4)$
8	52.53	9.95	37.52	8.62	3.77	87.61	$CaCr_2O_7 \cdot 4H_2O$
9	52.29	11.44	36.27	8.59	4.33	87.08	
10	47.39	18.39	34.22	8.22	7.36	84.42	
11	45.75	13.77	40.48	7.00	4.86	88.14	
12	45.52	22.77	31.71	8.29	9.56	82.15	$CaCr_2O_7 \cdot 4H_2O + (CaCrO_4)$
13	43.25	16.37	40.38	6.60	5.76	87.64	
14	39.80	30.65	29.55	7.50	13.32	79.18	
15	37.88	20.25	41.87	5.57	6.87	87.56	
16	19.79	47.29	32.92	3.31	18.27	78.42	$CaCl_2 \cdot 2H_2O + (CaCrO_4)$
17	14.32	49.55	36.13	2.23	17.79	79.98	
18	12.83	50.56	36.61	1.98	17.99	80.09	
19	11.08	51.24	37.68	1.66	17.77	80.57	
20	10.48	51.51	38.01	1.56	17.74	80.70	
21	7.30	52.95	39.75	1.05	17.58	81.37	
22	2.95	55.89	41.16	0.41	17.97	81.62	
23	0.31	56.80	42.89	0.04	17.67	82.29	
24	0.16	56.44	43.40	0.02	17.41	82.57	
25	—	56.88	43.12	—	17.62	82.38	$CaCl_2 \cdot 2H_2O$

TABLE 4

Solubilities of the Components in the System $CaCl_2 - K_2Cr_2O_7 - H_2O$ at 0°

Point No.	Solution composition, wt. %					Solution composition, in molar % per 100 moles of salts				Moles of H_2O per 100 moles of salts	Solid phase
	$K_2^{\cdot\cdot}$	$Ca^{\cdot\cdot}$	$Cr_2O_7^{''}$	$Cl_2^{''}$	H_2O	$K_2^{\cdot\cdot}$	$Ca^{\cdot\cdot}$	$Cr_2O_7^{''}$	$Cl_2^{''}$		
1	1.07	13.30	—	24.50	61.13	4.00	96.00	—	100	983	$CaCl_2 \cdot 6H_2O + KCl$
2	1.03	13.23	0.006	24.34	61.40	3.83	96.17	0.01	99.99	994	
3	1.10	13.32	0.96	24.25	60.37	4.06	95.94	1.28	98.72	968	$CaCl_2 \cdot 6H_2O + KCl + K_2Cr_2O_7 + (CaCrO_4)$
4	11.56	—	0.28	10.39	77.77	100	—	0.90	99.10	2923	$K_2Cr_2O_7 + KCl$
5	9.03	2.01	0.24	11.67	77.05	69.70	30.30	0.70	99.30	2583	
6	3.68	7.33	0.65	16.09	72.75	20.44	79.56	1.31	98.69	1757	$K_2Cr_2O_7 + KCl + (CaCrO_4)$
7	2.17	10.41	0.56	20.20	66.66	9.60	90.40	0.9	99.10	1288	
8	1.33	12.79	0.71	23.61	61.56	5.00	95.00	1.00	99.00	1017	
9	0.65	8.07	45.30	—	45.98	4.00	96.00	100	—	1218	$K_2Cr_2O_7 + CaCr_2O_7 \cdot 6H_2O$
10	0.71	8.74	38.26	3.55	48.74	4.00	96.00	78.00	22.00	1192	
11	0.63	9.56	30.65	7.42	51.74	3.25	96.75	57.60	42.40	1166	
12	0.46	11.34	16.60	15.03	56.57	2.00	98.00	26.60	73.40	1089	
13	0.61	12.86	8.84	20.40	57.29	2.40	97.60	12.50	87.50	969	
14	0.65	12.94	8.52	20.69	57.20	2.50	97.50	11.90	88.10	960	
15	0.80	12.90	8.79	20.67	56.84	3.10	96.90	12.25	87.75	951	$K_2Cr_2O_7 + CaCr_2O_7 \cdot 6H_2O + CaCl_2 \cdot 6H_2O + (CaCrO_4)$
16	—	13.30	8.12	20.86	57.72	—	100	11.33	88.67	967	$CaCr_2O_7 \cdot 6H_2O + CaCl_2 \cdot 6H_2O$
17	0.23	13.03	7.86	20.69	58.19	0.91	99.09	11.09	89.02	985	
18	0.90	13.15	1.38	23.63	60.94	3.40	96.60	1.90	98.10	997	$CaCl_2 \cdot 6H_2O + K_2Cr_2O_7$
19	0.71	13.22	1.95	23.45	60.67	2.90	97.10	2.70	97.30	992	
20	0.53	13.14	4.62	22.21	59.50	2.00	98.00	6.39	93.60	988	$CaCl_2 \cdot 6H_2O + K_2Cr_2O_7 + (CaCrO_4)$
21	0.46	12.94	7.72	20.78	58.10	1.80	98.20	10.87	89.13	982	

TABLE 5

Solubilities of the Components in the System $CaCl_2 - K_2Cr_2O_7 - H_2O$ at 25°

Point No.	Solution composition, wt. % $K_2^{\cdot\cdot}$	$Ca^{\cdot\cdot}$	$Cr_2O_7^{''}$	$Cl_2^{''}$	H_2O	Solution composition, in molar % per 100 moles of salts $K_2^{\cdot\cdot}$	$Ca^{\cdot\cdot}$	$Cr_2O_7^{''}$	$Cl_2^{''}$	Moles of H_2O per 100 moles of salts	Solid phase
1	1.61	16.28	—	30.26	51.85	5.00	95.00	—	100	674.8	$CaCl_2 \cdot 6H_2O + KCl$
2	2.26	15.23	3.91	27.71	50.89	7.00	93.00	4.43	95.57	691.5	$CaCl_2 \cdot 6H_2O + KCl + (CaCrO_4)$
3	2.48	15.36	4.47	27.95	49.74	7.60	92.40	5.00	95.00	666.0	$CaCl_2 \cdot 6H_2O + KCl + K_2Cr_2O_7 + (CaCrO_4)$
4	14.08	—	0.89	12.48	72.55	100	—	2.30	97.70	2238	$K_2Cr_2O_7 + KCl$
5	9.89	2.98	0.82	13.97	72.34	62.96	37.04	1.89	98.11	2002	
6	5.67	6.64	0.84	16.62	70.23	30.40	69.60	1.63	98.37	1217	$K_2Cr_2O_7 + KCl + (CaCrO_4)$
7	3.46	16.56	3.81	31.19	44.98	9.68	90.32	3.90	96.10	546	
8	0.99	8.84	50.37	—	39.80	5.40	94.60	100	—	948	$K_2Cr_2O_7 + CaCr_2O_7 \cdot 5H_2O$
9	1.00	9.63	42.85	3.88	42.64	5.05	94.95	78.40	21.60	936	
10	1.03	11.67	29.25	11.98	46.07	4.32	95.68	44.50	55.50	841	
11	1.08	12.77	22.60	16.16	47.39	4.20	95.80	31.50	68.50	792	$K_2Cr_2O_7 + CaCr_2O_7 \cdot 5H_2O + (CaCrO_4)$
12	—	15.31	14.35	22.39	47.95	—	100	17.38	82.62	697	$CaCr_2O_7 \cdot 5H_2O + CaCl_2 \cdot 6H_2O + (CaCrO_4)$
13	1.79	15.03	12.20	23.66	47.32	5.00	95.00	15.00	85.00	668	$CaCr_2O_7 \cdot 5H_2O + CaCl_2 \cdot 6H_2O + K_2Cr_2O_7 + (CaCrO_4)$

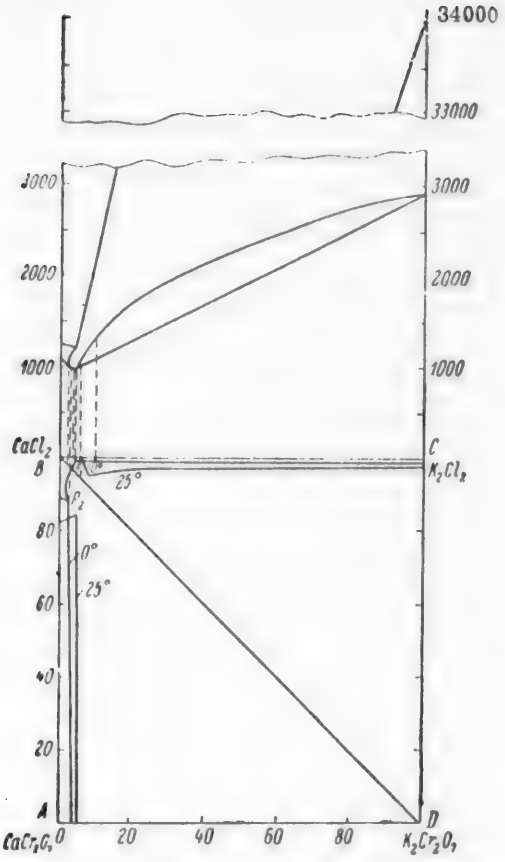

Fig. 2. Solubility diagram of the 4-component system $CaCl_2 - K_2Cr_2O_7 - H_2O$ at 0° and 25°.

The results of the investigation are presented in Tables 1, 2, and 3 and in Fig. 1. The solubility data are average values from several analytical determinations.

Examination of the solubility isotherms at 0, 25, and 50° shows that despite the precipitation of the hydrolysis product of the dichromate ion – solid calcium chromate – at 25 and 50°, the curves are of the same general character for all three temperatures. The break in the solubility isotherm at 50° at the points of highest Ca^{++} concentration in the solution is due to the fact that it is impossible to attain equilibrium between the solutions and the main solid phases: $CaCr_2O_7 \cdot 4H_2O$ and $CaCl_2 \cdot 2H_2O$. The branch of the isotherm for saturated solutions of calcium dichromate is forked, probably owing to the formation of metastable solutions in equilibrium with metastable calcium chromate.

The shape of the solubility curves shows the reciprocal influence of the salts on their solubilities. Thus, the solubility of calcium dichromate greatly decreases in presence of calcium chloride, and the solubility of calcium chloride is changed little by additions of calcium dichromate.

The solid phases for the univariant branches of the isotherms are individual salts, and for the eutonic points, mixtures of these salts. Observations of the solid phases under the microscope showed that they consist of hydrated crystals of the salts, the compositions of which were determined earlier by ourselves and others, namely: for calcium dichromate at 0° $CaCr_2O_7 \cdot 6H_2O$, at 25° $CaCr_2O_7 \cdot 5H_2O$ and at 50° $CaCr_2O_7 \cdot 4H_2O$ [2, 4], for calcium chloride at 0 and 25° $CaCl_2 \cdot 6H_2O$ (hexahydrate) and at 50° $CaCl_2 \cdot 2H_2O$ [5] (crystalline dihydrate).

The quaternary reciprocal system $CaCl_2 - K_2Cr_2O_7 - H_2O$. In the aqueous quaternary reciprocal double-decomposition system $CaCl_2 + K_2Cr_2O_7 \rightleftharpoons CaCr_2O_7 + 2KCl$ the reciprocal salt pairs are $CaCl_2 + K_2Cr_2O_7$ and $CaCr_2O_7 + KCl$. The solubilities of these salts were studied only at 0° and partially at 25°. Determinations were not carried out at 50° because of the sharp displacement of the equilibrium between dichromate and chromate ions in the direction of chromate, with formation of the sparingly soluble calcium chromate, which turned the solution into a pasty mixture. The same effect hindered studies of the solubilities of the components of the system at 25°.

The Jänecke method [6] was used for graphical representation of the 4-component system; in this method, the contents of the salt anions are taken along one side of the base of the diagram (square), and the cation contents are taken along the other. The numbers of moles of water dissolving a definite number (1 or 100) moles of the salt mass are taken along perpendiculars to the corresponding points in the square.

Studies of the triple points of the quaternary system were based on saturated solutions of the eutonic points of the ternary systems in equilibrium with the corresponding solid phases, to which increasing amounts of the third salt were added until it was found in the precipitate. Equilibrium was confirmed by agreement between results obtained in determinations from two binary points. In this way it was possible to determine intermediate points corresponding to univariant solutions of the quaternary system.

To determine points on the solubility curve for the stable reciprocal salt pair, saturated solutions of the salts with excess of solid phases were used, adding different amounts of one of the 2nd reciprocal pair's salts.

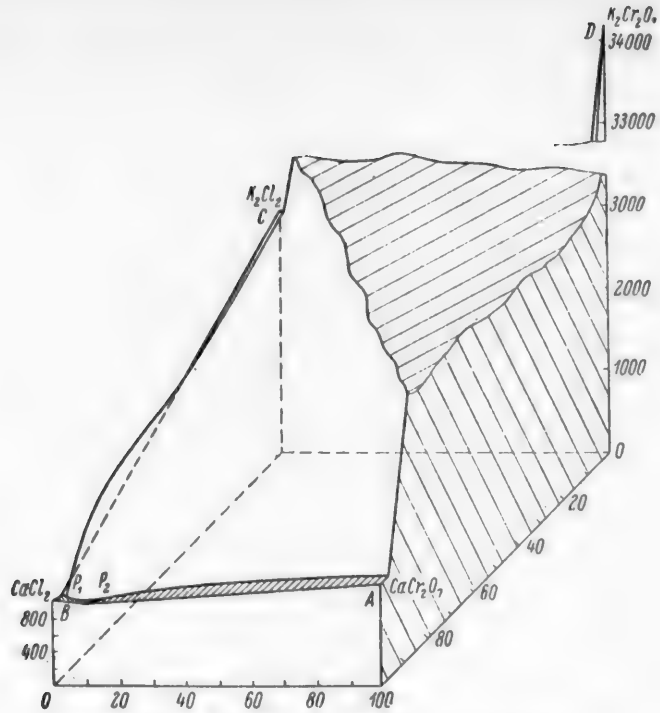

Fig. 3. Space solubility diagram for the 4-component system $CaCl_2 - K_2Cr_2O_7 - H_2O$ at 0°.

The solution compositions were expressed in molar percentages of gram ions per 100 moles of salts, and in numbers of moles of water per 100 moles of salt mixtures.

For observations of changes in the solid phase, the external appearance and form of the crystals were viewed under the microscope.

Data on the solubilities of the salts in the system are presented in Tables 4 and 5 and Figs. 2 and 3.

Fig. 2 shows the horizontal and vertical projections of the isotherm for the system at 0°, and an incomplete horizontal projection of the isotherm at 25°. The horizontal projection gives the ionic composition of the salt mass in the saturated solutions; the side AB shows the contents of the salt anions, and AD, of cations. The corners of the square correspond to the pure salts: A to the salt $CaCr_2O_7$, B to $CaCl_2$, C to K_2Cl_2, and D to $K_2Cr_2O_7$. The formula of potassium chloride is doubled to correspond to the other salts in the system. The sides of the square represent ternary systems: AB represents the system $CaCr_2O_7 - CaCl_2 - H_2O$, BC, the system $CaCl_2 - KCl - H_2O$, CD, the system $K_2Cr_2O_7 - KCl - H_2O$ and AD, the system $CaCr_2O_7 - K_2Cr_2O_7 - H_2O$. The points within the square represent the quaternary system. P_1 and P_2 are triple points of the system: 1) $CaCl_2 - KCl - K_2Cr_2O_7$ and 2) $CaCr_2O_7 - K_2Cr_2O_7 - CaCl_2$. The vertical projection shows the water content in moles per 100 moles of salt mass for the univariant and invariant points of the system at 0°.

Fig. 3 is a space model of the solubility isotherm for the system $CaCl_2 - K_2Cr_2O_7 - H_2O$ at 0°.

Examination of the experimental results shows that no new solid phases were found in the given 4-component system: the diagram contains four crystallization fields for the salts: $CaCr_2O_7$, $K_2Cr_2O_7$, $CaCl_2$ and KCl. The largest crystallization field, both at 0° and at 25°, is that of potassium dichromate, which occupies about 95% of the whole diagram area. The stable salt pair in double decomposition in this 4-component system is the pair $CaCl_2 + K_2Cr_2O_7$.

The curve P_1P_2 represents the conditions of coexistence of quaternary solutions with these two solid phases; it is cut by the diagonal BD. This shows that the solutions of the triple points P_1 and P_2 are congruently saturated with salts of the stable pair and one of the salts of the unstable pair.

The potassium dichromate content of saturated calcium chloride solution along the curve P_1P_2 lies within a narrow range — from 1.7 to 2.5 wt. % at 0°.

In additional experiments on the influence of the amount of added potassium dichromate on the freezing point of calcium chloride solution it was found that addition of 2.5% of $K_2Cr_2O_7$ to a 28% $CaCl_2$ solution raises the freezing point of the latter from $-49°$ to $-20°$.

SUMMARY

1. Studies of salt solubilities in the ternary system $CaCr_2O_7 - CaCl_2 - H_2O$ and the quaternary system $CaCl_2 - K_2Cr_2O_7 - H_2O$ showed that the components of these systems do not interact, and do not form double salts or solid solutions.

2. The presence of a large amount of Ca^{++} ions in the solutions of these systems results in a sharp shift of equilibrium between dichromate and chromate ions in the chromate direction, with formation of sparingly soluble calcium chromate.

3. Solubility studies of the quaternary system showed that addition of $K_2Cr_2O_7$ as inhibitor to $CaCl_2$, within the permissible concentration limits, would not ensure adequate protection of metals against corrosion and would have an adverse effect on the low-freezing properties of the solution.

4. The relative extents of the crystallization fields of the salts in the system make the double decomposition reaction, $CaCl_2 + K_2Cr_2O_7 \rightleftharpoons CaCr_2O_7 + 2KCl$, unsuitable as a method for production of calcium dichromate.

LITERATURE CITED

[1] I. L. Rozenfel'd, Corrosion Inhibitors in Neutral Media (1953). [In Russian]

[2] D. N. Tarasenkov and Z. I. Konopkina, J. Appl. Chem. 27, 2, 198 (1954).*

[3] Iu. V. Kariakin, Pure Chemical Reagents (1947). [In Russian]

[4] Z. I. Konopkina, J. Appl. Chem. 29, 1, 22 (1956).*

[5] G. I. Druzhinin and A. I. Shepelev, Proc. Acad. Sci. USSR 4, 703 (1950).

[6] V. A. Anosov and S. Ia. Pogodin, Fundamentals of Physicochemical Analysis (1947). [In Russian]

Received February 4, 1957.

*Original Russian pagination. See C. B. Translation.

STUDY OF THE STRUCTURE AND SORPTIONAL PROPERTIES OF CHARCOALS OXIDIZED BY HYDROGEN PEROXIDE

I. A. Kuzin, T. G. Plachenov, and V. P. Taushkanov

When charcoal is activated by means of gaseous activating agents, oxides are formed on its surface; these may be alkaline or acidic, according to the treatment conditions. In aqueous solutions, these oxides may undergo hydration with formation of surface compounds which dissociate and split off hydrogen or hydroxyl ions.

The literature contains no information on the secondary structure or sorptional properties of charcoals oxidized at low temperatures. However, studies of such properties would extend our knowledge of the nature of charcoal surfaces and would assist in investigations of the possible production of ion-exchange sorbents with a rigid structure, more stable toward acids and alkalies than the known ion-exchange sorbents.

The purpose of the present investigation was to determine the possibility of increasing the ion-exchange groups on the surface of activated charcoal by low-temperature oxidation.

EXPERIMENTAL

Oxidized charcoals were prepared by the treatment of "BAU" activated birchwood charcoal, 0.5-1.0 mm fraction, with 30% hydrogen peroxide solution. The degree of oxidation was varied by increase or decrease of the hydrogen peroxide – carbon ratio. The oxidation was carried out in a beaker, into which hydrogen peroxide was carefully added, and the mixture was then heated to the boiling point of the solution. After the oxidation the charcoal was washed with distilled water and dried at 105° to constant weight.

The charcoal structure was studied by the sorption method [1] and the mercury-penetration method [2]. The surface area of the different types of pores was calculated from the porosity diagrams determined by the mercury method. In calculations of the volume of the micropores and intermediate pores, a correction was introduced for the volume of the adsorption film in macropores and intermediate pores [3].

The results of studies of the structure of oxidized charcoals by the sorption method are given in Table 1, while the results obtained by the mercury-penetration method are plotted in Figs. 1 and 2.

The porosity diagrams were used for calculations of the pore surfaces and volumes V (Table 2).

The tabulated data show that extensive structural changes take place in the charcoal during oxidation.

It follows from the data in Table 1 that the total pore volume increases as the result of an increase in the volume of the macropores and intermediate pores, which amounts to 0.196 cc/cc for charcoal D. This is accompanied by a decrease of the micropore volume from 0.120 to 0.033 cc/cc.

Table 2 shows that an increase of pore volume by 0.283 cc/g in the effective-radius (r) range of $3.7 \cdot 10^{-6}$–$-6 \cdot 10^{-4}$ cm is accompanied by a decrease of the surface by 0.71 m^2/g, whereas an increase of pore volume by 0.167 cc/g in the effective-radius range of $4.7 \cdot 10^{-7}-3.7 \cdot 10^{-6}$ cm leads to an increase of the surface by 47.17 m^2/g. It also follows from the same table and Fig. 1 that (except in the case of sample B) the volumes of the macropores and intermediate pores increase regularly with increasing oxidation of the charcoal, in the pore-radius range studied.

Fig. 2 shows variations of pore-volume distribution by effective radius during oxidation of the charcoals. The maximum in the macropore distribution is shifted from an average effective radius of $8.7 \cdot 10^{-5}$ to $1.5 \cdot 10^{-4}$ cm^3/cm

TABLE 1

Structural Characteristics of Oxidized Charcoals

Charcoal	Amount of 30% H_2O_2 (ml) used per 20 g of "BAU" charcoal	Density (g/cc)		Volume					Charcoal yield (%)
		true, d	apparent S	W_S, maximum volume of the sorption space (cc/g)	V_ε, total (cc/cc)	V_{ma}, of macropores (cc/cc)	V_i, of intermediate pores (cc/cc)	V_{mi}, of micropores (cc/cc)	
1	—	1.860	0.54	0.386	0.707	0.499	0.088	0.120	100
A	500	1.855	0.46	0.384	0.754	0.586	0.057	0.110	97.5
B	1000	1.865	0.45	0.377	0.756	0.588	0.068	0.101	94.0
C	1750	1.910	0.42	0.406	0.780	0.605	0.095	0.075	77.3
D	3000	1.850	0.34	0.426	0.816	0.671	0.112	0.033	52.1

TABLE 2

Structural Characteristics of Oxidized Charcoals*

Charcoal	Amount of 30% H_2O_2 (ml) used per 20 g of charcoal	Charcoal surface (m^2/g)			Pore volume (cc/g)		
		S	S_1	S_2	V	V_1	V_2
1	—	—	2.60	—	—	0.688	—
A	500	17.96	2.20	15.76	0.788	0.718	0.070
B	1000	12.29	1.44	10.85	0.701	0.644	0.057
C	1750	26.56	1.62	24.96	0.973	0.882	0.091
D	3000	64.82	1.89	62.93	1.208	0.971	0.237

* In Table 2 the symbols S, S_1, and S_2 denote the surfaces and V, V_1, and V_2 the volumes of the pores in the effective-radius ranges of $4.7 \cdot 10^{-7}$–$6 \cdot 10^{-4}$cm, $3.7 \cdot 10^{-6}$–$6 \cdot 10^{-4}$cm, $4.7 \cdot 10^{-7}$–$3.7\ 10^{-6}$cm.

as the result of oxidation, and there is a total increase of volume of the pores in the effective-radius range of $3.7 \cdot 10^{-6}$–$6 \cdot 10^{-4}$ cm, and intermediate pores in the range of $3.7 \cdot 10^{-6}$–$4.7 \cdot 10^{-7}$ cm.

The ion-exchange and sorptional properties of the charcoals change with variations of the nature of their surface and structure

Investigation of the sorptional properties of charcoals. The sorptional properties of the oxidized charcoals were studied in relation to water vapor and to Ba^{2+}, Na^{+}, and Cl^{-} ions. The experiments on the sorption of water vapor were performed at $t = 17.5 \pm 0.5°$ over sulfuric acid solutions of different concentrations.

Data on the sorption of water vapor are presented in Table 3.

It follows from Table 3 that with increasing oxidation of "BAU" charcoal by hydrogen peroxide the sorption of water vapor increases, from 18.5 millimoles/g for charcoal 1, to 25.70 millimoles/g for charcoal D at $P/P_0 = 0.9770$.

The maximum volume of the sorption space W_S increases for oxidized charcoal D over the value for charcoal 1 by 0.040 cc/g, because of the increase in the volume of the intermediate pores, while the volume of sorbed water increases by 0.140 cc/g. This increase in the sorption of water vapor, as compared with the sorption of benzene vapor, is the result of oxidation of the charcoal surface. The oxygen compounds on the charcoal surface, having polar properties, may act as centers of water-vapor sorption. Benzene is a nonpolar compound, and its sorption is not significantly influenced by the presence of oxygen compounds on the charcoal surface [4].

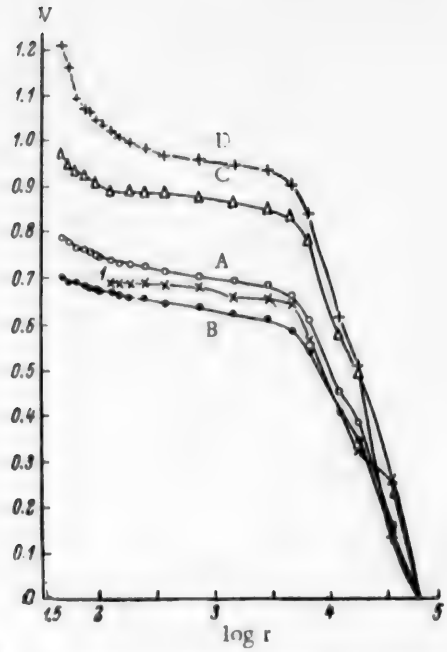

Fig. 1. Integral structural curves for charcoals oxidized by hydrogen peroxide.
Amount of 30% hydrogen peroxide (ml) used for oxidation of BAU charcoal: 1) 0, A) 500, B) 1000, C) 1750, D) 3000.

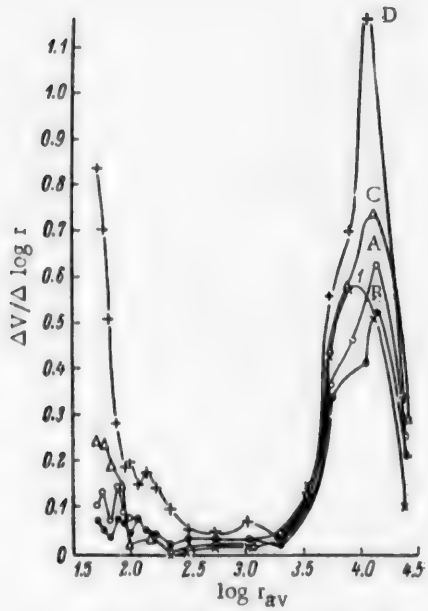

Fig. 2. Differential volume-distribution curves for macropores and intermediate pores in charcoals oxidized by hydrogen peroxide.
Curve designations as in Fig. 1.

TABLE 3

Sorption of Water Vapor by Charcoals Oxidized by Hydrogen Peroxide (t = 17.5 ± 0.5°)

$\frac{P}{P_0}$	Sorption of water vapor (millimoles/g)				
	1	A	B	C	D
0.0053	0.19	0.14	0.20	0.27	0.36
0.0435	0.22	0.17	0.22	0.34	0.40
0.1630	0.86	1.16	1.97	3.22	4.09
0.3570	4.00	4.96	6.20	7.50	8.75
0.5700	8.85	9.80	11.00	12.45	13.80
0.8370	15.15	16.20	17.75	20.90	21.60
0.9770	18.05	17.95	19.40	22.70	25.70

The sorptional properties of the charcoals with respect to Na^+ and Cl^- ions were studied by Nikol'skii's method [5]. Titration data were used to determine the effect of pH on the sorption of Na^+ and Cl^- ions, and the sorption of barium ions was also studied.

The results of these investigations are given in Table 4 and Fig. 3, which show the effects of pH on the sorption capacity of the charcoals for sodium and chloride ions. Fig. 3 indicates the changes in the ion-exchange properties of "BAU" charcoal in the course of oxidation. Titrations of NaCl solutions with different content of HCl and NaOH in presence of "BAU" charcoal showed the presence of oxides of an alkaline nature on the surface of the latter. The amount of alkaline groups decreases, and that of acidic groups increases with increasing oxidation; this is confirmed by the sorption of cations and anions.

TABLE 4

Capacity of Charcoals Oxidized by Hydrogen Peroxide

Charcoal	Amount of 30% H_2O_2 (ml) used per 20 g of "BAU" charcoal	Sorption capacity (meq/g) at pH = 4			pH = 7	
		Ba^{2+}	Na^+	Cl^-	Na^+	Cl^-
1	—	0.073	—	0.600	—	0.280
A	500	0.160	—	0.501	—	0.040
B	1000	0.265	—	0.320	0.120	—
C	1750	0.975	0.240	—	0.805	—
D	3000	1.235	0.402	—	1.060	—

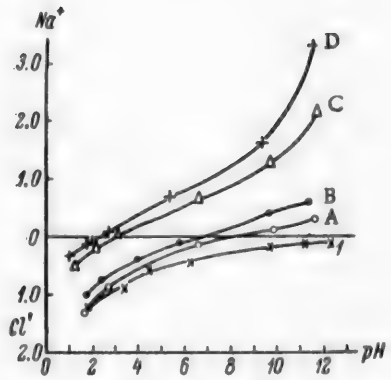

Fig. 3. Effects of pH on the sorption capacity of charcoals oxidized by hydrogen peroxide, with respect to sodium and chloride ions. Na^+, Cl^- – amounts of ions sorbed (meq/g).

The degree of dissociation of the acid and alkaline groups respectively differs at different pH; for example, in an acid medium mainly the alkaline groups dissociate, whereas at high pH the acid groups dissociate. In the region of intermediate pH values dissociation of both types of ion-exchange groups is possible, and therefore a case is possible in which no hydrolytic adsorption occurs. This is found at the points of intersection of the curves with the straight line corresponding to "zero" sorption of ions (Fig. 3).

It follows from the data in Table 4 that the oxidized charcoals adsorb barium ions in preference to sodium ions. These differences in the sorbability of ions differing in valence are specific for sorbents containing weakly-dissociating groups of the – COOH and –OH types [6].

As was shown in Table 1, oxidation of the charcoal is accompanied by a decrease of the micropore volume from 0.120 to 0.033 cc/cc, which corresponds to a 3-fold decrease of the specific surface of the micropores, while the surface of charcoal D increased 3.6-fold as compared with charcoal A in the effective-radius range of $4.7 \cdot 10^{-7}$–$6 \cdot 10^{-4}$ cm. The sorption capacity of oxidized charcoal D with respect to barium ions increased over that of the original "BAU" charcoal at pH=4 from 0.073 to 1.235 meq/g. These results lead to the conclusion that the ion-exchange groups are carried mainly on the surfaces of the intermediate pores.

SUMMARY

1. Oxidation of "BAU" charcoal results in extensive structural changes due to increase of the pore volume. Oxidation of this charcoal by hydrogen peroxide increases the volume of the macropores and intermediate pores and decreases the micropore volume; the specific surface of the macropores decreases, and that of the intermediate pores increases.

2. The sorption capacity of charcoals depends on the degree of oxidation and the extent of the oxidized surface of the intermediate pores and macro pores.

3. Charcoal samples were prepared with a sorption capacity of 1.2 meq/g for barium ions at pH=4.

LITERATURE CITED

[1] M. M. Dubinin, Jubilee Volume on the 30th Anniversary of the Great October Socialist Revolution, 1 (1947). [In Russian]

[2] T. G. Plachenov, J. Appl. Chem. 28, 3, 245 (1955). *

[3] M. M. Dubinin, Progr. Chem. 24, 3 (1955).

[4] M. M. Dubinin, Progr. Chem 24, 513 (1955).

[5] B. P. Nikol'skii and V. I. Paramonova, Progr. Chem. 8, 1535 (1939).

[6] E. A. Materova and V. I. Paramonova, Theory and Practice of the Use of Ion-Exchange Materials (Izd. AN SSSR, 1955), 8. [In Russian]

Received June 13, 1957.

* Original Russian pagination. See C. B. Translation.

ABSORPTION OF SO_2 AND CS_2 BY CERTAIN HYDROCARBONS OF THE DIPHENYLMETHANE SERIES

N. I. Gel'perin, I. G. Matveev, and K. V. Vil'shau

The removal of acid gases from dilute mixtures is a very important problem in a number of regions of our country and in some branches of industry. In some cases the removal of acid gases is necessary on grounds of industrial hygiene (decontamination of the atmosphere), and in others on economic grounds (utilization of certain gases). In particular, sulfur dioxide and carbon disulfide present in the waste gases from a number of chemical industries are valuable chemical materials, but often make the atmosphere highly toxic not only at the plants but at considerable distances beyond their limits.

Despite its great importance, the problem of extraction of acid gases from industrial exit gases is still very far from being solved. None of the methods proposed so far for the extraction of acid gases is free from important defects which restrict their fields of application to various extents. The main reason why the problem is so difficult to solve is that it is necessary to treat very large volumes of dilute gaseous mixtures, which, moreover, contain chemically-aggressive components. Further difficulties in the solution of the problem are introduced by the very rigorous economic requirements with regard to low capital and operational costs of industrial units for the extraction of acid gases.

The very extensive literature on extraction of acid gases shows that research in this field has been mainly concerned with the chemical binding of SO_2. The question of SO_2 removal by absorption methods remained almost untouched, both with regard to searches for suitable absorbents, and in relation to the process kinetics. However, it is evident that if absorbents of low vapor pressure, available in practice, and chemically inert toward SO_2 were used, absorption of SO_2 from dilute gaseous mixtures might be very advantageous in some cases. It was shown by I. G. Matveev as long ago as 1951 that certain hydrocarbons of the diphenylmethane series can act as absorbents of this type. The present paper deals with studies of the possible use of these substances as absorbents for SO_2 and CS_2.

The substances mainly studied were two hydrocarbons of the diphenylmethane series – ditolylmethane and and dicumylmethane. For comparison, a diisopropylbenzene fraction from a cracking plant was used as a third absorbent. Ditolylmethane and dicumylmethane were in the form of mixtures of the corresponding o-, m-, and p-isomers; constant composition of these mixtures is ensured by the method used for their synthesis. This fact is confirmed by the identity of the Raman spectra of a number of ditolylmethane samples made in different plants from different raw materials.

Studies of the absorption capacity of these hydrocarbons were preceded by determinations of certain physicochemical constants needed for calculations relating to the design of the absorption units.

Variations of the densities of ditolylmethane (DTM), dicumylmethane (DCM), and diisopropylbenzene (DIPB) with temperature are given below:

Temperature (in °C)	20	35	50	65	80	95	120
Density (g/cc)							
DTM	0.9825	0.9710	0.9600	0.9490	0.9382	0.9274	0.9098
DCM	0.9475	—	0.9288	0.9190	—	0.8993	—
DIPB	0.8628	—	—	0.8275	—	—	—

The viscosities of the absorbents in the 20-150° temperature range are given below:

Temperature (in °C)	20	35	50	65	80	95	150
Viscosity (centipoises)							
DTM	5.27	3.66	2.59	1.90	1.39	1.017	0.636
DCM	8.70	4.05	2.65	1.90	1.32	0.989	—
DIPB	1.443	1.082	0.834	0.646	0.508	0.411	—

Experimental determinations showed that the heat capacities of the absorbents can be calculated with sufficient accuracy from Kurbatov's formula [1]

$$C = \frac{a + bt}{M} \text{ (kcal/kg °C)}, \quad (1)$$

where t is the temperature of the liquid absorbent (in °C), M is the molecular weight of the absorbent, and a and b are constants the values of which are given below:

	a	b
DTM	70.05	0.1337
DCM	83.65	0.1337
DIPB	65.30	0.1722

The vapor pressures of the absorbents in the 30-128.5° range, measured by the method of vapor efflux from small orifices are given below:

Temperature (in °C)	30	50	90	108.5	128.5
Vapor pressure (mm Hg)					
DTM	0.00581	0.01700	0.26875	0.93200	2.49000
DCM	—	0.00275	0.04090	0.08500	0.41800

The boiling points (t_b), solidification points (t_s), flash points (t_f), and surface tension (σ) of DTM and DCM are given below:

	t_b at one atmos (in °C)	t_s (in °C)	t_f (in °C)	at 21° (dynes/cm)
DTM	292 - 293	−32 - −36	142	38.2
DCM	335 - 336	−22 - −24	160	34.4

The solubility of sulfur dioxide in DTM, DCM, and DIPB was determined gravimetrically, by saturation of a weighed sample of absorbent, kept in a thermostat, to constant weight at a definite temperature and a definite SO_2 concentration in the gas phase. The results obtained by the gravimetric method were in good agreement (within 1-2%) with the results obtained by titration of the solutions with 0.1 N KOH solution with the use of phenolphthalein indicator.

Data on the solubility of concentrated (100%) SO_2 in these absorbents at standard pressure and temperatures in the 3-140° range are presented in Table 1.

Data on the solubility of SO_2 in the absorbents, with different SO_2 concentrations in mixtures with air, and at different temperatures, are given in Table 2.

The data of Tables 1 and 2 are represented by the group of curves in Fig. 1 where the abscissas represent the temperature, and the ordinates, the solubility of SO_2 in the absorbents. The different curves correspond to different concentrations of SO_2 in the air mixtures, and to different absorbents. The top right-hand corner of Fig. 1 shows separate curves for the solubility of SO_2 in the absorbents, from a gas mixture containing 1.7 vol. % of SO_2.

Fig. 1 shows that DTM has the highest and DIPB the lowest absorption capacity for SO_2. The absorption capacities of all the absorbents depend on the temperature; the effect of temperature is especially pronounced below 20°, and increases with increase of SO_2 content in the gas mixture.

The most likely operating temperature under practical conditions is 25°. The relationships between the solubility of SO_2 in the absorbents and the SO_2 content of the gas mixture (in the 0-100% range) at 25° are plotted in Fig. 2. Fig. 2 also contains separate solubility curves for 20°, with 0-14% of SO_2 in the gas mixture.

The curves in Fig. 2 show that the absorption capacities of all the absorbents greatly depend on the SO_2 content of the gas mixture.

The solubility of carbon disulfide in DTM, DCM, and DIPB from gas mixtures containing different concentrations of it was determined iodometrically, the dissolved CS_2 being first converted into potassium xanthate. Carbon disulfide was absorbed from mixtures with nitrogen, the maximum concentration of the former being 1.04% at 20°. The results of the determinations are given in Table 3.

TABLE 1

Solubility of Concentrated (100%) SO_2 in the Absorbents

Absorbents	Solubility (g SO_2/100 g of absorbent) at temperature (in °)														
	3	4.5	9	17.5	25	34.5	42	54.5	60	65	70	75	89.5	130	140
DTM . .	—	59	45	19.9	14.5	10.8	9.17	5.92	5.19	3.96	3.79	3.27	2.06	1.65	0.95
DCM . .	35.2	29.2	21.5	13.3	10.8	8.25	7.58	3.87	—	3.54	—	2.62	1.65	—	—
DIPB . .	—	26.5	—	—	10.7	—	7.5	—	—	—	—	—	—	—	—

TABLE 2

Solubility of SO_2 (x—g SO_2/100 g of absorbent) as a Function of its Concentration (y—vol. %) in Mixtures with Air

$y = 57.75$			$y = 21$			$y = 7.08$			$y = 1.7$		
	x			x			x			x	
t° C	DTM	DCM	t° C	DTM	DCM	t° C	DTM	DCM	t° C	DTM	DCM
3	21.9	14.9	3.5	9.68	6.95	8.5	2.95	2.17	20.3	0.385	0.321
14.5	14.2	10.8	14.8	5.69	4.74	14.5	1.92	1.55	25	0.32	0.26
25.8	9.14	6.62	25	3.8	3.11	26	1.34	1.058	35	0.180	0.119
35.6	6.46	4.77	35.6	3.02	2.21	36	0.932	0.721	—	—	—
49	4.22	3.18	49.6	1.97	1.46	43.8	0.716	0.589	—	—	—
74	2.32	1.80	74.6	0.94	0.70	56.3	0.516	0.393	—	—	—
—	—	—	—	—	—	66	0.408	0.328	—	—	—
—	—	—	—	—	—	75.2	0.354	0.275	—	—	—

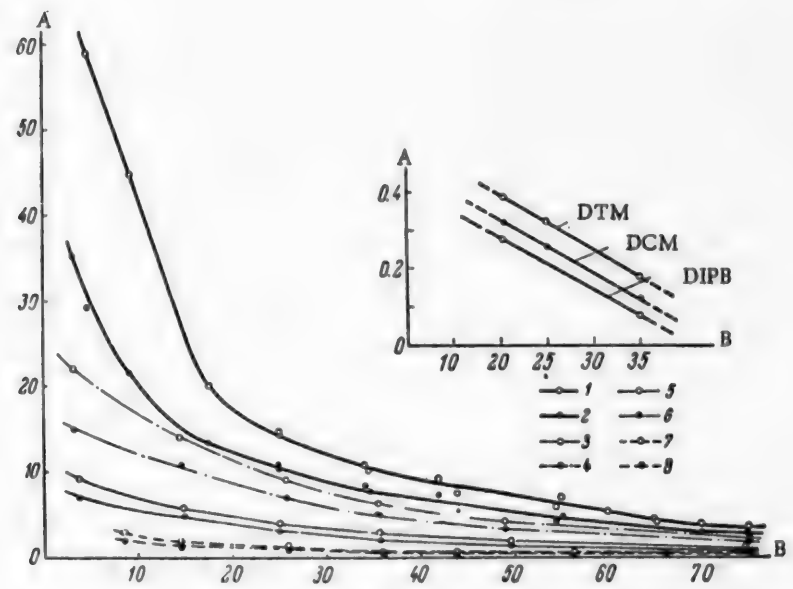

Fig. 1. Solubility of SO_2 in DTM, DCM, and DIPB at different temperatures. A) Solubility of SO_2 (g/100 g of solvent), B) temperature (in °). Absorbent: 1, 3, 5, 7 — DTM; 2, 4, 6, 8 — DCM. SO_2 concentration (vol. %): 1, 2 — 100; 3, 4 — 57.75; 5, 6 — 21.0; 7, 8 — 7.08. The upper graph shows the solubility curves of SO_2 with 1.7 vol. % of SO_2 in the gas phase.

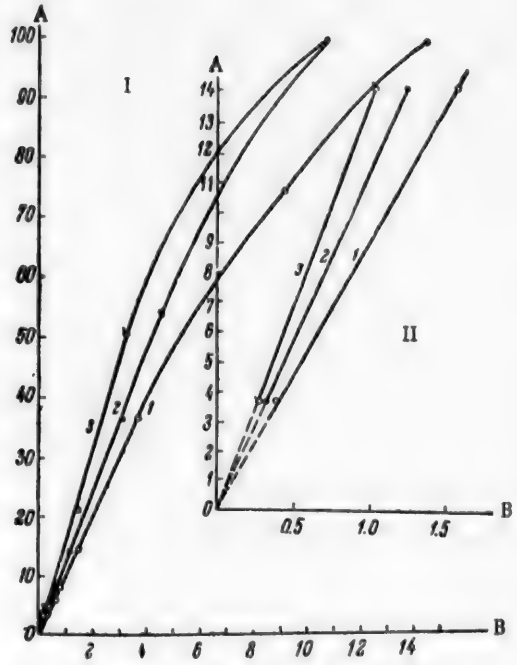

Fig. 2. Effects of SO_2 concentration in the gas mixture on the solubility of SO_2 in DTM, DCM, and DIPB at 25° (I) and 20° (II).
A) SO_2 content of gas (wt. %), B) solubility of SO_2. Absorbent: 1) DTM, 2) DCM, 3) DIPB.

TABLE 3

Solubility of Carbon Disulfide, from Gas Mixtures of Different Concentrations, in DTM, DCM, and DIPB (g CS_2/100 g of absorbent) at 20°

Absorbent	Solubility of CS_2/100g of absorbent) at concentration (wt. %)			
	0.115	0.440	0.625	1.040
DTM	0.0435	0.181	0.265	0.650
DCM	—	0.164	0.249	0.569
DIPB	0.0330	—	0.224	0.460

The effects of temperature on the solubility of carbon disulfide (in g CS_2/100 g of absorbent), with 1.04 wt. % CS_2 in the gas mixture, are given in Table 4.

The data in Tables 3 and 4 show that DTM has the highest absorption capacity for CS_2. The solubility of CS_2 in all three absorbents increases at a greater rate than the concentration of CS_2 in the gas mixture.

Finally, the solubility of CS_2 in all three absorbents falls with increase of temperature, especially at temperatures below 45-50°.

For comparison, we determined the solubility of carbon disulfide in solar and transformer oils from a gas mixture containing 0.5% CS_2 by weight at 20°. It was found that the solubility of CS_2 in solar oil is 12% lower, and in transformer oil 38% lower, than in ditolylmethane.

TABLE 4

Effect of Temperature on the Solubility of CS_2 in DTM, and DIPB, with 1.04% wt. % of CS_2 in The Gas Mixture

Absorbent	Solubility of CS_2 (g/100 g of solvent) at temperature (in °)					
	20	40	80	100	120	150
DTM	0.650	0.161	—	0.135	0.125	0.037
DCM	0.565	0.153	0.107	—	0.096	0.037
DIPB	0.46	—	0.08	—	—	—

The coefficients of absorption of SO_2 and CS_2 in these absorbents were determined with the aid of countercurrent packed columns of the same active height (2.5 m) but of different internal diameters (35, 44, 52.5, and 69 mm). Each column consisted of three sections, at the lower ends of which supporting grids were fixed, with open sections equal to 60% of the column cross-section. The packing consisted of Raschig rings, d_{int} (internal diameter) = 2.71 mm, d_{ext} (external diameter) = 4.61 mm, height 4.46 mm; $9275 \cdot 10^3$ rings per 1 m^3, specific surface of packing 1154 m^2/m^3, free volume 0.62 m^3/m^3.

The diluted gas mixtures were fed into the column through a flow meter. Sulfur dioxide was obtained from a cylinder, measured by means of a flow meter, and was mixed with air in a special mixer.

For reasons of safety, carbon disulfide was mixed with nitrogen and was metered by the method described by Rapoport [2].

The absorbents entered the absorption column through a metering valve from a header tank which was kept at constant level in each series of experiments. The flow rate of the absorbent was measured with the aid of a measuring vessel at the column exit. For determination of the SO_2 concentration before and after the column, the gas mixture was passed through an absorption flask containing 50 ml of 0.1 N caustic potash and a few drops of phenolphthalein. The required SO_2 content was calculated from the time (τ) required for decolorization of the solution in the absorption flask, and from the gas rate ($\underline{a}$ liters per hour). The KOH solution is decolorized when the hydroxide has been converted into sulfite. Completeness of absorption of SO_2 was confirmed by the absence of an acid reaction to Congo Red in the gases leaving the absorption flask. For determination of the CS_2 concentration before and after the column, the gas mixture was passed at a definite rate through flasks filled with 20% alcoholic alkali solution. The CS_2 content was determined by iodometric titration of the xanthate formed.

In the studies of absorption kinetics, 328 experiments were performed in these absorption columns; 187 with sulfur dioxide and 141 with carbon disulfide. In these experiments the linear velocity of the gas mixture in the open sections of the absorption columns was varied in the range of 0.0127-0.098 m/second, the linear velocity of the absorbent in the range of 0.027-2.19 mm/second, the SO_2 concentration of the original gas mixture in the range of 0.05-19.1 wt. %, and the CS_2 concentration, in the range of 0.05-0.75%.

The theoretical analysis of the experimental data was based on the mass-transfer equation

$$M = K \cdot \Delta_x \cdot F, \qquad (2)$$

where M is the amount of substance absorbed (kg), K is the coefficient of mass transfer (absorption), Δ_x is the average driving force of mass transfer (kg/kg), and F is the phase-contact area (m^2).

The valves of M were calculated from the experimental data with the aid of the material-balance equation

$$M = W(x_2 - x_1) = D(y_1 - y_2).$$

where W is the absorbent rate (kg/hour), x_1 and x_2 are the initial and final concentrations of the absorbed substance in the liquid phase (kg/kg of absorbent), D is the flow rate of the inert gas (kg/hour), y_1 and y_2 are the initial and final concentrations of the absorbed substance in the gas phase (kg/kg of inert gas).

Since the main resistance to mass transfer is in this instance concentrated in the liquid phase (because of the relatively low solubilities of SO_2 and CS_2 in the absorbents used), it follows that

$$\Delta_s = \frac{(x_{1e} - x_2) - (x_{2e} - x_1)}{\ln \frac{x_{1e} - x_2}{x_{2e} - x_1}},$$

where x_{1e} and x_{2e} are the concentrations of the absorbed substance in the liquid phase, in equilibrium with the concentrations of these substances in the initial and final gas mixtures.

Use of the logarithmic mean difference of the concentrations is justified in this instance by the fact that the systems in question conform fairly accurately to Henry's law in the ranges of SO_2 and CS_2 concentrations studied.

The phase-contact area was taken to be equal to the total surface of the packing rings, and Equation (2) was then used to calculate the values of the mass-transfer coefficient K for all the experiments. As is known, the π-theorem gives the relationship, for mass-transfer processes in absorption, between the mass-transfer coefficient, the Reynolds number (Re), the Prandtl diffusion number (Pr'), and the dimensional geometrical parameter ($\frac{H}{D_c}$), where H is the active height of the column and D_c is its diameter. The implicit form of this functional relationship is given by the equation

$$Nu' = f\left(Re_L,\ Re_G,\ Pr'_L,\ \frac{H}{D_c}\right), \tag{3}$$

where $Nu' = K \cdot D_c / D \cdot \gamma_L$ is the Nusselt diffusion number, $Re_L = W_L \cdot D_c \cdot \gamma_L / g \cdot \mu_L$ and $Re_G = W_G \cdot D_c \cdot \gamma_L / g \cdot \mu_G$ Reynolds numbers for the liquid and gas phases, $Pr'_L = \mu_L \cdot g / \gamma_L \cdot D$ is the Prandtl diffusion number for the liquid

γ_L, γ_G are the denities of the liquid and gas (kg/m³),

μ_L, μ_G are the viscosities of the liquid and gas phases (centipoises), W_L, W_G are the linear liquid and gas velocities in the open section of the column (m/second), and g = 9.81 m/second².

Equation (3) does not contain the Prandtl diffusion number for the gas phase, as this is virtually constant. The reason for the choice of the column diameter as the determining geometrical dimension is that all the experiments were performed with columns containing the same type of packing but of different diameters.

Analysis of the experimental data also showed that the mass-transfer coefficient depends not only on the above-named parameters, but also on the concentration ranges of the absorbed substances. The following functional relationship is satisfactorily applicable:

$$Nu' = f_1\left(Re_L,\ Re_G,\ Pr'_L,\ S,\ \frac{H}{D_c}\right),$$

where $S = \int_{x}^{x_e} \frac{dx}{x_e - x}$ is the number of transfer units.

The values of γ_L and μ_L determined experimentally for all the absorbents studied are given above. The liquid-phase diffusion coefficients were calculated from the formula [3]:

$$D = \frac{0.00278}{\sqrt{\mu_L}\left(V_A^{1/3} + V_B^{1/3}\right)^2} \sqrt{\frac{1}{M_A} + \frac{1}{M_B}}\ \text{m}^2/\text{hour} \tag{4}$$

where μ_L is the viscosity of the absorbent (in centipoises), V_A, V_B – are the molecular volumes of the absorbed

substance and absorbent, and M_A, M_B – are the molecular weights of the absorbed substance and absorbent.

The calculated diffusion coefficients (D) and Prandtl numbers (Pr'_L) for the six systems studied at 20° are given below:

System	$D \cdot 10^6$ (m^2/hour)	Pr'_L
DTM – sulfur dioxide	1.940	8950
DCM – sulfur dioxide	1.017	27300
DIPB – sulfur dioxide	3.760	1601
DTM – carbon disulfide	1.610	10790
DCM – carbon disulfide	1.225	32800
DIPB – carbon disulfide	3.120	1932

Finally, it should be noted that the experiments on the absorption of sulfur dioxide were carried out in the range Re_L = 1.004–52 and Re_G = 40.2–312, and the experiments on the absorption of carbon disulfide, in the range Re_L = 0.284–43.2 and Re_G = 62.4–268.

The relationships between the Nusselt number and each of the determining criteria were established consecutively, and the results were used to plot the generalized graph in Fig. 3.

Fig. 3 shows that in the selected coordinate system all the experimental points fit satisfactorily around a straight line represented by the equation:

$$Nu' = 245 \cdot 10^{-7} \cdot Re_L \cdot Re_G^{0.15} S \cdot Pr'_L \cdot \left(\frac{H}{D_C}\right)^{0.5}. \qquad (5)$$

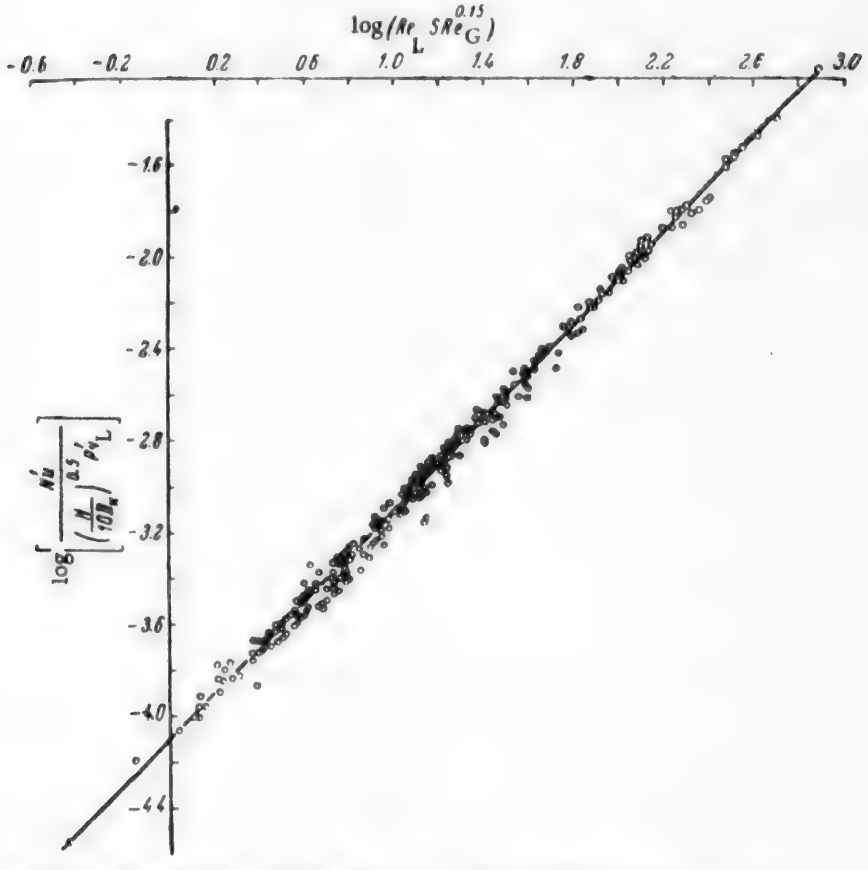

Fig. 3. The function $Nu' = f_1(Re_L, Re_G, Pr'_L, S, H/D_C)$.
The points correspond to different systems and different column diameters.

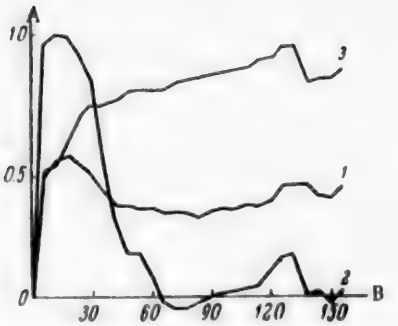

Fig. 4. Results of corrosion tests on seamless steel plates in conditions of SO_2 absorption.
A) Weight increase (% of original weight), B) time (hours). Plates: 1) Immersed in DTM, 2) half-immersed in DTM, 3) above DTM.

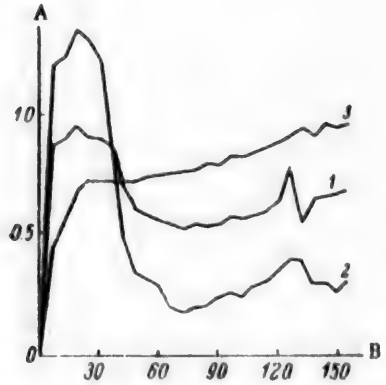

Fig. 5. Results of corrosion tests on welded steel plates in conditions of SO_2 absorption. Designations as in Fig. 4.

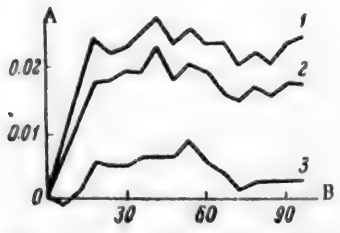

Fig. 6. Results of corrosion tests on seamless steel plates in conditions of SO_2 desorption. Designations as in Fig. 4.

Equation (5) can evidently be used for determinations of mass-transfer coefficients of the systems in question, for the packing of the dimensions used. For conversion to other packing dimensions, the appropriate relationships published in the literature may be used.

For investigation of the chemical resistance of the equipment in absorption and desorption of sulfur dioxide by these absorbents, corrosion tests were carried out on polished plates made from St-3 steel. In experiments on the absorption of SO_2 by ditolylmethane two plates were tested (with and without a welding seam), and in the experiments on SO_2 desorption, only a seamless plate was used. The tests were performed in glass cylinders, a gas – air mixture containing 1% SO_2 (by volume) being bubbled through a layer of ditolylmethane. Before the air was mixed with SO_2 it was passed through a layer of water 75-100 mm high, heated to 30°, to saturate it with water vapor. Three plates were suspended from glass hooks in each cylinder; one was completely immersed in DTM, the second was half-immersed, while the third was above the liquid surface (in the gas phase). Before the tests the plates were degreased, dried in a vacuum dessicator and weighed on an analytical balance.

The total exposure time of the plates in the cylinders was 156 hours, check weighings being carried out every 6 hours (after removal of the corrosion products, washing, and drying).

The corrosion tests under desorption conditions differed by the fact that the DTM temperature was maintained at 80°, and 100% SO_2 saturated with water vapor was bubbled through it. The total exposure time of the test plates in the cylinders in the desorption experiments was 96 hours.

The results of tests on seamless plates in absorption conditions are represented by the three curves in Fig. 4, where change of weight (% of the original) is plotted against time (hours). Curve 1 refers to the immersed plate, Curve 2 to the half-immersed plate, and Curve 3, to the plate in the gas phase.

It follows from these graphs that after 156 hours the steel plates kept under conditions of absorption of SO_2 by DTM increased and not decreased in weight. This weight increase was caused by the formation of an extremely strong protective film, difficult to scrape off with a knife blade. Only one of the six specimens (Fig. 4), tested under absorption conditions, showed a weight loss of 0.05% after 72 hours, and this loss was completely balanced by the weight increase at the end

of the test. Incidentally, this weight loss corresponded to a corrosion rate of 0.0562 mm/year. Fig. 3 shows that the test results for the welded plates are almost the same as for the seamless plates. Steel plates tested under desorption conditions showed some gain in weight after 96 hours, owing to the formation of a strong protective film (similar to that on the plates tested under absorption conditions).

The results of these corrosion tests show that St-3 steel is chemically resistant in DTM in which sulfur dioxide is being absorbed or desorbed.

LITERATURE CITED

[1] V. Ia. Kurbatov, J. Gen. Chem. 17, 18, 1999 (1947); 22, 7, 1139 (1950). *

[2] F. M. Rapoport, Zav. Labs. 5, 560 (1950).

[3] L. Andrussow, Z. Elektroch. 54, 566 (1950); 55, 51 (1951).

Received February 22, 1957.

* Original Russian pagination. See C. B. Translation.

KINETICS OF THE ABSORPTION OF WATER VAPOR BY SULFURIC ACID UNDER TURBULENT (FOAM) CONDITIONS

M. E. Pozin and E. Ia. Tarat

(The Lensoviet Technological Institute, Leningrad)

Absorption of water vapor by sulfuric acid, widely used in industry in gas drying [1], is usually effected in 2-3 packed towers connected in series. Among the disadvantages of this method of gas drying are the large size of the equipment (packed towers), the need for pumping and cooling equipment, criculation of large amounts of acid, etc.

It was therefore of interest to study the rate and degree of absorption of water vapor by sulfuric acid under effective foam conditions [2-4].

The available literature data on the kinetics of absorption of water vapor by sulfuric acid relate mainly to the use of packed towers. It has been shown [5-7] that the coefficient of absorption (and desorption) of H_2O is proportional to $w_G^{0.8}$ (w_G is the virtual linear gas velocity in the scrubber). Moreover, it was found that the liquor rate has no appreciable influence on the absorption coefficient. This shows that the principal diffusional resistance in the absorption of water vapor is in the gas phase; in such cases the use of high-turbulence foam conditions is especially effective. Certain data [8] indicate that the air-drying efficiency increases with intensification of foaming which occurs under ordinary bubbling conditions.

EXPERIMENTAL

The laboratory unit used for studies of air drying in foam apparatus is shown schematically in Fig. 1.

Air was heated in the coil 1 by the gas burner 2, and passed into a humidifier 3, which was an auxiliary single-tray foam apparatus. Water, heated to 40-50° in the flask 4 by means of the heater 5, was fed continuously to the humidifier grid. The water supply to the humidifier was regulated by means of the tube 6 so that air completely saturated with moisture at 30 ± 0.5° entered the working model of the foam apparatus (drier) 7. The air humidity was determined from the readings of the dry and wet-bulb thermometers 8, installed at the gas entry and exit of the foam apparatus 7. The gas pipe from the humidifier 3 and the lower part of the drier were insulated. The dried air was sucked out by means of a fan through the spray traps 9 and 10. The air rate was regulated by means of the stopcock 11, according to the readings of the differential manometer at the diaphragm 12. The rarefaction at the entry to the drier was measured by means of the manometer 13, and the total hydraulic resistance of the apparatus tray (grid with foam), by means of the differential manometer 11. The active liquid (92-93% sulfuric acid) at a temperature of 15-20° (measured by the thermometer 15) entered the drier 7 from the constant-level header 16 through the flow meter 17 and the regulating valve 18. The acid overflowed from the overflow section of the drier body into the receiver 19, while part of it, which flowed through the grid openings under certain operating conditions, flowed into the vessel 20.

For determination of the gas humidity after drying, the gas was drawn through two U tubes 21 containing phosphorus pentoxide, and through the gas meter 22. The duration and rate of gas sampling were so regulated that the water vapor was absorbed completely, the amount being 0.5-1.0 g. This ensured adequate accuracy in determinations of the moisture content.

The foam apparatus (drier) was a glass model, with an overflow device for removal of liquid. The model consisted of two columns with a grid clamped between them by means of flanges. The column above the grid was equipped with an overflow chamber for removal of the foamed acid from the apparatus; this was 100 mm

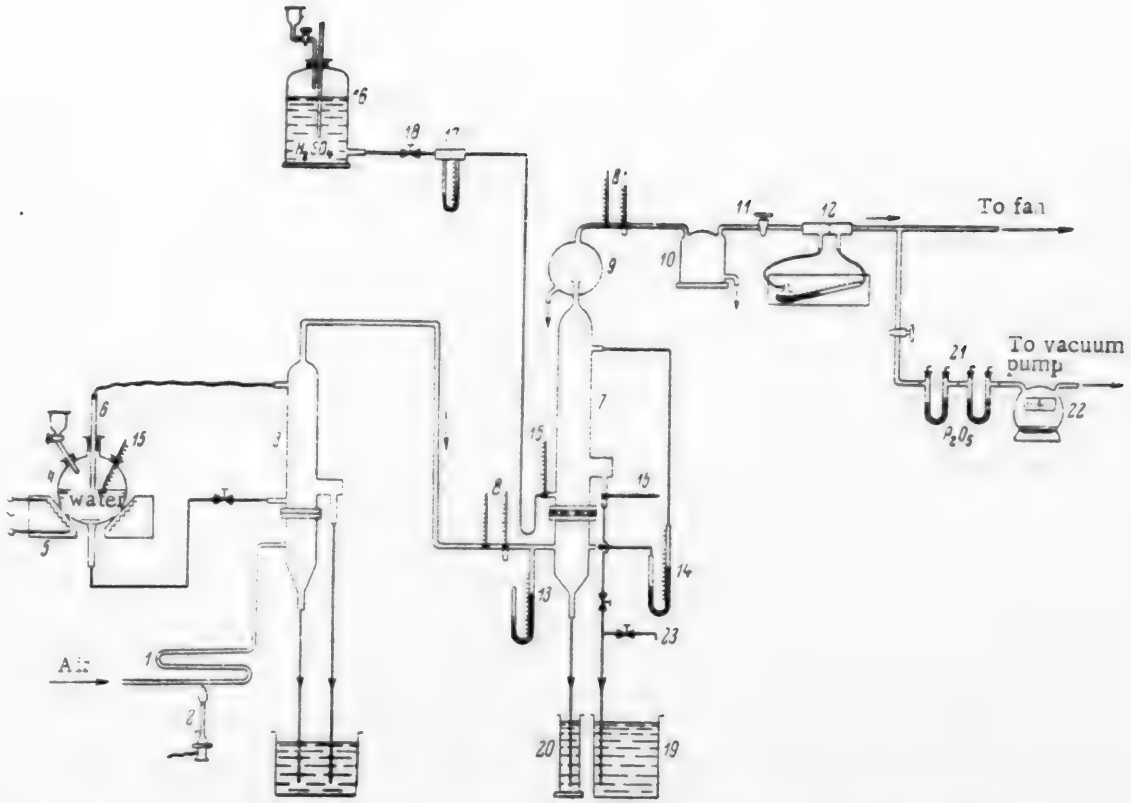

Fig. 1. Laboratory unit for absorption of water vapor by sulfuric acid in a foam apparatus. Explained in text.

above grid level, so that the weir height in this model, h_w, was 100. The overflow chamber was of rectangular section, 20 mm wide; thus, a liquid feed rate of 20 liters/hour corresponds to a rate $i = 1\ m^3/m \cdot hour$ [2]. The cross-sectional area of the model and grid was 10 cm^2 (d = 36 mm). A grid of the 5/2 type with openings 2 mm in diameter and 5 mm apart (open section $S_0 = 17\%$) was used in all the experiments.

A definite air rate in the upper portion of the drier, and a definite acid rate, were established in the experiments. After a stable hydrodynamic regime, which was then strictly maintained, had been reached, the humidity of the air at the drier exit was determined for 5-10 minutes, and the instrument readings were taken.

The results given below for each set of conditions are average values from several determinations.

The coefficient of absorption of water vapor by sulfuric acid was calculated from the formula

$$K = \frac{G}{S \cdot \Delta C}, \quad \frac{kg}{m^2 \cdot hr \cdot kg/kg}, \tag{1}$$

where G is the amount of moisture absorbed (kg/hour); S is the grid area (m^2); ΔC is the driving force of absorption (kg/kg); the latter was calculated from the formula

$$\Delta C = \frac{y_i + y_f}{2} - y_e, \tag{2}$$

where y_i and y_f are the concentrations of water vapor in the gas before and after drying (in kg/kg of dry gas), y_e is the equilibrium concentration of water vapor over the sulfuric acid at its average temperature and concentration on the grid (in kg/kg).

The efficiency of a single-tray drier was calculated from the formula

$$\eta = \frac{y_i - y_f}{y_i - y_e} \cdot 100\%. \tag{3}$$

All the other measurements were performed as described earlier [2].

It follows from the data in Table 1 that the coefficients of absorption of water vapor by sulfuric acid in the foam apparatus reach 12,000-15,000 $kg/m^2 \cdot hour \cdot kg/kg$, or, calculated for 1 m^3 of apparatus volume (for a height of 0.5 m of reaction space above the grid), 24,000-30,000 $kg/m^3 \cdot hour \cdot kg/kg$. By means of Amelin's equation [7] it can be shown that the absorption coefficient of water vapor in a packed tower has an average value of 0.01 $kg/m^2 \cdot hour \cdot mm\ Hg$, or 650 $kg/m^3 \cdot hour \cdot kg/kg$. Comparison of these values shows that the process is much more rapid and intensive under turbulent foam conditions than in packed towers.

The very high drying efficiencies are also noteworthy – over 80% of the water vapor is absorbed on one tray of the foam apparatus, and under optimum conditions, over 90%. This shows that, despite the short time of phase contact, the system approaches fairly closely to the equilibrium state under turbulent conditions.

It follows from the graphs for K as a function of the gas velocity w_G in the full section of the apparatus, shown in Fig. 2, that, as in the systems studied earlier [2, 3, 9, 10], the mass-transfer coefficient increases sharply with the gas velocity because of the increase of foam height and greater turbulence of the system. For the system in question, K is directly proportional to w_G (it may be remembered that for packed columns the power of w_G is less than 1).

Fig. 3 shows graphs for drying efficiency η as a function of the gas velocity w_G. The values of η fall somewhat with increase of w_G, despite the accompanying increase of foam height, probably because decrease of the phase-contact time has the predominant influence. However, it is clear from Fig. 3 that the decrease of η is not large, being only about 3% when the gas velocity is increased from 0.75 to 2.5 m/second. Thus, the influence of gas velocity on tray efficiency is not, in this instance, significant in selection of the appropriate gas velocity in the apparatus.

Increase of w_G results in increase of the hydraulic resistance of the apparatus as well as of its operating rate. Therefore the most rational gas velocities are in the range of $w_G = 1.5$-2.5 m/second, as at these velocities the performance is the most economic, the efficiency of the apparatus remains at approximately the same level,

TABLE 1

Conditions and Results of Experiments in the Drying of Air by Sulfuric Acid (93% H_2SO_4)

Air velocity in apparatus w_G (m/sec)	Acid rate i (m^3/m · hour)	Acid temperature (in °) at		Hydraulic resistance ΔP (mm H_2O)	Foam Height H (mm)	H_2O content of gas (wt. %) at		Tray efficiency η (%)	Absorption coefficient K (kg/m^2 · hour · kg/kg)
		entry	exit			entry	exit		
0.75	0.5	16.7	30	103	150	2.73	0.42	84.6	4400
0.75	1.0	16.8	28	110	160	2.79	0.28	90.2	4900
0.75	2.0	16.7	24	118	170	2.67	0.25	91.0	5000
1.0	0.5	16.2	34	100	160	2.91	0.44	85.0	5900
1.0	1.0	16.3	30	110	170	2.79	0.34	88.2	6420
1.0	2.0	16.3	25	118	180	2.79	0.32	88.9	6500
1.5	0.5	17.5	41	100	170	2.79	0.45	84.0	8700
1.5	1.0	15.7	36	105	180	2.64	0.34	86.9	9190
1.5	2.0	15.8	29	115	200	2.79	0.34	88.2	9520
2.0	0.5	15.9	42	105	180	2.73	0.51	81.8	11400
2.0	1.0	16.7	36	110	200	2.73	0.39	86.1	12200
2.0	2.0	16.8	34	125	220	2.64	0.34	87.5	12600
2.5	0.5	17.0	47	90	190	2.73	0.52	84.5	14100
2.5	1.0	16.1	41	110	210	2.64	0.37	85.9	15150
2.5	2.0	16.1	37	130	240	2.73	0.35	87.5	15600

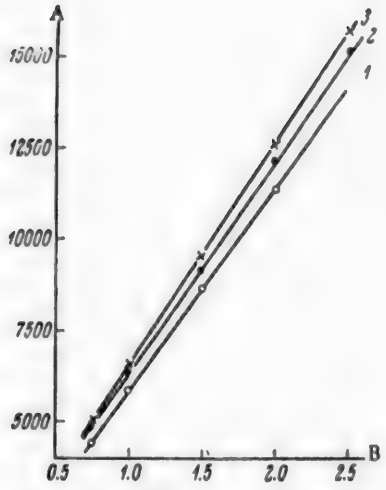

Fig. 2. Effect of gas velocity on the absorption coefficient of water vapor.
A) Absorption coefficient of water vapor, K (kg/m^2 · hour · kg/kg), B) gas velocity in full section of the apparatus, w_G (m/second). Acid flow rate i (m^3/m · hour): 1) 0.5, 2) 1.0, 3) 2.0.

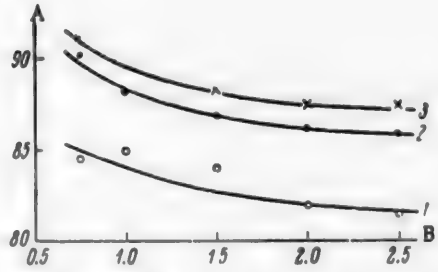

Fig. 3. Effect of gas velocity on drying efficiency.
A) Drying efficiency η (%), B) gas velocity w_G in the full section of the apparatus (m/second). Acid flow rate i (m^3/m · hour): 1) 0.5, 2) 1.0, 3) 2.0.

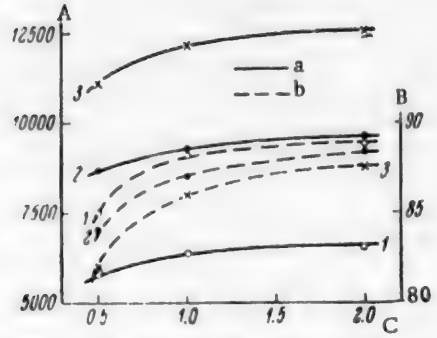

Fig. 4. Effect of acid flow rate on the absorption of water vapor.
A) Absorption coefficient of water vapor K ($kg/m^2 \cdot hour \cdot kg/kg$), B) drying efficiency η (%), C) acid flow rate $\underline{i}$ ($m^3/m \cdot hour$). a) Variation of K with $\underline{i}$, b) variation of η with $\underline{i}$. Gas velocity w_G (m/second): 1) 1.0, 2) 1.5, 3) 2.0.

while spray loss is still relatively small [2]. If the highest possible efficiency is required while the cross section of the apparatus is not important, lower values of w_G should be used.

The effects of the liquid flow rate $\underline{i}$ on the absorption characteristics of water vapor are illustrated by the graphs in Fig. 4. The experiments were performed at low values of $\underline{i}$, in the range of 0.5-2 $m^3/m \cdot hour$, with a high weir (h_w = 100 mm); the reasons are explained below. Under such conditions a normal foam regime is established and the foam apparatus operates at a high efficiency. Both the absorption coefficient K and the tray efficiency η gradually increase with increase of $\underline{i}$.

Experiments with a two-tray apparatus. To test the effectiveness of water-vapor absorption with several trays operating consecutively, experiments were carried out on the drying of air by 93% sulfuric acid in a two-tray apparatus. A diagram

TABLE 2

Experimental Conditions in the Drying of Air in a Two-Tray Model of the Foam Apparatus 5/2 grids. 100 mm weirs

Gas velocity in apparatus w_G (m/sec)	Acid flow rate i (m^3/m·hour)	Total resistance Δp (mm H_2O)	Foam height H on trays (mm)		H_2O content of gas (wt. %) at		Efficiency of apparatus η (%)	Absorption coefficient K (kg/m^2·hour·kg/kg)
			top	bottom	entry	exit		
1.0	0.5	210	160	160	2.73	0.14	94.8	6760
1.0	1.0	225	180	180	2.90	0.09	96.9	6900
1.5	0.5	210	170	170	2.64	0.18	93.0	9720
1.5	1.0	210	180	180	2.64	0.11	95.9	10950
2.0	0.5	210	180	180	2.55	0.25	90.1	12760
2.0	1.0	230	210	210	2.76	0.21	92.6	13900

of the glass model of the two-tray apparatus used in these experiments is shown in Fig. 5. The acid was fed from a header vessel to the upper tray, from which it passes to the lower tray through an overflow tube and hydraulic seal. This two-tray model was installed in place of the one-tray unit in the apparatus shown in Fig. 1. In this case, in calculations of K the driving force of absorption ΔC was calculated as for a counter-current column.

Comparison of the results obtained (Table 2) with the data for a one-tray model under similar operating conditions shows that the absorption coefficient does not decrease if two trays operate consecutively. However, the efficiency of the second tray is somewhat lower than that of the first.

For example, at w_G = 1 m/second and i = 1 m^3/m hour, the following values were obtained earlier (Table 1): K = 6420 $kg/m^2 \cdot$ hour · kg/kg, and η = 88.2%; for equivalent operation of two trays, this should give η = 98.6%; however, under the same conditions the values obtained in the two-tray apparatus were K = 6900 $kg/m^2 \cdot$ hour · · kg/kg, and η = 96.9%. Similarly, at w_G = 1.5 m/second and i = 1 $m^3/m \cdot$ hour, in the one-tray apparatus, K = 9190

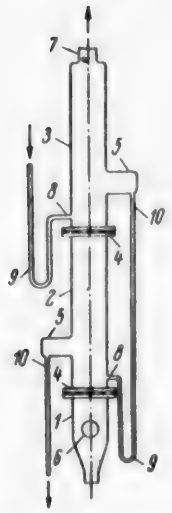

Fig. 5. Diagram of the two-tray model of the foam apparatus. 1) Bottom column, 2) intermediate section, 3) upper section, 4) grid, 5) overflow chamber, 6) gas inlet tube, 7) gas outlet tube, 8) acid inlet tube, 9) hydraulic seal (acid entry), 10) overflow tube (acid exit).

kg/m^2 · hour · kg/kg and $\eta = 86.9\%$ (which would correspond to $\eta = 98.3\%$ of a two-tray apparatus), while in the two-tray model K = 10,950 kg/m^2 · hour · kg/kg and $\eta = 95.9\%$, etc.

The results show that for adequate drying of gases, a single foam apparatus with 2-3 trays would be sufficient in place of the 2-3 packed towers as used at present. Circulation of acid then becomes unnecessary, as it is quite possible to operate a foam drier in such a way that concentrated sulfuric acid is fed to the top tray in a quantity at which dilute acid of the limiting permissible concentration flows from the bottom tray. This makes it necessary to operate at low acid flow rates, which is quite feasible without disturbance of the normal foam regime provided that high weirs and grids through which the liquid does not flow are used. These conditions were used in the experiments described.

If the amount of acid fed into the apparatus is small, the acid may become excessively hot owing to heat of dilution. Even in our experiments, where heat losses were relatively large, the acid was heated up to 40-50°, according to conditions. Therefore, if it is necessary to cool the acid, internal cooling coils may be installed on the trays of the foam drier, so that the acid can be cooled in the apparatus itself. It has been shown [2] that the heat-transfer coefficient in a heat exchanger situated in a layer of mobile foam has high values (~2000 kcal/m^2 · hour · degree), and the presence of coils on the trays of the foam apparatus does not disturb the efficiency of the main process.

TABLE 3

Conditions and Results of Experiments on the Drying of Air by 93% Sulfuric Acid, with Different Foam Heights

Pressure head h_p (mm)	Air velocity in apparatus w_G (m/sec)	Hydraulic resistance Δp (mm H_2O)	Foam height H (mm)	H_2O content of gas (wt. %) at entry	H_2O content of gas (wt. %) at exit	Tray efficiency η (%)	Absorption coefficient K (kg/m^2 · hour · kg/kg)
25	1.0	73	110	2.58	0.55	79.5	5320
	1.5	75	120	2.64	0.51	79.9	8000
	2.0	85	140	2.71	0.58	80.1	10860
	2.5	92	160	2.49	0.50	79.5	14000
50	1.0	120	200	2.71	0.25	91.1	6800
	1.5	126	220	2.64	0.31	88.9	9690
	2.0	130	240	2.64	0.32	88.8	12750
	2.5	130	260	2.73	0.34	87.7	15700
75	1.0	150	270	2.67	0.11	95.8	7600
	1.5	160	280	2.76	0.19	93.3	10500
	2.0	175	320	2.76	0.20	92.9	14100
	2.5	180	350	2.76	0.27	90.5	16500
100	2.0	240	390	2.67	0.08	97.5	15200

DISCUSSION OF RESULTS

The main factors which determine the rate and extent of mass-transfer processes in foam apparatus are the degree of turbulence of the gas – liquid system, and the interphase area which develops. However, their magnitudes cannot be determined quantitatively as yet. Nevertheless, the development of the interphase area can be estimated [2, 11] from the easily measured height of the layer of mobile foam on the apparatus grid. It is therefore more convenient to treat the experimental data as empirical relationships between K and η, and the foam height. These relationships can be used to calculate absorption characteristics under given operating conditions, and determine modeling conditions (for any actual given system).

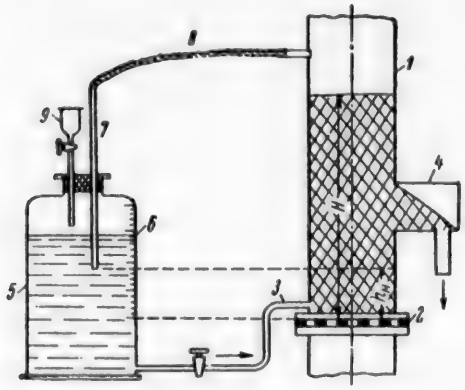

Fig. 6. Liquid feed into the foam apparatus at constant pressure head.
1) Top column of foam apparatus, 2) grid, 3) liquid inlet tube, 4) overflow chamber, 5) pressure vessel, 6) scale for measurement of pressure head, 7) movable tube for regulation of pressure head, 8) tube for equalization of pressure, 9) funnel for liquid feed.

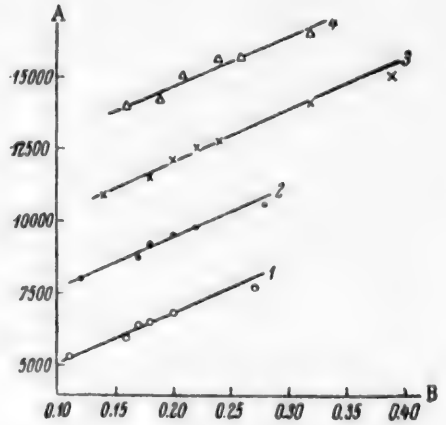

Fig. 7. Variation of the absorption coefficient of water vapor with foam height, for the system: air (saturated with water vapor at 30°) – 93% sulfuric acid.
A) Absorption coefficient of water vapor, K (kg/m^2 · hour · kg/kg), B) foam height H (m).
Gas velocity w_G (m/second): 1 – 1.0, 2 – 1.5, 3 – 2.0, 4 – 2.5.

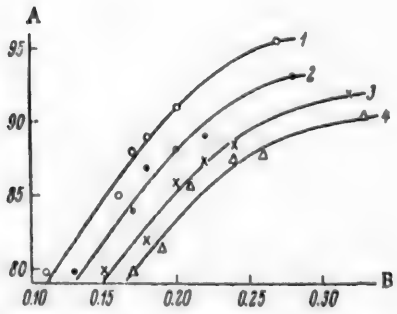

Fig. 8. Variation of drying efficiency with foam height, for the system: air (saturated with water vapor at 30°) – 93% sulfuric acid.
A) Drying efficiency η (%), B) foam height H (m).
Gas velocity w_G (m/second): 1 – 1.0, 2 – 1.5, 3 – 2.0, 4 – 2.5.

For derivation of calculation formulas relating to the absorption of water vapor by sulfuric acid, additional experiments were performed with the laboratory unit described above, with different heights of foam on the grid. In these experiments the sulfuric acid was fed into the foam apparatus from a special pressure vessel. The pressure head h_p was varied by the raising or lowering of a tube hermetically clamped in the bung of the vessel. In this way it was possible to set up on the grid a given initial layer of acid of height h_0, and therefore a definite foam height H, which was automatically maintained throughout the experiment under the given conditions, as the acid leaving the grid was replaced by exactly the same amount of fresh liquid. The average results of these experiments are given in Table 3.

Fig. 7 shows the average values of the absorption coefficient of water vapor with variations of the foam

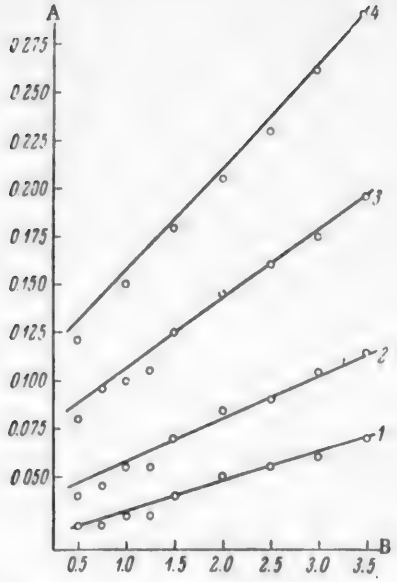

Fig. 9. Foaming in the system air —96% sulfuric acid. Apparatus without liquid overflow. 5/2 grid (S_0 = 17%). A) Foam height H (m), B) air velocity in the full section of the apparatus, w_G (m/second). Height of original acid layer h_0 (m): 1 — 0.01, 2 — 0.02, 3 — 0.04, 4 — 0.06.

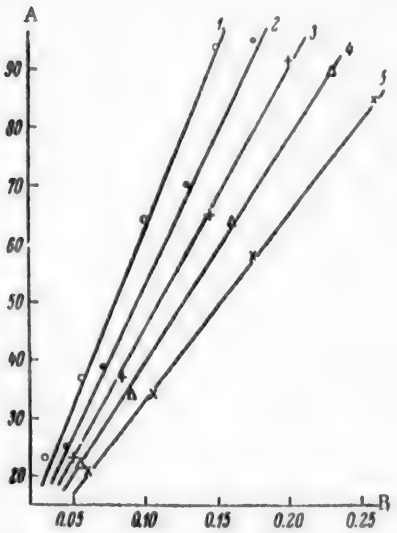

Fig. 11. Effect of foam height on its hydraulic resistance in the system air — — 96% sulfuric acid. 5/2 grid (S_0 = 17%). A) Hydraulic resistance of the foam ΔP_2 (mm H_2O), B) foam height H (m). Gas velocity w_G (m/second): 1 — 1.0, 2 — 1.5, 3 — 2.0, 4 — 2.5, 5 — 3.0.

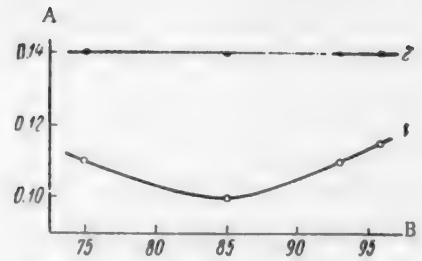

Fig. 10. Effect of sulfuric acid concentration on foam height. Height of original acid layer h_0 = 0.04 m. A) Foam height H (m), B) sulfuric acid concentration (%). Gas velocity w_G (m/second): 1) 1.0, 2) 1.75.

height between 100 and 350 mm, at the gas velocities used (w_G from 1 to 2.5 m/second). In the absorption of water vapor, as in other processes [2, 12], the absorption coefficient is proportional to the foam height over a considerable range of the latter. The reason for the slight scattering of the points around the straight lines in Fig. 7 is that, in addition to small fluctuations of the initial air temperature and humidity under different conditions, there were larger fluctuations of the final acid temperature (the acid was not cooled in the laboratory experiments).

The group of straight lines in Fig. 7 can be represented by the generalized equation

$$K = 17500H + 5200w_G - 1900, \qquad (4)$$

where K is in kg/m^2 · hour · kg/kg, H is in m, and w_G is in m/second.

This equation, or Fig. 7, may be used for determination of the absorption coefficient of water vapor in sulfuric acid as a function of the foam height on the grid. The absorption of water vapor by sulfuric acid is more complete, i. e., the drying efficiency η increases, with increase of the foam height on the grid (Fig. 8). This relationship is represented by a group of curves, each of which corresponds to a definite linear gas velocity; the greater the value of w_G, the lower does the corresponding curve lie. The curves in Fig. 8 are, with an accuracy adequate for practical purposes, represented by the equation

$$\eta = (1.33 - 0.075w_G)\, H^{0.2}, \qquad (5)$$

where η is expressed as a fraction of unity.

This equation, and the graphs in Fig. 8, can be used for determination of the foam height, and therefore of the operating conditions in the foam apparatus, for a given drying efficiency.

The foregoing equations are graphs and empirical in character, and therefore they give reliable results only within the ranges of process conditions studied; these largely correspond to the operating conditions for works driers.

These relationships must be correlated with the hydrodynamic conditions before they can be applied. A study was therefore made of the foaming of 96% sulfuric acid by the action of air, in a model apparatus without overflow of the liquid from the grid (i. e., with the height of the original acid layer known). The variations of H with h_0 and w_G in this system are presented in Fig. 9. This group of curves is represented by the equation

$$H = 0.7w_G(h_0 + 0.012) + 1.75h_0, \quad (6)$$

where H and h_0 are in meters, and w_G is in m/second.

It may be noted that Equation (6) is identical to the one derived earlier [2] for the system air – 76% sulfuric acid. It seems that the height of the mobile foam is independent of the sulfuric acid concentration in the range in question (76 – 96% H_2SO_4). To test this, experiments were performed on the foaming of sulfuric acid solutions of different concentrations; the results are plotted in Fig. 10. At a low gas velocity in the apparatus, the foam height is at a minimum at 85% concentration of sulfuric acid. This variation of foam height is associated with changes in the physical properties of sulfuric acid solutions, the influence of which is more pronounced at low values of w_G [9], i. e., when the turbulence of the system is less.

However, the absolute changes of foam height with variation of the sulfuric acid concentration are not large even at low gas velocities, and they may be neglected in practical calculations. At higher values of w_G there are no changes of foam height with variations of the H_2SO_4 concentration.

This fact is significant, as it makes it possible to apply the above relationships to the operating conditions on all the trays of the foam drier, despite the variations of sulfuric acid concentration at different heights (on different trays) of the apparatus. Incidentally it may be noted that the absorption coefficient has been reported to be independent of the concentration of strong sulfuric acid [13].

Experimental data for the system air – 96% sulfuric acid are plotted in Fig. 11; it is seen that the hydraulic resistance of the foam, ΔP_2, is proportional to the foam height at constant gas velocity. As the structure of the foam (at a given height) depends on the gas velocity in the apparatus, ΔP_2 also depends on w_G. The higher the gas velocity, the lower are the density and hydraulic resistance of the foam.

The empirical formula for calculation of the hydraulic resistance of the foam formed from 96% sulfuric acid is

$$\Delta P_2 = 765H - 150w_G H = 150\,(5.1 - w_G)\,H \text{ mm } H_2O. \quad (7)$$

In selection of the optimum operating conditions of the foam drier it must be taken into account that although increase of foam height increases K and η, it involves an increase of the hydraulic resistance of the apparatus. Therefore the foam height should be increased only up to a certain limit, usually up to 150-200 mm.

SUMMARY

1. When sieve apparatus is operated under foaming conditions, absorption of water vapor by sulfuric acid proceeds at high rates, and the system approximates closely to the equilibrium state. The absorption coefficient reaches values of 12,000-15,000 kg/m^2 · hour · kg/kg, and the tray efficiency, 80-90%.

2. The drying of gases by means of sulfuric acid under foaming conditions is highly effective, as the process can be carried out to the required extent in one small apparatus instead of several cumbersome packed towers, and recirculation of the acid becomes unnecessary.

3. From the operational characteristics of the foam drier, determined in the present investigation, the following conditions may be recommended: foam height on grid 150-200 mm, gas velocity in the full section of the apparatus 1.5-2.5 m/second.

The number of trays in the apparatus depends on the initial and final moisture contents of the gas; in most industrial cases 2-3 trays are sufficient for good drying of gases.

LITERATURE CITED

[1] V. M. Ramm. Absorption Processes in Chemical Industry (Goskhimizdat, 1951). [In Russian]

[2] M. E. Pozin, I. P. Mukhlenov, E. S. Tumarkina, and E. Ia. Tarat, The Foam Method of Treatment of Gases and Liquids (Goskhimizdat, 1955). [In Russian]

[3] M. E. Pozin, I. P. Mukhlenov, E. S. Tumarkina, and E. Ia. Tarat, J. Appl. Chem. 27, 1, 12 (1954).*

[4] M. E. Pozin, I. P. Mukhlenov, and E. Ia. Tarat, The Foam Method of Gas Purification (Goskhimizdat, 1953). [In Russian]

[5] D. A. Kuznetsov, I. M. Egorkina, and A. S. Pospelova, J. Chem. Ind. 18, 13, 5 (1941).

[6] E. Ia. Turkhan and E. A. Andreeva, J. Chem. Ind. 16, 6, 18 (1939).

[7] A. G. Amelin and M. M. Sharov, J. Chem. Ind. 2, 7 (1945).

[8] I. G. Bliakher, Trans. Ural Chemical Scientific Research Institute, 1 (Goskhimizdat, 1954).**

[9] M. E. Pozin, B. A. Kopylev, and E. Ia. Tarat, J. Appl. Chem. 30, 5, 674 (1957).*

[10] M. E. Pozin and B. A. Kopylev, J. Appl. Chem. 30, 3, 362 (1957).*

[11] M. E. Pozin, I. P. Mukhlenov, and E. Ia. Tarat, J. Appl. Chem. 30, 1, 45 (1957).*

[12] M. E. Pozin and E. Ia. Tarat, Trans. Lensoviet Technol. Inst. Leningrad 36, 139 (1956).

[13] E. Ia. Turkhan and K. P. Zhideleva, J. Chem. Ind. 11, 6 (1946).

Received April 18, 1957.

*Original Russian pagination. See C. B. Translation.

**In Russian.

KINETICS OF HEAT AND MASS TRANSFER IN A FOAM LAYER•

I. P. Mukhlenov

(The Lensoviet Technological Institute, Leningrad)

Under industrial conditions, with direct contact between gas and liquid, heat transfer usually takes place simultaneously with mass transfer, and it is therefore important to carry out simultaneous studies of these processes, with derivation of calculation formulas of the same type. This was the purpose of our investigations performed with sieve equipment under foaming conditions.••

The general differential kinetic equations are usually written as follows:

$$\text{for heat transfer} \quad \frac{dQ}{d\tau} = k_H F \cdot \Delta t, \tag{1}$$

$$\text{for mass transfer} \quad \frac{dG}{d\tau} = k_M \cdot F \cdot \Delta C, \tag{2}$$

where Q and G are the amounts of heat (in kcal) or matter (in kg) transferred, K_H and k_M are the coefficients of heat transfer (in kcal/m². hour. degree) and mass transfer (in kg/m². hour. kg/m³ of gas), F is the area of contact between gas and liquid (m²), and Δt and ΔC are the driving forces of heat transfer (in deg.) and mass transfer (in kg/m³).

In Equations (1) and (2) the driving force of the process does not depend on the turbulence of the interacting gas and liquid. The phase-contact area increases very rapidly with increasing turbulence of the system, but it is not measurable in turbulent systems. Therefore in calculations of heat-and mass-transfer rates it is usual to refer it to the reaction volume (volume of packing, volume of apparatus, volume of liquid) or, arbitrarily, to a characteristic area which can be measured exactly (surface area of the packing, tray area, etc.). Here heat and mass transfer are calculated for the total area of all the grids in the sieve apparatus, the grid area being assumed equal to the cross section of the apparatus.

In the usual method, the whole complexity of the varied effects of the geometrical, physical, and chemical parameters of a system on the rate of heat or mass transfer is referred to the coefficient of heat transfer k_H or of mass transfer k_M. Determination of these coefficients usually comprises the main task in studies of the process kinetics.

Diffusion and heat-transfer processes have been studied fundamentally for conditions of film, drop, and bubbling interaction between gases and liquids. For a number of conditions, with geometrical and hydrodynamic similarity of the systems, these processes have been shown to be analogous. Equations have been derived for calculation of heat- and mass-transfer coefficients under experimental conditions.

It has been shown in our investigations [1, 2] that the hydrodynamic conditions in a foam layer differ greatly from those in all other methods of gas – liquid interaction studied previously. Therefore the empirical equations for quantitative determination of heat- and mass-transfer coefficients, applicable to the other methods, cannot be applied to the foam layer. However, the criterial equations should largely retain their essential structure when applied to foam layers.

•Communication 1.

•• Experiments carried out jointly with M. E. Pozin, E. S. Tumarkina, and E. Ia Tarat.

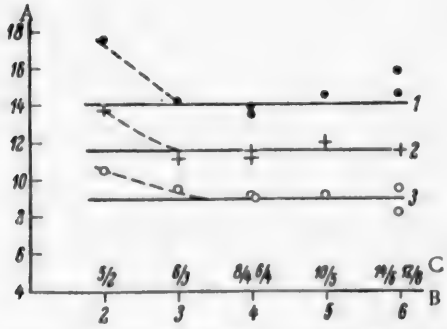

Fig. 1. Variation of the heat-transfer coefficient with the diameter of the grid orifices.
A) Coefficient of heat transfer $K_H \cdot 10^{-3}$ (kcal/m^2 · hour · degree), B) orifice diameter d_0 (mm), C) ratio of orifice spacing to diameter m/d_0.
Air velocity w_G (m/second): 1 – 3.0, 2 – – 2.5, 3 – 2.0.

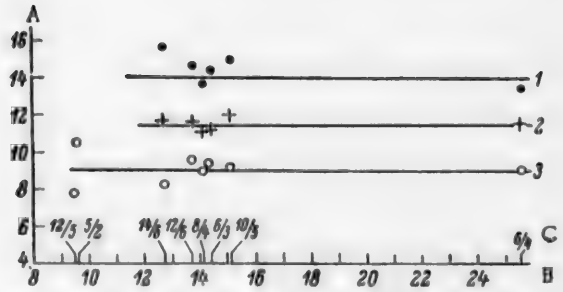

Fig. 2. Coefficient of heat transfer on grids of different S, d_0, and m.
A) Coefficient of heat transfer $k_H \cdot 10^{-3}$ (kcal/m^2. hour · degree), B) Open section of grid S (%), C) ratio of grid orifice spacing to diameter m/d_0.
Air velocity w_G (m/second): 1 – 3.0, 2 – 2.5, 3 – 2.0.

Berman [3, 4] correctly points out that, in addition to the general criteria which determine the process kinetics: the Reynolds number Re, the Prandtl thermal criterion Pr, the Prandtl diffusion criterion Pr', the geometrical criteria Γ_1, Γ_2, etc., in many cases it is necessary to introduce into the criterial equations additional criteria, which characterize the hydrodynamic characteristics of this method of gas – liquid interaction. Such a criterion, which determines the kinetics of mass- and heat-transfer processes in a foam layer, is the specific foam height H_{sp}, calculation formulas for which were derived by us earlier [1]. As the determined criterion in equations representing processes in a foam layer it is convenient to use the Margulis criterion M [5], recommended by Frank-Kamenetskii for turbulent conditions [6].

$$\text{For heat transfer} \quad M = \frac{k_H}{w_G \cdot c_G \cdot \gamma_G}, \tag{3}$$

$$\text{For mass transfer} \quad M' = \frac{k_M}{w_G}, \tag{4}$$

where w_G is the linear gas velocity in the apparatus (m/second), c_G is the heat capacity of the gas (in kcal/kg. degree), and γ_G is the density of the gas (in kg/m^3).

The criteria M and M' are particular cases of Diakonov's [7] contact criterion Co, which represents the ratio between the rates of restoration and breakdown of thermodynamic equilibrium. If k_G, k_M and w_G are regarded as inversely proportional to time, M and M' can be considered to represent the ratio of the duration of the heat- or mass-transfer process to the contact time between gas and liquid.

In a foam layer the gas phase is subjected to the greater turbulence, and therefore the use of the foam regime is most effective for processes limited by gas-phase transfer, i.e., mass transfer of readily soluble gases, and heat transfer. Therefore the investigations the results of which are presented in this paper were carried out in relation to processes the rate of which is determined by diffusion (molecular or turbulent) in the gas phase.

Generalization of our own and published experimental data showed that, for layers of mobile foam, heat- and mass-transfer processes determined by gas-phase diffusion may be represented by analogous criterial equations

$$M = A \cdot Re^{m} \cdot H_{sp}^{n} \cdot Pr^{q} \cdot G_1^{r} \cdot \Gamma_2^{s} \quad \text{or}$$

$$\frac{k_M H}{w_G \cdot c_G \cdot \gamma_G} = A \left(\frac{w_r \cdot D_e}{\nu_G} \right)^{m} \left(\frac{H}{h_0} \right)^{n} \left(\frac{\nu_G}{a} \right)^{q} \cdot \left(\frac{h_0}{D_e} \right)^{r} \left(\frac{m}{d_0} \right)^{s}, \tag{5}$$

$$M'_1 = B \cdot Re^{m} \cdot H_{sp}^{n} \cdot Pr'^{q} \cdot \Gamma_1^{r} \cdot \Gamma_2^{s} \quad \text{or}$$

$$\frac{k_M}{w_G} = B \left(\frac{w_G \cdot D_e}{\nu_G} \right)^{m} \cdot \left(\frac{H}{h_0} \right)^{n} \left(\frac{\nu_G}{D} \right)^{q} \cdot \left(\frac{h_0}{D_e} \right)^{r} \left(\frac{m}{d_0} \right)^{s}, \tag{6}$$

where A and B are constants, D_e is the equivalent diameter of the apparatus (in m), d_0 is the diameter of an orifice in the apparatus grid (in m), m is the spacing between the orifice centers (m), H is the height of the foam layer on the grid (in m), h_0 is the height of the original layer of pure liquid, from which the foam is formed on the grid (in m), ν_G is the coefficient of kinematic viscosity of the gas (in m^2/second or m^2/hour), $a = \lambda / c_G \cdot \gamma_G$ is the coefficient of temperature conductivity (in kcal/m^2. hour. degree), λ is the coefficient of thermal conductivity (in kcal/m. hour. degree), and D is the gas-phase diffusion coefficient (in m^2/hour).

Equation (6) is valid only at high values of M', i. e., for readily soluble gases (M' > 1). Absorption of gases of moderate and low solubility corresponds to moderate and low values of M' respectively, and is represented by equations containing different criteria from those in Equation (6) [8].

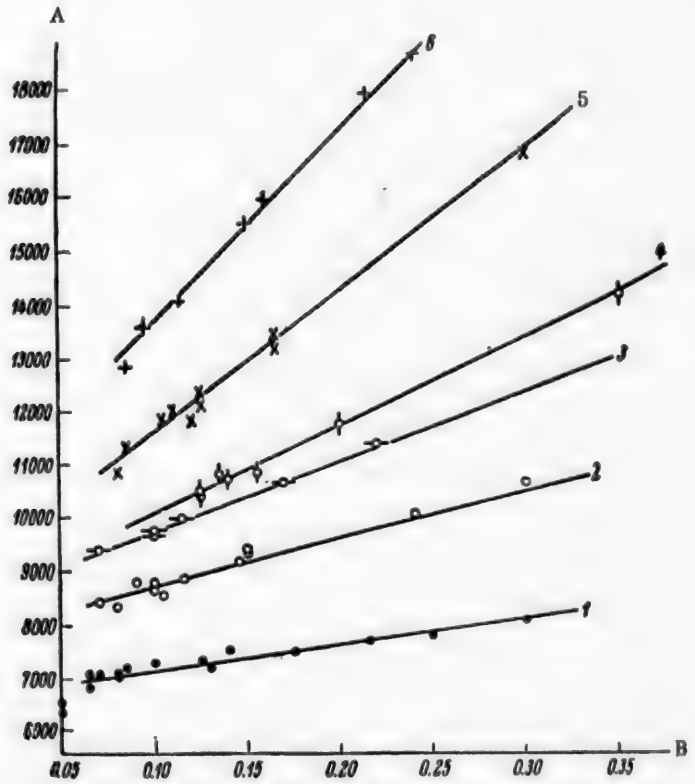

Fig. 3. Effect of foam height on the condensation coefficient of water vapor.

A) Condensation coefficient k_a (kg/m^2 · hour · kg/m^3), B) foam height H (m). Air velocity w_G (m/second): 1 – 1.5; 2 – 2.0, 3 – 2.3, 4 – 2.5, 5 – 3.0, 6 – 3.5.

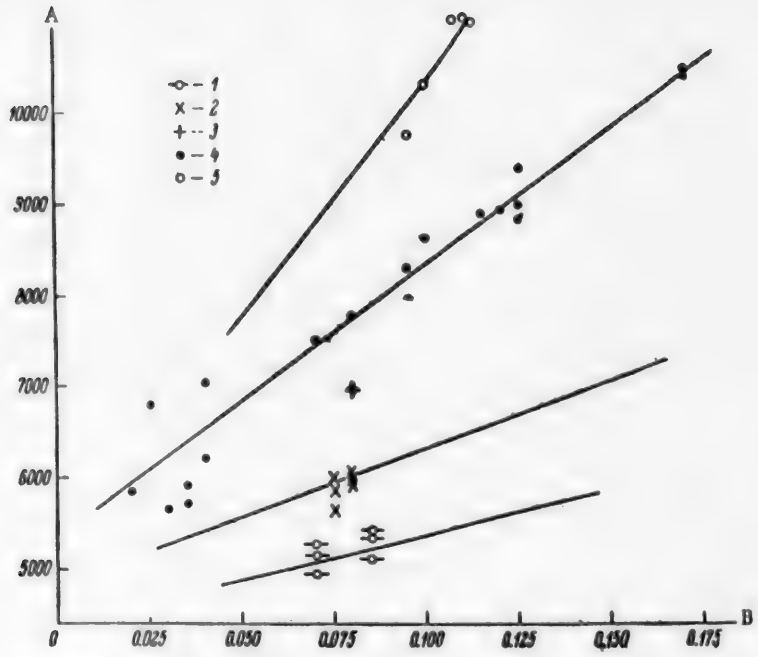

Fig. 4. Effect of foam height in the system: air mixed with ammonia — — water, on the coefficient of absorption of ammonia in water. A) Absorption coefficient k_a (kg/m^3· hour · kg/ m^3), B) foam height H (m). Grids of m/d_0: 5/2; 6/2; 6/4. Gas velocity w_G (m/second): 1 — — 1.25, 2 — 1.5, 3 — 1.75, 4 — 2.0, 5 — 2.75.

The purpose of the experimental work was to determine the effects of the parameters in Equation (5) and (6) on k_H and k_M, and to find the numerical values of the indices: m, n, q, r, and s, both in Equation (5) and in (6). The present paper contains the results of determinations of the effects of the geometrical (constructional) parameters and of the height of the foam layer on k_H and k_M.

The experiments were performed with the use of laboratory units described previously [1, 2, 8, 9], and industrial foam equipment. The process conditions and grid types were varied most widely in experiments with a 3-tray model of the foam apparatus [1, 9]. This model was used for tests on more than 20 grids, with orifices from 2 to 8 mm in diameter, with from 5 to 14 mm spacing between the orifice centers, and with from 9 to 25% open section. The height of the overflow weir was varied from 0 to 30 mm, and the height of the overflow orifice from 70 to 100 mm (the length of the overflow orifice was always equal to the width of the grid). The gas velocity in the open section of the apparatus was varied from 0.4 to 3.5 m/second, and the water rate i from 2 to 40 m^3 per meter of grid width per hour (m^3/m. hour).

The hydrodynamic conditions were regulated and checked largely as in the experiments on the hydrodynamics of foaming, described previously. In some experiments the foam height was not measured, but calculated from the formulas derived earlier. The height of the original liquid layer was always calculated by means of the formula derived earlier [1, 2, 8]. The method used in the experiments on heat transfer was similar to that described in our investigation performed jointly with Tumarkina [9]. In the absorption experiments, the absorbed component was fed into the pipe leading to the foam apparatus from cylinders (NH_3, CO_2, Cl_2, SO_2) or from special generators (Br_2, NO + NO_2). In experiments on desorption, the solutions for investigation were prepared in separate vessels (reservoirs), and then introduced into the bottom tank of the apparatus. In all the absorption and desorption experiments gas samples were taken on each side of the apparatus tray by means of evacuated bulbs or aspirators. In a number of experiments, liquid from the inlet pipes and hydraulic seals beyond the tray of the foam apparatus was withdrawn through side tubes simultaneously with the gas samples.

Equations (1) and (2) (in integrated form) were used for calculations of k_H and k_M; the driving force (Δt, ΔC) was calculated from M. E. Pozin's equations [10]. The method used for calculation of k_H was analogous to that described previously [9]. Data obtained in experiments on heat transfer from moist air to water were also used to calculate the mass-transfer coefficient or, more accurately, the condensation coefficient of water vapor k_a (analogous to β_x [4, 10]), which can also be described as the absorption coefficient of a gaseous component infinitely soluble in the liquid. The values of the criteria in Equations (5) and (6) were calculated from experimental and reference data (c_G, γ_G, ν_G, λ, D).

The results of the experiments are presented in Figs. 1-4.

Influence of design parameters. Many workers have studied the influence of the dimensions and design details of the apparatus on heat and mass transfer between gases and liquids.

Some investigators [11-13] found that the diameter of the apparatus has only a small influence on the processes in it. Others concluded that the diameter of an industrial apparatus does not influence the rate of mass or heat transfer if it does not affect the hydrodynamics of the streams. Under laboratory conditions the diameter may have an influence if the tubes used are too narrow to serve as models of industrial equipment. Our experiments showed that changes of the diameter of the foam apparatus from 0.055 to 2.5 m have no effect on the coefficients of mass and heat transfer between gas and liquid. Therefore, in order that the criteria containing D_e in Equations (5) and (6) should remain dimensionless, D_e must be taken as constant, as was done in the hydrodynamical studies ($D_e = 1.13$ m) [1].

The influence of the ratio m/d_0 in Equations (5) and (6) was tested for a number of models of the foam apparatus, and for different gas – liquid systems. The experiments showed that variations of the orifice diameter d_0 between 6 and 3 mm, and of the open section of the grid S from 25 to 5%, with m = 4-16 mm, have no effect on k_H or k_M if the influence of liquid flow through the grid orifices is eliminated. With grids of $d_0 = 2$ mm, heat and mass transfer are somewhat more intensive, because of a small increase of foam height and improvement of the foam structure. This is illustrated by the experimental data in Figs. 1 and 2.

In conformity with economic requirements, grids with $d_0 > 2$mm and $S > 10\%$ are largely used in industrial equipment; therefore in calculations relating to such equipment the influence of d_0 and m on k_H and k_M may be disregarded, i. e., S may be taken as 0 in Equations (5) and (6).

Thus, our experiments showed that heat- and mass-transfer processes in foam equipment are "automodeling".

Influence of foam height. It was shown earlier [1, 2, 8] that the foam height H is the principal factor which determines the mass- and heat-transfer coefficient. The time of contact between gas and liquid on the tray of the foam apparatus is directly proportional to the height of the foam layer. Therefore the relationships between the heat- and mass-transfer coefficients and the height of the foam layer should, under constant conditions, also be linear; this was confirmed experimentally. In illustration, the variations of the absorption coefficient k_a with H at different gas velocities are shown in Figs. 3 and 4. Graphs of the same type are obtained for heat transfer and desorption. If the foam height is decreased to below 40-80 mm (according to the gas velocity), the relationships between k_H, k_M, and H cease to be linear. The decreases of k_H and k_M become more rapid.

The experiments on absorption of ammonia in water were less exact than the other series of experiments, because of the previously described [2] foam-suppression effect, i. e., an irregular decrease of foam height H on addition of ammonia to air. Therefore the lines drawn in Fig. 4 were actually calculated from other experimental data, and the experimental points were added subsequently; the points lie satisfactorily close to the lines.

For each straight line in Figs. 3 and 4 all the determining parameters in Equations (5) and (6) are virtually constant, with the exception of H and h_0.

The function $k = f(H)$ can be represented by equations of the form $k = aH + bc$ for all the experiments, with variable values of the coefficients a and b, or by equations of the form $k = A_1 \cdot H^n$, more convenient for inclusion in the criterial equation, where k is the rate coefficient of the process (mass or heat transfer), and n varies from 0.3 to 0.4.

The experimental data were also used to calculate the tray efficiencies, i. e., the degree of heat transfer, the extraction coefficient in absorption, and the enrichment coefficient in desorption of gases. In all cases the curves obtained gradually flatten out, like those described earlier [9]; the increase of efficiency with H gradually diminishes.

The above data show that the intensity of heat and mass transfer on the tray of a foam apparatus is proportional to the foam height H. However, large increases of H are unsuitable for two reasons. First, because the efficiency approaches 100%, the increase of tray productivity with increasing foam height almost ceases, although k continues to increase. Second, if the foam height exceeds 400 mm the foam quality and efficiency deteriorate while the hydraulic resistance increases. In practice, foam heights between 50 and 300 mm are usually attained in foam equipment, according to the required efficiency and to the possibility of attaining it.

SUMMARY

1. Analysis of experimental and literature data yielded general criterial Equations (5) and (6) which represent heat transfer and absorption of readily soluble gases in a foam layer.

2. Experiments showed that heat- and mass-transfer processes in foam apparatus are "automodeling" in particular, it is shown that these processes are not influenced by the diameter of the apparatus, diameter of the grid orifices, and free grid section, in the range of practical variations of these parameters.

3. The coefficients of heat and mass transfer are shown to be proportional to foam height.

LITERATURE CITED

[1] I. P. Mukhlenov, J. Appl. Chem. 31, 1, 45 (1958).*

[2] M. E. Pozin, I. P. Mukhlenov, E. S. Tumarkina, and E. Ia. Tarat, The Foam Method for Treatment of Gases and Liquids (Goskhimizdat, 1955). [In Russian]

[3] L. D. Berman, Heat Engineering 5, 25 and 6, 3 (1954); 8, 10 (1955).

[4] L. D. Berman, Evaporative Cooling of Circulation Water (Gosenergoizdat, 1949). [In Russian]

[5] W. Margulis, Chaleur et Industrie 134, 269, 352 (1931).

[6] D. A. Frank-Kamenetskii, Diffusion and Heat Transfer in Chemical Kinetics (Izd. AN SSSR, 1952). [In Russian]

[7] G. K. D'iakonov, Bull. Acad. Sci. USSR, OTN 7-8, 473 (1944); Proc. Acad. Sci. USSR 57, 7, 701 (1947).

[8] I. P. Mukhlenov, Doctorate Dissertation, Lensoviet Technological Inst.(Leningrad, 1955).

[9] I. P. Mukhlenov and E. S. Tumarkina, J. Appl. Chem. 28, 2, 135, and 4, 345 (1955).*

[10] M. E. Pozin, J. Appl. Chem. 25, 10, 1032 (1952);* 26, 11, 1133 (1953).*

[11] N. M. Zhavoronkov and I. E. Furmer, Oxygen 5, 9 (1947).

[12] M. D. Kuznetsov, J. Appl. Chem. 21, 1, 48 (1948).

[13] V. G. Levich, Physicochemical Thermodynamics (Izd. AN SSSR, 1952). [In Russian]

Received March 20, 1957.

* Original Russian pagination. See C. B. Translation.

ROTATION SPEEDS OF STIRRERS IN THE STIRRING OF TWO MUTUALLY INSOLUBLE LIQUIDS

I. S. Pavlushenko and A. V. Ianishevskii

(The Lensoviet Technological Institute, Leningrad)

Mechanical stirring is very extensively used in different branches of chemical technology. Stirring is especially important in continuous processes; this accounts for the considerable interest of numerous workers in the problem. In recent years most attention has been devoted to determination of quality characteristics of the mechanical stirring process. However, because of the diversity of the technological requirements, a general solution to the problem has not yet been found.

The stirring of two mutually insoluble liquids and the production of suspensions are among the most common examples of stirring. In considerations of the mechanical stirring of two mutually insoluble liquids under the conditions used for various technological processes, attention must evidently first be devoted to the question of the creation of conditions which ensure a uniform distribution of the liquids in the stirred volume. Studies of this aspect of the problem have been totally inadequate. The most interesting paper from this aspect is that by Miller and Mann [1], who characterized the homogeneity of the stirred volume in terms of uniformity of the phase distribution, while the uniformity was defined as the arithmetic mean of the relative phase contents in a series of samples taken simultaneously. No analytical relationships were derived between the physicochemical properties of the stirred liquids, the geometrical dimensions of the apparatus and stirrer, and the stirrer speed necessary to produce uniform distribution.

In the case of mechanical emulsification, the intensity of stirrer operation is characterized not only by uniformity of the phase distribution, but also by the dispersity of the disperse phase. A considerable number of studies deal with this problem. They include the work of Harkins and Beeman [2], Stamm [3], Moore [4], Stamm and Kraemer [5], Clayton and Morse [6], Nagata [7], Vermeulen et al. [8], Padger et al. [9], and others.

The present paper contains some results of a study of emulsification by means of mechanical stirring, from the aspect of uniform phase distribution.

The view was advanced earlier [10] that the relationship between the physicochemical properties of the stirred liquids, the geometrical dimensions of the apparatus and stirrer, and the stirrer speed necessary to give uniform distribution may be found with the use of the concept of the determining stirrer speed. In the case of mechanical emulsification, we define as the determining speed, the number of revolutions n_0 of the stirrer in unit time, at which the relative concentration of the disperse phase reaches 100% over the entire stirred volume.

The formation of an emulsion when two mutually insoluble liquids are stirred, and its breakdown when stirring is discontinued, indicate that a dynamic equilibrium between emulsion formation and breakdown exists during the stirring process.

The process of emulsification, which was elucidated by Kremnev and Ravdel [11], can be confirmed by visual observation, and depends on the following factors:

$$\rho_m, \rho_p, \mu_m, \mu_p, \sigma, V_m, V_p, d_s, D, H_0, h, n, g.*$$

According to numerous investigations [12], the stability of two-component emulsions depends on the following factors:

$$\rho_m, \rho_p, \mu_m, \mu_r, d_d, \sigma, V_m, V_p$$

The dynamic equilibrium between the two processes, with uniform phase distribution, may be represented by the expression

$$n_0 = \varphi(\rho_m, \rho_p, \mu_m, \mu_p, \sigma, d_S, D, H_0, h, g, V_m, V_p). \quad (1)$$

Expansion of the functional relationship (1) by the usual methods of dimensional analysis••• yields ten criterial equations, representing variations of the relationships between the variables. The effect is most conveniently represented by an expression of the following form:

$$\frac{\rho_m n_0 d_S^2}{\mu_m} = C\left(\frac{\rho_m^2 d_S^3 g}{\mu_m^2}\right)^a \left(\frac{\rho_m d_S \sigma}{\mu_m^2}\right)^b \left(\frac{\mu_p}{\mu_m}\right)^e \left(\frac{\rho_p}{\rho_m}\right)^f \times \times \left(\frac{D}{d_S}\right)^i \left(\frac{H_0}{d_S}\right)^m \left(\frac{h}{d_S}\right)^k \left(\frac{V}{d_S^3}\right)^r \left(\frac{V}{d_S^3}\right)^t \quad (2)$$

or, in abbreviated form

$$Re_c = C \cdot Ga^a \left(\frac{Re_c^2}{We_c}\right)^b S_\mu^e S_\rho^f \Gamma_D^i \Gamma_{H_0}^m \Gamma_h^k K_p^r K_m^t. \quad (3)$$

Experiments were carried out to determine the indices of the similarity criteria and the coefficient in Equation (3).

EXPERIMENTAL

The experiments were performed in two special units, in which the stirrer speeds could be varied smoothly from 60 to 1600 revolutions per minute. The liquids were stirred in glass vessels, 300 mm in diameter, with standardized spherical bottoms [14]. In addition to vessels without internal devices, vessels each containing four glass baffle-partitions 3 mm thick and 24 mm wide were used [15]. The partitions were placed vertically near the vessel walls, in two planes at right angles to each other. The lower edges of the partitions were 90 mm from the vessel floor. The stirrers used were 3-blade screws of pitch 1, and turbines 50, 75, 100, 125, 150, 175 mm in diameter, made from stainless steel in conformity with standards NMP-298-49 and NMP-300-49 of the Scientific Research Institute of Chemical Machinery Construction [14].

In every experiment the vessel was filled to a height equal to its diameter, i. e., $H_0 = D$. Uniformity of phase distribution was checked by sampling. Samples of the emulsions were withdrawn by means of a "Record"

• The following notation is used: ρ_m, ρ_p, the densities of the dispersion medium and the disperse phase (kg · · second^2/m^4); μ_m, μ_p, the viscosities of the dispersion medium and the disperse phase (kg · second/m^2); σ, the interfacial tension (kg/m); V_m, V_p, the volumes of the dispersion medium and the disperse phase (m^3); d_S, the stirrer diameter (m); D, the vessel diameter (m); H_0, the total height of the liquid layer (m); h, the distance between the median line of the stirrer and the bottom of the vessel (m); n, the stirrer speed (revolutions/second); g, the acceleration due to gravity (m/second^2); d_d, the diameter of a disperse-phase droplet (m).

•• The variable d_d does not enter the function, as it is not determining with regard to the speed n, but is a function of n.

••• By the practical methods described previously [13].

TABLE 1

Characteristics of the Systems*

System No.	System	ρ_p (kg·sec²/m⁴)	ρ_m (kg·sec²/m⁴)	μ_p (kg·sec/m²)	μ_m (kg·sec/m²)	$\sigma \cdot 10^4$ (kg/m)
I	Water in carbon tetrachloride	102.0	162.6	$1.02 \cdot 10^{-4}$	$0.98 \cdot 10^{-4}$	46.4
II	Carbon tetrachloride in water	162.6	102.0	$0.98 \cdot 10^{-4}$	$1.02 \cdot 10^{-4}$	46.4
III	Glycerol in carbon tetrachloride	126.0	162.6	$1.94 \cdot 10^{-2}$	$0.98 \cdot 10^{-4}$	17.6
IV	Carbon tetrachloride in glycerol	162.6	126.0	$0.98 \cdot 10^{-4}$	$1.94 \cdot 10^{-2}$	17.6
V	Kerosene in glycerol	84.4	126.0	$2.15 \cdot 10^{-4}$	$1.94 \cdot 10^{-2}$	26.8
VI	Glycerol in kerosene	126.0	84.4	$1.94 \cdot 10^{-2}$	$2.15 \cdot 10^{-4}$	26.8
VII	Kerosene in water	84.4	102.0	$2.15 \cdot 10^{-4}$	$1.02 \cdot 10^{-4}$	44.0
VIII	Water in kerosene	102.0	84.4	$1.02 \cdot 10^{-4}$	$2.15 \cdot 10^{-4}$	44.0
IX	Machine oil in water	93.5	102.0	$2.53 \cdot 10^{-2}$	$1.02 \cdot 10^{-4}$	24.5
X	Octane and carbon tetrachloride in water	104.0	102.0	$0.66 \cdot 10^{-4}$	$1.02 \cdot 10^{-4}$	49.5
XI	Aqueous solution of glycerol a in carbon tetrachloride	115.4	162.6	$1.07 \cdot 10^{-3}$	$0.98 \cdot 10^{-4}$	39.8
XII	Carbon tetrachloride in aqueous solution of glycerol a	162.6	115.4	$0.98 \cdot 10^{-4}$	$1.07 \cdot 10^{-3}$	39.8
XIII	Kerosene in aqueous solution of glycerol b	84.4	119.2	$2.15 \cdot 10^{-4}$	$1.54 \cdot 10^{-3}$	10.6
XIV	The same, glycerol c	84.4	122.8	$2.15 \cdot 10^{-4}$	$4.98 \cdot 10^{-3}$	9.4

medical syringe, 20 cc in volume, through a tube at 3 different points. The first sampling point was 295 mm from the bottom of the vessel, the second, 150 mm, and the third, 30 mm; these distances corresponded to 0.983 H_0; 0.5 H_0 and 0.1 H_0, respectively. The volume ratio of disperse phase to dispersion medium in each sample was determined by the usual sedimentation method.

The systems used in the experiments are given in Table 1. The total number of experiments was 303. For each experiment, the uniformity of phase distribution J was plotted against the stirrer speed n, and the determining speed n_0 was found from the graph. One such graph is shown in Fig. 1, where the Curves I, II, and III represent the duration of individual experiments, which varied from 1 to 14 hours (the uniformity of distribution of the disperse phase at points 1, 2, and 3 respectively).

DISCUSSION OF RESULTS

It was found in preliminary experiments that the determining speed decreases with increasing immersion depth of the stirrer. Data on this relationship, studied for System IX (Table 1) are presented in Table 2.

Most of the experiments were performed with the stirrer at the minimum possible distance from the bottom of the vessel, given by the condition $\frac{h}{d_S} = \frac{1}{5}$. Experiments with Systems III, IV, VII, and VIII were carried out for different concentrations of the disperse phase (from 10 to 70 vol.%). The experiments showed that the influence of the disperse phase concentration on the determining stirrer speed is relatively small and is random in character.

In view of this, it is possible to simplify Equation (2), by elinimation of the ratio $\frac{h}{d_S}$, which was constant in

* The physicochemical constants were measured at 20°; aqueous glycerol solutions (a, b, c) were made from different batches of glycerol.

TABLE 2

Variation of Determining Stirrer Speed with the Immersion Depth (1) Determining speed in revolutions/minute, for distance from the bottom (mm). (2) Experimental series:

	Determination speed in revolutions/min, for distance from the bottom (mm)					
	30	40	60	80	100	150
Experimental series:						
I	285	280	320	325	400	425
II	280	315	315	325	375	425

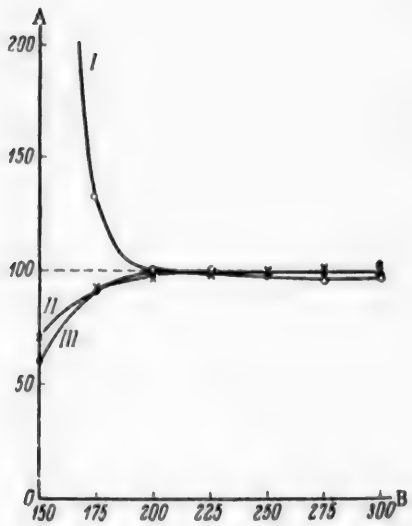

Fig. 1. Variation of the uniformity of phase distribution J with stirrer speed. System kerosene – water, $V_p : V_m$ = 30:70, propeller stirrer, d_S = 0.15 m, vessel of D = 0.3 m with four partitions. A) Uniformity of phase distribution J (%), B) revolutions per minute, n. Explanation in text.

our experiments, $\frac{H_0}{d_p}$ which was equal to $\frac{D}{d_S}$, and the ratios $\frac{V}{d_S^3}$, $\frac{Vm}{d_S^3}$. Moreover, it proved convenient to replace the ratio $\frac{\rho}{\rho_m}$ by $\frac{\Delta\rho}{\rho}$. These simplifications give

$$\frac{\rho_m n_0 d_S^2}{\mu} = C\left(\frac{\rho_m^2 d_S^3 g}{\mu_m^2}\right)^d \left(\frac{\rho_m d_S^2}{\mu_m^2}\right)^b \left(\frac{\mu_p}{\mu_m}\right)^e \left(\frac{\Delta\rho}{\rho_m}\right)^f \left(\frac{D}{d_S}\right)^i \quad (4)$$

or, in contracted form

$$Re_c = CGa^a \left(\frac{Re_c^2}{We_c}\right)^b S_\mu^e S_{\Delta\rho}^f \Gamma_D^i. \quad (5)$$

The most difficult step in analysis of the experimental data was determination of the influence of individual physicochemical properties of the stirred liquids. In the usual graphical and analytical methods for analysis of experimental data, only one parameter must be changed, while all the others remain constant. This is not possible with such properties of liquids as density, viscosity, and surface tension.

After the indices and coefficients had been determined (by trial and error), the following equations were obtained in explicit form:

In a Vessel without Baffle Partitions

a) For the propeller stirrer

$$Re_c = 68.9 Ga^{0.01} \left(\frac{Re_c^2}{We_c}\right)^{0.47} S_\mu^{0.03} S_{\Delta\rho}^{0.13}, \quad (6)$$

b) for the turbine stirrer

$$Re_c = 62.9 Ga^{0.01} \left(\frac{Re_c^2}{We_c}\right)^{0.47} S_\mu^{0.03} S_{\Delta\rho}^{0.13}. \quad (7)$$

In a Vessel with Four Baffle Partitions

a) For the propeller stirrer

$$Re_c = 2.85Ga^{0.3}\left(\frac{Re_c^2}{We_c}\right)^{0.15} S_\mu^{0.04} S_{\Delta\rho}^{0.08} \Gamma_D^{1.25}, \tag{8}$$

b) for the turbine stirrer

$$Re_c = 2.85Ga^{0.3}\left(\frac{Re_c^2}{We_c}\right)^{0.15} S_\mu^{0.04} S_{\Delta\rho}^{0.08} \Gamma_D^{0.92}. \tag{9}$$

By solving Equations (6, 7, 8, 9) for the determining stirrer speed n_0, we obtain the following calculation formulas:

In a Vessel without Baffle Partitions

a) For the propeller stirrer

$$n_0 = 4.23 \cdot 10^3 \frac{\Delta\rho^{0.13}\mu_m^{0.01}\mu_p^{0.03}\sigma^{0.47}}{\rho_m^{0.64} d_S^{1.5}} \frac{\text{rev}}{\text{min}}, \tag{10}$$

b) for the turbine stirrer

$$n_0 = 3.86 \cdot 10^3 \frac{\Delta\rho^{0.13}\mu_m^{0.01}\mu_p^{0.03}\sigma^{0.47}}{\rho_S^{0.64} d_m^{1.5}} \frac{\text{rev}}{\text{min}}. \tag{11}$$

In a Vessel with Four Baffle Partitions

a) For the propeller stirrer

$$n_0 = 3.4 \cdot 10^2 \frac{\Delta\rho^{0.08}\mu_m^{0.06}\mu_p^{0.04}\sigma^{0.15} D^{1.25}}{\rho_m^{0.33} d_S^{2.2}} \frac{\text{rev}}{\text{min}} \tag{12}$$

b) for the turbine stirrer

$$n_0 = 3.4 \cdot 10^2 \frac{\Delta\rho^{0.08}\mu_m^{0.06}\mu_p^{0.04}\sigma^{0.15} D^{0.92}}{\rho_m^{0.33} d_S^{1.87}} \frac{\text{rev}}{\text{min}}. \tag{13}$$

Examination of these equations shows that the mechanical stirring of two mutually insoluble liquids by means of propeller and turbine stirrers in vessels without baffle partitions is represented by Equations (6) and (7), which differ only by the numerical values of the coefficients. The presence of baffle partitions in the vessel changes the situation sharply. In this case the stirring processes are represented by the new Equations (8) and (9), which are also very similar to each other. The only difference lies in the powers of the geometrical similarity criteria Γ_D.

It should be specially noted that, for stirring processes in vessels without baffle partitions, the index i of the geometrical criterion Γ_D is zero, i. e., n_0 calculated from Equations (10) and (11) is virtually independent of Γ_D. This result may be explained as follows. When the stirrer diameter is varied, the determining speed n_0 in a vessel without baffles changes correspondingly in such a way that the Weber criterion • remains constant.

• The Weber criterion $\left(\frac{\rho_m n_0^2 d_S^3}{\sigma}\right)$, which represents the ratio of inertia forces to surface tension forces, characterizes the possibility of emulsification of the system in general.

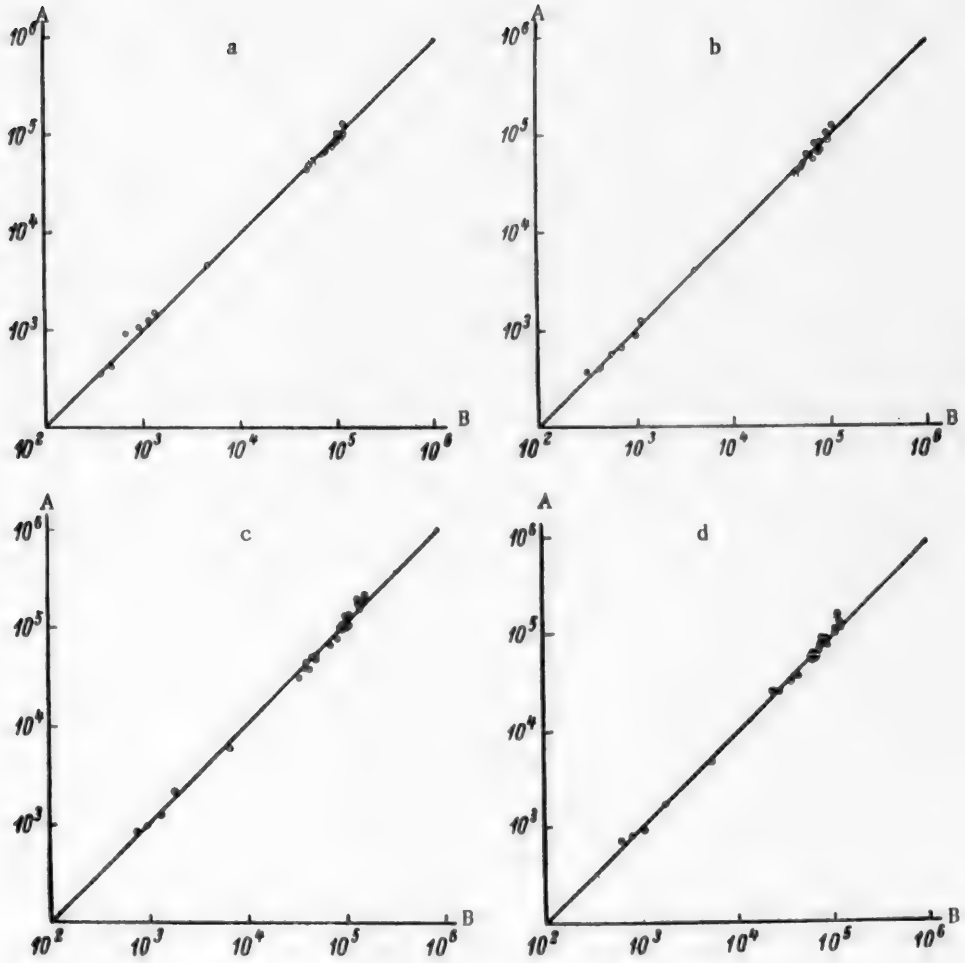

Fig. 2. Comparison of experimental and calculated data.
A) Experimental values of Re_C, B) calculated values of Re_C. a) Propeller stirrer, in vessel without baffles, b) turbine stirrer, in vessel without baffles, c) propeller stirrer, vessel with baffles, d) turbine stirrer, vessel with baffles.

The experimental values are compared with those calculated from Equations (6, 7, 8, 9) in Graphs a, b, c, d (Fig. 2). The average deviation is in the range of 7-15%.

The equations are valid for the following ranges:

$$Re_C = 3.38 \cdot 10^2 - 2.00 \cdot 10^5, \quad Ga = 1.74 \cdot 10^5 - 1.24 \cdot 10^{11},$$
$$\left(\frac{Re_C^2}{We_C}\right) = 2.45 \cdot 10 - 1.18 \cdot 10^7, \quad S_\mu = 0.005 - 246,$$
$$S_{\Delta\rho} = 0.02 - 0.594, \qquad \Gamma_D = 1.72 - 4.00.$$

SUMMARY

1. A theoretical analysis of the mechanical stirring of two mutually insoluble liquids has been carried out, and a mathematical expression has been derived for the conditions at which uniform distribution of the phases is attained.

2. It is shown that, in the ranges studied: a) turbine stirrers are more efficient than propeller stirrers; b) the determining stirrer speed decreases with decreasing distance of the stirrer from the bottom of the vessel and increases with stirrer diameter; c) the determining speed increases with increasing vessel diameter if baffles are present, but is independent of the vessel diameter in absence of baffles; d) variations of the disperse-phase concentration have virtually no effect on the determining speed; e) the determining stirrer speed decreases with increasing density of the medium, and increases with increases in interfacial tension, and of the density and viscosity differences between the two liquids.

3. Equations have been derived for calculation of the determining speeds of propeller and turbine stirrers.

LITERATURE CITED

[1] S. A. Miller and C. A. Mann, Tr. Am. Inst. Chem. Engrs. 40, 709 (1944).

[2] W. D. Harkins, and N. Beeman, J. Am. Chem. Soc. 51, 1688 (1929).

[3] A. J. Stamm, Colloid Symposium Monograph, 3, 251 (1925).

[4] W. C. Moore, J. Am. Chem. Soc, 41, 944 (1919).

[5] A. J. Stamm and E. O. Kraemer, J. Phys. Chem. 30, 992 (1926).

[6] W. Clayton and J. F. Morse, Chemistry and Industry, 304 (1939).

[7] S. Nagata, Chem. Eng. (Japan), 15, 49 (1951).

[8] T. Vermeulen, G. Williams and G. Langlois, Ch. Eng. Prog., 51, 85 (1955).

[9] W. Padger, V. Trice and J. Rushton, Ch. Eng. Prog., 52, 515 (1956).

[10] I. S. Pavlushenko, N. M. Kostin, and B. N. Iachkula, Trans. Lensoviet Technol. Inst. Leningrad, 41 (Goskhimizdat, 1957).

[11] L. Ia. Kremnev and A. A. Ravdel', Colloid J. 16, 1, 17 (1954).

[12] W. Clayton, Theory of Emulsions and Their Technical Treatment (Moscow, IL, 1950) [Russian translation].

[13] I. S. Pavlushenko, N. M. Kostin and S. F. Matveev, J. Appl. Chem. 30, 8, 1160 (1957).

[14] Standards in Chemical Machinery Construction, 1 [In Russian] (Sci. Res. Inst. Chem. Machine Construction, Mashgiz, 1950).

[15] E. J. Lyons, Ch. Eng. Prog., 44, 341 (1948).

Received April 7, 1958.

TESTS OF EXPERIMENTAL STORAGE CELLS WITH GRIDS MADE FROM ALLOYS CONTAINING IMPURITIES*

V. P. Mashovets

Publication of Dasoian's paper [1] on the use of low-grade lead and antimony in storage cells led us to return to an investigation which was carried out several years ago, but remained unpublished. This work completed a series of studies [2-4] on the effects of impurities in lead – antimony alloy on the corrosion and electrochemical properties (overvoltage) of the alloy, and consisted of tests on cells with grids cast from impure alloys. The choice of the impurities tested was governed by considerations of the possible use of incompletely refined lead. The characteristics of the alloys used, methods of preparation, and casting of the specimens are described in an earlier paper [2].

Storage-cell grids 60 x 45 x 4 mm were cast from the alloys, and the weight of each grid was adjusted to 40 ± 0.5 g. The paste was made by one of the powder techniques, and the filled plates were adjusted to weigh 71 ± 1 g. The cells were assembled from three plates each (one positive and two negative, or vice versa), with mipor separators, and tested after assembly and aging runs (7-8 cycles). Two series of tests were carried out, in which not only the alloys but the test methods were different; they are therefore considered separately.

First test series. The metals tested in the first series were pure lead, L_0, an alloy with 5.72% Sb without additions, "synthetic" bismuth alloys Nos. 12 and 14 (the same numbering is used as before [2]), i. e., containing deliberate additions of Bi (0.01 and 0.10%), and "technical" alloys Nos. 13 and 15, with a high Bi content (0.04 and 0.28%) in the original lead (with 5.72% Sb in all cases).

For each alloy 6 cells were assembled; three of these had one positive plate, each with a grid made from the test alloy, and two negative plates made from standard lead – antimony alloy; the other three cells each had one negative test plate and two standard positive plates. The cell capacity was always determined by the test plate, as the presence of two plates of the opposite sign always ensured that their capacity was in excess.

The cells were assembled in RG-1 vessels, which gave a very compact assembly.

After aging (with the cells in the discharged state) the acid density was adjusted to 1.28, and tests were started under accelerated conditions, in which grid corrosion was intensified. The cells were charged at 0.3 amp for 10 days, and a control discharge at 0.26 amp was then carried out; the potential of the single plate, – 1.97 v for the positive plate and 0.25 v for the negative plate (against the cadmium electrode), determined the end of the discharge; this cycle was followed by a 10-day charge and control discharge, etc. The control discharges gave an indication of the state of the plates, as shown by their capacity. In addition, on the day before each discharge the block was removed from the vessel and the plates examined. The temperature was maintained at 26-30° throughout the test period.

Capacity changes of the cells during the tests are shown in Fig. 1. The agreement between the results obtained with three similar specimens is fairly good. The capacity curves for cells with single positive plates, of pure Pb – Sb alloy (No. 4), and alloys containing up to 0.1% Bi (Nos. 12, 13, 14), show capacity increases for 40-50 days, followed by a decrease and finally by an abrupt drop caused by breakdown of the grid and loss of the active paste. In some cases the abrupt drop of capacity could not be observed, as when the cell was inspected before the discharge during which this drop was to be expected, the positive plate broke when removed from the vessel. In such cases the date on which the grid broke was taken as the date on which the service life of the grid ended. If the break was preceded by the abrupt drop of capacity during the previous discharge, the end of the

*Communication IV in the series on the influence of impurities in lead – antimony alloys on grid performance in lead storage cells.

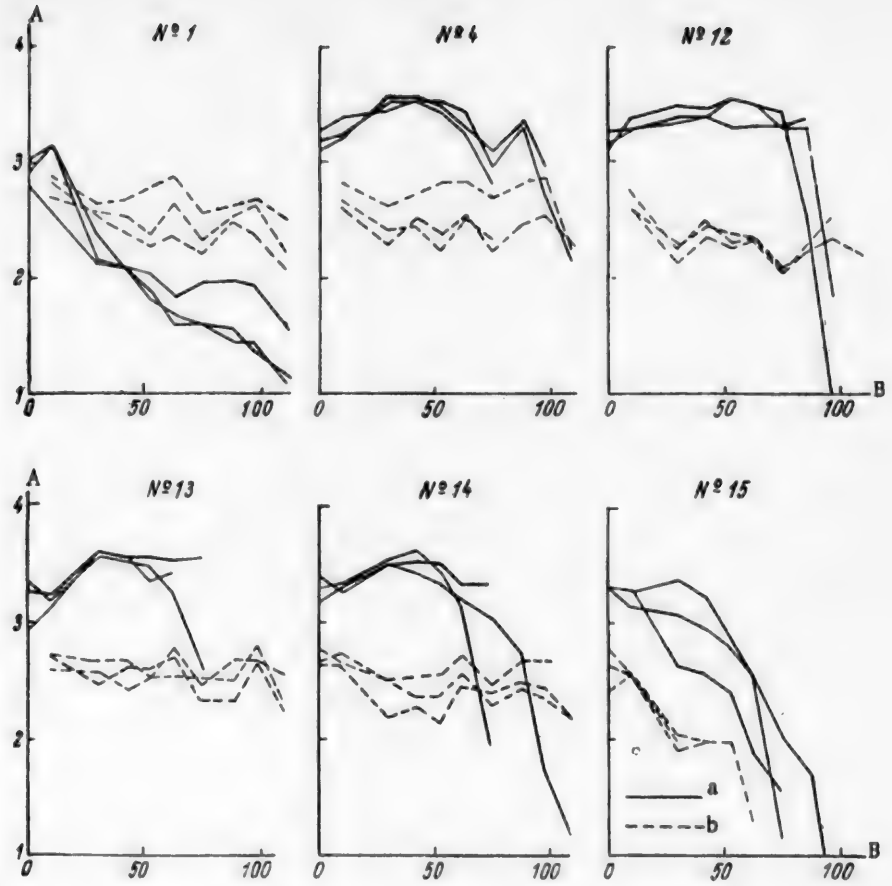

Fig. 1. Capacity curves in the first series of tests on cell discharge.
A) Capacity (amp-hrs), B) time (days). a) One test positive, two standard negative plates; b) one test negative, two standard positive plates. Alloy numbers are given in Table 1.

service life was taken to be intermediate between the last discharge and the break. An error of ± 4 days is possible in this method of evaluation.

Pure lead (No. 1), and alloy No. 15 containing 0.28% Bi, showed capacity decreases right from the start. It is interesting, however, that the pure lead grids remained whole until the end of the tests, and the paste did not fall out, although the capacity fell continuously. The examples in Fig. 2 show that, with the exception of pure lead, not only were the internal ribs broken down completely in all the grids at the end of the tests, but the outer frames were cracked or destroyed.

The grid lives are given in Table 1. The most durable were the lead grids, while the Pb-Sb grids had a somewhat shorter life. In bismuth alloys, the grid life was only a little shorter, by 12-13% as compared with the Pb-Sb alloy, even with 0.28% Bi. The abnormally short life of alloy No. 13 (0.04% Bi) is probably an accidental result, as this alloy proved to be fairly resistant in corrosion tests [2].

Tests on cells containing one negative plate with a grid made from the test alloy, and two standard positive grids, did not yield any characteristic results. Fig. 1 shows that all the cells had virtually the same capacity; the final charge voltage was also the same for all the cells. Therefore neither antimony nor bismuth in the grid of the negative plate had any effect on hydrogen overvoltage. It was found in our measurements on smooth electrodes [4] that these impurities lower overvoltage. It seems, however, that in a storage-cell plate the influence of the grid on overvoltage is negligible in comparison with the influence of the active mass. Therefore this type of assembly was not tested in the second test series.

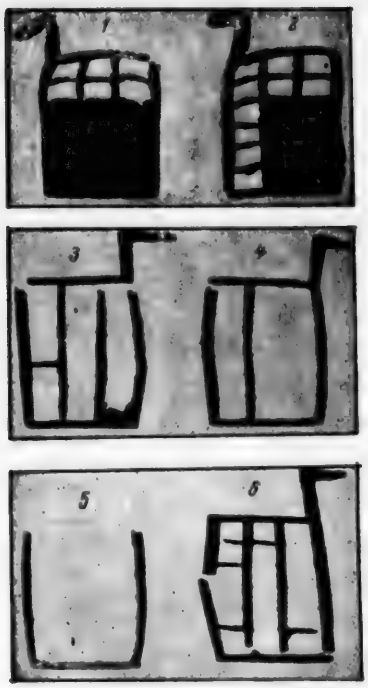

Fig. 2. State of grids after tests. 1 and 2) Pure lead after 109 days, 3) alloy with 5.72% Sb, after 81 days, 4) the same, after 108 days, 5) alloy with 0.28% Bi, after 81 days, 6) the same, after 102 days.

Second test series. In the second series, 18 alloys were tested in the same assembly as in the first series – one positive plate with a grid of the test alloy, and two standard negative plates. In addition, 10 alloys were tested in a new form of assembly – one standard negative plate, and two positive plates of the test alloy. In this version the influence of the impurity might be that, by intensifying the corrosive breakdown of the positive grid, it would increase transfer of antimony to the negative plate, and thereby lower the final charge potential of the negative plate and intensify self-discharge and gas evolution during storage. The test procedure was somewhat modified. The current strength in the 10-day charges was raised to 0.50 amp in order to intensify breakdown and accelerate the tests. The control discharge current was 0.30 amp. The cells were assembled in RG-2 vessels; because of the increase in the amount of acid, the capacities were higher than in the first test series. The method for estimation of the grid stability was also changed. The plates were not inspected before each control discharge. The abrupt fall of capacity in all the cells took place after 6-day or 10-day cycles. All the cells were then dismantled, and the state of the positive plates was evaluated on a 5-point scale:

5 – whole grid intact, paste completely retained in plate;
4 – some ribs destroyed, most of the paste retained;
3 – grid broken down considerably, paste retained in a few cells;
2 – ribs completely destroyed, no paste, only the the frame present;
1 – frame destroyed;
0 – cell withstood less than six cycles.

All the 18 test alloys were divided into 4 groups (I, the most resistant, to IV, the least resistant to corrosion), based on a combined evaluation of the state of three grids made from each alloy.

TABLE 1

Grid Lives in the First Test Series

Alloy No.	Details of alloy	Life (days)			
		individual values			average
1	Pure Pb (L_0)	> 109,	> 109,	> 109	> 109
4	5.72% Sb (without impurities)	87,	108,	109	101
12	0.01% Bi (synthetic)	102,	96,	102	100
13	0.04% Bi (technical)	74,	87,	87	83
14	0.10% Bi (technical)	87,	109,	81	92
15	0.28% Bi (technical)	81,	102,	81	88

TABLE 2

Evaluation of the Corrosion Resistance of Grids from Different Alloys, in the Second Test Series

Alloy No.	Details of alloy	Characteristic impurity (%)	Sb content (%)	State of grids in individual cells (5-point scale)	Group
--	L_0 lead with different antimony grades:				
40	electrolytic	—	5.51	0, 2, 1	III
42	antimony conforming to All-Union Standard 662	—	5.85	0, 2, 1	III
43	refined from slag	As 0.0052 Fe 0.0070	5.79	4, 4, 5	I
44	unrefined Chinese	As 0.012 Fe 0.0038	5.89	4, 5, 5	I
45	crude	As 0.0017 Fe 0.0038	4.93	4, 4, 5	I
	Alloys with lead from the Harris process:				
34	end of process	Zn 0.0005	5.63	2, 2, 4	II
36	the same	Zn 0.0003	5.76	2, 4, 3	II
37	middle of process	Zn 0.0317	5.94	0, 0, 0	IV
38	start of process	Zn 0.1138	5.97	0, 0, 0	IV
	Alloys with artificially introduced impurities:				
7	silver	Ag 0.001	5.72	0, 1, 1	III
9	the same	Ag 0.0118	5.72	5, 1, 3	II
17	arsenic	As 0.0038	5.72	2, 2, 5	II
20	iron	Fe 0.0031	5.76	4, 2, 3	II
23	zinc	Zn 0.0017	5.72	0, 0, 1	IV
26	magnesium	Mg 0.011	5.31	0, 0, 0	IV
31	calcium, without antimony	Ca < 0.02	—	5, 5, 5	I
32	the same	Ca 0.05	—	5, 5, 5	I

The results of these evaluations are summarized in Table 2, and some examples of capacity changes are shown in Fig. 3 (the numbering and exact details of the alloys are given in an earlier paper [2]).

In Table 2, alloys Nos. 40 and 42 with high-grade antimony, and Nos. 34 and 36 with lead from the completed Harris process (treatment of lead with caustic soda and saltpeter) may be considered as standard of the kind generally used in the battery industry. They are classed in Groups III and II. It is interesting to note that alloys with low-grade antimony (Nos. 43, 44, and 45) proved to be more resistant to corrosion, and are classed in Group I. This is probably due to the effect of arsenic and sulfur present in low-grade antimony. These alloys, and alloys Nos. 17 and 20 with artificially added arsenic and iron, give no evidence of any adverse effects of As and Fe. Silver had a protective effect only when its content was relatively high, 0.01% in alloy No. 9. Zinc (alloys Nos. 37, 38, and 23) and magnesium (No. 26) are definitely dangerous impurities. The behavior of antimony-free alloys containing calcium is peculiar. They showed very high corrosion resistance, like pure lead in the first test series but, like pure lead, they produced very rapid decreases of cell capacity even in the first few cycles (Fig. 3). The peculiar nature of the surface film formed as the result of corrosion on lead and on lead – calcium antimony-free alloys probably interrupts contact between the paste and the grid.

Cell assemblies of the second type (one negative plate from the standard alloy, and two positive plates from the test alloy), had lower capacities than those of the first type; this was also found in the first test series. All the grids, positive and negative, were in excellent condition after 6 cycles. The final charge voltage remained fairly stable during all the 6 test cycles, and showed good reproducibility in each group of three cells of the same type. It is therefore permissible to use average values. In cells with positive grids from standard alloy with 5.72% Sb the final charge voltage of the negative plates was 0.27 v (against the cadmium electrode). When positive plates containing silver (up to 0.0118%), bismuth (up to 0.28%), and arsenic (up to 0.012%) were used, the charge

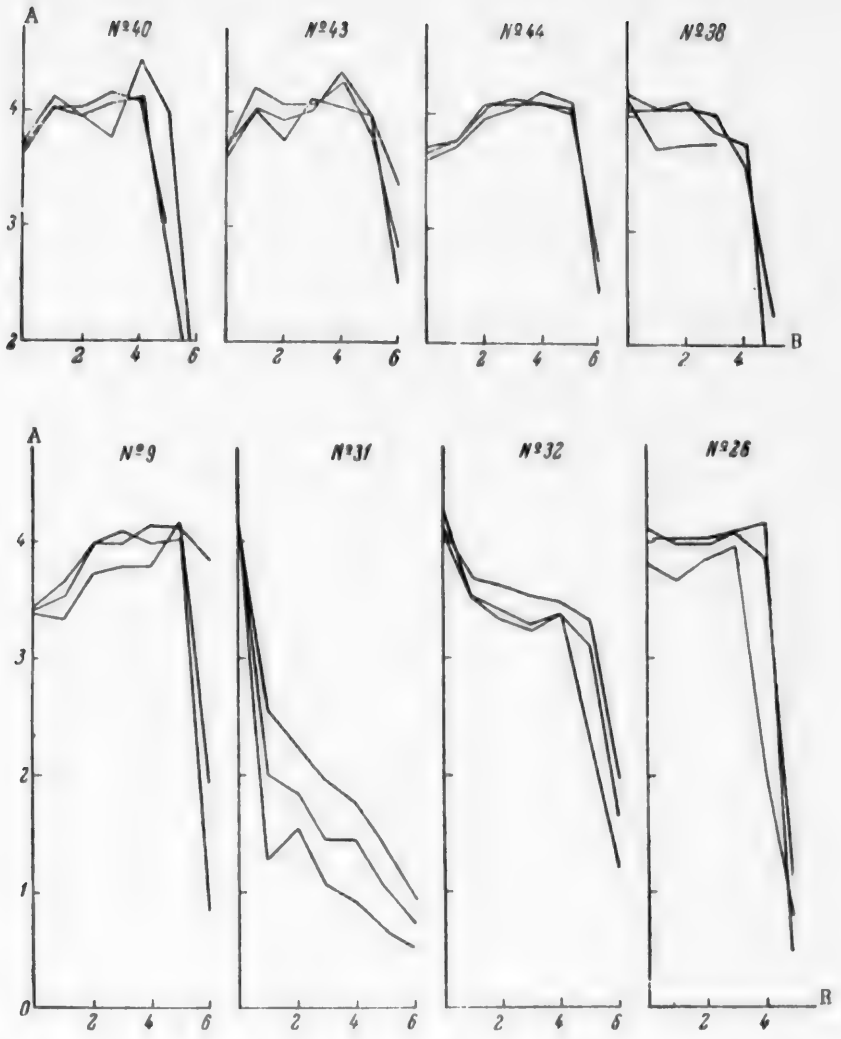

Fig. 3. Capacity curves in the second series of tests on cell discharge.
A) Capacity (amp-hrs), B) cycle number. Alloy numbers are given in Table 2.

voltage of the negative plates did not fall, but even rose to 0.28-0.31 v; this may still lie within the error limits. In any case, there is no evidence of an adverse effect of the impurities, consisting of intensified transfer of antimony to the negative plate and decrease of hydrogen overvoltage. When the calcium alloys Nos.31 and 32 were used in the positive grid, the charge voltage of the negative plate rose to 0.34 v, probably because of the total absence of antimony in these alloys.

It may be concluded from these tests that pure lead is more resistant to corrosion in storage cells than lead – antimony alloy (of course, pure lead cannot be used for grid casting because of its mechanical properties). Admixtures of silver and arsenic in lead – antimony alloy increase its resistance. The use of low-grade antimony has the same effect. Iron, within certain limits, is,at least,harmless as an impurity. Bismuth is a harmful impurity, but its harmful effect has been greatly exaggerated in battery practice. None of these impurities, when present in positive grids, decreases the charge voltage of the negative plate, and therefore none has an adverse effect on cell performance. Zinc and magnesium, even in small amounts, are definitely harmful and sharply lower the corrosion resistance of positive grids. Antimony-free lead – calcium alloys are very resistant to corrosion, but when used for grids they lower the cell capacity; the causes of this are not quite clear, although the effect may be due to the formation of a peculiar intermediate layer which breaks down the contact between the paste and grid.

All these findings are in agreement with the results of our earlier studies [2-4], and support Dasoian's conclusion that it is necessary to revise the standards for lead and antimony used in the storage-battery industry.

SUMMARY

Tests were carried out on laboratory specimens of storage cells, with impurities introduced artificially into the grids of the positive plates; it was found that the stringent specifications for lead and antimony in the storage-battery industry are not justified, and require modification, with an extension of the permissible levels of impurities.

LITERATURE CITED

[1] M. A. Dasoian, J. Appl. Chem. 29, 1827 (1956).*

[2] V. P. Mashovets and A. Z. Liandres, J. Appl. Chem. 21, 347 (1948).

[3] V. P. Mashovets and A. Z. Liandres, J. Appl. Chem. 21, 441 (1948).

[4] V. P. Mashovets and V. N. Fateeva, J. Appl. Chem. 21, 448 (1948).

Received April 5, 1957.

*Original Russian pagination. See C. B. Translation.

INFLUENCE OF ALUMINUM ON THE ANODE EFFECT IN THE ELECTROLYSIS OF CRYOLITE – ALUMINA MELTS

A. I. Beliaev and L. A. Firsanova

Our earlier papers dealt with the influence of excess (undissolved) alumina in the electrolyte [1] and of the composition of the gas phase [2] on the anode effect in electrolysis of cryolite – alumina melts.

Since in industrial aluminum cells the electrolyte is in constant contact with melted aluminum, it was also important to study the influence of aluminum on the anode effect in the electrolysis of cryolite – alumina melts.

This study was carried out by determinations of the critical current density at a carbon anode by the usual method [3], with the difference that the critical current (I_{cr}) was measured in presence of aluminum previously introduced into the electrolyte. In addition, in various experiments the critical current strength was either read visually (by means of an ammeter) or determined from anode-effect oscillograms. Finally, either a dynamotor or a selenium rectifier was used as the direct-current source.

It is known that in acid electrolytes (containing AlF_3 in excess over the composition of cryolite) aluminum reacts with aluminum fluoride, with formation of aluminum subfluoride (univalent aluminum ions), which is surface-active at the carbon boundary,

$$2Al + AlF_3 \leftrightarrows 3AlF$$

or

$$2Al + Al^{3+} \leftrightarrows 3Al^{+}, \qquad (I)$$

and in presence of which the critical current density should increase. In alkaline electrolytes (with excess NaF above the cryolite composition) aluminum displaces sodium, which may partially react with sodium fluoride, likewise forming sodium subfluoride (semivalent sodium ions) which is also surface-active at the carbon boundary.

$$Na^{+} + NaF \leftrightarrows Na_2F$$

or

$$Na + Na^{+} \leftrightarrows Na_2^{+}. \qquad (II)$$

It is therefore to be expected that the critical current density would also increase in alkaline electrolytes in presence of aluminum.

In the first series of experiments the critical current density was measured at 1000° in melts with different cryolite ratios (CR) NaF/AlF_3 (molar), without addition of alumina*; at first the critical current density was measured in absence of metal (the first points), and it was then measured every 30 seconds after immersion of aluminum in the melt.

The results are plotted in Fig. 1. It is seen that about 1 minute after immersion of the metal (which corresponded to the time required for the aluminum to melt) the critical current density rose sharply. In very acid electrolytes (CR = 2) this rise is less than in less acid electrolytes (CR = 2.5 and over) or in alkaline electrolytes, where the critical current density becomes almost double the initial value (measured in absence of metal). However, subsequently the critical current density falls again, the fall being more rapid in acid electrolytes; after

*Certain amounts of the latter were introduced only with aluminum fluoride.

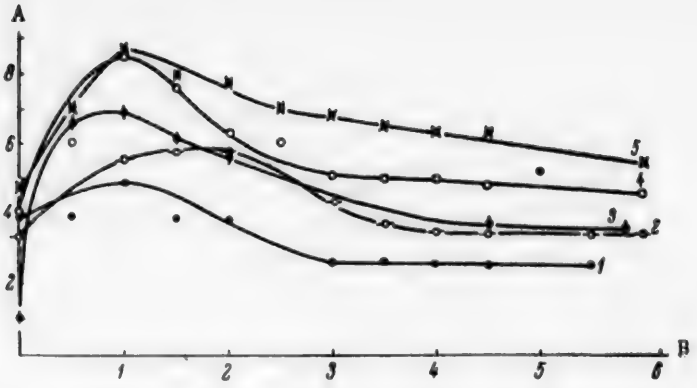

Fig. 1. Effect of the time of contact between cryolite melts and aluminum on the critical current density for melts of different cryolite ratios.
A) Critical current density (amps/cm^2), B) contact time (minutes). Cryolite ratios: 1 – 2, 2 – 2.5, 3 – 3, 4 – 4, 5 – 5.

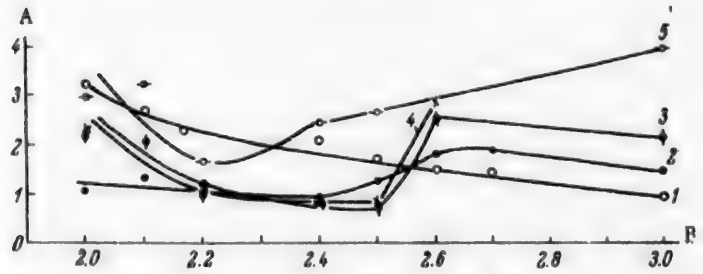

Fig. 2. Variation of critical current density with cryolite ratio of the melt; determinations 5, 10, 15, and 25 minutes after immersion of aluminum in the melt.
A) Critical current density (amps/cm^2), B) cryolite ratio. Time after immersion of Al (minutes): 1) Al and Al_2O_3 absent, 2) 5, 3) 10, 4) 15, 5) 25.

this the critical current density becomes constant, at lower values (even somewhat lower than the initial value) than those for alkaline electrolytes, where the fall of critical current density is slower.

The maxima on the "critical current density – time" curves, found soon after immersion of the metal, may be attributed to the fact that immediately after immersion of aluminum into the melt the metal is dissolved rapidly with formation of surface-active Al^+ ions (in acid melts) or Na^+_2 ions (in alkaline melts), which sharply lower the interfacial tension between the electrolyte and the carbon anode and correspondingly raise the critical current density. The reason why the maxima on the critical current density curves are higher for alkaline electrolytes is probably that, in accordance with the values of the generalized moments* of Na^+_2 and Al^+ ions, which are 0.55 e and 2.05 e respectively, semivalent sodium ions are more surface-active than univalent aluminum ions.

However, reactions take place in the anolyte layer, as the result of which these ions are expended by interaction of the corresponding subhalides with the CO_2 liberated at the anode; in acid electrolytes

* The generalized moment $M=\frac{n \cdot e}{r}$, where e is the electronic charge, n is the valence, and r is the ionic radius (in A).

$$3AlF + 3CO_2 \rightarrow AlF_3 + Al_2O_3 + 3CO \quad \text{(III)}$$

or

$$Al^+ \rightarrow Al^{3+}$$

and in alkaline electrolytes

$$2Na_2F + CO_2 \rightarrow 2NaF + Na_2O + CO$$

or

$$Na_2^+ \rightarrow 2Na^+, \quad \text{(IV)}$$

the current density therefore decreases rapidly again; its ultimate steady value depends not only on the influence of Al^+ or Na_2^+ ions, formed in the melt by the interaction of the electrolyte with aluminum and on the interfacial tension between the electrolyte and anode, but also on the influence of the substances formed in the anolyte layer by the interaction of these ions (subhalides) with CO_2.

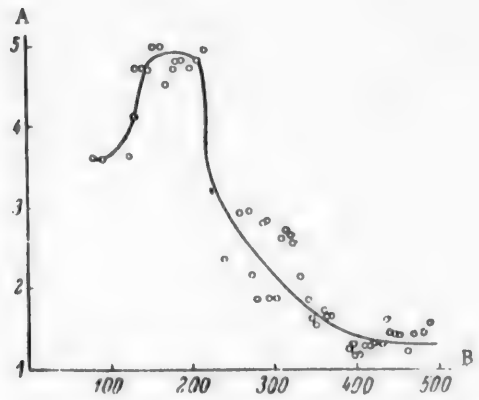

Fig. 3. Effect of the time of contact between the melt (CR = 2) and aluminum on the critical current density, measured by means of a loop oscillograph.
A) Critical current density (amps/cm^2), B) time (seconds).

The anolyte layer of the melt becomes enriched either with aluminum fluoride(Al^{3+} ions), which is not surface-active, or sodium fluoride (Na^+ ions) which is surface-active, but less so than sodium subfluoride (Na_2^+ ions). Moreover, by Equation (III), Al_2O_3 is formed at the anode; this dissolves slowly in very acid electrolytes (CR = 2), and therefore it remains in the melt in a state of suspension for a certain time. It was shown earlier [1] that the presence of this aluminum oxide greatly lowers the critical current density. This probably accounts for the fall of critical current density in acid electrolytes (CR = 2-2.5) in presence of aluminum (after the maximum has been reached) to values even lower than those found in absence of the metal.

In alkaline melts the critical current density also falls after the maximum has been reached, but the critical current density in alkaline melts is always higher in presence of aluminum than in its absence. This is explained by the surface activity of NaF and Na_2O, which are formed by Reaction (IV) near the anode, and which dissolve readily in the electrolyte.

Fig. 2 shows the effect of cryolite ratio of the melt on the critical current density, measured 5, 10, 15, and 25 minutes after immersion of aluminum in the melt, i. e., after the maximum critical current density has been reached, which usually occurs 1-2 minutes after immersion of the metal. It is seen in this graph that in all cases the critical current density for acid electrolytes (CR = 2-2.5) is lower than the critical current density measured in absence of aluminum. It is true that the critical current density measured in electrolytes after they had been in contact with aluminum for 25 minutes increased somewhat, probably because of the increased contents of dissolved alumina, formed by Reaction (III), in such melts. For melts with cryolite ratios of 2.6 and over the critical current density is always higher in presence of aluminum than in its absence, and it increases if the aluminum is present for a long time in the melts owing to increased concentration of surface-active NaF and Na_2O, formed in the anolyte space by Reaction (IV).

Fig. 3 shows the results of determinations of the critical current densities for electrolytes in presence of aluminum, measured by means of a loop oscillograph, for a melt with a cryolite ratio of 2 at 1000°. These results fully correspond to the variations of critical current density in presence of aluminum in acid electrolytes, as described earlier in this paper.

Fig. 4 shows photographs of some actual anode-effect oscillograms for these experiments. The oscillograms

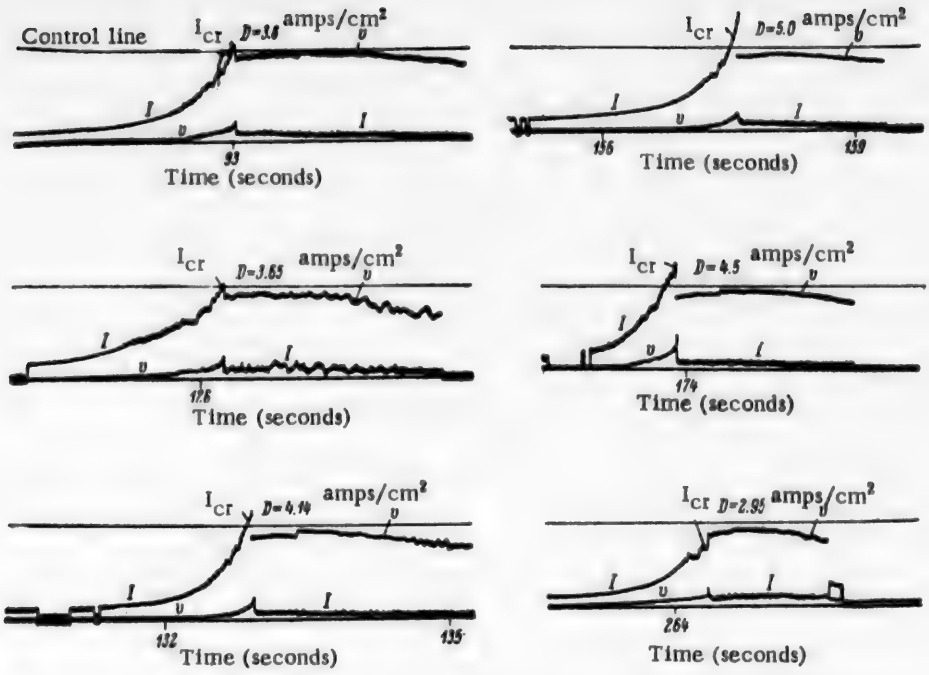

Fig. 4. Anode-effect oscillograms in measurements of the critical current in presence of aluminum in cryolite melts.

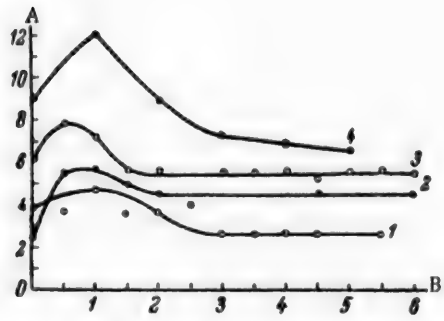

Fig. 5. Effect of the time of contact between cryolite – alumina melts and alumina on the critical current density, with direct current supplied to the cell from a dynamotor. A) Critical current density (amps/cm²), B) time after immersion of Al (minutes). Al_2O_3 content (%) and cryolite ratio respectively: 1) 0 and 2.0; 2) 0 and 3.0; 3) 5 and 2.0; 4) 5 and 3.0.

can be used for very exact determinations of the true critical current (I_{cr}) before the anode effect occurs, and the potential of the anode effect.

In the subsequent experiments the critical current density was measured in cryolite melts of cryolite ratios from 2 to 4, but with a constant alumina content (5%).

The results of these measurements are presented in Figs. 5 and 6; in the former case, direct current was supplied to the cell from a dynamotor, and in the latter, from a single-phase selenium rectifier.

It follows from these results that the relationship between the critical current density for melts containing dissolved alumina, and the time of contact between the melt and metal, is analogous to the relationship for melts without alumina. The only difference lies in the higher absolute values of current density for melts containing alumina.

SUMMARY

1. The effect of aluminum in contact with the electrolyte on the critical current density at a carbon anode in the electrolysis of cryolite – alumina melts was studied; the "critical current density – time" curves for cryolite melts exhibit early maxima, due to formation of Al^+ ions (in acid melts) and Na_2^+ ions (in alkaline melts), which are surface-active at the carbon boundary, in the anolyte layer.

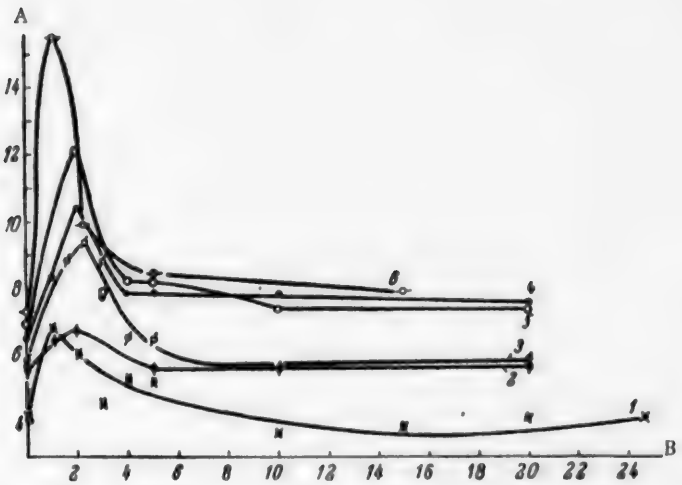

Fig. 6. Effect of the time of contact between a cryolite – alumina melt and aluminum on the critical current density, with direct current supplied to the cell from a single-phase selenium rectifier. A) Critical current density (amps/cm^2), B) time (minutes). Cryolite ratio: 1) 2.0, 2) 2.4, 3) 2.5, 4) 2.7, 5) 3.0, 6) 4.0.

2. The rapid disappearance of these maxima is accounted for by the expenditure of the surface-active Al^+ and Na_2^+ ions by their reaction with the CO_2 liberated at the anode; in consequence (when the steady state has been reached) the presence of aluminum in the electrolyte has no significant influence on the anode effect in the electrolysis of cryolite – alumina melts.

3. The critical current density (I_{cr}) before the anode effect occurs can be accurately determined by means of anode-effect oscillograms.

LITERATURE CITED

[1] A. I. Beliaev, L. A. Firsanova, and E. A. Zhemchuzhina, Nonferrous Metals 3, 35 (1954).

[2] A. I. Beliaev, E. A. Zhemchuzhina, and A. D. Gerasimov, J. Appl. Chem. 29, 12, 1843 (1956).*

[3] A. I. Beliaev, Physicochemical Processes in the Electrolytic Production of Aluminum [In Russian] (Metallurgy Press, 1947), 140.

Received February 18, 1957.

*Original Russian pagination. See C. B. Translation.

CORROSION OF STAINLESS STEELS AT POINTS OF CONTACT WITH NONMETALLIC MATERIALS

I. B. Ulanovskii and Iu. M. Korovin

Mettalic constructions undergocharacteristic corrosion in sea water, in narrow gaps at points of contact with nonmetallic materials [1-4]. Corrosion of this type was observed by the authors in tests on stainless steels in the Black Sea. In many instances it was exceptionally severe. One of the main causes of this characteristic form of attack is considered in this paper.

The degree of attack at the points of contact varied within wide limits for different kinds of stainless steel, but its nature was roughly the same in all cases. This suggests that the destruction mechanism is probably a common one for many kinds of stainless steels. Therefore we confined the study to one kind of steel, others being used only for comparison. Steel 1Kh13 (GOST 5632-51), which is particularly strongly attacked, was taken for the laboratory studies. The specimen surfaces were polished and degreased before the experiments. The nonmetallic materials used were rubber, Plexiglas, and "Textolite". The corrosive medium was Black Sea water. To eliminate changes of concentration, the tests were carried out in large 6 liter glass vessels, and, in some cases, 20 liters in capacity. The temperature of the water was in the 15-16° range. In prolonged tests the water was changed every 48 hours.

The experiments showed that the attack observed at the points of contact is the result of the action of contact – surrounding surface galvanic couples. This follows from the following facts:

1. The breakdown is concentrated in appearance, characteristic of the action of galvanic couples. The contact points are surrounded by loose hydroxides precipitated by alkali from the anodic products.

2. When a galvanic couple acts in sea water, increase of the cathode area intensifies the attack [5]. This was found to be the case in studies of the couples formed by the contact and the surrounding surface (Fig. 1).

The magnitude of the breakdown at the contact points, as a function of the cathode area (anode area 0.8 cm^2, action time of the couple 24 hours) is given below:

Cathode area (cm^2)	540	270	145	80	45
Weight loss (mg)	2.2	1.0	0.8	0.6	0.4

3. The breakdown originates at the boundary and only then spreads and gradually covers the whole contact area. Our investigations showed that this form of attack is characteristic for any anode in contact with a nonmetallic material.

Action mechanism of the couple: contact – surrounding surface. It is known from the literature that, if the electrolyte contains chloride ions, the corrosion products at the anode and in the stagnant zone consist mainly of concentrated solutions of ferrous chloride and chlorides of other metals present in the stainless steel [3]. These solutions, which are acid as the result of hydrolysis [6], break down the passivity of stainless steel [7, 8] and shift the electrode potential in the negative direction. A galvanic couple which arises for any reason can continue to operate for a long time under such conditions, as its subsequent "steady-state" operation is maintained by the anodic process.

Such a breakdown mechanism is quite possible at the points of contact, as the gaps formed there are "ideal" stagnant zones, while sea water contains considerable amounts of chloride ions [9]. To clarify this

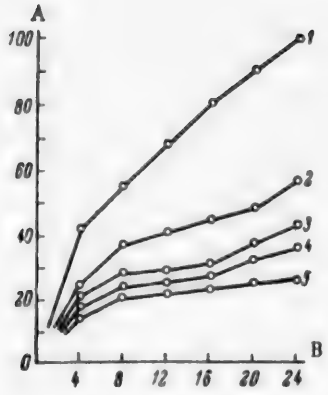

Fig. 1. Effect of cathode size on the current strength in the couple: contact – surrounding surface.
A) Current strength (μa), B) time (hours). Cathode area (cm^2): 1) 540, 2) 270, 3) 145, 4) 80, 5) 45. Anode area 0.8 cm^2; duration of test 24 hours. The zero on the graph corresponds to the instant when current begins to flow in the couple.

Fig. 2. Variation of pH with anodic current density (polarization time 24 hours).
A) pH, B) current density (ma/cm^2) × 10^{-2}.

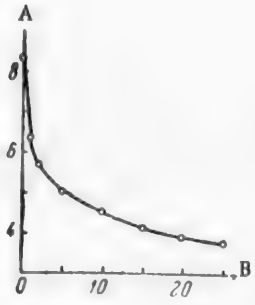

Fig. 3. Variation of pH with the time of anodic polarization (current density 0.12 ma/cm^2).
A) pH, B) time (hours).

question, experiments were performed to determine the possible decrease of pH in the gap, and to study the effect of decreased pH on the electrode potential.

The pH was determined directly at the points of contact by the potentiometric method, and by means of paper and liquid indicators. The minimum pH value recorded was ~3. In order to obtain more exact quantitative data, and to study the influence of a number of factors on pH, cylindrical specimens 20 cm^2 in area were subjected to anodic polarization in a glass cylinder; the amount of electrolyte was 5 cc.

The experiments showed that the pH decreases considerably in the anode space, even at low current densities. The pH decreases with increases of current density and polarization time (Figs. 2 and 3), and with decrease of the volume of water per unit anode area.

The effects of pH on the electrode potential of stainless steel were studied in sea water with additions of HCl. It was found that as the pH decreases the electrode potential is shifted in the negative direction; this shift is especially large at pH < 4, and the potential which results is stable in character (Fig. 4).

Initial breakdown of passivity at the regions of contact. It was stated above that initial formation of an anode is sufficient for prolonged and intense activity of a contact – surrounding surface couple. What is the cause of the initial anodic polarization of the contact surface? To answer this question, numerous contacts were studied immediately after breakdown (which was readily revealed by the appearance of current in the circuit) commenced. It was found that any corrosion point in the contact regions can cause initial anodic polarization. The latter leads to formation of metal-chloride solutions, decrease of pH, and a consequent lowering of the electrode potential of the whole contact area. In the great majority of cases the initial corrosion site originates at the perimeter. The probable explanation is that the steel surface at the contact points and the free surface are not under the same conditions. Because of this, the passive film on the metal surface at the contact differs in properties from the film on the surface outside this contact. It is therefore reasonable to suppose that the junction of these films along the contact perimeter should have many vulnerable points.

In some instances the cause of initial anodic polarization is restricted access of oxygen to the contact gap, and decrease of the amount already available as the result of spontaneous dissolution [3].

Course of attack in the contact regions. For a detailed study of the attack, the Plexiglas used as the nonmetallic material was applied in such a way that the whole contact area remained clearly visible. It was thereby possible to observe and record the origin and subsequent development of the attack (Fig. 5). At the initial instant, points of corrosion arise along the perimeter; their number increases continuously and after some time they form

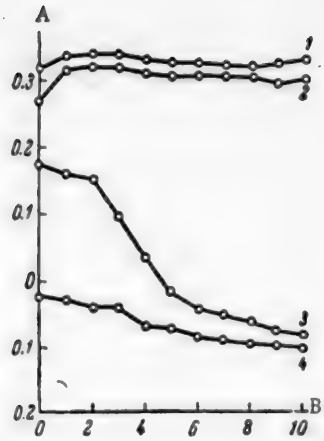

Fig. 4. Electrode potentials of 1Kh13 steel at different values of electrolyte pH.
A) Negative potential (v), B) time (hours). pH: 1) 2.3, 2) 3.0, 3) 4.3, 4) 5.5

an interrupted or continuous thin line. This attack, in the form of a line, gradually widens and migrates toward the center. Simultaneously it increases in depth*. The attack follows exactly the same course in anodic polarization of stainless steel by an external current source, in contact with a nonmetallic material. Because of the speed and convenience of such experiments, this method was used by us in a number of cases.

Fig. 5 represents a case of "ideal" attack at regions of contact. Such attack was observed if the contacting surfaces were strictly parallel, with the presence of a very thin continuous layer of water in the gap, etc. If these conditions are not fulfilled, the attack develops at individual points of the contact surface (Fig. 6). If the cathodic area is small or entirely absent, the attack does not originate at the perimeter, but occurs inside even under "ideal" conditions, although occasional corrosion points may also appear at the perimeter. The nature and intensity of the attack did not differ with the different materials, listed above, in contact with the steel surface. The shape of the nonmetallic body likewise has no influence on the attack (Fig. 7).

Fig. 5. Consecutive development of corrosion in the contact area.
A) Attack after 120 hours, b) after 240 hours, c) after 360 hours.

Fig. 6. Irregular attack in contact region.

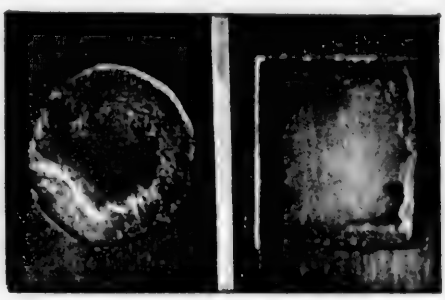

Fig. 7. Attack on contact with nonmetallic bodies of different shapes. Test time 240 hours.

* The literature contains numerous descriptions of corrosive attack in the form of lines at the regions of contact between metallic and nonmetallic surfaces [1]. It seems likely that, in some cases at least, this form of attack was similar to that reported by us, but either only the initial stage was observed, or the attack was greatly retarded.

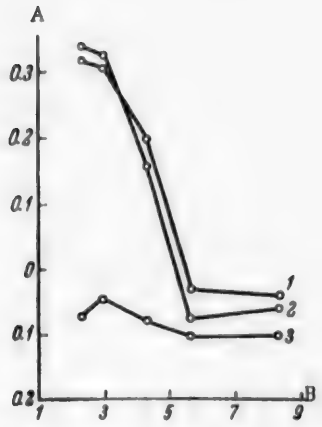

Fig. 8. Variation of electrode potential with pH (after 2 hours of exposure in the electrolyte).
A) Negative potential (v), B) pH. 1) 2Kh13 steel, 2) 1Kh13 steel, 3) 1Kh18N9T steel.

The mechanism of attack at the regions of contact, considered for 1Kh13 steel, is the same for other kinds of stainless steel. However, the intensity of the attack varies very much. For example, 2Kh13 steel is attacked as strongly, while the attack on 1Kh18N9T steel is very much less. Experiments showed that the different rates of attack can be explained as follows: many different kinds of stainless steel show similar large decreases of pH at the anode. However, the effects of the decrease of pH on the electrode potential are different (Fig. 8); this effect is one of the principal factors which determines the rate of attack at the regions of contact. This was confirmed by tests on the specimens under laboratory conditions and in the sea itself. The tendency of stainless steels to undergo attack at regions of contact with nonmetallic materials can be rapidly determined with the aid of graphs similar to that shown in Fig. 8; the degree of displacement of the electrode potential in the negative direction is a measure of the possible attack.

SUMMARY

1. One of the principal causes of corrosion of stainless steels at regions of contact with nonmetallic materials is activation of the metal surface owing to decreased pH of the electrolyte in the gap. This results in prolonged and stable action of couples formed by the contact and the surrounding surface.

2. The results provide a simple accelerated method for determination of the tendency of stainless steels to undergo corrosion at regions of contact.

LITERATURE CITED

[1] U. R. Evans, Metallic Corrosion, Passivity, and Protection (1941). *

[2] I. L. Rozenfel'd and I. K. Marshakov, J. Phys. Chem. 30, No 12 (1956).

[3] H. Uhlig (editor), Corrosion Handbook, 1 (1952). *

[4] K. M. Huston and R. B. Teel, Corrosion, No 7, 251 (1952).

[5] G. V. Akimov, Fundamentals of Corrosion and Metal Protection (1946). [In Russian]

[6] V. N. Alekseev, Course in Analytical Chemistry (1951). [In Russian]

[7] G. V. Akimov, Proc. Commission on Prevention of Metal Corrosion, 2 (1956). [In Russian]

[8] N. L. Tomashov, Corrosion and Metal Protection, 1 (1952). [In Russian]

[9] V. I. Vul'fson, Proc. Commission on Prevention of Metal Corrosion, 1 (1951). [In Russian]

Received February 8, 1957

* Russian translation.

MECHANISM OF THE CHEMICAL PROCESSES TAKING PLACE IN CYANIDING BATHS

V. A. Shushunov

(The Gor'kii Chemical Scientific Research Institute)

Studies of the mechanism of reactions taking place in liquid mixtures of cyanides, chlorides, and carbonates of the alkali and alkaline-earth metals are of considerable interest in relation to the cyaniding of steels. Definite views can be advanced on this problem as the result of our researches [1-5].

First, it should be noted that a study of the literature on the cyaniding of steels [6-9] led us to the conclusion that the mechanism of the chemical processes taking place in cyaniding baths has not yet been elucidated. Some of the papers cited [6, 7] contain discussions of chemical reactions, said to take place in cyaniding baths, which are quite impossible to carry out under these conditions. For example, Minkevich [7] considers that denitriding of steel occurs with formation of nitrogen trichloride and liberation of metallic barium. This is quite incorrect, as NCl_3 cannot exist, especially in presence of metallic barium, at the cyaniding temperature (800-950°). It is known that this compound decomposes explosively even at 100°.

The results of our investigations make it possible to put forward a scheme to represent the mechanism of the reactions taking place in liquid mixtures of cyanides with chlorides of the alkali and alkaline-earth metals, which is in full agreement with experimental results and literature data. This scheme may be successfully extended to processes in cyaniding baths.

Accordingly, the subsequent discussion of the data in this paper is divided into two parts: the first deals with low-temperature cyaniding, and the second, with high-temperature cyaniding, also known as liquid case-hardening of steel.

1. Low-temperature cyaniding of steel. In low-temperature cyaniding, the steel articles are placed in a fused mixture of cyanides, chlorides, and carbonates of alkali metals (potassium, or more often sodium) at 650-800°.

Potassium and sodium cyanides are thermally-stable compounds, but at high temperatures they can decompose slowly according to the equation

$$MCN = M + C + N. \qquad (1)$$

Liberation of the alkali metal (M) in this reaction was confirmed earlier.

Reaction (1) proceeds slowly at the cyaniding temperature, but it is greatly accelerated by iron. This is convincingly confirmedby our experiments, the results of which are partially summarized in Table 1. These experiments were performed in a quartz vessel in nitrogen, to avoid oxidation of cyanide by atmospheric oxygen. It follows from the data in Table 1 that the presence of iron in fused potassium cyanide favors thermal decomposition of this compound.

Reaction (1) accounts for the possibility of carrying out the cyaniding process in presence of nitrogen over the fused salt mixture, which was established a long time ago [10].

It is known that cyaniding is accelerated by the presence of an oxidizing medium, such as air or carbon dioxide, over fused mixtures of cyanides with other salts [6, 7]. For this reason certain oxides, such as silica, are sometimes even added deliberately to cyaniding baths.

TABLE 1

Effect of Iron on the Thermal Decomposition of Potassium Cyanide at 800°

Reaction time (minutes)	Contents of cyanide nitrogen in reaction product (%)	
	without iron	with iron powder
0	21.5	21.5
5	20.0	19.6
10	18.3	16.3
15	18.7	11.6
20	18.1	9.8
30	—	7.2

TABLE 2

Thermal Decomposition of Potassium Cyanide and Cyanate in Presence of Iron Powder

Reaction time (minutes)	Degree of decomposition (%)	
	KCN	KNCO
5	0	65
10	23	—
15	46	—
20	55	75
30	67	—
40	—	82

The favorable effect of such oxides on the cyaniding of steels is attributed to the formation of alkali-metal cyanates as intermediate compounds

$$2MCN + O_2 = 2MNCO, \quad (2)$$

$$2MCN + SiO_2 = 2MNCO + Si, \quad (3)$$

$$MCN + CO_2 \rightleftarrows MNCO + CO. \quad (4)$$

The alkali-metal cyanates formed in Reactions (2) - (4) have high thermal stability. However, in presence of certain metals which act as catalysts these compounds decompose fairly rapidly even at 650° with formation of cyanides and carbonates.

The mechanism of thermal decomposition of alkali-metal cyanates can be represented by the following reaction stages.

Alkali-metal cyanates exist in two tautomeric forms, the equilibrium between which is far on the right-hand side

$$MOCN \rightleftarrows MNCO. \quad (5)$$

One of these forms, MNCO, in our opinion, decomposes at high temperatures according to the equation

$$MNCO = M + N + CO. \quad (6)$$

The carbon monoxide liberated in Reaction (6) reduces the cyanate to cyanide according to Equation (4). We showed earlier [1] that this is a reversible process. It proceeds in both directions at considerable rates even at 700°, and very rapidly at 800°.

The alkali metal liberated in Reactions (1) and (6) reacts with carbon dioxide, cyanate, or carbonate present in the melt

$$2M + CO_2 = M_2O + CO, \quad (7)$$

$$2M + MNCO = M_2O + MCN, \quad (8)$$

$$2M + M_2CO_3 = 2M_2O + CO. \quad (9)$$

Moreover, the carbon dioxide liberated in Reactions (6), (7), and (9) undergoes a further change

$$2CO \rightleftarrows C + CO_2. \quad (10)$$

The reversible Reaction (10) is catalyzed by iron [11], and therefore this process occurs predominantly on the surfaces of the treated articles.

The atomic carbon liberated by Reactions (1) and (10) dissolves in iron, forming a solid solution or iron carbide. The atomic nitrogen, liberated in Reactions (1) and (6), behaves similarly and forms a solid solution or iron nitride.

The alkali-metal oxide formed in Reactions (7) - (9) readily reacts with carbon dioxide

$$M_2O + CO_2 = M_2CO_3. \quad (11)$$

The dissociation pressures of sodium and potassium carbonates do not exceed 15 mm Hg even at the highest temperatures used in low-temperature cyaniding; therefore these salts do not dissociate within the melt, but only on the surface of the cyaniding bath.

TABLE 3

Conversion of Cyanides into Cyanamides in Presence of Barium and Strontium Chlorides

Original mixture	Temperature (in °C)	Reaction time (minutes)	Nitrogen content (% of sample)	
			cyanide	cyanamide
$2NaCN + BaCl_2$	600	0	28.5	0
		3	18.3	
		5	14.5	
		10	16.8	Traces
		20	16.0	
	550	0	28.5	0
		5	21.6	1.3
		10	22.6	1.5
		20	20.4	1.9
		30	20.3	2.3
$2NaCN + SrCl_2$	600	0	28.5	0
		5	25.9	2.3
		10	20.5	3.2
		20	15.9	3.6
		40	16.0	5.4
	550	0	28.5	0
		5	22.5	3.8
		10	16.2	8.0
		20	12.0	11.0
		30	12.2	11.8

TABLE 4

Thermal Decomposition of Barium Cyanamide

Reaction time (minutes)	Degree of decomposition of barium cyanamide (%)	
	without iron	with iron powder
3	—	80
5	28	87
10	30	94
15	35	94

The above stages in the thermal decomposition of alkali-metal cyanides account for the formation of their carbonates and cyanides, carbon monoxide and dioxide, and iron nitrides and carbides, and also for the liberation of elemental carbon and nitrogen. We found that the amounts of carbonates, cyanides, and carbon monoxide and dioxide can be either more or less than the amounts corresponding to the over-all reaction which is assumed [6, 7] to take place:

$$4MNCO = M_2CO_3 + 2MCN + CO + N_2. \quad (12)$$

Equation (12) does not take into account a number of other processes, such as Reactions (7) and (10), which greatly influence the balance of the final reaction products.

In studies of the kinetics of the thermal decomposition of potassium cyanate we found that the amount of cyanide formed by the reaction in presence of iron first increases with the reaction time, reaches a maximum, and then decreases, often to a very small value. This relationship between cyanide concentration and reaction time is the result of competition between Reactions (4) and (8) on the one side, and Reactions (1) and (6) on the other.

The amount of potassium carbonate increases continuously in the decomposition of potassium cyanate, although oxidation of MCN and MNCO by atmospheric oxygen was quite impossible in our experiments.

The increase of the cyaniding power of cyaniding baths caused by the presence of alkali-metal cyanates was first observed a relatively long time ago. In our opinion this effect is due to the easier thermal decomposition of cyanates as compared with cyanides. Two series of special experiments were carried out to test this view. In the first series, potassium cyanide mixed with iron powder was thermally decomposed in a quartz tube in a nitrogen medium at 800°, and in the second series, a mixture of potassium cyanate with iron powder was heated in nitrogen at 600°. The results of these experiments are summarized in Table 2.

It follows from Table 2 that, in presence of metallic iron, potassium cyanate decomposes much more rapidly even at 600° than the cyanide does at 800°. If KNCO is thermally decomposed at 800°, the process is complete within only 5-10 minutes.

Therefore low-temperature cyaniding is effected mainly as the result of oxidation of cyanide to cyanate; subsequent rapid decomposition of the latter on the surface of the treated articles results in saturation of their surface layers with nitrogen and carbon.

A brief discussion of the nature of the catalytic effect of metals on the thermal decomposition of cyanates is necessary.

We showed earlier [1] that the catalytic effect in the thermal decomposition of cyanates depends very strongly on the nature of the metal.

Differences in the abilities of the metal catalysts to form carbides, nitrides, and oxides have no effects at all on their catalytic properties with respect to the reaction in question. Thus, according to our data, the catalytic power of silver is greater than that of copper, but much less than that of iron. Copper and iron form thermally-stable oxides, whereas silver oxide dissociates readily at the experimental temperature (above 600°). There is thus no connection between the oxide stability and catalytic activitity of these three metals.

Copper and silver do not form thermally-stable nitrides and carbides. Nitrogen and carbon are virtually insoluble in these metals [12], whereas boron and iron form solid solutions with nitrogen and carbon, and also give nitrides and carbides. However, the catalytic activity of iron is much higher than that of boron. Boron is close to copper and silver in this respect, although the latter differ from each other in catalytic properties [1].

These facts indicate that in this instance metals are typical catalysts of the thermal decomposition of cyanates, while formation of iron nitrides and carbides, and of solid solutions of nitrogen and carbon in iron, constitutes secondary processes.

2. High-temperature cyaniding or liquid case-hardening of steel. The mechanism of the chemical processes in liquid salt baths used for high-temperature cyaniding differs from the mechanism of the reactions in salt mixtures used for low-temperature cyaniding. There are two main causes of this difference: 1) addition of barium or strontium salts to the mixture, and 2) the low degree of oxidation of cyanides due to the formation of a protective layer of graphite or other substances on the surface of the melt.

In these liquid salt mixtures, which consist mainly of alkali-metal cyanides and chlorides, and barium chloride or (more rarely) strontium chloride, the following equilibrium is rapidly established:

$$2MCN + BaCl_2 \rightleftarrows 2MCl + Ba(CN)_2. \quad (13)$$

The barium cyanide formed dissociates according to the equation

$$Ba(CN)_2 \rightleftarrows BaCN_2 + C. \quad (14)$$

The results of some of our experiments, presented in Table 3, illustrate the nature of reactions (13) and (14).

It follows from the data in Table 3 that the cyanamide content of the salt mixture decreases with increasing temperature. Strontium chloride is more active than barium chloride in preventing the conversion of cyanide into cyanamide, while calcium chloride is even more active in this respect.

The equilibrium in Reaction (14) is shifted far to the left at temperatures of 900° and over [13]. However, this reaction does not reach the equilibrium state in cyaniding baths, as the final reaction products are consumed all the time; atomic carbon dissolves in iron, thereby carburizing the steel, while barium cyanamide is expended as the result of a further reaction

$$2MCl + BaCN_2 \rightleftarrows M_2CN_2 + BaCl_2. \quad (15)$$

It has been shown [4] that cyanamides of the alkali metals decompose at high temperatures according to the equation

$$M_2CN_2 = MCN + M + N. \quad (16)$$

Our quantitative determinations showed that in some cases the amount of cyanide formed reached 90-95% of the theoretical amount corresponding to Equation (16). Somewhat low results (85-90% of the theoretical) were obtained in determinations of alkali metals and nitrogen in these experiments.

The decomposition of barium cyanamide proceeds similarly, but at a considerably lower rate

$$2BaCN_2 = Ba(CN)_2 + Ba + N_2. \quad (17)$$

We found [4] that metallic iron catalyzes reactions (16) and (17), and therefore decomposition of cyanamides, like Reactions (1) and (6), occurs mainly at the surface of the treated articles. The catalytic effect of iron powder on Reaction (17) is illustrated by the data in Table 4, determined at 940°.

The cyanides formed in Reactions (16) and (17) again take part in Reactions (13) and (14).

The alkali metal liberated by Reactions (16) displaces barium from its chloride

$$2M + BaCl_2 \rightleftarrows 2MCl + Ba. \quad (18)$$

The metallic barium liberated in Reactions (17) and (18) reacts with the nitrogen present in the free state in the liquid salt mixture, or with nitrogen dissolved in the surface layer of the metal articles undergoing treatment, to form a very stable compound, barium nitride. Because of this reaction, the concentration of metallic barium in the liquid salt mixture is vary low, and the equilibrium in Reaction (18) is therefore shifted far to the right.

Moreover, barium may react with iron nitride, reducing it to the metal.

The reactions of barium with nitrogen and with iron nitride result in denitriding of the surface layers of the treated articles. Increase of the degree of dissociation of iron nitrides with rise of temperature also favors denitriding.

SUMMARY

A mechanism is suggested for the reactions taking place in salt mixtures in low-temperature and high-temperature cyaniding of steels. The proposed scheme accounts satisfactorily for the carburizing and nitriding of treated iron articles and for the formation of the final reaction products, and is fully consistent with all the process characteristics determined experimentally.

LITERATURE CITED

[1] V. A. Shushunov and N. K. Serdiuk, Proc. Acad. Sci. USSR 93, 507 (1953).

[2] V. A. Shushunov and A. M. Pavlov, Proc. Acad. Sci. USSR 89, 1033 (1953).

[3] V. A. Shushunov and A. M. Pavlov, J. Appl. Chem. 28, 1, 98 (1955). *

[4] V. A. Shushunov and A. M. Pavlov, J. Appl. Chem. 28, 9, 934 (1955). *

[5] V. A. Shushunov and A. M. Pavlov, J. Appl. Chem. 28, 10, 1161 (1955). *

*Original Russian pagination. See C. B. Translation.

[6] S. Z. Regirer, Liquid Case-Hardening of Steel (Mashgiz, 1949). [In Russian]

[7] A. N. Minkevich, Chemicothermal Treatment of Steel (Mashgiz, 1950). [In Russian]

[8] D. A. Prokoshkin, Theory and Practice of the Cyaniding of High-Speed Steels (Moscow, All-Union Scientific Society of Mechanical Engineers and Technicians, 1940). [In Russian]

[9] S. M. Liass, Cyaniding of Steel and its Industrial Applications (GONTI, 1939). [In Russian]

[10] G. Barsky, Trans. Am. Soc. Steel Treat. 20, 347 (1932).

[11] S. Berkman, J. C. Morell, and G. Egloff, Catalysis (State Fuel Press, 1949) [Russian translation].

[12] M. Hansen, Structure of Binary Alloys (GONTI, 1941) [Russian translation].

[13] H. Frank, and R. Neubner, Z. Elektroch. 40, 693 (1934).

Received July 8, 1956.

KINETICS OF THE EVAPORATION OF PETROLEUM OILS

F. K. Volynets

Evaporation of volatile components of petroleum lubricating oils causes a number of undesirable effects [1-5]. Therefore, the volatility characteristics of an oil are important in evaluation of its suitability under given conditions of use. In most cases these characteristics should give an indication of the amount of oil which evaporates under specified conditions in a given time. This is necessary for estimation of the effects of evaporation of the volatile components of the oil on its other properties. In some instances they should also indicate the vapor pressure of the oil (in the case of compressor oils and oils used in optical instruments).

The widely used method for evaluation of oil evaporation by determination of the weight loss of a sample under fixed evaporation conditions does not provide answers to any of the above questions, and is therefore unsatisfactory, and suitable only for control tests. A measure of oil evaporability which provides answers to these questions can at the present time be obtained only from data on evaporation kinetics. This explains why all recent work in this field deals with this problem [3, 4]. However, no relationships between the evaporation rate or weight loss and the evaporation conditions have been determined as yet, and the equations which have been proposed cannot be regarded as satisfactory.

For example, Fuks and his associates [2, 3] expressed the relationship between the weight loss of an oil sample and its evaporation time at constant temperature by the following equation:

$$U = K_1 + K_2 t, \tag{1}$$

where K_1 and K_2 are constants determined from experimental data; t is the evaporation time (hours); U is the weight loss for a given evaporation area (%).

The evaporation rates of petroleum oils, which are complex mixtures, are not constant. Therefore Equation (1) is applicable to only very narrow ranges of the U – t relationship. The effect of temperature on the volatility of the oils was represented in terms of the weight loss as a function of temperature for a constant evaporation time [2, 3], by the following equation:

$$U_t = K_1 + K_2 T, \tag{2}$$

where U_t is the weight loss (%) in a fixed evaporation time, and T is the temperature (in °).

In the case of petroleum oils, the relationship between the weight loss and temperature for a constant evaporation time characterizes the fractional composition of the oil. This was the basis of the method proposed by Papok et al. [6] for estimation of the fractional composition of oils. In the case of petroleum oils, however, this relationship does not represent the effect of temperature on the evaporation rate, and therefore Equation (2) cannot be used for quantitative evaluation of oil volatility over prolonged periods under actual service conditions.

Martynov [4] represented the evaporation kinetics of petroleum oils by the following equation, which he derived analytically:

$$\frac{at}{g_0} = \nu + b \lg (1 - \nu), \tag{3}$$

where a and b are constants, determined from experimental data; t is the evaporation time (minutes); g_0 is the initial weight (mg), and ν is the fraction of the sample evaporated.

Martynov considers Equation (3) to be so sound theoretically that even the constants a and b can be calculated in advance. This seems to us to be an exessively optimistic view, because the assumptions on which the equation is based cannot be regarded as completely substantiated. Moreover, as will be shown later in this paper, it is not in satisfactory agreement with experimental data.

On the assumption that the evaporation rate is determined by the vapor pressure, Martynov expresses the relationship between the evaporation rate and temperature by an equation analogous to the known equation for vapor pressure as a function of temperature:

$$\lg V = A + B/T, \tag{4}$$

where A and B are constants, T is the temperature (in ° K), and V is the evaporation rate.

However, calculation of the latent heat of evaporation from his data on the slope of the line $\log V = f(\frac{1}{T})$ gives a value of about 8000 cal/mole, which differs from known data. In our opinion, this indicates that the evaporation rate of a petroleum oil is not a function of its vapor pressure alone.

The volatility of petroleum oils was studied by the method described previously [7]. The oils were evaporated from paper strips 20 x 25 mm in a current of nitrogen; the original weight taken was 10-60 mg, the evaporation surface was 10 cm^2, and the average velocity of the nitrogen stream was 1.38 cm/second (1 liter per minute). The following oils were studied: MVP instrument oil, transformer oil, AU spindle oil, and MS-14 aviation oil. Since the laws found for evaporation from thin layers proved to be generally applicable to all the oils, the results presented here, for the sake of brevity, are mainly those obtained for MVP oil.

Table 1 contains data on the evaporation kinetics of different initial weights of MVP oil at 90°. It follows from these results that the evaporation rate of the oil, in contrast to individual liquids, is not constant, and the weight loss depends on the initial weight taken – for a constant evaporation time, the greater the initial weight, the greater is the weight loss. This makes the determination of an equation for the evaporation kinetics of petroleum oils much more difficult.

TABLE 1
Effect of Evaporation Time on Weight Loss for Different Initial Sample Weights of MVP Oil, 90°

Evaporation time (minutes)	Weight loss m (mg) from an initial sample weight g_0 (mg)										Amylnaphthalene
	60.95	56.00	51.25	47.20	37.75	32.75	27.35	21.35	16.65	11.95	
5	—	—	—	—	2.80	—	2.35	2.50	2.10	1.80	3.05
15	7.00	6.00	6.80	6.45	5.85	5.60	5.00	4.35	4.05	3.30	9.05
30	10.75	10.40	9.95	9.70	8.55	8.15	7.20	6.20	5.65	4.50	—
45	13.50	12.90	12.30	12.00	10.45	9.90	8.65	7.35	6.60	5.25	—
60	15.60	14.90	14.15	13.75	—	11.15	9.80	8.50	—	—	—
75	—	—	15.75	15.25	—	—	—	—	—	—	—

To determine the effect of the initial sample weight on the weight loss, the time required for evaporation of a constant fraction of the sample was determined for different initial sample weights. It was found that this time is directly proportional to the weight of the initial sample, and the relationship can therefore be represented by the linear equation

$$t_\nu = a g_0, \tag{5}$$

where t_ν is the time required for evaporation of a fixed fraction of the sample (minutes), and a is a constant.

The constant a or the ratio t/g_0, is a function of the fraction of the sample evaporated. Therefore, if the experimental data are plotted in $\nu - t/g_0$ coordinates, all the points lie on one curve, regardless of the initial weight taken. This simplifies the search for an equation for the evaporation kinetics. However, the relationship between

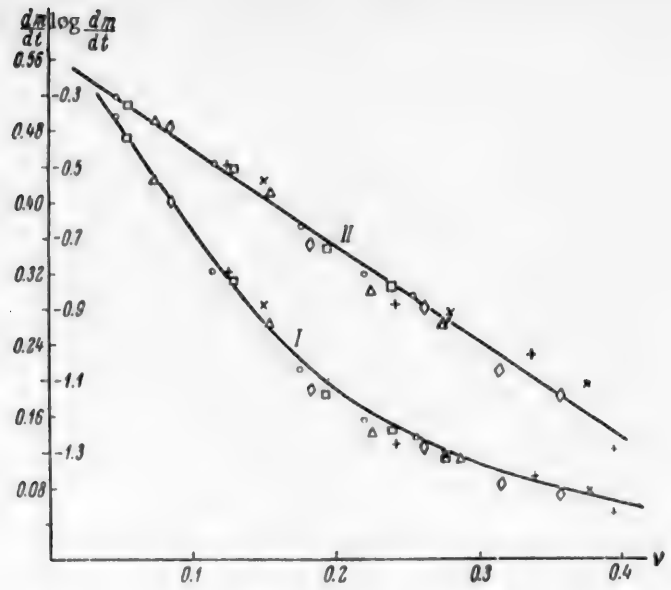

Fig. 1. Relationship between the true evaporation rate and the fraction of the sample evaporated. The points in Figs. 1, 2, and 3 correspond to initial samples weighing from 60.95 to 11.95 mg.

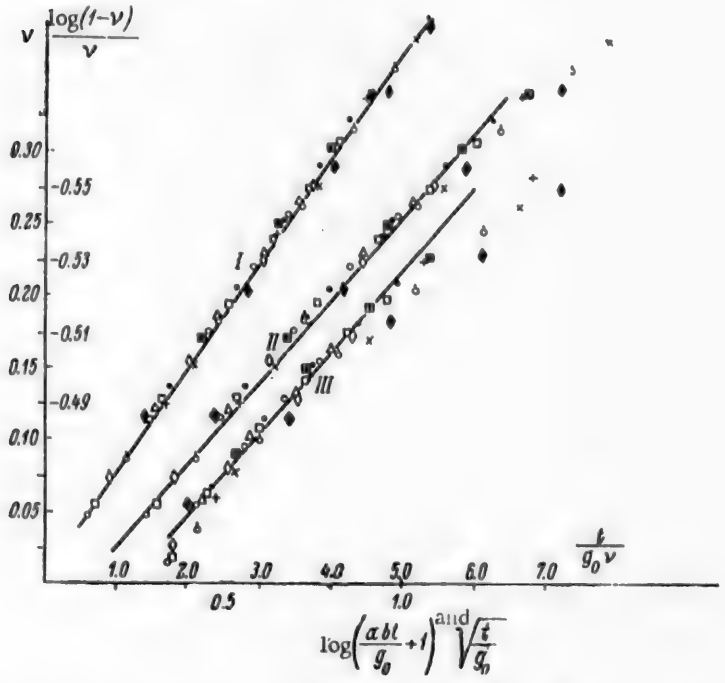

Fig. 2. Agreement between experimental data and different equations for the kinetics of oil evaporation.
I) Equation (7), II) Equation (13), III) Martynov's equation (3).

t/g_0 and the fraction of the sample evaporated is rather complex, and we did not succeed in determining it. It was noted that the constant a is directly related to the average rate of evaporation; this follows from its dimensions (minutes/mg). Therefore the average evaporation rate, like the constant a, should be a definite

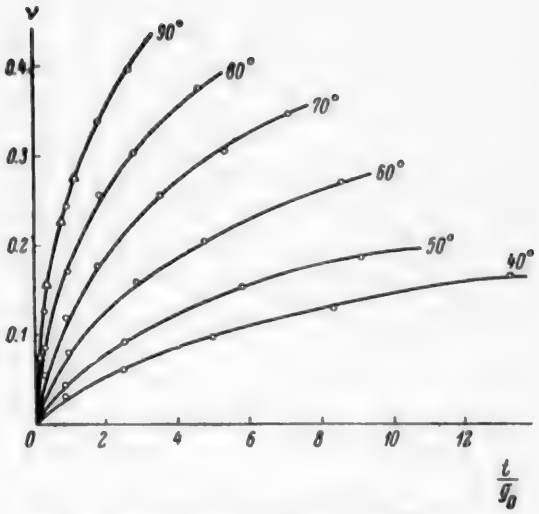

Fig. 3. Volatility of MVP oil at different temperatures.

function of the evaporated fraction of the initial sample. Accordingly, the relationship between the true rate of evaporation and the fraction of the sample evaporated was used for determination of the kinetic equation. The true evaporation rate was found by graphical differentiation of the function m = f(t). The relationship between the true evaporation rate of MVP oil and the fraction of the sample evaporated at 90° is plotted in Fig. 1 (Curve 1). It is seen that all the points, irrespective of the initial sample weight, lie on the same curve; this confirms that the evaporation rate is directly associated with the fraction of the sample evaporated. This relationship proves to be linear if plotted in semilogarithmic coordinates (Line II). It may therefore be expressed by the following exponential equation, which is the equation for the evaporation kinetics of petroleum oils:

$$\frac{dm}{dt} = ae^{-bv}, \qquad (6)$$

where $\frac{dm}{dt}$ is the true evaporation rate (mg/minute).

TABLE 2

Values of the Constants a and b at Different Temperatures

Temperature (in °)	MVP oil		Transformer oil		AU oil		Evaporation rate of amylnaphthalene (mg/minute)
	a (mg/minute)	b	a (mg/minute)	b	a (mg/minute)	b	
90	0.631	6.12	0.348	6.67	0.1335	6.73	0.600
80	0.354	6.71	0.208	7.20	0.0742	7.71	0.320
70	0.2095	7.23	0.118	8.45	0.0361	8.80	0.180
60	0.116	8.39	0.0768	10.46	0.0191	10.47	0.080
50	0.0604	9.89	0.0441	12.70	—	—	0.0425
40	0.0357	11.46	—	—	—	—	0.02335

Integration of Equation (6) yields the following expression for the relationship between the fraction of the sample evaporated, evaporation time, and initial sample weight:

$$\frac{t}{g_0} = \frac{1}{ab}(e^{bv} - 1). \qquad (7)$$

To test its agreement with experimental data, Equation (7) was transformed into the linear equation

$$\lg\left(\frac{abt}{g_0} + 1\right) = \frac{bv}{2.3}, \qquad (8)$$

and the experimental data were accordingly plotted in $v - \log[(abt/g_0 + 1)]$ coordinates (Fig. 2). Despite the great variations of the initial weight, and with variations of the fraction evaporated up to $v = 0.4$, when the support does not yet have an effect, the results of all the experiments fit quite satisfactorily on the straight line.

For evaluation of oil volatility under real conditions, it is not enough to know the equation for the kinetics of oil evaporation at constant temperature. The volatility of MVP oil at different temperatures is represented in

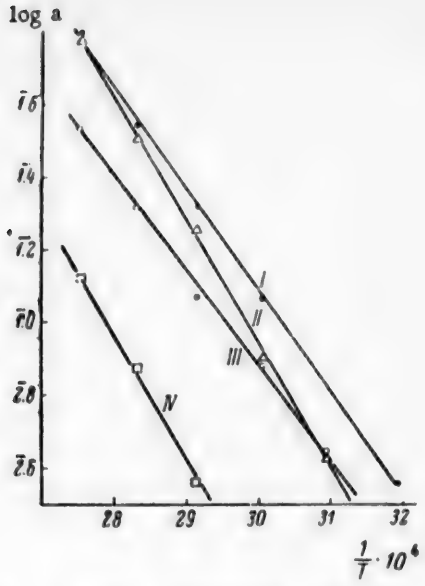

Fig. 4. Effect of temperature on the constant a. Oils: I) MVP, II) amylnaphthalene, III) transformer oil, IV) AU.

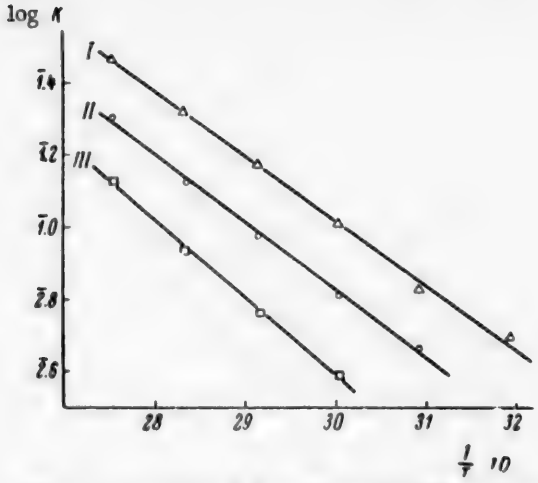

Fig. 5. Variation of the constant K with temperature. Oils: I) MVP, II) transformer oil, III) AU.

Fig. 3, where the experimental data are plotted in $\nu - t/g_0$ coordinates; as was noted earlier, the influence of the initial weight on the fraction evaporated is eliminated by the use of this coordinate system. In order to establish the influence of temperature on the evaporation rates of oils, it is necessary to find the effects of temperature on the constants a and b in Equation (6). Two methods may be used to find the values of these constants from experimental data at different temperatures. The first, graphical method involves the use of the linear relationship between the logarithm of the evaporation rate and the fraction of the sample evaporated. This method was used to find Equation (6) for the kinetics of evaporation. The second method is based on the use of the kinetic Equation (7). Experimental data can be used to obtain a system of two equations, in which the unknowns are the constants a and b:

$$\lg\left(\frac{abt'}{g_0}+1\right)=\frac{b\nu'}{2.3},$$
$$\lg\left(\frac{abt''}{g_0}+1\right)=\frac{b\nu''}{2.3}, \qquad (9)$$

where t' is the time for evaporation of a fraction ν' of the sample; t" is the time for evaporation of a fraction ν''.

This system of equations is easily solved if the values of ν' and ν'' are chosen so that $\frac{\nu'}{\nu''} = 2$. This method is less laborious than the graphical method, and it was used for determinations of the constants a and b for different temperatures. The results are given in Table 2.

It follows from Equation (6) that the constant a has a perfectly definite physical meaning. It is the initial evaporation rate of the oil, when the fraction evaporated is zero. For this reason, in Table 2 the constant a is given in the dimensions of evaporation rate. At the initial instant the evaporation rate is determined mainly by the vapor pressure, as the other factors which influence the evaporation rate do not yet come into operation. It is therefore natural to assume that the relationship between the constant a and the temperature should be similar to the relationship between the vapor pressure and the temperature, and therefore the logarithm of the constant a should be a linear function of the reciprocal absolute temperature. This assumption is confirmed in Fig. 4, where the logarithm of the constant a for three oils is plotted against the reciprocal temperature. On the basis of these results, the relationship between a and the temperature can be represented by the equation:

$$a = a_0 e^{-E_1/RT}, \qquad (10)$$

where a_0 is a constant, R is the gas constant, T is the temperature (° K), and E_1 is the activation energy.

Further, if the initial evaporation rate is determined mainly by the vapor pressure, then the activation energy found from the slope of the log $a = f(\frac{1}{T})$ plot should be equal to the latent heat of evaporation of the oil. This gave the following values for latent heats (in cal/mole): MVP instrument oil, 13,000; transformer oil, 12,500; AU spindle oil, 15,200; amylnaphthalene, 14,500.

These results are in good agreement with the results of direct determinations of the heats of evaporation of the corresponding petroleum fractions [8].

In the light of these results it is possible to use the constant a as a measure of the maximum vapor pressure, i. e., the vapor pressure observed at very high ratios of the oil volume to the gas phase, by comparing it with the evaporation rates of individual liquids.

It might be thought that the constant b is independent of the temperature because, as Equation (6) shows, it determines the relationship between the evaporation rate and the fraction of the sample evaporated, i. e., the fractional composition of the oil. However, it follows from the data in Table 2 that this constant also depends on the temperature and, unlike the constant a, decreases with rise of temperature. The logarithm of the constant b is also a linear function of the reciprocal absolute temperature, and therefore the relationship between this constant and temperature be expressed in the form of the exponential equation

$$b = b_0 e^{E_2/RT}, \tag{11}$$

where b_0 is a constant, T is the temperature (° K), and E_2 is the activation energy.

It is noteworthy that the constant b changes similarly to viscosity with decrease of temperature. It is therefore of interest to compare the activation energies calculated from the slopes of the lines $\log b = f(\frac{1}{T})$ and $\log \nu = f(\frac{1}{T})$ (where ν is the kinematic viscosity of the oil).

MVP oil		Transformer oil		MS-14 oil		
E_ν	E_b	E_ν	E_b	E_ν	E_b	
5200	2900	6000	3700	9000	8500	cal/mole

These results show that the activation energies for viscosity and the constant b are of the same order of magnitude. It follows that the evaporation rate is significantly influenced by the oil viscosity, and its changes in the course of evaporation. The reason for this influence is that viscosity of the oil determines the rate of diffusion of the volatile components from within the layer to the evaporation surface; as the viscosity increases, the surface layer loses its volatile components more rapidly than changes in the oil composition would indicate.

Substitution of the expressions found for a and b as functions of the temperature into Equation (6) gives the following differential equation for the evaporation kinetics of petroleum oils:

$$\frac{dm}{dt} = a_0 e^{-E_1/RT} e^{-b_0 e^{E_2/RT}}. \tag{12}$$

Equation (12) satisfactorily represents the evaporation kinetics of petroleum oils, and makes it possible to estimate their volatility under actual use conditions.

Analysis of the relationship between the evaporation rate of petroleum oils, temperature, and evaporation time (or fraction of sample evaporated) showed that the evaporation rate is mainly determined by two factors: the vapor pressure of the oil (its fractional composition), and diffusion of volatile components from within the layer to the evaporation surface. The influence of the latter factor increases rapidly with fall of temperature. Because of this, the evaporation of petroleum oils at moderate temperatures can be regarded, with some degree of approximation, as a diffusion process. Accordingly, the experimental data were plotted in $\nu - \sqrt{t/g_0}$ coordinates, which represent the well-known diffusion equation (Fig. 2). It is seen that the experimental points do not fit strictly on a straight line, but the dependence of ν on $\sqrt{t/g_0}$ may be assumed linear, with an accuracy adequate for practical purposes, for values of ν up to 0.25. The following expression is therefore proposed for representing the relationship between ν and t/g_0 within these limits:

$$v = C + K\sqrt{\frac{t}{g_0}}, \qquad (13)$$

where C and K are constants, and t is the evaporation time (minutes).

The results of the same experiments are plotted in Fig. 2 in $\frac{t}{g_0 v} - \frac{\log(1 - v)}{v}$, coordinates, corresponding to the linear form of Martynov's Equation (2) (Curve III). It is seen that despite its greater complexity this equation does not give better agreement with the experimental data than Equation (13).

The effect of temperature on oil volatility may be expressed in terms of the slope of the lines $v = f(\sqrt{t/g_0})$, i. e., of the coefficient K in Equation (13). Fig. 5 shows a plot of log K against the reciprocal absolute temperature. As the points fit satisfactorily on a straight line, the relationship may be expressed by the following equation:

$$K = K_0 e^{-\frac{d}{T}}$$

where K_0 and d are constants, and T is the temperature (° K).

The preceding results can therefore be used for estimation of the volatility of petroleum oils under use conditions, with an accuracy adequate for practical purposes, by means of the simpler Equations (13) and (14).

In conclusion, I offer my deep gratitude to Professor A. F. Dobrianskii for valuable advice and guidance in the course of this investigation.

SUMMARY

1. It is shown that the evaporation rate of petroleum oils is a function of the fraction of the sample evaporated; i. e., a function both of the oil composition and its viscosity, which vary continuously during evaporation.

2. The following empirical differential equations describe the kinetics of evaporation of petroleum oils from thin layers:

$$\frac{dm}{dt} = ae^{-bv} \text{ and } \frac{dm}{dt} = a_0 e^{-E_1/RT} \cdot e^{-b_0 v e^{E_2/RT}}.$$

These equations can be used for estimating the evaporation losses of an oil under actual use conditions, and also its vapor pressure.

3. An approximate equation for the evaporation kinetics of petroleum oils is proposed.

LITERATURE CITED

[1] K. K. Papok, V. P. Danilin, and V. S. Zuseva, Proc. 2nd Conference on Friction and Wear in Machines 3, 233 (1949). [In Russian]

[2] G. I. Fuks, M. S. Borovaia, and A. F. Liashenko, Trans. Sci. Res. Inst. for Transport, Storage, and Use of Petroleum Products 3, 174 (1952).

[3] G. I. Fuks and N. E. Gol'tsova, Zav. Labs. 2, 183 (1952).

[4] V. V. Martynov, Investigation Methods for Petroleum and Petroleum Products (State Fuel Tech. Press, 1955), 157. [In Russian]

[5] T. M. Makarova and V. S. Molchanov, Optico-Mechanical Ind. 3, 54 (1957).

[6] K. K. Papok, B. S. Zuseva, and V. P. Danilin, Chem. and Technol. of Fuels and Oils 3, 48 (1957).

[7] F. K. Volynets, J. Appl. Chem. 31, 6, 863 (1958). [See C. B. Translation]

[8] M. M. Kusakov, Methods for Determination of the Physicochemical Characteristics of Petroleum Products 288, (1936). [In Russian]

Received March 27, 1958.

INFLUENCE OF SULFUR COMPOUNDS ON THE SERVICE PROPERTIES OF HYDROCARBON FUELS*

Ia. B. Chertkov and V. N. Zrelov

The composition of sulfur compounds in petroleum is complex and has not been studied sufficiently [1]. Most of the studies relate to compounds which cause, because of their corrosive nature, destruction of the equipment and other technological difficulties in petroleum processing. The effects of sulfur compounds on the performance of fuels are also studied in so far as they involve destruction of the combustion mechanism of the motor and formation of residues insoluble in the fuel.

Because of the diverse structure of the sulfur compounds in fuels and other petroleum compounds, apart from their harmful effects, they can be regarded as constituting an almost untapped source of new compounds which will undoubtedly become of industrial importance in the future.

The present paper constitutes an attempt to determine the group composition of the sulfur compounds in fuels boiling in the ligroine – kerosene range, in relation to their thermal stability and the influence of some of them on the corrosive activity and precipitate formation of fuels.

The experimental data and conclusions are not claimed to be exhaustive and complete, but merely form a step toward classification of sulfur compounds by their influence on fuel quality.

It is known that the oxidation potentials of even the most unstable hydrocarbons, such as alkene-substituted aromatics, are considerably higher than the oxidation potentials of most sulfur compounds, which increase in the following sequence: mercaptans – sulfides – disulfides – thiophenes [2]. However, not all sulfur compounds were found to be equivalent in gum and precipitate formation in fuels.

The work of the Division of Chemistry of the Bashkir Branch of the Academy of Sciences USSR, and of other authors, has shown that the thermal stability of organic sulfur compounds differs in petroleums of different origin [3-9].

In the fuel system of an engine a fuel is heated less strongly than it is during production, but the process takes place in contact with catalytically active copper or its alloys, in an oxidizing medium. Very little is known about the behavior of sulfur compounds in fuels under these conditions.

It is now believed that the nonhydrocarbon components of fuels, including sulfur compounds, lower the thermal stability of fuels [10]; the sulfur compounds form the following sequence, in order of decreasing harmfulness: polysulfides – higher aliphatic mercaptans – thiophenols – lower aliphatic mercaptans. Other sulfur compounds are virtually inert [11].

In addition, there are increasingly frequent reports of sulfur compounds which confer positive qualities on hydrocarbon and other mixtures. For example, phenols with their molecules bridged by sulfur atoms are highly effective antioxidant additives to cracking kerosenes, and remain effective up to 175°.

Derivatives of 2,5-dimercapto-1,3,4-thiodiazole can be used as polyfunctional additives in oils [13]. β-Alkylmercaptoketones [14] were found to be effective antioxidants for fats.

It is evident that among the complex mixtures of sulfur compounds present in petroleum products there may be not only harmful but also inert and even useful compounds, which may have favorable effects on the fuel performance.

---

*N. A. Afanas'eva took part in the experimental work.

TABLE 1

Composition of Sulfur Compounds in Fuels (as % of the Sulfur Contents)

Sulfur compounds*	Direct distillation				Thermal cracking		
	I	II	III	IV	I	II	III
Mercaptans	3.26	18.53	23.63	12.35	0.67	9.57	1.18
Sulfides							
Aliphatic	51.10	47.50	26.50	63.00	14.25	32.80	13.60
aromatic	8.15	Nil	7.08	8.97	31.20	40.80	35.20
Disulfides	2.97	14.80	9.74	14.00	Nil	8.10	0.26
Extracted by Hg	4.72	9.20	15.98	1.68	2.66	0.83	7.70
including elemental sulfur	2.38	2.96	0.20	1.68	Not determined		
Residual compounds	29.80	9.97	17.07	Nil	51.22	7.90	42.06
Total:	100	100	100	100	100	100	100

TABLE 2

Characteristics of the Gummy Portion of Fuels

	Direct distillation				Thermal cracking		
	I	II	III	IV	I	II	III
Yield (wt. %)	0.065	0.103	0.041	0.092	0.632	0.364	0.474
Elementary composition (%)							
C	79.25	72.85	73.49	76.60	77.41	75.13	77.30
H	11.77	10.85	11.81	11.27	9.56	9.33	9.81
S	2.56	11.53	10.05	3.71	3.63	5.10	4.11
N	0.30	0.67	0.10	0.49	1.13	1.09	1.23
O	6.12	4.10	4.55	7.93	8.27	9.35	7.55

TABLE 3

Sulfur Compounds Entering the Gummy Portion of the Fuel (% of the original sulfur contents)

Sulfur compounds	Direct distillation				Thermal cracking		
	I	II	III	IV	I	II	III
Mercaptans	20.2	18.0	0	10.9	100	35.0	100
Sulfides:							
aliphatic	4.7	40.4	0	19.0	70.0	23.2	64.0
aromatic	100	100	0	25.0	0	0	18.2
Disulfides	17.8	0	0	10.7	—	0	0
Extracted by mercury	100	100	83	100	98.0	72.0	100
Including elemental sulfur	100	100	100	100	Not determined		
Residual compounds	0	95	100	—	48.5	41.0	0
Total:	14.5	39.5	20.0	18.5	20.0	14.0	27.5

In our work we used Ball's scheme for analysis of sulfur compounds [15], with certain modifications; despite certain defects, this scheme gave some indication of the group composition of the sulfur compounds in fuels.

*Hydrogen sulfide absent.

TABLE 4

Service Characteristics of Fuels

Characteristics	Direct distillation								Thermal cracking					
	I		II		III		IV		I		II		III	
	original	after removal of gums	original	after removal of gums	original	after removal of gums	original	after removal of gums	original	after removal of gums	original	after removal of gums	original	after removal of gums
Corrosion of bronze (g/m^2)	0.5	0.5	5.5	0.6	4.0	0.8	0.3	0.3	4.2	1.7	2.9	0.7	0.5	0
Deposits on bronze (g/m^2)	0	0	1.0	0.5	0.5	0	0.2	0	1.7	0	0.4	0	0.1	0
Precipitate in fuel, from difference in light absorption (%).	20	10	37	1	27	8	24	7	38	8	16	6	48	7

The total sulfur in fuels was determined by combustion of weighed samples in tubes [16]. Mercaptans were determined argentometrically. Free sulfur was determined by means of metallic mercury, and, in colorless direct-distillation fuels, also photocolorimetrically [17]. Disulfides were reduced to mercaptans, which were also determined by argentometric titration. Aliphatic sulfides were separated by means of mercurous nitrate, and aromatic sulfides and thiophenols, by means of mercuric nitrate. The balance of the group composition of the sulfur compounds in fuels was determined. The total losses did not exceed 5% of the total sulfur compounds, and were distributed in proportion to the group composition. The deficiency to 100% was classified as a group of undetermined sulfur compounds.

In determinations of the group composition of the sulfur compounds, the cracking products were diluted with petroleum spirits so that the total sulfur content of the mixture did not exceed 0.3%. The sulfur compounds were investigated in 7 typical mass-produced fuels, boiling in the 80-280° range, and obtained from sulfurous petroleums from different large oilfields. Four of the fuels were direct-distillation products of the TS-1 type, and three were commercial kerosenes made by thermal cracking.

The sulfur contents (%) of the fuels are given below:

Direct distillation				Thermal cracking		
I	II	III	IV	I	II	III
0.123	0.219	0.220	0.178	0.941	0.647	0.506

The direct-distillation fuels II and III were of nonstandard quality because of their high mercaptan contents: 0.045 and 0.050% of the sulfur contents respectively.

Table 1 shows the sulfur distribution in the fuels by different groups of sulfur compounds.

In direct-distillation fuels a considerable proportion of the sulfur compounds consists of aliphatic sulfides, and in fuels made by thermal cracking, of aromatic sulfides. The disulfide content is much lower in the cracking-process fuels than in direct-distillation fuels. These differences are caused by the different temperature conditions in which the fuels are produced.

The results show that metallic mercury extracts not only elemental sulfur but also sulfur compounds, probably unsaturated. Therefore the content of elemental sulfur determined by this method should be regarded critically. The amounts of sulfur in the compounds of the undetermined group differ for different fuels.

It was very interesting to determine the proportion of the sulfur compounds concentrated in the gummy portion of the fuel, and their group composition. For this, the fuels were percolated through "ShSM" silica gel of 28-65 mesh at a space velocity of 1 $hour^{-1}$. The desorbent used for the hydrocarbon portion was isopentane, and for the gummy portion, methanol. After separation of the gummy portion, the remaining sulfur compounds in the fuels were again investigated as described above.

The characteristics of the gummy portions of the fuels are given in Table 2, and the fractions of the different groups of the sulfur compounds found in the gummy portion are given in Table 3.

The total gum contents of direct-distillation fuels were 0.04-0.10%, and of the cracking products, 0.40-0.60%. The sulfur content of the gums in the direct-distillation fuels was in the range of 3-12%, whereas it did not exceed 0.22% in the original fuels. In fuels II and III, which had very high contents of mercaptans and compounds extracted by mercury, the sulfur contents in the gums were 3-4 times as high as in gums from fuels which did not contain over 0.005% mercaptans, and from which much smaller amounts of sulfur compounds were extracted by mercury.

The gums from the thermal-cracking fuels contained 4-5% sulfur, whereas the original fuels contained 0.941%.

In general, 15-40% of the total sulfur compounds in the fuels passed into the gums. Group composition of the sulfur compounds showed that the sulfur compounds extracted by mercury, including elemental sulfur, pass almost completely into the gums. The other groups of sulfur compounds pass into the gums in various quantities, which apparently depend not only on the functional groups but also on the structure of the sulfur-compound molecules as a whole.

For example, in the case of direct-distillation fuels I, II, and IV, 10-20% of the mercaptans pass into the gums, while in fuel No III, where their content was high, they were completely retained. An interesting fact is that the results for all the fuels indicate that only a small proportion of the disulfides passes into the gums. The same is true of aromatic sulfides in the fuels made by thermal cracking. This leads to the conclusion that accumulation of sulfur compounds in the gummy portion of fuels depends, on the one hand, on their absolute contents in the fuel and on the other, not only on the group composition but also on the chemical structure of compounds containing the same types of functional groups. This last fact was confirmed in one of our investigations on the evaluation of deposit formation in fuels containing mercaptans differing in chemical structure [18].

The following question naturally arises: to what extent do the gummy compounds, separated from the fuel on silica gel, determine the corrosive action and gum and deposit formation of fuels?

We carried out tests on the fuels, both in their original state and after separation of the gummy portion, at 120° for 6 hours in contact with antimony bronze, with 100 ml per 0.002 m^2 surface area; the weight loss of the metal, amount of gum adhering to the metal surface, and the amount of precipitate insoluble in the fuel were determined [19]. The amount if insoluble precipitate was determined in terms of the difference between the light absorption by the fuel before and after separation of the solid particles on a No. 4 porous glass filter. Light absorption was determined by means of the "FEK-3" electrophotocolorimeter.

The results of the tests are summarized in Table 4; it is seen that the fuel quality was sharply improved by separation of the gummy portion (consisting to a considerable extent of sulfur compounds) on silica gel. The corrosive activity, and gum and precipitate formation were decreased. It is interesting to note that fuels made by thermal cracking were not inferior to direct-distillation fuels in these respects after purification.

Tests showed that 60-85% of the sulfur compounds remanining in the fuel after separation of the gummy portion were inert under the test conditions used; they produced no harmful effects and did not undergo any appreciable decomposition with formation of new compounds with an adverse action. This conclusion was confirmed with the use of individual sulfur compounds.

Tests were performed under the same conditions on a sulfur-free and very stable fuel, white spirit, to which various sulfur compounds, kindly supplied by Professor S. E. Krein, were added in considerable amounts. These compounds included: 1) mercaptans (nonyl-, decyl-, benzyl-, and α-phenylethylmercaptan, thiophenol, α-thionaphthol, dithioresorcinol), 2) sulfides (dioctadecyl, cyclopentyldecyl, cyclohexyldecyl, phenylnonyl, diphenyl and dibenzyl sulfides), and 3) disulfides (dicyclopentyl disulfide).

In addition, the effects of α-decylthiophene and elemental sulfur were tested.

Corrosion of the bronze, and gum and precipitate formation took place only in tests in which petroleum spirits contained aliphatic mercaptans of high molecular weight, or elemental sulfur. None of these effects was observed to any practical extent in presence of any of the other individual compounds, or in the original petroleum spirits.

SUMMARY

1. The gummy portion separated on silica gel from fuels boiling in the ligroine – kerosene range contains 15-40% of the total contents of sulfur compounds in the fuel. The sulfur compounds remaining in the fuels after separation of the gummy portion were thermally stable and inert in contact with bronze for 6 hours at 120°.

2. Separation of the gummy portion from fuels made by thermal cracking yields products which are not inferior to direct-distillation fuels in corrosiveness, and in gum and deposit formation.

3. The sulfur compounds which appreciably increase corrosion and gum and precipitate formation in the conditions described include all compounds extracted by mercury (including elemental sulfur) and the mercaptans present.

LITERATURE CITED

[1] J. B. Hill, Ind. Eng. Ch. 45, 7 (1953).

[2] V. G. Luk'ianitsa and G. D. Gal'pern, Bull. Acad. Sci. USSR, OTN 1, 30 (1956).

[3] W. L. Nelson, G. T. Fombona and L. Cordera, 4th International Petroleum Congress, 6 (State Fuel Tech. Press, 1956), 49 [In Russian]

[4] R. B. Tompson, L. W. Druge, J. A. Chenicek, Ind. Eng. Ch. 41, 12, 2715 (1949).

[5] C. M. Barringer, M. W. Corsilins, and J. D. Rogers, Petrol. Processing 12, 1909 (1955).

[6] V. Ia. Masumian and M. R. Musaev, Azerbaidzhan Petroleum Economy 11, 26 (1955).

[7] E. F. Nixon, Chem. and Ind. 13,332 (1955).

[8] H. I. Coleman, C. J. Thompson, H. T. Rall, and H. M. Smith, Ind. Eng. Ch. 45, 12, 2706 (1953).

[9] A. Marakaev and A. Efimov, Advances in Petroleum Technology, Bureau of Technical and Economic Information, Central Scientific Research Institute for the Organization and Mechanization of Labor in the Petroleum Industry, Petroleum Processing 3, 21 (1955).

[10] Oil and Gas J. 69, VI, 20 (1955).

[11] C. R. Johnson, D. F. Fink, and A. C. Nixon, Ind. Eng. Ch. 46, 10, 2166 (1954).

[12] G. Müller, Lab. Praxis, 8, 8, 87 (1956).

[13] H. Krzikalla, H. Engel, W. Wolf, and H. Pohlemann, German Patent 943,790 (1956).

[14] R. B. Tompson, Ind. Eng. Ch. 43, 1638 (1951).

[15] J. Ball, U. S. Bureau of Mines, Report 3591.

[16] G. I. Chernov and I. K. Chudakova, Zav. Labs., 2, 151 (1954).

[17] G. E. Mapstone, Ind. Eng. Ch. 18, 8, 498 (1946).

[18] Ia. B. Chertkov, V. N. Zrelov, N. I. Marinchenko, and V. M. Shchagin, Chem. and Technol. of Fuel 12, 47 (1956).

[19] Ia. B. Chertkov, V. M. Shchagin, and V. V. Rudakov, Advances in Petroleum Technology, TsNIITE Petroleum, Petroleum Processing 2, 3 (1956).

Received April 5, 1957.

WATER-REPELLENT IMPREGNATION OF COTTON FABRICS BY ORGANOSILICON COMPOUNDS*

N. V. Kalugin and M. G. Voronkov

Studies of the water-repellent impregnation of fabrics by aluminum soaps, preparations of the "Velan" type, etc., show that the protective coatings so obtained are not sufficiently stable, and deteriorate rapidly in use.

A new trend in improvement of the water repellency of fabrics is the use of organosilicon compounds for this purpose [1-6].

The organosilicon compounds suitable for conferring water-repellent properties on fabrics may be divided into three groups according to the method of application: 1) easily hydrolyzed organosilicon compounds (acyloxy silanes, polyalkyl silazanes, etc.), which are used for fabric impregnation in the form of solutions in organic solvents (toluene, carbon tetrachloride, etc.), 2) polyalkyl hydrosiloxanes and their copolymers with polydialkyl siloxanes, used in the form of aqueous emulsions; 3) water-soluble organosilicon compounds, such as polyalkyl siloxanolates ("alkyl siliconates") of metals, alkyl acetoxysilanes, etc.

The formation mechanism of a water-repellent film on textile fibers depends on chemical action of the active groups (H, OCOR, NH, OH, etc.) attached to the silicon atoms in the organosilicon compounds with hydroxyl groups in cellulose and with water adsorbed by the fibers.

The water-repellent properties of the films are due to orientation of the organosilicon molecules, in which the polar $-Si-O-$ bonds are directed toward the fiber (or fabric) surface, while the hydrophobic organic radicals form an external layer (Langmuir layer), which makes the fabric water-repellent.

The chemical bonding between an organosilicon polymer and the fibers in a fabric may be schematically represented as follows:

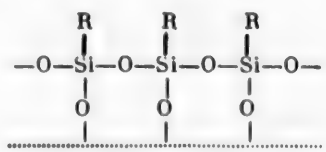

The organosilicon films formed on the fibers are invisible. They are about 10^{-6} cm thick, which is equivalent to a layer consisting of some tens of molecules [1].

Hydrophobic organosilicon films are stable in use, resistant to friction, are not washed off by soap, are insoluble in the common solvents, withstand the effects of high and low temperatures, and are resistant to the action of oxidizing agents, light, and other factors [1].

M. G. Voronkov, Ia. V. Kolesnikov, S. A. Iakubov, and V. P. Davydova synthesized 50 water-repellent organosilicon preparations in the Institute of Silicate Chemistry of the Academy of Sciences USSR, and tested the water repellency of underwear and outer-wear fabrics impregnated with them. As a result of this work, preparations which gave the best water-repellent properties, such as A-4, EN-2, EN-8, etc., were developed and recommended for production use.

*Communication IV in the series on the water-repellent treatment of materials by organosilicon compounds.

TABLE 1

Conditions for Treatment of Cloth Samples by 3% Solutions of Preparations A-4 and A-19 in CCl_4

Sample No	Cloth	Drying before impregnation: time (minutes)	Drying before impregnation: temperature (in °)	Preparation used	Impregnation time (minutes)	Heat treatment: temperature (in °)	Heat treatment: time (minutes)
1	Orekhovo tenting, not desized, rotproofed No 565	60	110	A-4	60	110	60
2	The same	60	110	A-4	60	110	120
3	Egor'ev tenting, desized, No 610	60	110	A-4	60	120	120
4	Orekhovo tenting, not desized, rotproofed No 565	60	110	A-4	60	130	120
5	Egor'ev tenting, desized, No 610	60	100	A-19	60	130	120
6	Orekhovo tenting, rotproofed, No 565	60	100	A-4	1	110	120
7	Egor'ev tenting, desized, No 610	60	110	A-19	1	110	120
8	Orekhovo tenting, rotproofed, No 565	60	110	A-4	5	110	120
9	Egor'ev tenting, desized, No 610	60	110	A-19	5	110	120
10	Orekhovo tenting, rotproofed, No 565	15	110	A-4	30	110	120
11	Egor'ev tenting, desized, No 610	15	110	A-19	30	110	120
12	Orekhovo tenting, rotproofed, No 565	15	110	A-4	60	143	45
13	Egor'ev tenting, desized, No 610	15	110	A-19	60	143	5
14	Orekhovo tenting, rotproofed, No 565	15	110	A-4	60	110	180
15	Egor'ev tenting, desized, No 610	15	110	A-19	60	110	180
16	Orekhovo tenting, rotproofed, No 565	15	110	A-4	60	110	240
17	Egor'ev tenting, desized, No 610	15	110	A-19	60	110	240
18	Orekhovo tenting, rotproofed, No 565	15	110	A-4	60	110	120
19	Egor'ev tenting, desized, No 610	15	110	A-4	60	110	120
20	The same	15	110	A-19 *	60	110	120
21	Egor'ev tenting, desized, rotproofed No 610	15	110	A-4	60	110	120
22	The same	15	110	A-19	60	110	120

Unfortunately, however, these preparations are not yet being produced on the large scale for the textile industry.

We investigated the following preparations of the Institute of Silicate Chemistry, Academy of Sciences USSR: A-4 (methyldiacetoxystearoxysilane, $CH_3Si(OCOCH_3)_2OCO_{17}H_{35}$), A-19 (polytetramethyldiacetoxytrisil-

* 1% solution.

TABLE 2

Stability of Tent Cloths Impregnated with A-4 Organosilicon Preparation, After 3 Months of Use in Kalinin

Sample No.	Before use				After 90 days of use				
	water imbibition in 1 hour (%)	degree of polymerization of fiber cellulose*	molecular weight of fiber cellulose*	specific viscosity of cellulose fiber	water imbibition in 1 hour (%)	degree of polymerization of fiber cellulose*	molecular weight of fiber cellulose*	specific viscosity of cellulose fiber	% degradation of cellulose (from viscosity)
Control combined impregnation	11.3	4649	753203	2.3247	23.7	1820	294840	0.91	60.8
1	8.3	2586	418867	1.2928	22.5	1484	240376	0.7419	42.6
2	6.2	2302	372859	1.1508	23.8	1384	224176	0.6919	39.9
4	8.3	2572	416599	1.2859	17.6	1339	216983	0.6697	47.9
6	5.3	2014	326268	1.0070	20.1	1424	230720	0.7121	29.3
8	4.4	2841	460242	1.4205	22.7	1601	259427	0.8007	43.6
10	4.7	2529	409730	1.2646	21.2	1576	255377	0.7882	37.7
12	8	1474	238723	0.7368	19.1	1163	188341	0.5813	21.1
14	6.6	1830	296492	0.9151	23.7	1158	187531	0.5788	36.7
16	6.6	2280	369392	1.1401	22.4	1210	196085	0.6052	46.9
18	10.1	1403	227318	0.7016	16.9	1378	223236	0.689	1.8
21	6.2	1435	232438	0.7174	16.1	1072	173599	0.5358	25.3
22	4.7	1137	184129	0.5683	22.2	800	179600	0.400	29.6

oxane)[$(CH_3)_2SiOSi(OCOCH_3)_2OSi(CH_3)_2O)_n$]MSN (sodium polymethylsiloxanolate), and GKZh-94 liquid [polyethylhydrosiloxane, $(C_2H_5SiHO)_n$].

This last preparation (Technical Specification EU-124-56) [3, 7] is already in use for water-repellent treatment of various materials (fabrics, paper, cellulose, leather, concrete, plaster, slate, etc.). GKZh-94 is readily emulsified in water, and is marketed both as the 100% substance, and as 50% aqueous emulsion.

Two gray tent cloths were used for impregnation with A-4 and A-19: gray cotton tent cloth No.565 of the Orekhovo Cotton Combine, and gray cotton tent cloth No.610 of the Egor'evsk Cotton Combine. The Orekhovo cloth had been given the usual rotproofing treatment (tanbark extract 30 g/liter, copper sulfate 10 g/liter, potassium dichromate 5 g/liter).

The No.610 tent cloth was de-sized and thoroughly scoured. The cloths prepared in this case were first dried, and then impregnated by immersion in 3% solutions (by volume) of A-4 and A-19 organosilicon preparations in carbon tetrachloride. 22 samples 20 x 40 cm were impregnated. They were then dried in air and heat-treated at 110°. The impregnation conditions used for the tent-cloth samples are summarized in Table 1.

Gray tent cloth No.563 of the Orekhovo Cotton Combine was used for impregnation with MSN preparation. Rotproofed, gray, and scoured fabrics were impregnated at the Orekhovo Cotton Combine. Each piece was 6 m in size.

Subsequent impregnation was carried out by us at the 1st Moscow Cotton Printing Works.

Before the rotproofing treatment, the cloths were scoured at the boil in 1.5% caustic soda solution in a dye jig for 1 hour, and then rinsed in the same jig.

The rotproofing of both cloth samples was carried out in a continuous machine, the recipe and procedure being that generally adopted in our works. After the rotproofing, the cloths were washed, squeezed out, and dried on drums. The prepared samples were then impregnated at 60° in 1% aqueous solution of MSN preparation in a 3-roller padding mangle (tank volume 300 liters). The cloth was passed twice through the machine, dried on drums, and heated at 150° for 5 minutes in the special ager of the 1st Moscow Cotton Printing Works.

The above procedure was adopted after preliminary laboratory selection of the optimum impregnation conditions.

TABLE 3

Wear Resistance and Water Repellency of Tent Cloths Impregnated with Organosilicon Preparations, after 5 Months of Use in Leningrad

Sample No. and cloth	Treatment	Before use		After use	
		strength of a single warp thread (g)	water repellency (cm H_2O)	Strength of a single warp thread $\left(\frac{\text{in g}}{\text{in \%}}\right)$*	water repellency (cm H_2O)
Control	Combined	804.6	27	668.9 / 16.9	18.3
the same	Water-repellent	517.47	21	407.1 / 21.33	20
1	A-4	679.9	36.6	674.7 / 0.8	23.3
2	A-4	670.6	37.0	642.6 / 4.2	21.5
4	A-4	319 weft	36.3	339.6 / +6.4	24.5
6	A-4	402.8 Gray	38.6	420.6 / +4.4	25.5
8	A-4	685.6	36.6	648 / +5.5	21.5
10	A-4	685.3	35.6	665.3 / 2.9	23.5
12	A-4	625	35	573.7 / 8.3	21.5
14	A-4	729.7	34.7	660.7 / 9.5	22.5
16	A-4	609.3	34	633.4 / +3.9	25
18	A-4	645.1	34.3	630.9 / 2.2	22.5
21	A-4	720.3	35.3	593 / 17.7	24
22	A-4	395.4	34.3	358.9 / 9.3	28.3
Gray	MSN	818.6	36	744.86 / 9	28.4
Scoured	MSN	816.6	36	744.86 / 9	28.4
Gray	GKZh-94	741.3	29	594.2 / 19.85	31.3
Scoured	GKZh-94	721.3	26	601.3 / 16.64	31.8

For impregnation with GKZh-94 liquid, two samples of rotproofed tent cloth No. 565 were taken – 6 m of each–one of which was in the gray state and the other had been scoured before the rotproofing treatment. The rotproofing procedure was the same as described earlier.

The rotproofed samples were obtained from the finishing section of the Orekhovo Cotton Combine. They were treated by immersion of the cloths for 30 minutes into a 0.5% solution of GKZh-94 in benzene. 3 liters of

* The numerator represents the strength of a single warp thread in grams, and the denominator gives the strength decrease as a percentage. A plus sign indicates a strength increase.

solution were taken per kg of cloth. After the treatment the cloths were dried in air and heated on drying drums at 120° for 15 minutes at the finishing plant of the Kalinin Cotton Combine. The cloth was in close contact with the drum surface during the drying. The cloth was not washed after the heat treatment.

High temperatures and long drying times were used in our experiments; investigations of the Institute of Silicate Chemistry of the Academy of Sciences USSR have shown that the temperatures can be reduced to 110-115° if catalysts such as ethyl orthotitanate $Ti(OC_2H_5)_4$ are used.

The results of wear tests on tent cloths impregnated with A-4 organosilicon preparation are given in Table 2.

Studies of preparation GKZh-94 and MSN showed that the water repellency of fabrics treated with them persists after five months of use, although it is lower, as measured by the hydrostatic-head method, than that of fabrics given the usual combined impregnation treatment.

The results of comparative tests on cloths impregnated with the organosilicon preparations are given in Table 3; it is seen that the loss of strength is less in cloths treated with A-4 and MSN than in control samples given the combined treatment or the water-repellent treatment. Their better resistance to weathering is probably due to the absence of aluminum salts in the treatment. GKZh-94 results in approximately the same fall of strength in the cloths as is found in the control samples.

The water repellency of the control samples, and samples treated with A-4, MSN, and GKZh-94, decreases during use. The smallest decrease was found in samples treated with GKZh-94. Scouring of the cloths before impregnation with MSN and KGZh-94 for improvement of water repellency does not produce any significant advantages as compared with gray cloths. The water repellency of the two kinds of cloth remains at about the same level. Therefore preliminary scouring of the fabrics is not necessary before the use of these preparations, as it has no significant influence on water repellency.

Trials of organosilicon preparations A-4, A-19, MSN, and GKZh-94 showed that they confer water repellency on tent cloths, and are compatible with rotproofing treatment, so that they can replace the usual combined impregnation. It is thereby possible to avoid the use of aluminum salts in the production of cloths subjected to the combined treatment; our tests showed that aluminum salts accelerate degradation of textile fibers.

The water repellency of cloths differs in stability with different organosilicon preparations. For example, whereas cloths treated with A-4, MSN, or KGZh-94 retain water repellency after 90 days of use, this is not the case for samples treated with A-19, which rapidly lose water repellency during use.

In the selection of a technological process for fabric impregnation, the nature of the solvent used for the water-repellent substances is very important. For example, A-14 can only be used in organic solvents, which makes its industrial use difficult. On the other hand, MSN and GKZh-94 can be used as aqueous solutions or emulsions, which is very convenient in the textile industry.

Special impregnation equipment is not required for the application of organosilicon preparations; the equipment available in finishing plants, such as jigs, padding mangles, and continuous machines may be used. One great obstacle to the industrial adoption of organosilicon finishes is the need for heat treatment of the treated cloths at 140-150° at the end of the process; this has to be done in special gas-heated or electric agers. A longer time (1-3 hours) is required for heat treatment at lower temperatures (100-110°).

Moreover, the mechanical strength of the cloth is decreased considerably in all the variants of the heat treatment, and this may reduce its service life. Whereas the specific viscosity of the cellulose in a control sample after the ordinary combined impregnation was 2.3247, in samples impregnated with A-4 it fell (after heat treatment) to between 0.563 and 1.42.

However, if we examine the changes in the chemical characteristics of wear resistance at the end of three months of use, we find that the control cloth after the usual combined impregnation is degraded at a greater rate than samples treated with preparation A-4. The specific viscosity of the cellulose in the control cloth fell by 60.9% in three months, while the corresponding fall in the samples treated with A-4 was 25.3-47.9%. This shows that A-4 has better protective properties than the existing combined impregnation. In some instances we even found an increase of cloth strength during use; this was probably caused by further polymerization of the organosilicon preparation under the influence of sunlight.

The results of water-imbibition tests on the cloths show that the water-repellent film formed by A-4 preparation is more resistant to weathering than the combined impregnation treatment. The water imbibition of the control cloth is higher than that of cloth treated with A-4, both after the treatment and after 3 months of use. Whereas the imbibition of a cloth treated with A-4 was 17% after three months of use, the imbibition of the ordinary cloth subjected to the combined treatment was 24% after the same period.

The organosilicon preparations tested give a good external water-repellent effect, but lower water-repellency values in hydrostatic-head tests; these may be improved by increasing the cloth density by application of agents such as melted paraffin in thin layers, etc., in addition to the organosilicon material, or by the use of organic polymers in conjunction with the latter.

The following procedure is recommended for impregnation of fabrics with preparation A-4. The preliminary drying may be carried out on drying drums at their lowest speeds (variations of the drying time from 15 to 60 minutes do not have any great influence on the water repellency), or it may be omitted altogether. The immersion time of the fabric in the organosilicon solution need not exceed one minute. The solution temperature is not significant. The different procedures used for heat treatment of the fabrics after the impregnation are all unsatisfactory, as they are either lengthy (1-4 hours at 100-110°) or cause a loss of mechanical strength (at 150°), with an ultimate low productivity of the equipment and of the undertaking as a whole. It is therefore necessary to concentrate on a drying procedure with the use of catalysts for the condensation of the organosilicon compounds (orthotitanate esters, etc.).

For successful industrial development of the organosilicon treatment, production of the preparations must be organized on a large scale. At present they are being produced in limited amounts.

This investigation has shown that the organosilicon preparations A-4, MSN, and GKZh-94 confer water repellency, stable in use, on fabrics, while A-4 and MSN also confer increased protection against weathering. A disadvantage of A-4 is that it must be used in organic solvents, so that special equipment must be designed for industrial impregnation and drying of fabrics. Organosilicon compounds which can be dissolved or emulsified in water are the most promising for use in textile finishing works with the existing equipment.

SUMMARY

Organosilicon preparation A-4, in conjunction with rotproofing treatment, confers good water repellency and resistance to weathering on fabrics. The water repellency of fabrics treated with it persists after five months of use. A combined impregnation treatment, stable in prolonged use, is obtained by the use of organosilicon compounds in conjuction with salts of copper and chromium. The increase of water imbibition during use is slower in fabrics treated with the organosilicon impregnating agents than those subjected to the usual combined treatment.

Organosilicon preparations A-4, MSN, and KGZh-94 can be used in combined treatments, without the use of aluminum salts, which are stable to weathering. Fabrics so treated do not undergo any significant changes of water repellency during five months of use.

Fabrics impregnated with organosilicon preparations show considerably less strength loss during use than fabrics treated by the standard combined method, and sometimes their strength even increases. This shows that organosilicon treatment in conjunction with rotproofing has better protective properties.

LITERATURE CITED

[1] M. G. Voronkov and B. N. Dolgov, Nature 5, 22 (1954); J. Leningrad Univ. 5, 185 (1954).

[2] R. R. McGregor, Silicones and Their Uses (New York, 1954), 83.

[3] K. A. Andrianov, Heat-Resistant Organosilicon Dielectrics (Moscow, State Power Institute, 1957) 264. [In Russian]

[4] F. Fortess, Ind. Eng. Ch. 46, 2325 (1954).

[5] W. Weltzien, G. Hauschield. Uber Silikone ind ihre Anwendung in der Textilveredlung, Koln (1955).

[6] H. Reuthe, S. Sliwinskii, and C. Schneider, Chem. Technik, 5, 694 (1953); 6, 381 (1954).

[7] K. A. Andrianov, V. M. Romanov, and S. A. Golubtsov, J. Chem. Ind. 3, 14 (1956).

Received April 3, 1958.

EFFECT OF PLASTICIZER EFFICIENCY ON THE VISCOSITY OF POLYVINYL CHLORIDE COMPOSITIONS*

Sh. L. Lel'chuk and V. I. Sedlis

(The Leningrad Scientific Research Institute of Polymerization Plastics)

It is known that the viscosity and plasticity of polymers are interconnected, and that viscosity can serve as a certain measure of plasticity. We attempted to determine the replationships between plasticizer efficiency and the viscosity of polyvinyl chloride (PVC) compositions. One of us has shown that the viscosity – temperature relationship for melted polymers and polymer compositions can be expressed by the following formula (the viscosimetric characteristic of the material):

$$\lg \eta_T = B - AT, \qquad (1)$$

where η_T is the viscosity of the material at temperature T (in poises); T is the temperature (in °); B and A are characteristic constants of the following physical meaning: B is log η at T = 0°; A is the temperature gradient of log η for a 1° temperature decrease, $A = \frac{\log \gamma_0 - \log \eta_T}{T}$; A is always > 0.

We determined the viscosimetric characteristics of PVC compositions with different plasticizers, the results being given in Table 1; the same table also gives the viscosities of these compositions at 100°, and the temperatures used in industry for their molding (extrusion temperature and hot-compression molding temperature).

It follows from Table 1 that there is a close connection between the efficiency of plasticizers and the viscosity of compositions containing them; the lower the composition viscosity, the higher is the plasticizer efficiency. This suggests that the greater efficiency of the plasticizer, which is manifested in greater plasticity of the composition, greater mobility of the polymer macromolecules, lowering of the glass-transition temperature, and lowering of the molding temperature, should be attributed to the decrease in the viscosity produced by the given plasticizer in the composition.

Addition of a plasticizer produces the same effect as heat, i. e., it lowers the viscosity of the material. However, in order to decrease the viscosity of pure PVC from $3.7 \cdot 10^9$ poises (the viscosity of pure PVC at 100°) to 10^8 poises (the viscosity of a composition containing 8 molar % of TCP at 100°) PVC must be heated to a temperature above 138°; to produce a viscosity of $1.85 \cdot 10^7$ poises (the viscosity of a composition containing 8 molar % of DOS) in PVC it must be heated to above 157°; and to reduce the viscosity of PVC to $3 \cdot 10^6$ poises (the viscosity at the extrusion temperature of a composition containing 8 molar % of DOS) it must be heated to 175°. It is known that PVC undergoes decomposition and degradation at such temperatures, especially if subjected to them for long periods. Of course, this is true, to various extents, of most polymers. That is why plasticizers are used so widely in the production of plastics, in order to lower the processing temperatures. Polymer viscosities are reduced to tenths or hundredths of their initial values by the use of plasticizers.

We derived the following empirical formulas which connect the viscosity of a plasticized PVC composition with the plasticizer efficiency, plasticizer content in the composition, and the temperature; these formulas can be used to find the viscosimetric characteristics of the compositions, represented by Formula (I):

*Communication V in the series on the influence of plasticizers on the properties of polyvinyl chloride.

TABLE 1

Viscosimetric Characteristics of PVC Compositions with Different Plasticizers, Their Viscosities at 100°, and Molding Temperatures with Plasticizer Contents n = 8 molar %

PVC – plasticizer	Efficiency number E (in °)	Glass-transition temperature T_g (in °)	Swelling of PVC at 90° (%)	Viscosimetric characteristics $\log \eta = B - AM$	Viscosity at 100° (poises)	Extrusion temperature (in °)	Compression-molding temperature (in °)
0	—	65	—	$\log \eta = 13.665 - 0.041\ T$	$3.7 \cdot 10^9$	175	163
Tricresyl phosphate (TCP)	9.4	−10	80	$\log \eta = 10.758 - 0.0269\ T$	$1 \cdot 10^8$	158	139
Diethyl phthalate (DEP)	9.8	−13	300	$\log \eta = 10.653 - 0.0267\ T$	$1.03 \cdot 10^8$	155	137
Dibutyl phthalate (DEP)	10.6	−19	120	$\log \eta = 10.504 - 0.0261\ T$	$7.8 \cdot 10^7$	153	134
Dioctyl phthalate (DEP)	11.9	−30	35	$\log \eta = 10.238 - 0.0254\ T$	$5 \cdot 10^7$	147	127
Dibutyl adipate (DBA)	12.4	−32	128	$\log \eta = 10.190 - 0.0253\ T$	$4.6 \cdot 10^7$	145	125
Dioctyl adipate (DOA)	13.1	−39	0.79	$\log \eta = 10.029 - 0.0249\ T$	$3.5 \cdot 10^7$	141	121
Dibutyl sebacate (DBS)	13.8	−44	22	$\log \eta = 9.909 - 0.0248\ T$	$2.9 \cdot 10^7$	138	118
Dioctyl sebacate (DBS)	15.1	−54	0.70	$\log \eta = 9.690 - 0.0242\ T$	$1.85 \cdot 10^7$	132	111

TABLE 2

Viscosimetric Characteristics and Other Physical Properties of Copolymers of Vinyl Chloride with Acrylate Esters. Acrylate contents 5 molar % per mole of vinyl chloride

Copolymer	Efficiency number (in °)	Glass-transition temperature (in °)	Copolymer viscosity (poises)	Viscosimetric characteristics $\log \eta = B - AT$	Heat resistance Martens test (in °)	Molding temperature (in °)	
						extrusion	compression
Pure polyvinyl chloride	—	65	$3.7 \cdot 10^9$	$\log \eta = 13.665 - 0.041\ T$	78	175	163
VC + MA	1.60	55	$3.6 \cdot 10^9$	$\log \eta = 12.738 - 0.0316\ T$	70	197	181
VC + EA	2.31	51	$2.8 \cdot 10^9$	$\log \eta = 12.600 - 0.0314\ T$	65	194	146
VC + BA	3.74	42	$1.64 \cdot 10^9$	$\log \eta = 12.294 - 0.0308\ T$	58	184	170
VC + OA	6.70	23	$5.4 \cdot 10^8$	$\log \eta = 11.672 - 0.0292\ T$	48	177	160

$$A = \frac{11 A_0}{16.400 - 0.041\,[65 - (0.55n + 3.5)\,E]}, \qquad \text{(II)}$$

$$B = 11 + A\,[65 - (0.55n + 3.5)\,E], \qquad \text{(III)}$$

where n is the molar % of plasticizer, E is the efficiency number, and A_0 is a constant for pure PVC, equal to 0.041.

These formulas were used for calculation of the viscosimetric characteristics and viscosities at 100° (η_{100}), given in Table 1.

The above considerations are also applicable to vinyl chloride (VC) copolymers, if the second monomer is regarded as a plasticizer, and copolymerization as internal plasticization.

TABLE 3

Characteristics of PVC Compositions Containing Plasticizer Mixtures Total Plasticizer contents 8 molar %

No.	PVC + plasticizer mixture	Efficiency number E of plasticizer (in °)	Viscosity of plasticizer mixture (centipoises)	Glass-transition temperature of composition (in °)	Viscosity of composition at 100 ° (poises)	Extrusion temperature (in °)	Compression-molding temperature (in °)
1	TCP + DOP (4:4)	10.6	74.0	—19	$7.4 \cdot 10^7$	152	133
2	TCP + DOS (5:3)	11.5	42.0	—26	$5.8 \cdot 10^7$	150	129
3	DEP + DOS (5:3)	11.8	17.16	—29	$7.0 \cdot 10^7$	155	134
4	DEP + DBS (5:3)	11.3	10.6	—26	$6.3 \cdot 10^7$	150	131
5	TCP + DOP(5:3)	10.3	76.0	—16	$8.9 \cdot 10^7$	155	136
6	TCP + DBS (5:3)	11.0	35.0	—22	$6.9 \cdot 10^7$	152	132
7	TCP + DOP + DOS (5:2:1)	10.7	39.2	—19.5	$7.8 \cdot 10^7$	153	134

Table 2 gives the viscosimetric characteristics and various physical properties of a series of copolymers of vinyl chloride with acrylate esters: methyl acrylate (MA), ethyl acrylate (EA), butyl acrylate (BA), and octyl acrylate (OA). All contained 5 molar % of the second monomer per mole of vinyl chloride monomer.

Our calculation formulas can be used to calculate, for example, the composition of a vinyl chloride copolymer which is equivalent in its main physical and mechanical properties to a PVC composition containing an ordinary low-molecular plasticizer. For instance, a copolymer of vinyl chloride with 8.8 molar % of octyl acrylate would have the same viscosimetric characteristic as a composition containing 30 weight parts of TCP. They would both have the same values of T_g, the same heat resistance and hardness, and the same molding temperatures.

Here again, as the efficiency number of the plasticizer (second monomer) increases, the copolymer viscosity decreases regularly, and this is accompanied by an increase in the plasticity of the product (decrease of the glass-transition temperature, heat resistance, and molding temperatures). In this case one cannot speak of the viscosity of the plasticizer, but only of the viscosity of the composition (the plasticized product) which, as can be seen, is closely associated with the efficiency number of the second monomer.

It follows from the data in Tables 1 and 2 that the temperature gradient of the logarithm of the viscosity, A, decreases regularly with increase of the efficiency number; in other words, the compositions become less sensitive to temperature changes.

The fact that the plasticity of a material can be increased by decrease of polymer viscosity, which makes manipulation of the material easier by a decrease of the molding temperature, has long been known and used in practice. For example, it is known that polystyrene made by block polymerization, which has lower molecular weight and viscosity, is easier to work than polystyrene made by emulsion polymerization, which has high molecular weight and viscosity. Low-viscosity grades of PVC are used for molding of hard articles from the unplasticized material. Another fact which has been known and used for a long time is that the plasticity of rubbers can be increased by means of cold mastication, as by the repeated passage of the rubber between cold rolls, which causes some degradation of the rubber, shortening of the chains, and decrease of its viscosity.

In the light of the preceding, it is possible to account for the validity of the relationship, established by Orlova and Sedlis [1] and by Leilich [2], between plasticizer viscosity and efficiency. Both components, the polymer and the plasticizer, should influence the viscosity of a plasticized composition. If a polymer – plasticizer system is regarded as a solution of the former in the latter, it follows that a low-viscosity plasticizer should lower the viscosity of the composition as a whole, and increase its plasticity, i. e., the efficiency of the plasticizer. However, this rule does not always hold, and cannot be generally applicable, as it does not take account of another important factor, namely the solvating or gelating power of the plasticizer and its compatibility with the polymer.

It is known that good solvents yield solutions of higher viscosity, and vice versa [3]. Consider a low-viscosity plasticizer, with good solvent power with respect to PVC. The low viscosity of the plasticizer should make the viscosity of the composition low, but its high solvent power would produce the opposite effect – an increase of viscosity – which may overlap or mask to some extent the effect produced by the low viscosity of the plasticizer itself. Therefore the viscosity of a plasticizer cannot serve as a measure of its efficiency. An example is provided by diethyl phthalate, which has low viscosity, but a high solvent power with respect to PVC.

The swelling of PVC in DEP was 300% at 90° in 3 hours; this was the highest value obtained with any of the plasticizers tested. However, the viscosity at 100° (η_{100}) of a composition containing DEP is the same as that of a composition containing the high-viscosity TCP (the viscosities of these plasticizers are 13.22 and 79.20 centipoises respectively). It follows from Table 1 that their molding temperatures and values of T_g also differ little.

Accordingly, the efficiency numbers of the systems PVC – DEP and PVC – TCP also differ little, being 9.8 and 9.4 respectively.

Our method for characterization of plasticizer efficiency in terms of the lowering of the glass-transition temperature of the composition (efficiency number E), on the other hand, allows for the combined effect of these factors, the "resultant" of two opposing effects. Our views are illustrated especially clearly by data for compositions containing mixed plasticizers, presented in Table 3.

A mixture of equal amounts of TCP and DOP has fairly high viscosity (74 centipoises), several times that of DBP (19.4 centipoises). By the viscosity criterion, a composition containing this mixture (8 molar %) should be considerably inferior to a composition containing DBP only. In fact, however, a composition with this mixture has the same plasticity as a composition with DBP (equal glass-transition temperatures, viscosities at 100°, and molding temperatures). This is understandable, as the efficiency numbers of the systems PVC – TCP + DOP and PVC – DBP are equal (10.6).

In this instance plasticizers of approximately the same solvating power were used. We now consider a mixture of TCP (which has high viscosity), a plasticizer which has good compatibility with PVC, and DOS, which has relatively low viscosity and poor compatibility, taken in 5:3 ratio (Composition 2). The viscosity of the mixture is fairly high, although lower than that of TCP. The plastic properties of the composition with this mixture are close to the plastic properties of a composition with DOP, although somewhat inferior to the latter; this is to be expected from the efficiency numbers (the efficiency number of the mixture, 11.5, is close to that of DOP, 11.9).

The plasticity of the composition is increased considerably by the addition of a relatively small amount of DOS to TCP. We are inclined to attribute this effect not only to the better plasticizing power of DOS, but also to its poor compatibility with PVC. This may be confirmed by comparison of Compositions 4 and 6. In the latter, DBS, which is also a very effective plasticizer but which is more compatible with PVC, was added in the same ratio to TCP. It is seen that the plasticity of Composition 6 is somewhat less than that of 4, in agreement with their efficiency numbers (11 and 11.3 respectively). Comparison of Compositions 5 and 7 is also interesting. The only difference of plasticizer composition between them is that, in Composition 7, 1 molar % of DOP is replaced by 1 molar % of the poorly compatible DOS. The plastic properties of Composition 7 are seen to be superior to those of Composition 5.

Mixed Compositions 2 and 3 are also of interest. To 5 molar % of the low-viscosity plasticizer DEP, which is well compatible with PVC, there was added 3 molar % of the low-viscosity DOS, of poor compatibility. The viscosity of the mixture is somewhat higher than the viscosity of pure DEP (17.16 and 13.22 centipoises respectively). The efficiency of the mixed plasticizer is considerably higher, and the plastic properties of the composition containing it are almost the same as those of the composition with DOP (their efficiency numbers are also very similar: 11.8 and 11.9). Somewhat worse results are obtained for a composition in which DBS, which has very low viscosity but better compatibility with PVC than DOS has, is added to DEP in the same ratio (Composition 4). The viscosity of the mixture is very low, lower than that of pure DEP (10.6 as compared with 13.26 centipoises). The plastic properties of the composition are worse than those of Composition 2, as indicated by the efficiency numbers (11.3 and 11.5 as compared with 11.9 with DOP). Further confirmation of the preceding is provided by the following example, relating to the use of a polymeric plasticizer, namely, butadiene – nitrile rubber (SKN). SKN-18 (18% of nitrile groups in the rubber), which is badly compatible with PVC, produces a much higher plasticization effect than SKN-35, which has good compatibility with PVC; this is shown by the following data: a PVC composition containing 31 centimoles of SKN-18 has $T_g = -18°$, whereas a composition

containing the same amount of SKN-35 has $T_g = +10°$. The first composition is much easier to mill and work than the second. The viscosity of the first composition at 100° is $\eta_{100} = 4 \cdot 10^7$ poises, and of the second $\eta_{100} = 2 \cdot 10^9$. These values correctly reflect the efficiency numbers, 1.60 and 1.11 respectively.

Thus, the plastic properties and plasticizer efficiency are determined by the viscosity of the composition, and not of the plasticizer.

The preceding considerations partially account for and justify the procedure often used in practice, where a certain amount of a nongelating, badly compatible plasticizer (known as a "secondary plasticizer" or softener) is added to the principal gelating plasticizer of good compatibility. Such a mixture has better plasticizing action than the gelating plasticizer alone especially in relation to the shift of the glass-transition temperature (increase of the frost resistance of the material) toward lower value.

SUMMARY

1. There is a systematic relationship between plasticizer efficiency and viscosity of plasticized PVC compositions, which indicates that the action of a plasticizer consists primarily of a decrease in the viscosity (η) of the composition, and is predetermined by the latter.

2. Empirical formulas are derived, representing the quantitative relationships between the viscosity of PVC compositions, plasticizer efficiency and content, and temperature. The viscosimetric characteristics of PVC compositions containing different plasticizers are compared, their viscosities at an elevated temperature (100°) were calculated, and the temperatures used for their molding by the usual industrial methods are given.

3. The claim that plasticizer efficiency and plasticity of compositions can be characterized and predicted in terms of plasticizer viscosity only is shown to be unsound. The viscosity of a polymer – plasticizer system depends not only on the polymer and plasticizer viscosities, but also on compatibility – the solvating effect of the plasticizer on the polymer; the lower the latter, the lower is the viscosity.

4. The influence of all these factors is indicated by the efficiency number, which represents the decrease of the glass-transition temperature in a plasticized composition as compared with that of the pure polymer; it is therefore a reliable measure of true plasticizer efficiency.

5. A number of effects observed in the industrial applications of plasticizers in plastics production are explained in the light of the preceding theoretical considerations.

LITERATURE CITED

[1] V. I. Sedlis, Proc. 1st and 2nd Conf. on High-Molecular Compounds (Izd. AN SSSR, 1945). [In Russian]

[2] K. Leilich, Koll. Z. 99, 107 (1942).

[3] A. Alfrey, A. Bartovics and H. Mark, J. Am. Chem. Soc. 64, 7, 1557 (1942).

Received February 1, 1957.

POLYMERIZATION OF DIVINYLACETYLENE*

I. M. Dolgopol'skii, A. L. Klebanskii, and D. M. Krasinskaia

It is known that divinylacetylene is readily oxidized with formation of peroxide compounds [1].

It has been shown [2, 3] that quantitative formation of peroxide compounds takes place at the initial oxidation stage, and the peroxides then decompose slowly with formation of oxidation and polymerization products. In the light of the work of Medvedev and his associates [4] it may be assumed that both reactions (oxidation and polymerization) are initiated by the same mechanism – under the influence of free radicals formed in the decomposition of peroxides.

The polymerization of pure divinylacetylene under the influence of oxygen is difficult to bring about in practice because of the formation of very explosive peroxides, and also because the polymers pass into a gelatinous insoluble state even at a relatively low degree of conversion. The polymers are unsuitable for technical purposes in this form.

As the polymerization of divinylacetylene proceeds, the properties of the polymerization product gradually change. At the initial stage of the reaction the polymers are soluble in the monomer, and also in aromatic, chlorinated, and other solvents; solutions of divinylacetylene polymers have a liquid oily consistency. As the extent of reaction increases, the viscosity of the polymerization product rises, and the latter gradually passes into a gelatinous state. In the early stages of gel formation the polymers are partially soluble in the above solvents. With further polymerization, when a gel of low mobility is formed, the product becomes insoluble, and then passes into a solid resin. This resin is not soluble in any known solvent.

Only soluble polymers can be used industrially as film formers, and therefore one of our main tasks was to determine the conditions in which soluble polymers are formed, with the maximum possible degree of conversion. In the light of the existing extensive data on the effect of polymer structure on properties it may be assumed that the soluble polymers have a linear structure, while the insoluble polymers have a network or space structure. It should be pointed out that the literature data on the polymerization of divinylacetylene are very scanty, and consist mainly of patents. Still less is known on the structure of divinylacetylene polymers.

The literature contains only one paper [5] on the subject, with only tentative data. In the authors' opinion, the polymerization of divinylacetylene is a thermal reaction. They isolated and investigated only the first member of the series, divinylacetylene dimer; the next member, the trimer, could not be isolated because of its instability. This polymer was obtained in the form of its hydrogenation product. It was suggested by the authors [5] that divinylacetylene polymers have the structure of cyclobutane derivatives.

Divinylacetylene polymers have a number of valuable technical properties and can be used as film formers. We therefore studied the conditions for their formation, and means of improving their properties.

Because of the tendency of vinylacetylene hydrocarbons to spontaneous polymerization and oxidation by atmospheric oxygen, with formation of explosive compounds, we studied the polymerization of divinylacetylene in solution in presence of stabilizers, i. e., in conditions in which safety was ensured. Under these polymerization conditions, soluble polymers of low molecular weight are formed. However, these polymers are highly unsaturated and have a strong tendency to autooxidation and further polymerization under the influence of peroxide compounds,

*Communication III.

TABLE 1

Polymerization of Divinylacetylene and its Mixtures with Acetylenyldivinyl at Various Temperatures

Experiment No.	Amounts taken (wt.%)		Composition of gaseous medium (%)		Reaction temperature (in °)	Reaction time (hours)	Polymer yield (%)	Properties of polymerization product
	Divinylacetylene	Acetylenyldivinyl	CO_2	N_2				
1	97.75	2.25	100	—	16—20	275 cyt.	19.5	Hard insoluble resin
2	97.75	2.25	—	96 + 4% O_2	16—20	275 cyt.	50.3	
3	100	—	100	—	50	26.5	4.3	Oily soluble liquid
4	100	—	100	—	50	27.5	5.4	
5	100	—	100	—	50	31.5	6.8	Gelatinous insoluble mass
6	100	—	100	—	50	39.0	9.0	
7	100	—	100	—	80	46.0	21.0	Oily soluble liquid
8	100	—	100	—	80	53.0	24.1	
9	100	—	100	—	80	62.0	38.9	
10	100	—	—	100	100	0.5	9.7	
11	100	—	—	100	100	1.0	33.2	
12	100	—	—	100	100	1.5	50.1	
13	100	—	—	100	100	2.0	67.6	Gelatinous insoluble resin
14	100	—	—	100	100	3.0	78.2	

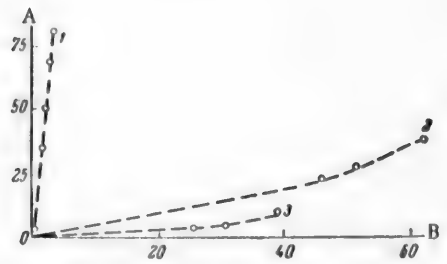

Fig. 1. Effect of reaction temperature on the polymerization rate of divinylacetylene. A) Polymer yield (%), B) time (hours). Temperature (in °): 1) 100, 2) 80, 3) 50.

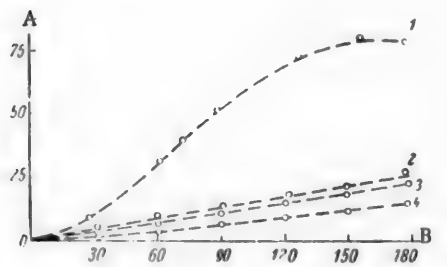

Fig. 2. Effect of heating time on the yield of divinylacetylene polymers. A) Polymer yield (%), B) time (minutes). 1) 100% divinylacetylene, 2) 98% divinylacetylene + 2% α-napthylamine, 3) 40% divinylacetylene + 60% xylene, 4) 40% divinylacetylene + 60% xylene + 2% α-naphthylamine.

with formation of cross-linked insoluble polymers. This cross linking of the low-molecular polymers initially formed probably occurs during film formation, when films dry and harden under the influence of atmospheric oxygen and light. This process probably consists of the conversion of linear macromolecules into polymers with a spatial network structure, which are insoluble in all the known organic solvents.

The mechanism of divinylacetylene polymerization in presence of solvents and reaction inhibitors, in an inert gas medium, is still not quite clear. Studies of the mechanism and kinetics of polymerization, carried out by a number of authors (Lebedev, Staudinger, Carothers, Medvedev, Mark, and others), have shown that polymerization of unsaturated compounds proceeds by a chain mechanism.

If this mechanism is considered in relation to the conditions used for polymerization of divinylacetylene (by the action of heat, in a solvent, in an inert gas medium, and in presence of inhibitors), the following conclusions may be drawn: polymerization of divinylacetylene is initiated thermally or under the influence of small amounts of peroxides formed by the reaction of the hydrocarbon with atmospheric oxygen; the presence of solvent and inhibitor favors chain termination with formation of low-molecular soluble polymers, probably of linear structure; the process of divinylacetylene polymerization culminates in a stage of film formation under the influence of atmospheric oxygen and light, by cross linking of the molecules with conversion of the soluble forms, probably of linear structure, into an insoluble polymer, probably of a network spatial structure. These conversions of the polymeric forms are associated with the con-

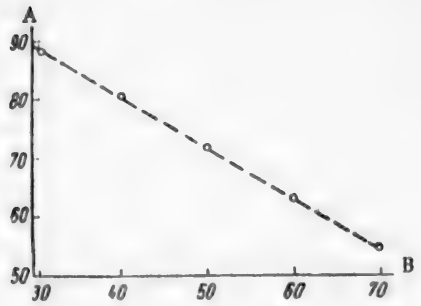

Fig. 3. Variation of polymer content with the monomer concentration in solution (to the start of gel formation).
A) Polymer yield (%), B) concentration of vinylacetylene hydrocarbons in xylene solutions (%).

siderable unsaturation of the polymers initially formed.

In the light of the foregoing considerations, the polymerization of divinylacetylene was studied from the following aspects: 1) study of the conditions for the polymerization of divinylacetylene in air and in an inert gas; 2) determination of the effects of reaction temperature and divinylacetylene concentration in solution, both on the reaction rate and on the extent of reaction at which the soluble polymers are converted into the insoluble form; 3) the effects of inhibitors on the reaction rate and on the polymer properties.

As the result of this investigation, the optimum conditions for divinylacetylene polymerization were established. It was shown that the process may be regulated if polymerization is carried out in dilute solutions in an inert gas medium in presence of stabilizers. Under these conditions the heat of reaction is led away most effectively, and polymers of valuable technical properties are formed.

EXPERIMENTAL

Both pure divinylacetylene and its mixtures with acetylenyldivinyl (containing about 10% of the latter) were polymerized. For determination of the effect of reaction temperature on the polymerization rates of these hydrocarbons, the experiments were performed in sealed bulbs at room temperature and at 50, 80 and 100°. The reactions were carried out in absence of solvents or stabilizers.

The data in Table 1 and Fig. 1 show that the yield of soluble polymers depends both on the temperature and on the extent of reaction. The amount of soluble polymers increases with the temperature. For example, when a mixture of divinylacetylene and acetylenyldivinyl was kept in an inert gas atmosphere in sealed bulbs at room temperature for 9 months, the polymer yield was 19%, and the polymers formed were insoluble and hard, probably with a branched cross-linked structure. The extent of polymerization increased in the presence of 4% oxygen in the gas phase.

Increase of the polymerization temperature of divinylacetylene to 50° (Experiments 3-6, Curve 3) also resulted in the formation of insoluble gelatinous polymers, with a low degree of conversion (5.4-9%). At 80°, liquid oily soluble polymers were obtained, the degree of conversion being up to 39%. The solubility of these polymers is probably the consequence of their lower molecular weight as compared with the polymers obtained at the lower temperature. At 100° (Experiments 10-14, Curve 1), liquid soluble polymers are formed, with a degree of conversion of about 50%; if the latter is increased, insoluble gelatinous polymers are formed.

For determination of the effects of stabilizers and solvents on the polymerization process, parallel experiments were performed on the polymerization of pure divinylacetylene, and its solutions in xylene (40% concentration), in presence and in absence of stabilizer. The experiments were performed in an atmosphere of pure nitrogen in sealed bulbs at 100°. Soluble polymers were formed in these experiments.

It follows from the data in Fig. 2 that the polymerization reaction is retarded in presence of solvent and anti-oxidant. Taken separately, these substances produce somewhat weaker effects (Curves 2 and 3). It follows that to retard the spontaneous polymerization of divinylacetylene in storage, it must be diluted by a solvent and stabilizers must also be added. The polymerization should be carried out in a similar solution.

It was shown as the result of a series of experiments that polymerization of vinylacetylene cannot be continued to 100% conversion of the monomer, owing to the complete insolubility of the polymers formed. If soluble polymers are to be obtained, the polymerization must be terminated before it is complete, and the optimum degree of conversion depends on the temperature, monomer concentration in solution, and inhibitor content and effectiveness. The unpolymerized monomer must be distilled off in order to avoid further polymerization and conversion of the product into the gel state. The polymerization product is highly unstable in that

TABLE 2

Experiments on Polymerization of Acetylene Trimers (9 wt. Parts of Divinylacetylene and 1 wt. Part of Acetylenyldivinyl) at Different Temperatures

Amounts taken (%)			Reaction time (hours)	Reaction temperature (in °)	Yield of soluble polymers (%)
vinylacetylene hydrocarbons	α-naphthylamine	chlorobenzene			
30	0.3	69.7	6	120	53.6
30	0.3	69.7	6	130	64.7
30	0.3	69.7	6	140	66.4
30	0.3	69.7	6	150	69.5

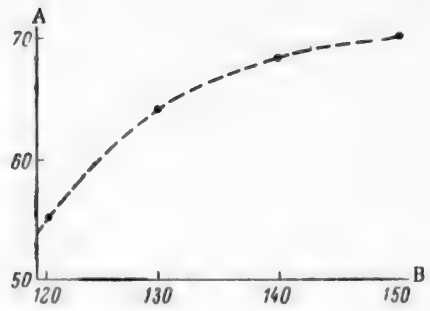

Fig. 4. Effect of polymerization temperature on the polymer yield in the polymerization of technical divinylacetylene; duration of experiments 6 hours, monomer concentration in solution 30%.
A) Polymer yield (%), B) temperature (in °).

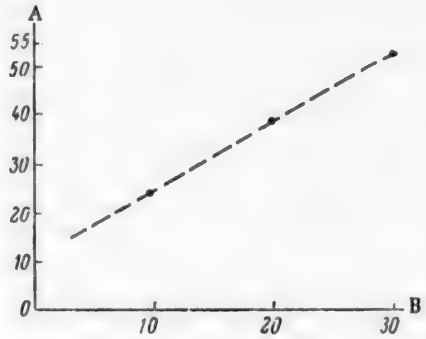

Fig. 5. Effect of concentration of technical divinylacetylene in solution on the polymer yield; heating time 5 hours, reaction temperature 140°.
A) Polymer yield (%), B) concentration of technical divinylacetylene in solution (%).

state, and often undergoes further spontaneous polymerization, which is often explosive in character. This last effect is the result of ineffective removal of the heat of reaction because of the viscosity of the mass, with resulting accumulation of heat, so that the temperature rises sharply above the temperature at which the polymers decompose explosively.

The unpolymerized monomer can be distilled out of the polymer solution only if the solution is sufficiently diluted with some high-boiling solvent, which boils at a higher temperature than the monomer. The unchanged monomer can then be removed completely from the polymers during distillation of the added excess solvent. After removal of the excess solvent, the polymers remain in solution. They can be stored for considerable periods in that form without undergoing noticeable changes.

For selection of the most effective solvent, series of experiments were carried out on the polymerization of technical divinylacetylene in kerosene, various solvent naphtha fractions, chlorobenzene, and xylene. It was found that polymers of vinylacetylene hydrocarbons are insoluble in kerosene and are precipitated during the reaction. Of all the solvent naphtha fractions tested, the most suitable was the xylene fraction (boiling range 130-145°). As the result of a number of experiments it was found that xylene and chlorobenzene are satisfactory solvents for polymers of vinylacetylene compounds. Moreover, these solvents are available industrially.

For determination of the optimum concentration of monomer* in the solutions, polymerization experiments were performed in xylene solutions containing 10, 20, 30, 40, 50, and 70% of the hydrocarbon, at 110°.

* The technical divinylacetylene had the following composition: acetylene trimers 76%, acetylene tetramers + nonvolatile polymers 22%, and vinylacetylene 2%.

The results of these experiments, plotted in Fig. 3, show that as the concentration of technical divinylacetylene in the solution increases, gel formation occurs at a lower degree of conversion and after a shorter time. Dilute solutions, containing about 20% of the monomer, are the most suitable for polymerization of vinylacetylene hydrocarbons, and ensure greater safety in the reaction. With such solutions the degree of conversion before the product passes into the gel state is 70-80% of the original monomer weight. The unpolymerized monomers are distilled off together with excess solvent under vacuum. With higher monomer concentrations in solution (60-70%), 35-45% of the monomer mixture remains at the end of the reaction (in absence of gel formation), and this makes the product unstable. When the monomers are distilled from such concentrated solutions, the products pass into the insoluble state. Conditions for the polymerization of technical divinylacetylene at higher temperatures (120-150°) were also studied. In these experiments the monomer concentration was varied over the 3-30% range. The results in Table 2 and Fig. 4 show that the yield of soluble polymers increases from 54% to 70% (in 6 hours) with increase of the reaction temperature from 120 to 150°.

For determination of the effect of concentration of vinylacetylene hydrocarbons in solution in high-temperature polymerization, comparative experiments were carried out at 140°. In these experiments the monomer concentration was varied from 5 to 30%. The composition of the mixture of acetylene trimers was the same as in the preceding series of experiments. The mixtures were heated on an oil bath at 140°. As in the previous experiments, the yields of nonvolatile polymers were determined in order to follow the course of the reaction. The polymerization time in the experiments of this series was 5 hours. Fig. 5 shows the variations of polymer yield, in polymerization at 140°, with the concentration of the monomer solution.

The results obtained in the polymerization of acetylene trimer mixture in chlorobenzene solutions of different concentrations (Fig. 5) show that the polymer yield increases in proportion to the trimer concentration in solution; the viscosity of the product increases, and its transition into the insoluble gelatinous state is accelerated, with increasing monomer concentration in solution.

Polymers of divinylacetylene and acetylenyldivinyl, formed in dilute solutions (3-10%) at 140°, are soluble and are not precipitated during polymerization, even when the degree of conversion of the monomers is raised to 92-93%.

SUMMARY

The effects of various factors (heating temperature and duration, nature and concentration of solvent and inhibitors) on the polymerization of divinylacetylene was studied, and it was shown that the following are the most favorable conditions for polymerization: the use of dilute solutions (5-20% of divinylacetylene), in an inert gas atmosphere, in presence of 0.5-1% of polyphenols or aromatic amines at 120-150°.

LITERATURE CITED

[1] J. Nieuwland, W. Calcott, B. Downing, and A. Carter, J. Am. Chem. Soc. 53, 4, 197-200 (1931).

[2] A. L. Klebanskii and E. B. Askilazi, Coll. Trans. State Inst. Appl. Chem. 38, 88 (Goskhimizdat, 1947). [In Russian].

[3] I. M. Dolgopol'skii and V. A. Bartashev, J. Appl. Chem. No 12 (1946); Trans. All-Union Sci. Res. Inst. Synthetic Rubber, 1 (State Chem. Press, 1948), 99.

[4] S. S. Medvedev and P. Tseitlin, J. Phys. Chem. 18, 1-2, 13 (1944).

[5] W. Carothers and M. Cupery, J. Am. Chem. Soc. 56, 1167 (1934).

Received June 28, 1957.

THERMAL LIQUEFACTION OF COTTON-HULL LIGNIN*

V. G. Panasiuk

(The Dnepropetrovsk Agricultural Institute)

For comparison of the efficiency of different thermal methods for the conversion of hydrolytic cotton-hull lignin, we determined the degree of liquefaction and the yields of principal products obtained from lignin in thermal liquefaction, and compared the results with the results obtained by dry distillation and vacuum-thermal decomposition in the liquid phase. All the three methods of thermal treatment have certain steps in common, but they differ in the nature of the processes.

Very little information is available in the literature on the thermal liquefaction of hydrolytic lignin.

D'iakova and Melent'eva [1], in their study of the thermal liquefaction of solid fuels and coal-formers, also studied wood lignin, and obtained the following yields (in %), with tetralin as solvent (1:3) at 400° in 30 minutes: gas 7.4; gasoline 8.57; extract soluble in benzene 62.51 (by difference); water 7.62; insoluble residue 13.9; extraction of organic matter, 86.1.

There are no other data on the thermal liquefaction of lignin. Neither is it known what substances, and in what amounts, are obtained from hydrolytic lignin by this method of thermal treatment.

Cotton-hull lignin was used almost exclusively, and the optimum process conditions were used in determinations of the yields obtained from hydrolytic wood lignin.

The experiments on thermal liquefaction were performed in a stirred autoclave, 0.5 liter in capacity, and in a rotary autoclave 2 liters in capacity.

The yields of insoluble residue, gas, water, and tar (solution) were determined by the method prescribed by the Thermal-Liquefaction Group of the Institute of Combustible Minerals of the Academy of Sciences USSR.

Two paste-forming solvents were used in the experiments on thermal liquefaction; one was anthracene oil, boiling in the 230-360° range, which swells hydrolytic lignin, and the other, which has no swelling action, was a solar oil fraction boiling in the same range. These solvents were chosen in order to determine the effect of swelling of lignin on the yields of substances obtained in thermal liquefaction under pressure.

Our work on the vacuum-thermal decomposition of lignin in various paste formers indicated that the best results are obtained with the use of a paste former which swells the lignin. It is not known what paste-formers are the best liquefiers for lignin. According to Sudzilovskaia [2], who worked on the liquefaction of coal, solvents which have a strong swelling effect on coal at low temperatures give low degrees of liquefaction under the solution conditions used.

The results of experiments with anthracene oil as the solvent are given in Table 1.

With anthracene oil as solvent, the best results were obtained at 360°, in 1 hour. The amount of organic matter liquefied in the lignin reached nearly 45%. The amount of gas liberated was much greater than that liberated in 30 minutes.

The yields obtained at 380° in 30 minutes were almost the same as those obtained at 360° in 1 hour. In-

*Communication V in the series on the thermal conversion of hydrolytic lignin.

TABLE 1

Yields of Substances from Cotton-Hull Hydrolytic Lignin in Thermal Liquefaction

Experiment No.	Paste	Process temperature (in °)	time (minutes)	Yield (% on dry lignin)			
				insoluble residue	tar	pyrolytic water	gas
20	Lignin and anthracene oil, 1 : 1.8	360	30	66.0	20.1	5.5	8.4
4	The same	360	60	55.5	21.8	6.4	16.3
27	» »	380	30	62.4	18.4	6.1	13.1
25	» »	400	30	60.4	12.8	6.7	20.1
3	» »	420	30	60.4	8.4	8.7	22.5
16	Lignin and solar oil, 1 : 1.5	360	60	58.8	15.5	8.2	17.5
43	The same	380	60	48.8	23.5	7.2	20.5

crease of the temperature to 400° has an adverse effect on the tar yield, while the gas yield increases considerably. Further rise of temperature leads to a sharp decrease in the yields of insoluble residue and tar, with corresponding increases of the yields of water and gas.

The yield of the most valuable liquefaction product, tar, from cotton-hull hydrolytic lignin can be raised to nearly 22% with the use of anthracene oil as solvent. With the use of solar oil as solvent, in which lignin does not swell, the optimum temperature is 380°, and the time 1 hour. The amount of organic matter dissolved from the lignin is then over 51%, and the tar yield is 23.5%.

The substances formed by the thermal liquefaction of lignin were analyzed only in Experiments No. 4 and No. 43.

The gas had the following composition (vol. %):

	CO_2	CO	C_nH_m	CH_4	H_2	H_2S
Experiment No. 4	69.9	16.55	0.15	7.40	0.95	2.10
Experiment No. 43	53.1	16.07	1.0	22.33	1.10	2.30

It is seen that the gas formed in the thermal liquefaction of lignin in anthracene oil (Experiment No. 4) consists mainly of carbon dioxide and monoxide, their total content being over 86%. The amount of methane found was much less. With the use of solar oil (Experiment No. 43), the total content of carbon oxides is nearly 70%. The methane yield is higher, probably as the result of cracking of the solar oil. The presence of some hydrogen sulfide in the gas suggests that the SO_4'' ions adsorbed by hydrolytic lignin are probably reduced to hydrogen sulfide under the conditions of thermal liquefaction. The contents of unsaturated hydrocarbons and hydrogen in the gas are very low.

Only the tar which distilled up to 230° was investigated; above 230° the solvent remained. The freshly distilled tar fraction boiling up to 230° is yellow, and darkens during storage. The tar formed in Experiment No. 4 is rather high-boiling, and only 8% of it distills up to 230° (calculated on the original dry lignin). In Experiment No. 43 the amount distilled off up to 230° was even somewhat more than the amount of tar obtained from the lignin; this must be attributed to considerable cracking of the solar oil.

The group composition of this fraction is given below:

	Experiment No. 4		Experiment No. 43	
	% of fraction	% of lignin	% of fraction	% of lignin
Acids	2.1	0.18	3.2	1.0
Phenols	18.2	1.58	6.7	2.1
Bases	2.5	0.22	2.2	0.6
Neutral substances	70.1	6.09	79.4	24.6

TABLE 2

Yields of Products in the Thermal Liquefaction of Hydrolytic Hull Lignin

Experiment No.	Paste	Temperature (in °)	Time (minutes)	Yield (% on dry lignin)			
				insoluble residue	tar	pyrolytic water	gas and losses
52	Lignin and anthracene oil, 1:2.5	360	30	70.4	8.4	10.9	10.3
54	The same	360	60	58.7	7.7	14.1	19.5
55	» »	380	30	60.7	6.8	14.5	18.0
53	Lignin and solar oil, 1:2.5	380	30	53.7	12.2	13.6	20.5

Calculated on the original lignin, the phenol yields are 1.58% with anthracene oil as solvent, and 2.1% with solar oil.

Separation of the pyrolytic water during thermal liquefaction was very poor, and the water was therefore separated during distillation of the tar. The aqueous distillate had a weak acid reaction; its refractive index was $n_D^{20} = 1.3380$, and it was of no interest in the investigation.

It may be concluded from the data in Table 1 and from the group composition of the fractions up to 230° that anthracene oil is not the best lignin-swelling solvent, as the tar from the lignin contained only 1.5% of phenols. The process goes somewhat further in solar oil. Several experiments were carried out in order to determine the extent of lignin liquefaction with increased amounts of solvent. The results of these experiments are summarized in Table 2.

The results show that in Experiment No. 52 the liquefaction process was incomplete, as shown by the high value for the insoluble residue. This is confirmed by analysis of the tar, which contained only 1.3% of phenols, calculated on the lignin.

Liquefaction of lignin in Experiments No. 54 and No. 55 was accompanied by considerable cracking of the solvent, as shown by the high gas yields, and by the amounts of tar distilled off up to 230°. In Experiment No. 54 the amount of tar obtained by distillation was 39.2%, while the value by difference was only 7.7%; in Experiment No. 55, 37.9% by distillation and 6.8% by difference, and in Experiment No. 53, 33.7% by distillation and 12.2% by difference.

The group composition of the tar fractions up to 230°, made by thermal liquefaction of lignin, is given below:

	Experiment No. 54		Experiment No. 55		Experiment No. 53	
	% of tar fraction	% of lignin	% of tar fraction	% of lignin	% of tar fraction	% of lignin
Acids	2.67	0.87	4.80	1.42	1.98	0.55
Phenols	12.30	4.02	15.90	4.75	11.90	3.38
Bases	4.80	1.60	7.30	2.17	2.30	0.62
Neutral substances	78.40	25.70	69.70	20.70	76.80	21.90

These analytical results seem to suggest that the liquefaction was more extensive with large amounts of solvent, especially of anthracene oil. A somewhat strange fact is that we never before obtained such high yields of bases as those in Experiments No. 54 and No. 55. The phenols obtained were also different from those obtained previously from cotton-hull lignin. The refractive index of the phenols obtained from hydrolytic hull lignin was consistently (n_D^{20}) 1.52 – 1.54. The phenols isolated from the tar fraction up to 230° in Experiment No. 54 had a

TABLE 3

Yields of Products in the Thermal Liquefaction of Hull Lignin

Experiment No.	Paste	Temperature (in °)	Time (minutes)	Yield (% on lignin)			
				insoluble residue	tar	water	gas and losses
56	Lignin and phenol, 1:2.5	380	30	58.1	16.9	2.5	22.5
57	lignin and anthracene oil, 1:2.5	380	30	34.1	26.5	16.2	21.2

refractive index of 1.5710, and in Experiment No. 55, 1.5715; these values were very close together, but not typical of low-boiling phenols. It seemed likely that these phenols consisted partially of products formed by cracking of phenols from anthracene oil.

To test this hypothesis, we carried out experiments on the thermal decomposition of lignin in anthracene oil washed free from phenols, and also in pure phenol.

Anthracene oil, washed free from phenols by alkali solution, had little effect on the swelling of lignin in these experiments. Lignin showed good swelling in pure phenol (in the melted state).

The results of these experiments are given in Table 3.

Phenol differs little from unwashed anthracene oil as solvent; the yields of products, with the exception of pyrolytic water, were almost the same.

Quite different results were obtained with the use of phenol-free anthracene oil as solvent. The degree of liquefaction of lignin in it reached nearly 66%, which had not been obtained before.

The group composition was determined only in the case of the tar fractions in Experiment No. 57. This composition was not determined in Experiment No. 56, as it proved impossible during the analysis to separate the phenol solvent from the phenols formed from the lignin.

The composition of the 180-230° tar fraction is given below:

	Acids	Phenols	Bases	Neutral substances
Contents (%)				
of tar fraction	6.30	12.60	9.70	68.10
of lignin	0.97	1.95	1.50	10.50

The somewhat higher yield of bases must evidently be attributed to bases in the anthracene oil. The phenol yield was only 1.95% on the lignin. The refractive index was 1.5320, which agrees satisfactorily with the refractive index of low-boiling phenols. Therefore the phenols obtained in Experiments No. 54 and No. 55 must be partially attributed to phenols from the anthracene oil solvent. Therefore the yield of phenols from lignin in thermal liquefaction in anthracene oil is 2%, but no higher. Better results were obtained with solar oil, which does not swell lignin; the phenol yield was over 3%.

It follows from all the foregoing data on the thermal liquefaction of hydrolytic hull lignin in anthracene oil that the highest amount of the organic matter of the lignin which can be liquefied in the form of tar, pyrolytic water, and gas is 44.5%.

The yield of phenols from lignin can be up to 1.6% under the optimum experimental conditions. More extensive liquefaction of the lignin, with phenol yields up to 2%, can be attained with the use of phenol-free anthracene oil as solvent. This oil has little swelling effect on lignin. Better results are obtained with the use of solar oil as solvent. Thus, with lignin and solar oil in 1:1.5 ratio the phenol yield reaches 2.1%. With a higher proportion of solvent (1:2.5) the phenol yield can be raised to 3.4%.

TABLE 4

Yields of Products in the Thermal Liquefaction of Hydrolytic Wood Lignin

Experiment No.	Paste	Reaction temperature (in °)	Time (minutes)	Yield (% on dry lignin)			
				insoluble residue	tar	pyrolytic water	gas and losses
46	Wood lignin and solar oil, 1 : 1.5	360	30	61.0	13.8	11.2	14.0
50	The same 1: 1.5	380	30	59.5	16.0	13.8	11.7
47	» » 1 : 2.5	360	30	56.2	16.6	12.8	14.4
51	» » 1 : 2.5	380	30	54.3	18.4	10.8	16.5

TABLE 5

Group Analysis of Tar Fractions up to 230°

	Experiment No. 50		Experiment No. 51	
	% of tar fraction	% of lignin	% of tar fraction	% of lignin
Acids	1.8	0.3	3.0	1.3
Phenols	13.3	2.1	8.5	3.8
Bases	0.5	0.1	0.85	0.38
Neutral substances .	83.5	13.4	84.5	12.62

Fewer experiments were carried out with wood lignin; the results are given in Table 4.

Here, as in the experiments with hull lignin, there was considerable cracking of the solar oil; the yield of tar fraction distilled up to 230° was 34.4% in Experiment No. 50, and 72.2% in Experiment No. 51. Analysis of these fractions showed that, as the data in Table 5 show, considerably higher yields of valuable products such as phenols are obtained if larger amounts of solvent are used.

It is evident from the results in the table that increase of the amount of solvent favored deeper breakdown of the lignin molecules, and the phenol yield was nearly doubled.

Investigation of the substances obtained from lignin as the result of treatment by this method should make it possible to determine the differences between the substances obtained by different thermal methods of lignin conversion.

SUMMARY

1. For comparison of different thermal methods for the conversion of hydrolytic lignin, experiments were carried out on the thermal liquefaction of cotton-hull lignin in anthracene and solar oils.

2. The yield of the tar fraction (liquefied lignin) with the use of anthracene oil as solvent can be raised to 22%, with up to 1.6% of phenols on the dry lignin. With the use of solar oil, the tar yield is 23.5% of phenols on the lignin.

3. The degree of liquefaction was not increased by the use of pure phenol, which considerably assists the swelling of lignin, as solvent.

4. With the use of phenol-free anthracene oil as solvent, the percentage liquefaction of the lignin was raised to 66%.

5. Considerably higher yields of phenols are obtained at higher solvent ratios (1:2.5).

6. In the thermal liquefaction of wood lignin, better results were also obtained at higher solvent ratios. The phenol yield can be raised up to 3.8%.

7. The degree of liquefaction of lignin is somewhat lower in solvents which favor the swelling of lignin than in solvents which do not have a swelling effect, under analogous conditions. In this respect thermal liquefaction differs from vacuum-thermal decomposition of lignin in the liquid phase.

LITERATURE CITED

[1] M. K. D'iakova and N. V. Melent'eva, J. Appl. Chem. 15, 3 (1942).

[2] M. S. Sudzilovskaia, Trans. All-Union Sci. Res. Inst. Combustible Minerals 1 (1948).

Received March 4, 1957.

SYNTHESIS OF ALLYL ALCOHOL BY ISOMERIZATION OF PROPYLENE OXIDE

P. G. Sergeev, L. M. Bukreeva, and A. G. Polkovnikova

Literature data on the isomerization of propylene oxide are confined to a few papers and patents [1-6], which indicate that a mixture of propionic aldehyde and allyl alcohol is formed in the reaction. The production of allyl alcohol by isomerization of propylene oxide is undoubtedly a very attractive method if the yield of allyl alcohol could be increased and the amounts of by-products lowered. The best results in this respect were obtained with the use of Li_3PO_4 catalyst, first proposed in 1947 [7], but even with this catalyst a mixture of 80% allyl alcohol and 20% propionic aldehyde was obtained. This experiment was repeated in the USSR by P. V. Zimakov, who obtained the same results as those reported in the patent [7].

The purpose of the present investigation was to study the formation of allyl alcohol by isomerization of propylene oxide with the use of Li_3PO_4 as the most active catalyst, in order to develop an industrial process for the production of allyl alcohol.

EXPERIMENTAL

Experimental procedure. The catalysts used for isomerization of propylene oxide were Li_3PO_4, and Li_3PO_4 + filler. The Li_3PO_4 catalyst was made by precipitation from 15% lithium nitrate solution by the addition of 15% trisodium phosphate solution. The precipitate was washed with water to remove NO_3' ions, molded, and dried at 75-80°.

The Li_3PO_4 + filler catalysts were made by thorough mixing of a moist Li_3PO_4 paste with the filler. The amounts of filler were varied. The best results were obtained with catalysts containing 70% Li_3PO_4 and 30% filler.

The original propylene oxide boiled at 34° (756 mm) and had $d_4^{20} = 0.8304$, $D^{20} = 1.3657$.

The experiments were performed in a carbon-steel tube (20 mm in diameter and 1000 mm long), heated in an electric furnace.

The propylene oxide was fed from a water-cooled buret into an evaporator, from which it entered the furnace in vapor form. The liquid reaction products were collected in traps cooled in ice – salt mixture, and the gases were collected in a gas holder. Propylene oxide, allyl alcohol, and propionic aldehyde were determined in the condensate.

Propylene oxide was determined by the Deckert – Lubatti method, based on the quantitative reaction of oxides with metallic chlorides with formation of chlorohydrins. Allyl alcohol was determined by the bromide – bromate method, and also by acetylation of the hydroxyl group by glacial acetic acid in presence of BF_3. Propionic aldehyde was determined by means of hydroxylamine hydrochloride.

For confirmation of the analytical results, the condensate was distilled through a laboratory column and fractionated. It was found that the analytical data agree with the fractionation results.

Study of the isomerization of propylene oxide over Li_3PO_4 catalyst. The optimum process conditions were found to be a temperature of 280° in the contact zone, and a feed rate of 1600 ml of liquid propylene oxide per liter of catalyst per hour. Under these conditions the only reaction product is allyl alcohol, the yield of which, calculated on the propylene oxide decomposed, is 94-96%. Virtually no propionic aldehyde is formed. The amount of propionic aldehyde in the condensate increases, and the percentage of allyl alcohol decreases, with

TABLE 1

Effect of Temperature on the Yield of Allyl Alcohol. Feed rate of liquid propylene oxide 1200 ml per liter of catalyst per hour

Reaction temperature (in °)	Yield of allyl alcohol, calculated on the propylene oxide decomposed (% of theoretical)	Amount of allyl alcohol (in g per liter of catalyst per hour)
200	75	200
280	91.8	225
300	77.6	282
330	68.1	454
375	66.3	456

TABLE 2

Effect of the Feed Rate of Propylene Oxide on the Yield of Allyl Alcohol. Reaction temperature 280°

Feed rate of liquid propylene oxide, ml per liter of catalyst per hour	Yield calculated on the propylene oxide decomposed (% of theoretical)	
	allyl alcohol	propionic aldehyde
498	57.0	40.3
700	63.2	32.5
995	76.2	21.3
1100	84.0	10.1
1600	98.0	Traces

TABLE 3

Poisoning of Li_3PO_4 Catalyst. Feed rate of liquid propylene oxide 1600 ml/hour per liter of catalyst, temperature 280°

Service time of catalyst (hour)	Composition of condensate (wt. %)		Yield of allyl alcohol, calculated on the propylene oxide decomposed (% of theoretical)	Catalyst efficiency (g/liter · hour)
	allyl alcohol	propylene oxide		
6	27.1	69.5	96.9	351
14	27.6	68.5	96.1	351
22	28.1	66.3	94.4	364
30	20.2	77.6	97.8	260
38	18.8	79.3	98.8	247
47	14.9	83.8	100.0	238
56	12.8	86.2	99.0	195
63	11.1	87.4	98.5	143
70	10.9	86.6	97.5	141
80	8.3	90.7	99.0	104
After regeneration*				
6	5	93	98	65

decreasing feed rate of propylene oxide; the lower the space velocity, the more propionic aldehyde is formed (Tables 1 and 2).

A disadvantage of Li_3PO_4 catalyst is its instability. We found that after 70 hours of use it loses its activity completely, and none of the regeneration methods tried restored the activity (Table 3). This is probably the result of its great sensitivity to high temperatures. It is completely inactivated by calcination at 450°. When tars are burned out of the spent catalyst in a current of air or air – steam mixture, the temperature may rise at the active centers. The effects of dilution of the catalyst with fillers, as a means of reducing this process and preventing overheating, were tested.

Our hypothesis that the service life of Li_3PO_4 catalyst would be increased, and its regeneration facilitated, by the use of fillers was completely justified. Catalysts consisting of 70% Li_3PO_4 + 30% filler are effectively regenerated, and can be used for over 1000 hours with periodic regeneration at intervals of 70 to 80 hours.

* The catalyst was regenerated in a current of air – steam mixture for 3 hours at 375°.

TABLE 4

Tests of Catalyst Consisting of 70% Li_3PO_4 + 30% Filler. Temperature 280°, feed rate of liquid propylene oxide 1600 ml per liter of catalyst per hour

Service time of catalyst (hours)	Composition of condensate (wt. %)		Yield of allyl alcohol, calculated on the propylene oxide decomposed (% of theoretical)	Catalyst efficiency (g/liter · hour)
	allyl alcohol	propylene oxide		
8	29.8	70	99.8	387.4
17	28.8	71.0	99.8	374.4
24	32.1	60.8	92.9	416.0
31	23.4	73.2	96.6	304.2
40	20.6	76.1	96.7	267.8
47	20.0	74.5	94.5	267.4
57	15.4	83.2	98.6	200.2
65	14.4	85.1	99.6	187.2
70	12.5	85.9	98.4	162.5
79	10.55	88.1	98.6	136.5
85	9.8	90.1	99.9	127.4
After regeneration				
93	25.2	73.4	98.6	325
102	23.3	72.6	97.0	299
109	23.2	74.5	97.7	299
118	18.7	80.1	98.8	247
125	20.4	79.1	99.5	260
133	20.2	78.6	98.8	260
141	18.3	80.0	98.3	234
150	15.5	81.2	96.7	195
157	13.2	85.2	98.4	169
165	10.8	88.1	98.9	143
173	8.8	89.0	97.8	114.4

TABLE 5

Effect of Contact Time on the Yields of Allyl Alcohol and Propionic Aldehyde

Contact time (seconds)	Yield calculated on the propylene oxide decomposed (% of theoretical)	
	allyl alcohol	propionic aldehyde
18	40.3	58.1
15	57	40
10	78	21.5
6.7	88	10.5
4.8	90.2	8.2
3.5	99.8	Traces

TABLE 6

Isomerization of Allyl Alcohol to Propionic Aldehyde over Li_3PO_4 Catalyst. Contact time 25 seconds

Feed rate of 96% allyl alcohol, in g per liter of catalyst per hour	Temperature (in °)	Composition of condensate (%)		Yield of propionic aldehyde on the allyl alcohol decomposed (%)
		allyl alcohol	propionic aldehyde	
200	280	10.3	70.1	77
200	280	8.0	72.0	80.7

The regeneration is simple; it consists of calcination of the catalyst at 375° for 3 hours in a stream of steam – air mixture.

The results of tests of a catalyst consisting of 70% Li_3PO_4 + 30% filler are given in Table 4.

The catalyst was used under the same conditions for 1100 hours, with periodic regeneration at 80-hour intervals. Longer periods were not tried. The average output of the catalyst in 1100 hours was 240 g of allyl alcohol per liter of catalyst per hour.

Suggested Mechanism of the Isomerization of Propylene Oxide. The isomerization of propylene oxide has until now been represented as follows:

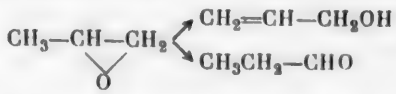

which suggests that the two reactions, i. e. isomerization of propylene oxide to propionic aldehyde, and isomerization of propylene oxide to allyl alcohol, occur simultaneously. We made the following observations in our study of the isomerization of propylene oxide over lithium phosphate catalyst. When propylene oxide is passed through the catalyst with a short contact time (3.5 seconds), the only reaction product is allyl alcohol, and only traces of propionic aldehyde (0.01-0.02%) were detected.

If the contact time is increased, the yield of allyl alcohol on the decomposed propylene oxide falls, while the yield of propionic aldehyde rises (Table 5). This led us to the conclusion that the primary isomerization product of propylene oxide is allyl alcohol, which is subsequently converted into propionic aldehyde.

The following experiment was carried out to confirm this conclusion: liquid allyl alcohol (96%) was passed at the rate of 200 g per hour per liter of catalyst (lithium phosphate) at 280°. It was found that the principal product of the conversion of allyl alcohol was propionic aldehyde (Table 6).

The data in Table 6 confirm our hypothesis that propionic aldehyde is a secondary conversion product of allyl alcohol in the isomerization of propylene oxide.

In our opinion, the isomerization of propylene oxide can be represented as follows:

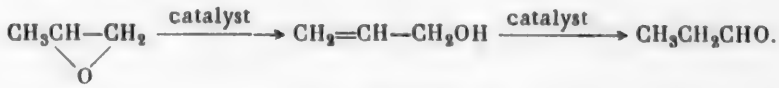

SUMMARY

1. The formation of allyl alcohol by isomerization of propylene oxide was studied, the reaction mechanism was determined, and it was shown that the primary reaction product is allyl alcohol, and the secondary, propionic aldehyde.

2. The best catalyst for the process is 70% Li_3PO_4 + 30% filler.

3. With a contact time of 3.5 seconds the yield of allyl alcohol on the decomposed propylene oxide is 94-98%. The reaction products consist of 20-30% allyl alcohol and 80-70% propylene oxide. Traces (0.01-0.02%) of propionic aldehyde were detected. Allyl alcohol can be easily separated from propylene oxide by rectification.

4. The catalyst of 70% Li_3PO_4 + 30% filler does not lose activity when used for over 1000 hours with periodic regeneration at intervals of 70-80 hours. The average output of the catalyst over 1000 hours of operation is 240 g of allyl alcohol per hour per liter of catalyst.

LITERATURE CITED

[1] Lester, Ind. Eng. Ch. 43, 728 (1951).

[2] Perry, Ind. Eng. Ch. 44, 2037 (1952).

[3] Perry, Ind. Eng. Ch. 42, 1715 (1950).

[4] A. P. Terent'ev, Proc. Acad. Sci. USSR 24, 5 (1950).

[5] German Patent 331,185 (1929).

[6] Canadian Patent 328,050 (1932); Chem. Abs, 27, 1012 (1933).

[7] U. S. Patent 2, 426, 264 (1947); Chem. Abs. 583 (1948).

Received February 25, 1957.

PREPARATION OF 2-ETHYLHEXANOL-1 BY CONDENSATION OF n-BUTANOL

A. I. Kutsenko and V. I. Liubomilov

(Organic Synthesis Laboratory, Scientific Research Institute of Plastics)

2-Ethylhexanol-1 was prepared by Guerbet [1], by condensation of n-butanol in presence of its own sodium alcoholate at 200-250° in a sealed tube. In addition to 2-ethylhexanol-1, the reaction products contained butyric and 2-ethylhexanoic acids. In further research, which is reviewed in papers by Machemer [2] and Kobayashi [3], a method was developed for condensation of alcohols in presence of alcoholates and dehydrogenation catalysts, in which the reaction temperature could be lowered. In addition to the main reaction of alcohol condensation

$$2RCH_2CH_2OH \longrightarrow RCH_2CH_2CHRCH_2OH + H_2O \qquad (1)$$

there is a side reaction in which the corresponding acid is formed because the water liberated in Reaction (1) decomposes the alcoholate present in the reaction mass, with formation of the alcohol and caustic alkali. The latter reacts with the alcohol in presence of catalysts, and at high temperature in absence of the latter, to form the salt of the carboxylic acid

$$RCH_2CH_2OH + NaOH \longrightarrow RCH_2COONa + 2H_2. \qquad (2)$$

Thus, one molecule of acid is formed for each molecule of alcohol with twice the number of carbon atoms.

Methods proposed for reduction of acid formation included condensation of alcohols with removal of the reaction water by distillation during the reaction [2, 4-6], or with binding of the water by various means [3, 7].

During the past 10 years we studied possible means of improving the process for condensation of n-butanol and, independently of the papers cited above, developed a method of condensation with removal of the reaction water by distillation. As the purpose was to develop an industrial method for production of 2-ethylhexanol-1, the alcoholate was prepared, not by dissolution of the alkali metal in n-butanol, but by dissolution of caustic soda in the latter followed by removal of water from the equilibrium mixture with the aid of a fractionating column; this method has long been known [8, 9]. Catalyst* was added to the sodium butylate solution, and the boiling was continued, the reaction water being distilled off; this gave yields of up to 78%, calculated from Equation (1), of 2-ethylhexanol-1.

These experiments showed that it is possible to use quite low concentrations of sodium butylate in n-butanol, and to carry out the reaction at 116-118° at the start and at 128-168° at the end of the process. Subsequently the method used for condensation of n-butanol was considerably simplified, the reactions of alcoholate formation and condensation being combined in one process. The yield of 2-ethylhexanol-1 was even increased somewhat; as a result, it reached 82.0% Such high yields in alcohol condensation have not been previously reported in the literature. It is interesting to note that the small amounts of salts of carboxylic acids formed when the condensation was performed with distillation of water contained only 25-40% of sodium butyrate, and a small amount of the sodium salt of 2-ethylhexanoic acid, and consisted mainly of the salt of a hydroxy acid which was isolated as the lactone $C_{12}H_{22}O_2$. We believe that the hydroxy acid was 2, 4-diethyl-5-hydroxycaprylic acid.

* The catalysts generally used for hydrogenation were used. They acted as dehydrogenation catalysts in this process.

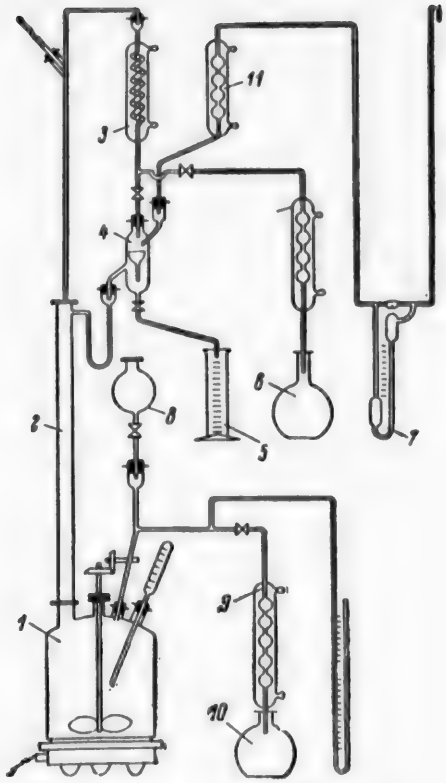

Preparation of 2-ethylhexanol-1.

Other by-products are higher saturated and unsaturated alcohols, formed in yields of 8-12% of the amount of 2-ethylhexanol-1.

It should be noted that the 2-ethylhexanol-1 fraction always contains an admixture of a few percent of the unsaturated alcohol 2-ethylhexanol-1 [10]. Completely pure 2-ethylhexanol-1 was obtained by catalytic hydrogenation. Butyraldehyde is always formed during the condensation of n-butanol; it is undoubtedly an intermediate reaction product in the formation of 2-ethylhexanol [11], and of butyric acid [12].

EXPERIMENTAL

Method. The apparatus shown in the diagram was used for the preparations. 5000 g of technical n-butanol (GOST 5208-51), 150-250 g of toluene, and technical caustic soda flakes were put into the steel vessel 1 equipped with a heater. The stirrer was switched on and the vessel was heated to ensure vigorous boiling. The vapors of n-butanol, toluene, and water passed through the column 2, 600 mm high and 40 mm in diameter, packed with Raschig rings 7 × 7 mm, and condensed in the condenser 3; the distillate passed into the water separator 4, where it separated into two layers. The upper layer was refluxed back into the column, while the lower layer (water) was periodically run off into the cylinder 5.

The formation of alcoholate was continued for 12-15 hours, at a temperature of 110-118° in the steel vessel, until liberation of water ceased. This was followed by distillation of 2.5-3.0 liters of a butanol – toluene fraction into the receiver 6; the temperature in the steel vessel rose to 120-122° in the process. A weighed quantity of the catalyst, basic copper carbonate previously dried for several hours in an oven at 120-135°, was added to the concentrated butylate solution. The steel vessel was heated at such a rate as to ensure that the distillate circulated vigorously through the water separator. As soon as reaction water began to separate in the water separator, the flow meter 7 began to indicate the liberation of hydrogen. When the hydrogen rate reached 80-100 ml/minute, the previously distilled butanol – toluene fraction was introduced into the steel vessel from the dropping funnel 8. The addition lasted about 2-4 hours. At the end of the addition, circulation of the reflux was continued until separation of water ceased; at this stage the liberation of hydrogen stopped almost entirely. Part of the unchanged n-butanol was distilled through the condenser 9 into the receiver 10, until the temperature in the vessel reached 134-136°. The reaction mass was treated by either of two methods to separate the reaction products: it was either removed from the apparatus, filtered free from catalyst, and washed with water, or it was distilled in steam. In both cases an alcoholic layer was obtained, containing 2-ethylhexanol, residual butanol, unsaturated alcohols and higher alcohols, and an aqueous solution of the sodium salts of butyric acid, 2-ethylhexanoic acid, 2, 4-diethyl-5-hydroxycaprylic acid, and higher acids. A sample of the alcoholic layer was distilled under atmospheric pressure through a laboratory dephlegmator, 20 cm high; fractions of aqueous n-butanol, and a 2-ethylhexanol fraction in the boiling range of 178-185°, were collected. The presence of n-butanol was also established in the wash waters by rectification of the wash waters, or of the condensates from the steam distillation. A sample of the solution of sodium salts was evaporated down, and the organic acids were isolated by addition of concentrated sulfuric acid. The liberated acids were dried over calcium chloride and fractionated.

Determination of the optimum alcoholate concentration. Table 1 contains the results of experiments carried out with equal amounts of catalyst, but with different amounts of caustic soda taken for preparation of the alcoholate. It is seen that the optimum amount of alkali (Experiment No. 39) is 150 g. If larger amounts are taken, n-butanol is consumed in acid formation, whereas with smaller amounts the conversion of n-butanol decreases sharply. With 150 g of caustic soda the concentration of sodium butylate is 7.1%.

TABLE 1

Determination of the Optimum Alcoholate Catalyst Concentration – 20 g of basic copper carbonate

Experiment No.	Amount of caustic soda (g)	Condensation time (hours)	Temperature at end of condensation (in °)	Yields (g)						Yield of 2-ethylhexanol-1 (% of theoretical)
				water*	unreacted n-butanol	2-ethylhexanol-1	higher alcohols	butyric acid	high boiling acids	
15	250	55	126	193	2900	1316	143	419	146	71.0
39	150	74	126	198	2948	1357	259	212	95	75.6
36	100	49	128	133	3736	832	174	135	74	74.7

TABLE 2

Tests of Different Catalysts. Sodium butylate concentration 7.1%, 40 g lots of catalysts

Catalyst	Condensation time (hours)	Condensation temperature (in °)	Yields (g)						Yield of 2-ethylhexanol-1 (% of theoretical)
			water*	unreacted n-butanol	2-ethylhexanol-1	higher alcohols	butyric acid	high-boiling acids	
Basic copper carbonate	73	128	221	3211	1205	125	122	302	76.5
Copper – chromium (Adkins)	49	126	123	3489	925	225	168	138	69.5
Nickel on chromium oxide	65	168	461	916	2807	339	92	229	78.0

TABLE 3

Experiments Without Preliminary Formation of Alcoholate. 150g of caustic soda and 60 g of catalyst taken

Catalyst	Condensation time (hours)	Temperature at end of condensation (in°)	Yields (g)						Yield of 2-ethylhexanol-1 (% of theoretical)
			water	unreacted n-butanol	2-ethylhexanol-1	higher alcohols	butyric acid	high-boiling acids	
Nickel on chromium oxide	58	140	595	879	2620	440	83	122	75.0
Nickel on aluminum oxide	62	126	354	2710	1378	286	48	193	69.2
Nickel on kieselguhr	98	140	560	1317	2350	523	93	108	72.8

Tests of different catalysts. The results of experiments with 40 g lots of different catalysts, with 7.1% butylate concentration in each case, are given in Table 2. In addition to basic copper carbonate, the copper – – chromium catalyst of Adkins [13], and an industrial nickel – chromium oxide catalyst, were tested. The best results were obtained with the last of these, with which the yield of 2-ethylhexanol-1 was 78% of the theoretical, calculated on the n-butanol consumed.

Experiments without preliminary preparation of alcoholate solution. It was noticed in one of the experi-

*Only the amount of water formed during condensation is given.

TABLE 4

Determination of the Optimum Amount of Catalyst (Nickel on Chromium Oxide) for the Combined Reaction. 150 g of caustic soda taken

Amount of catalyst (g)	Condensation time (hours)	Temperature at end of condensation (in °)	Yields (g)						Yield of 2-ethylhexanol-1 (% of theoretical)
			water	unreacted n-butanol	2-ethylhexanol-1	higher alcohols	butyric acid	high boiling acids	
40	99	169	639	541	3222	428	125	156	82.2
60	58	140	595	879	2620	440	83	122	75.0
200	13	150	625	610	2970	538	126	173	74.4
470	11.5	140	550	1108	2540	388	146	64	74.5

TABLE 5

Bromine Numbers of the 2-Ethylhexanol Fraction

Catalyst (g)		Caustic soda (g)	Bromine number
Basic copper carbonate	60	250	13.2
	20	250	39.4
	60	100	32.1
Nickel on chromium oxide	40	150	3.4
	40	150	8.8
	60	150	1.9
	180	150	3.5
Nickel on kieselguhr	60	150	9.3
	60	150	4.4

ments with the industrial nickel – chromium oxide catalyst that hydrogen was evolved during formation of the alcoholate. This was found to be a consequence of the fact that the catalyst from the previous experiment had not been completely removed from the reaction vessel. Earlier, in experiments with basic copper carbonate, it had been observed that the catalyst passed into the active form, i. e., is converted into copper oxides, only when added to the concentrated alcoholate solution, and especially if the sodium butylate solution does not contain caustic soda. In the presence of caustic soda the catalyst was not converted into the active form, but was evidently converted into metallic copper, which sometimes even formed a copper mirror on the vessel walls (if a glass flask was used). The active form of the catalyst from basic copper carbonate is less sensitive to the action of caustic soda, but loses its activity when treated with water, namely, during steam distillation of the reaction products, or during washing with water. The undoubted advantage of the nickel catalyst is that it is immeasurably less sensitive to the action of water or caustic soda. Experiments in which n-butanol, caustic soda, and nickel catalysts were put in together showed that it is possible to prepare 2-ethylhexanol-1 without a separate stage of sodium butylate formation. As a result, the time required for the process as a whole could be shortened considerably. The results of experiments carried out with industrial nickel catalysts by this method are given in Table 3. The best results, with regard to the yield of 2-ethylhexanol-1, the percentage conversion of n-butanol, and the reaction time, were again obtained with nickel – chromium oxide catalyst.

Determination of the optimum amount of catalyst. The results of experiments with different amounts of catalyst (nickel on chromium oxide) are compared in Table 4. It follows from Table 4 that with a small amount of catalyst about 90% of the butanol can be converted, the yield of 2-ethylhexanol-1 being 82.2% of the theoretical. However, this procedure is disadvantageous, because of the long reaction time needed. The reaction time can can be shortened to 11-13 hours by a considerable increase of the amount of catalyst, with a yield of over 74% of 2-ethylhexanol-1, and a high conversion of n-butanol. In experiments with other amounts of catalyst, the results of which are not given in the table, the whole process took 20-24 hours when 2 to 3% of catalyst on the weight

of n-butanol was taken, the concentration of sodium butylate being 7.1% as before. In this case the yield of 2-ethylhexanol-1 was 76-80%. This result was later confirmed on the industrial scale.

Regeneration of catalyst. As the catalyst (nickel on chromium oxide) did not lose its activity after treatment with water, it was possible to use the catalyst from preceding operations for the preparation of 2-ethylhexanol-1. Its activity remained at its initial level provided that it was washed with hot water to remove adsorbed salts of organic acids. It was therefore expedient to treat the reaction products by the second of the methods described earlier, i. e., by steam distillation. The catalyst was thereby automatically washed with water.

Losses of organic matter with the liberated hydrogen. The hydrogen liberated in the reaction always had a strong odor of butyraldehyde. To estimate the possible losses, the hydrogen was passed through columns filled with activated carbon type E. The weight increase of the columns indicated that the hydrogen, cooled in the condenser 11 (see diagram), carries away from 25 to 33 g of organic matter with it. This is a little more than 0.5% by weight of the n-butanol and toluene taken. Desorption by means of steam yielded about 8-10 g of butyraldehyde. It was identified by the formation of its 2, 4-dinitrophenylhydrazone of m.p. 121.5-122°, which agrees with literature data [14]. The remaining 15-23 g consisted of volatile hydrocarbons.

Preparation of pure 2-ethylhexanol-1. The 2-ethylhexanol fraction of b. p. 178-185° always had a measurable bromine number, owing to an admixture of 2-ethylhexanol-1. The bromine number depended on the catalyst efficiency and a number of other factors. The magnitude of the bromine numbers (determined by the Kaufmann method) is indicated in Table 5. As a rule, nickel catalysts operating at high efficiencies gave products of low bromine numbers. In order to obtain 2-ethylhexanol-1 free from impurities, the 2-ethylhexanol fraction was subjected to catalytic hydrogenation*, the product having zero bromine number. Subsequently it proved more advantageous to hydrogenate, not the 2-ethylhexanol fraction, but the reaction product after steam distillation and removal of the dissolved water and part of the n-butanol. The hydrogenation was carried out in a continuous unit, with the same catalyst (nickel on chromium oxide), under a hydrogen pressure of 120 atmos, at 135-140°, the feed rate being 0.5 liters/hour per liter of catalyst, with hydrogen: product in 4:1 molar ratio. The hydrogenation product had bromine number 0.5-0.7. This product was subjected to vacuum distillation through a column 650 mm high, packed with glass Raschig rings 5 × 5 mm; this gave 2-ethylhexanol-1 with the following properties: b. p. 183-183.5° (760 mm), d_4^{20} 0.8325, n_D^{20} 1.4325, bromine number not over 0.05. The constants correspond to the literature data for the pure compound [15]. The amount of pure 2-ethylhexanol-1 prepared in this way exactly corresponds to the percentage content of the 2-ethylhexanol fraction from the crude product.

The residue in the still after rectification of the hydrogenation product consists mainly of branched-chain alcohols with 12 and 16 carbon atoms in the molecule. Its bromine number is low, and can be reduced to zero by hydrogenation under harsher conditions.

Composition of the acid products. It follows from the data in Tables 1-4 that the ratio of butyric acid to high-boiling acids varies over a wide range. The high boiling acids was our term for the residue which remained after distillation of butyric acid. It was a dark liquid of acid number 70-74. Fractionation of this residue through a small column yielded 15-20% of 2-ethylhexanoic acid, b. p. 225-226° (760 mm); d_4^{20} 0.9115; n_D^{20} 1.4270; acid number 386.4.

$C_8H_{16}O_2$. Calculated: acid number 388.8. Lactone fraction in a yield of 65-70%, b. p. 131-123° (5 mm); d_4^{20} 0.9599; n_D^{20} – 1.4620; ester number 271.5.

$C_{12}H_{22}O_2$. Calculated: ester number 283.1.

SUMMARY

1. A method has been developed for preparation of 2-ethylhexanol-1 in yields of up to 82.0%, by condensation of n-butanol in presence of caustic soda and an industrial hydrogenation catalyst (nickel on chromium oxide), with removal of reaction water by distillation; the reactions of alcoholate formation and condensation are combined in a single process.

2. Pure 2-ethylhexanol-1 was prepared by catalytic hydrogenation of the reaction product, followed by rectification.

* The catalytic hydrogenation was performed under the guidance of P. A. Moshkin, to whom we offer our deep gratitude.

LITERATURE CITED

[1] M. Guerbet, C. r. 133, 1220 (1901).

[2] H. Machemer, Ang. Ch. 64, 213 (1952).

[3] R. Kobayashi, J. Soc. Organ. Synth. Chem. Japan, 13, 85 (1955).

[4] Belgian Patent 446,793 (1943).

[5] U. S. Patent 2,457,866 (1949).

[6] E. F. Pratt and D. G. Kubler, J. Am. Chem. Soc. 76, 52 (1954).

[7] I. Boll, C. r. 233, 1628 (1951).

[8] French Patent 653,818 (1929).

[9] U. S. Patent 1,712,830 (1929).

[10] V. I. Liubomilov, Candidate's Dissertation (Moscow, 1950). [In Russian]

[11] W. Hükkel and H. Naab, Ber. 64, 2137 (1931).

[12] V. I. Liubomilov, A. I. Kutsenko, and R. A. Abramova, J. Gen. Chem. 27, 2054 (1957).*

[13] Organic Syntheses (Moscow, IL, 1949), p. 301 [Russian translation].

[14] N. R. Campbell, Analyst, 61, 391 (1936).

[15] Dictionary of Organic Compounds, London, 2 (1953), 507.

Received January 29, 1957.

*Original Russian pagination. See C. B. Translation.

BRIEF COMMUNICATIONS

INVESTIGATION OF THE CONDITIONS FOR THE FORMATION OF LANTHANUM CARBIDE

M. S. Koval'chenko, V. S. Neshpor, and G. V. Samsonov

Lanthanum carbide may be formed as an impurity in lanthanum hexaboride when the latter is prepared by methods involving the use of carbon as reducing agent [1]; this may be shown by the characteristic odor of the carbide decomposition products, and by the results of chemical analysis. The emissive properties of the hexaboride are adversely affected by the presence of carbide and its solid decomposition products.

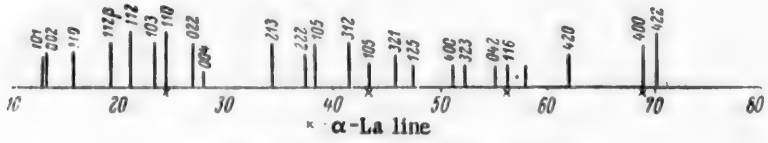

Line diagram of lanthanum carbide.

It was observed that the emission of lanthanum boride on a tungsten filament improves after the tube has been in operation for some time; this is possible due in part to gradual removal of lanthanum carbide and its decomposition products under the action of heat in a high vacuum. It is therefore important to find the technological conditions for formation of lanthanum hexaboride in pure form, without carbide as an impurity; for this, in turn, it is necessary to know the conditions in which lanthanum carbide is formed. There are no accounts of such conditions in the literature, although the existence of this compound was confirmed long ago [2], and it is reported that the carbides of the rare-earth metals may be formed when the oxides are heated with carbon. In the case of cerium carbide the reaction occurs at about 2000° [3].

In the present investigation lanthanum carbide was made by reduction of lanthanum oxide in a graphite tubular furnace at temperatures from 900 to 2000° (in 100° steps) for 1-2 hours, according to the equation

$$\underset{\downarrow}{3\overset{\times}{PbSO_4}} + 2K_3PO_4 \rightleftarrows \underset{\downarrow}{Pb_3(PO_4)_2} + 3\overset{\times}{K_2SO_4},$$

The lanthanum oxide was mixed with sufficient carbon black to complete the reaction. The mixture was molded in the form of briquets to improve contact between the oxide and carbon particles. The reaction product was analyzed chemically for total and free carbon, and the results were used to calculate the amount of combined carbon as the carbide phase.

The results of chemical analysis are presented in Table 1.

It is seen that active formation of lanthanum carbide begins at 1700° and over; the most favorable temperature for its formation being 1850° with an exposure of 2 hours. The specimens so formed are fused on the outside, and coated with a gray crust 1-2 mm thick.

Thus, the preparation of lanthanum hexaboride in a medium containing carbon must be carried out at the

TABLE 1

Results of Experiments on Preparation of Lanthanum Carbide

Temperature of carbide formation (in °)	Time (hours)	Carbon content (%)		
		C_{total}	C_{free}	C_{bound}*
1100	1	15.14	14.91	0.28
1200	1	17.20	16.45	0.90
1300	1	15.14	15.05	0.11
1400	1	16.70	16.70	0.00
1500	1	16.84	16.50	0.40
1600	1	14.85	13.90	1.10
1800	1	14.28	10.58	4.10
1900	1	12.03	1.18	11.00
2000	1	11.65	2.32	10.55
1850	2	14.05	0.41	13.70
1950	2	13.92	0.53	13.48

TABLE 2

X-ray Diagram of Lanthanum Carbide

hkl	θ°		intensity**	hkl	θ°		intensity**
	observed	calculated			observed	calculated	
101	13°00′	13°11′	M	312	41°33′	41°47′	S
002	13 24	13 33	M	105	43 21	42 54	W
110	15 51	16 07	M	321	45 48	45 51	M
112	21 12	20 52	VS	125	47 06	47 30	W
103	23 24	23 19	S	400	51 12	51 13	W
110***	24 24	24 18	VS	323	52 15	52 16	W
022	26 57	27 16	S	042	55 03	54 59	W
004	27 54	27 33	W	116***	58 00	58 03	W
213	34 18	34 18	S	420	62 00	61 21	M
222	37 03	37 05	M	400***	68 51	68 34	S
105***	38 18	38 16	S	422	70 06	69 57	VS

lowest possible temperature, in any case below 1650°, with a corresponding increase of the reaction time as compared with those used at higher temperatures.

Lanthanum carbide is a yellow compound which rapidly decomposes in air and in water with a characteristic odor of acetylene. According to literature data [2] the carbides of the rare earths decompose with evolution of acetylene (about 70%), methane (about 20%), and a small amount of ethylene. The residue consists of the metal oxide and small amounts of solid and liquid hydrocarbons. Lanthanum carbide is much less stable in air than calcium carbide.

The powder diagrams of lanthanum carbide were taken with copper radiation (λ_{Cu} = 1.539 A) in an RKD camera 57.3 mm in diameter. The cylindrical specimen was made with a paraffin-wax binder to prevent contact with air [4].

The line diagram of the compound is shown in the figure. Lanthanum carbide is known to have a tetragonal structure of the CaC_2 type (space group $I4/mmm - D_{4h}^{17}$) with lattice constants a = 3.92 and c = 6.55 A [5].

Comparison of the theoretically calculated positions of the lines for this structure with those found experimentally from the X-ray diagram (Table 2) confirms that this phase is correctly identified as lanthanum carbide, LaC_2.

*Calculated for the carbide (LaC_2) phase.

**M = moderate, VW = very weak, W = weak, S = strong, VS = very strong.

***α – La lines.

The lattice constants were found to be a = 3.95 A, and c = 6.54 A, in good agreement with literature data.

LITERATURE CITED

[1] G. V. Samsonov, Progr. Chem. 25, 190 (1956).

[2] G. Hevesy, The Rare Earth Elements (Sci. Chem. Tech. Press, 1929), 63 [Russian translation].

[3] J. De Villelume, Compt. rend. 231, 1497 (1950).

[4] V. P. Chalyi, Zav. Lab. 9, 1020 (1956), 6).

[5] G. B. Bokii, Introduction to Crystal Chemistry (Izd. MGU, 1954), 340. [In Russian]

Received July 8, 1957.

RADIOMETRIC DETERMINATION OF THE SURFACE AREAS OF DISPERSE AND POROUS SUBSTANCES

M. F. Skalozubov and V. I. Matsokin

(The Novocherkassk Polytechnic Institute)

The specific surface is a fundamental characteristic of powdered and porous substances, which determines many of their properties and their behavior in technological processes. Much attention is being devoted to development of methods for determination of specific surface. The particle sizes of powders can be determined by sedimentation methods, and the surface can be calculated from the results. The shapes and sizes of crystals and pores can also be determined under the microscope, the surfaces being calculated from the results of numerous measurements. This method, like the sedimentation method, gives inadequate results, as generally aggregates rather than individual crystals are examined, and their external outlines are insufficient for surface determination. Better results are obtained by the adsorption of gases or dyes on powders and porous substances, but this method is suitable only with specimens of high surface purity. Satisfactory results in determination of the specific surfaces of powders are also obtained by measurements of heats of wetting. Kabanov [1] determined the specific surface of lead dioxide, which is a conducting porous mass, from the capacity of the electric double layer.

Several methods have been proposed for determination of total porosity and pore size. Dumanskii [2] developed a method for determination of true pore size, based on measurement of the rate of air flow through a porous body immersed in water. Tovarov [3] designed an instrument for determination of the specific surface of dry cement by the flow of air through the pores in a layer of the powder. Kamakin [4], and also Plachenov, Aleksandrov, and Belotserkovskii, used the mercury-pressure method for characterization of porous structures. Zhdanov [5] investigated the possible application of the theory of capillary condensation in studies of the structure of porous substances. Systematic studies of disperse systems by means of the electron microscope have been started.

Determination of the specific surface of powders and porous substances by means of radioactive isotopes is of the greatest interest. Paneth and Vorwerk [6], and Paneth and Thimann [7], proposed a method based on the use of natural radioactive substances as long ago as 1922-1924. This method was improved by Khlopin and Merkulova [8]. Hahn's emanation method [9], which was used by Heckter [10] for determination of the surface of glass, and by Strassmann [11] for determination of the surface of crystalline powders, gives an indication of the surface area from the amount of radon or thoron emitted.

The emanation method and the adsorption of natural radioactive isotopes both give good results, but these methods involve difficulties in preparation of the specimens. It was reported by Astreeva [12] that Khusainova and Logvinov have developed a method for determination of the specific surface of cement, based on the adsorption of sodium tungstate containing tagged tungsten, on cement or sand surfaces. These workers also used adsorption of sodium tungstate for determinations of pore area in hardened cement.

We have attempted to find simple methods for the radiometric determination of the surface areas of powders and porous substances. The material mainly used for the investigation was paste from lead storage cells; it had been shown by us [13] that the grains in this paste consist of oxide particles coated with an external layer of lead sulfate. A powdered mass of lead sulfate was prepared by treatment of litharge with very dilute sulfuric acid solution. The specific surfaces of powders were determined by Tovarov's method in the T-3 apparatus, in-

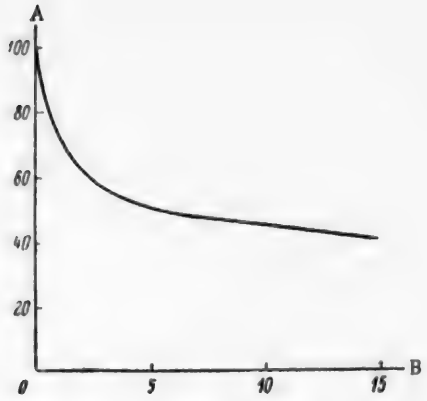

Fig. 1. Variation of solution activity with time.
A) Solution activity (%), B) time (minutes).

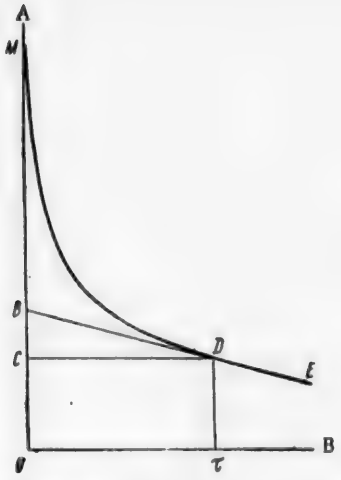

Fig. 2. Graphical determination of the surface of battery paste.
A) Solution activity, B) time. Explanation in text.

tended for technical determinations of the specific surface of dry cement. Adaptation of the apparatus for our purpose involved a correct choice of the weight of substance taken. The specific surface of the powder, prepared at room temperature, was 2000 cm^2/g. The same powder was also studied by the sedimentation method, under the following conditions: 1) the sedimentation medium was saturated $PbSO_4$ solution; 2) the balance was a steel spring with a rigidity of 25 mg/mm; 3) the weight of powder taken was 2 g; 4) the experiments were performed in a vessel 300 mm high and 0.5 liter in capacity.

Graphical analysis of the sedimentation curves showed that the specific surface was 778 cm^2/g. Evidently the particles settling on the balance cup were porous aggregates, the true surface of which was considerably greater than the calculated value.

For determinations by the tagged-atom method, lead sulfate powders were prepared by mixing of litharge with sulfuric acid containing tagged sulfur S^{35}. An attempt was first made to determine the specific surface from the rate of the exchange reaction

$$La_2O_3 + 7C = 2LaC_2 + 3CO.$$

where S^X is the radioactive sulfur isotope.

The equilibrium shifts in the direction of the less soluble lead phosphate more rapidly, the greater the surface of the original sulfate powder. The radioactivity reached a stable value after 20 minutes of shaking of the different specimens in potassium sulfate solution; this showed that the shift of equilibrium in the direction of lead phosphate had terminated. The specific surface of the powder was found to be 1940 cm^2/g.

On the assumption that powders with greater surfaces saturate the solution earlier, the duration of the dissolution process to saturation was determined. Weighed samples of 0.5 g of lead sulfate were put into flasks each containing 200 ml of distilled water; the flasks were shaken, and samples of solution were taken at 5-minute intervals for radioactivity determinations. The results proved to be suitable only for comparative evaluations of the specific surfaces of different samples.

An attempt was made to make use of the exchange of molecules between the solid and liquid phases, on the assumption that the exchange rate is directly related to the phase-contact area. It proved more convenient to prepare a saturated solution containing the tagged atoms, and to determine the solid phase area from the

loss of radioactivity in the solution, rather than to introduce the tagged atoms into the substance to be tested.

$PbSO_4$ powder was washed with pure saturated lead sulfate solution by threefold decantation. 5 g of the dried powder was shaken with 50 ml of saturated lead sulfate solution containing tagged sulfur

$$\underset{\downarrow}{m\mathrm{PbSO_4}} + n\mathrm{Pb\overset{\times}{S}O_4} \rightleftarrows \underset{\downarrow}{(m-l)\,\mathrm{PbSO_4}\cdot l\mathrm{Pb\overset{\times}{S}O_4}} + (n-l)\,\mathrm{Pb\overset{\times}{S}O_4} + l\mathrm{PbSO_4}.$$

The radioactivity of the solution fell rapidly during the first five minutes, and then the process slowed down sharply (Fig. 1).

The form of the curve suggests that the outer layer of solid particles took part in the molecular exchange, while diffusion of ions into the crystals was very slow.

The surface was calculated on the assumption that only molecules of the monomolecular layer on the surface of the solid particles are involved in the exchange:

$$F = \frac{v}{\sigma m} \cdot \frac{p}{100-p} = \frac{0.00415 \cdot 43}{4.3 \cdot 10^{-8} \cdot 5 \cdot 57} = 14500 \text{ cm}^2/\text{g}$$

where v is the volume of dry $PbSO_4$ dissolved in 50 ml of saturated solution (in cc); σ is the thickness of a monomolecular layer of lead sulfate, equal to $4.3 \cdot 10^{-8}$ cm; m is the weight of powder taken (in g); p is the % radioactivity absorbed from the solution.

It is more difficult to measure the surface of porous than of powdered substances. Only the through pores are determined by Dumanskii's method. An attempt to apply this method to battery paste proved unsuccessful -- its resistance to the passage of air bubbles was too great. The colorimetric method, in which methylene blue solution was forced through porous battery plates, gave data on the through pores only.

For radiometric determination of the surface area of a porous substance, battery pastes were molded into tablets, which were sulfated, washed with saturated sulfate solution, and dried. The weighed tablets were immersed in a saturated lead sulfate solution containing tagged sulfur, evacuated to remove air from the pores, and the progressive decrease in the solution radioactivity was measured. The process was much slower than with powders, because of the hindered diffusion of the tagged ions into the pores. Under these conditions, exchange with the monomolecular layer was followed by penetration of tagged ions into the crystals. It proved possible to differentiate between these two processes by a graphical method. Some time after the start of the experiment the decrease of solution radioactivity becomes linear. The diffusion rate of the tagged ions in the solid phase was determined from the linear portion of the curve, and data on the first process were obtained as follows: the straight line DE was produced to its intersection with the ordinate axis at B; from D, where exchange with the monomolecular surface layer ended, a parallel was drawn to the abscissa axis to cut the ordinate axis at C. The experimental data on the total fall of radioactivity of the solution in time τ were distributed between the first and second stages in the proportion of MB to BC.

This method proved to be suitable for determination of the surface area of the paste in negative battery plates in the discharged state.

In the case of the paste in positive plates of lead batteries, in the discharged state the lead dioxide particles become coated with a sulfate layer, and after the samples have been washed with saturated lead sulfate solution and dried this layer becomes complete, and the conditions are thereby created for determination of the surface area of the porous mass in positive battery plates.

LITERATURE CITED

[1] B. N. Kabanov and R. V. Iutkevich, J. Phys. Chem. 13, 813 (1939).

[2] A. V. Dumanskii, J. Russ. Phys. Chem. Soc. 61 (1929).

[3] V. V. Tovarov, Zav. Lab. 1 (1948). 8).

[4] N. M. Kamakin, Methods of Investigation of the Structure of Highly Disperse and Porous Bodies, Proc. Conf. Acad. Sci. USSR (1953). [In Russian]

[5] S. P. Zhdanov, ibid.

[6] F. Paneth and W. Vorwerk, Z. Phys. Ch. 101, 455 (1922).

[7] F. Paneth and W. Thimann, Ber. 57, 1215 (1924).

[8] V. G. Khlopin and M. S. Merkulova, J. Phys. Chem. 13, 9 (1939).

[9] O. Hahn, Naturwissenschaften, 17, 296 (1926).

[10] M. Heckter, Glastechn. Ber. 12, 156 (1934).

[11] F. Strassmann, Z. Phys. Ch. 26, 353 (1934).

[12] O. Astreeva, Construct. Materials 5 (1956).

[13] M. F. Skalozubov, J. Appl. Chem. 26, 7, 721 (1953). •

Received February 12, 1957.

• Original Russian pagination. See C. B. Translation.

USE OF RADIOACTIVE ISOTOPES IN STUDIES OF THE CONDITIONS OF FORMATION OF ELECTRIC ALLOYS*

S. M. Kochergin and G. R. Pobedimskii

One important problem in studies of the formation of electrolytic alloys is investigation of the effects of the electrodeposition conditions on the alloy composition. The radioactive-tracer method can be used with success to facilitate and accelerate quantitative analysis of electrolytic deposits.

EXPERIMENTAL

The electrodeposition of zinc – cobalt alloy was chosen for the study. The effects of electrodeposition conditions on alloy composition were studied with the aid of the radioactive isotopes Zn^{65} and Co^{60}. Zinc – Cobalt alloys were deposited from solutions of the following composition (in g/liter): 1) $ZnSO_4 \cdot 7H_2O$ #44, 25% NH_4OH 250, $(NH_4)_2SO_4$ 50; 2) $CoSO_4 \cdot 7H_2O$ 47.68, 25% NH_4OH 250, $(NH_4)_2SO_4$ 50. Radioactive zinc isotope Zn^{65}, equivalent to 3.84 millicuries per liter, was added to the zinc electrolyte. For determination of the specific activity of zinc in the solution, accurately measured amounts of 0.2 and 0.1 ml of the solution were dried on pieces of filter paper. The specimens were placed in packets made from tracing paper. The activity of the specimens was determined in the "B" unit by means of a cylindrical Geiger – Müller counter [1, 2]. The specific activity of the zinc, determined by this method, was 159±2 pulses per minute per mg of zinc. The solution containing zinc was electrolyzed. The electrolysis was performed in a 100 ml beaker placed in a thermostat. The zinc was deposited on weighed copper electrodes, 1× 2 cm; platinum anodes 1.5 × 1.5 cm were used. For determination of the weight of the electrolytic deposit, the electrodes were thoroughly washed after the deposition, dried to constant weight, and weighed again. The specific activity of the zinc was determined by measurement of the electrode activity in the "B" unit; a value of 152±1 pulses per minute per mg of zinc. The difference from the result of the preceding determination is beyond the accuracy limit of the weighing on an analytical balance (7 pulses corresponds to 0.000006 g).

For preparation of zinc – cobalt alloy, solution 1 containing zinc and solution 2 containing cobalt were mixed in various proportions. The mixed solutions were electrolyzed. In each case the total weight of the electrolytic deposit was found by weighing of the electrode on an analytical balance, while the zinc content of the alloy was determined by comparison of the specific activity of the alloy with the specific activity of zinc in the specimens prepared previously.

For example, if the specific activity of zinc is 152 pulses/minute · mg, and the specific activity of the alloy is 114 pulses/minute · mg, the zinc content of the alloy is 75%.

The results of experiments on the effect of the zinc – cobalt ratio in the electrolyte on the alloy composition, at different cathodic current densities and temperatures, are plotted in Figs. 1 and 2.

For comparison, experiments were carried out on the formation of electrolytic alloys from electrolytes with the same quantitative ratios of zinc to cobalt, but free from ammonia and ammonium salts (sulfate electrolytes). The results of experiments on the effect of the zinc – cobalt ratio in sulfate electrolytes on the composition of electrolytic alloys formed at different current densities are plotted in Fig. 3. It was found as the result of a series of experiments that temperature variations in the 20-60° range have no appreciable effect on the composition of alloys deposited from sulfate electrolytes.

---

*The results of the investigations were reported at the Scientific and Technical Conference of the Kazan' Institute of Chemical Technology on October 29, 1957.

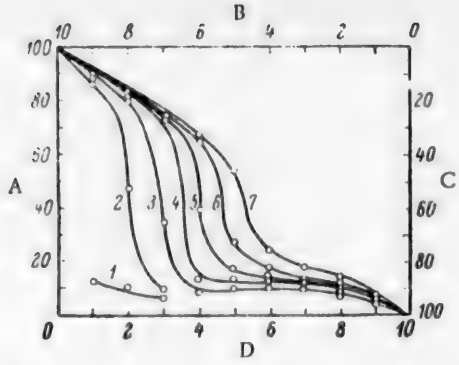

Fig. 1. Variation of alloy composition with the concentration ratio of zinc to cobalt in a mixed ammoniacal electrolyte at different current densities and at 20°.
A) Zn content of alloy (%), B) Zn content of solution, C) Co content of alloy (%), D) Co content of solution (g/liter). Current density (amps/dm^2): 1 – 0.25, 2 – 0.625, 3 – 1.25, 4 – 2.5, 5 – 3.75, 6 – 5.0, 7 – 7.5.

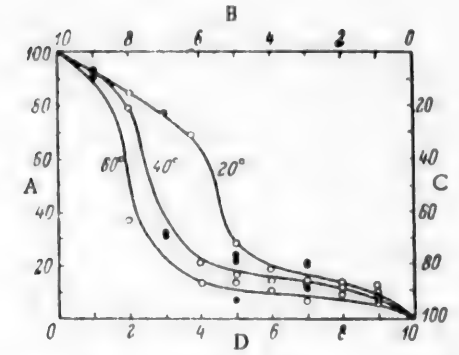

Fig. 2. Variation of alloy composition with the concentration ratio of zinc to cobalt in a mixed ammoniacal electrolyte at different temperatures and current density 5 amps/dm^2.
A, B, C, D – as in Fig. 1.

Duplicate and control experiments were carried out with the use of the radioactive tracer Co^{60}. The results of the experiments with the use of radioactive cobalt fully confirmed the earlier results*.

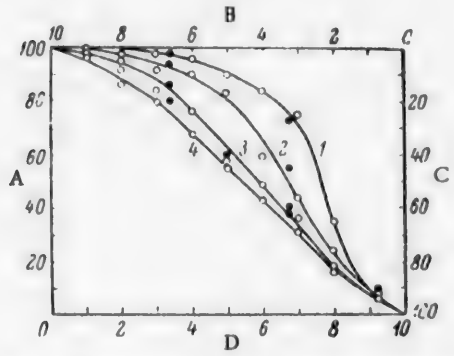

Fig. 3. Variation of alloy composition with the concentration ratio of zinc to cobalt in a sulfate electrolyte at different current densities and at 20°.
A, B, C, D – as in Fig. 1. Current density (amps/dm^2): 1 – 1.25, 2 – 2.5, 3 – 5.0, 4 – – 7.5.

SUMMARY

1. In the electrodeposition of zinc – cobalt alloy from mixed ammoniacal electrolytes and from sulfate electrolytes the zinc content of the alloy increases with increase of its content relative to cobalt in the electrolyte.

2. Increase of the cathodic current density favors an increase of the zinc content of the alloy deposited from mixed ammoniacal electrolytes, and of the cobalt content of the alloy deposited from sulfate electrolytes.

3. Increase of the electrolyte temperature in the 20-60° range lowers the zinc content of the alloy deposited from mixed ammoniacal electrolytes; temperature variations over the same range have no effect on the composition of the alloy deposited from sulfate electrolytes.

4. In studies of the effect of electrodeposition conditions on the composition of the electrolytic alloy, use of the radioactive-tracer method considerably accelerates quantitative analysis of the specimens, and gives quite reliable and fairly accurate results.

LITERATURE CITED

[1] Radiochemistry, Collected Papers edited by Prof. V. I. Spitsin (MGU, 1952). [In Russian]

* The data obtained with radioactive zinc are marked by white circles, and those with radioactive cobalt, by black circles in the graphs.

[2] V. Bochkarev, I. Keirim-Markus, M. L'vova, and Ia. Prusilin, Measurements of the Activities of Sources of Beta and Gamma Radiations (Izd. AN SSSR, 1953). [In Russian]

Received November 10, 1957.

SYNTHESES AND SOME TRANSFORMATIONS OF ORGANIC TIN AND SILICON COMPOUNDS*

M. F. Shostakovskii, V. N. Kotrelev, D. A. Kochkin, G. I. Kuznetsova, S. P. Kalinina, and V. V. Borisenko

(Institute of Organic Chemistry of the Academy of Sciences USSR, and the State Scientific Research and Planning Institute of the Plastics Industry)

This paper describes the syntheses and certain properties of silicon – tin and silicon organic compounds, prepared by the interaction of organotin oxides, such as hexaethylstannyl oxide $(C_2H_5)_3SnOSn(C_2H_5)_3$, with saturated and unsaturated organic and organosilicon alcohols and glycols, methacrylic acid, and a number of other substances.

It was found that the product of the reaction between hexaethylstannyl oxide and methacrylic acid – – triethylstannyl methacrylate – is a monomer which polymerizes in presence of peroxide catalysts to a transparent glassy substance, and which can form copolymers with methyl methacrylate, styrene, and other monomers.

The syntheses and reactions of the substances prepared by us may be represented by the following scheme:

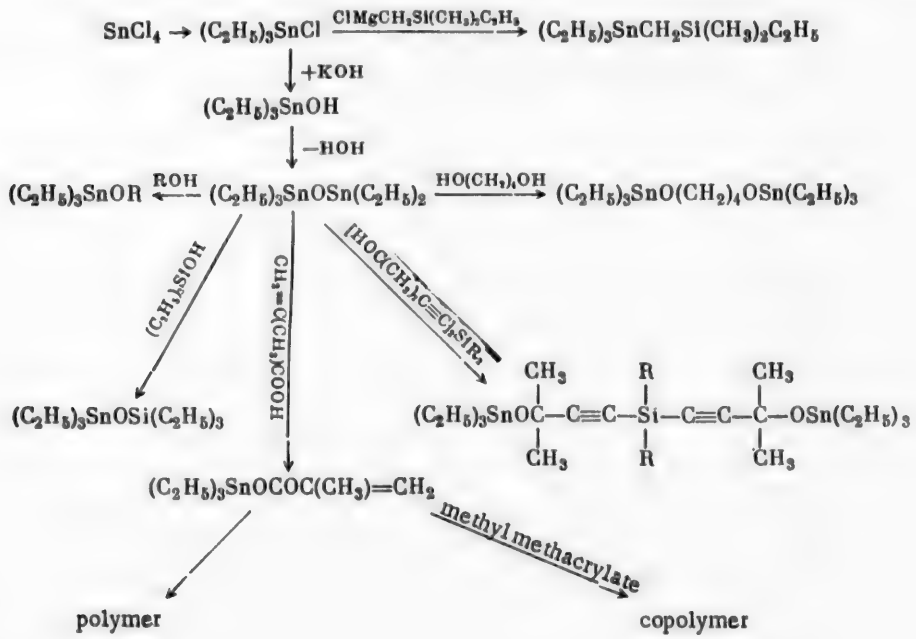

*Preliminary communication.

Physicochemical Properties of Certain Organic Compounds of Tin and Silicon

Compound	Formula	Boiling point (in °) under pressure of (mm Hg)	n_D^{20}	d_4^{20}	Molecular refraction MR		Molecular weight		Yields, as % of calculated
					found	calculated	found	calculated	
Cl-methylethyldimethylsilane	$ClCH_2Si(CH_3)_2C_2H_5$	124.5—125.5/739.5	1.4277	0.8899	39.47	39.75			60.0
γ-dimethylethylsilylpropanol	$(CH_3)_2C_2H_5SiCH_2CH_2CH_2OH$	92.5/20—94/20	1.4389	0.8478	45.38	45.8	148	146	
Dimethylethylsilyltriethylstannylmethane	$(CH_3)_2C_2H_5Si(CH_2)Sn(C_2H_5)_3$	99—100/3.5	1.4800	1.1135	78.50	78.98	295	306	58.43
Dimethylethylsilyltriethylstannyloxypropane	$(CH_3)_2C_2H_5Si(CH_2)_3OSn(C_2H_5)_3$	131—133/5	1.4769	1.1208	89.50	89.49	352	350	73.33
Full-substituted organotin ether of butanediol	$(C_2H_5)_3SnO(CH_2)_4OSn(C_2H_5)_3$	184—186/4	1.4975	1.201	121.0	121.13	472	499	39.4 31.25

EXPERIMENTAL

Reaction of hexaethylstannyl oxide with 1, 4-butanediol. To 4.13 g of hexaethylstannyl oxide 1.0 g of 1, 4-butanediol was added, and the mixture was fractionated under vacuum. A moderate amount of heat was evolved during the mixing.

As a result of twofold fractionation of the reaction products from the flask under vacuum, a fraction was obtained with b. p. 184-186° (4.5 mm), n_D^{20} 1.4975, d_4^{20} 1.2010, which was the fully substituted organotin ether of butanediol, $(C_2H_5)_3SnO(CH_2)_4OSn(C_2H_5)_3$. The yield was 39.4% of the theoretical.

Reaction of hexaethylstannyl oxide with γ-dimethylethylsilylpropanol. The experimental procedure was as before. Twofold fractionation yielded a product with b. p. 131-133° (5 mm), n_D^{20} 1.4769, d_4^{20} 1.1208, which corresponded to dimethylethylsilyltriethylstannyloxypropane, $(CH_3)_2SiCH_2CH_2CH_2OSn(C_2H_5)_3$. The yield was 73.3% of the theoretical.

Reaction of hexaethylstannyl oxide with methacrylic acid. When equivalent amounts of methacrylic acid and hexaethylstannyl oxide are mixed, much heat is evolved and triethylstannyl methacrylate $(C_2H_5)_3SnOCOC(CH_3)=CH_2$ is formed as a crystalline precipitate, which melted at 75° after complete removal of unreacted methacrylic acid and drying to constant weight. This ester readily polymerizes, and also copolymerizes with certain monomers.

The properties of the polymeric products are being studied.

The physicochemical constants of some of the compounds synthesized are given in the table.

Received May 21, 1958.

PRODUCTION OF SULFONATED NOVOLAC ION-EXCHANGE RESINS WITH INCREASED EXCHANGE CAPACITY

A. A. Vasil'ev and A. A. Vansheidt

(Institute of High-Molecular Compounds, Academy of Sciences USSR)

We showed earlier that strongly acidic cation-exchange resins (SN cation exchangers) are easily prepared by sulfonation of phenol – formaldehyde novolac resins by sulfuric acid or oleum, followed by heating of the sulfonated mass at temperatures above 150° [1]. The average exchange capacity of these resins was 3.2-3.6 meq/g, with low swelling coefficients and satisfactory mechanical strength.

It was subsequently found that sulfonated-novolac cation exchangers of even higher exchange capacities can be prepared if the sulfonation agent is chlorosulfonic acid, which had not previously been used in the production of sulfophenolic cation exchangers. The literature merely contains references to the possible use of chlorosulfonic acid in the production of soluble sulfonated phenol – aldehyde resins of the syntan type [2].

For preparation of cation exchangers with increased exchange capacities, the novolac resin was dissolved in chlorosulfonic acid at temperatures not over 30°; the mixture frothed violently and much heat was evolved, and the resin was therefore added gradually in powdered form. The resin usually dissolved completely after the mixture had been kept additionally at room temperature for several hours. For preparation of an insoluble sulfonation product, the sulfonation mass was heated at 170-190°. Subsequent heat treatment of the resultant gel reduced its swelling in water and made it mechanically stronger. At this stage the product contained $-SO_2Cl$ groups in addition to sulfo groups. The sulfonated resins, after the heat treatment, were therefore saponified by the action of hot water for 1-2 hours (or 10% alkali solution under the same conditions); the resin was then washed in water to remove acids and other water-soluble impurities, powdered, and dried in air.

Comparative data on sulfonated-novolac cation exchangers made with the use of chlorosulfonic acid (SN-2 resins) and of sulfuric acid (SN resins) are presented in the table.

SN-2 resins are more resistant than KU-1 sulfophenolic resins to the hydrolytic action of water and alkali. For example, the exchange capacities of KU-1 and SN-2 resins were 2.30 and 4.16 meq/g respectively, and after treatment with boiling water for one hour they were 2.02 and 4.09 meq/g. SN-2 resins are apparently somewhat inferior to SN resins in mechanical strength. The use of a large excess of sulfonation agent (10 weight parts of chlorosulfonic acid per 1 part of novolac) did not produce any further increase of exchange capacity of the resins, and gel formation then took place only at 230°.

Like SN resins, SN-2 resins contain about 2-2.5% of sulfur which cannot be determined by titration (inactive sulfur); in all probability, this is present in the cross-linking groups, which may be sulfonic ester or sulfone groups (or both).

Most of the SN-2 resin samples contained up to 2-3% of chlorine, which was probably not contained in $-SO_2Cl$ groups, as it could not be removed from the resin even when the latter was heated on a boiling water bath with 10% alkali solution for two hours.

Experiments on the determination of by-products in the sulfonation of novolacs by chlorosulfonic acid, followed by heating of the gels, showed that considerable amounts of sulfur dioxide are formed.

Therefore the formation of sulfonated-novolac SN-2 cation exchangers (like the formation of SN resins)

Comparative Properties of SN-2 and SN Sulfonated Ion-Exchange Resins*

new tech-

Resin	Weight ratio of sulfonation agent to resin	Heating conditions		Swelling coefficient of resin	Active sulfur content (%)	Total capacity (meq/g of dry resin)	Exchange capacity under dynamic conditions, to breakthrough (meq/liter)
		temperature (in °)	time (hours)				
SN-2	4 : 1	130	5	2.5	12.57	3.93	—
SN-2	4 : 1	150	5	—	13.34	4.17	—
SN-2	4 : 1	180	5	1.5	13.25	4.14	980
SN-2	5 : 1	130	30	2.3	16.32	5.10	—
SN	4 : 1	180	8.5	1.8	10.34	3.23	670
SN	4 : 1	180	3	2.3	12.03	3.76	660

involves oxidation – reduction processes, which in all probability play some part in the formation of insoluble products.

The data presented in this note are preliminary**.

SUMMARY

1. Ion-exchange resins were prepared by sulfonation of novolacs by chlorosulfonic acid, followed by heating of the sulfonated mass until an insoluble product was formed, heating of the gel, saponification of the polysulfochloride, powdering, washing, and drying of the resin.

2. Cation exchangers of the SN-2 type have low swelling coefficients, and high exchange capacities, exceeding those of the known sulfophenolic resins.

LITERATURE CITED

[1] A. A. Vasil'ev and A. A. Vansheidt, J. Appl. Chem. 31, 8, 1273 (1958).***

[2] French Patent 757, 725; Chem. Abs. 28, 2933 (1934).

[3] A. A. Vansheidt, A. A. Vasil'ev, and O. I. Okhrimenko, in the book: Theory and Practice of the Use of Ion-Exchange Materials (Moscow, Izd. AN SSSR, 1955), 110. [In Russian]

Received April 8, 1958.

*The exchange capacity, corresponding to the content of active sulfur (present in the sulfo groups), was determined by titration of weighed samples of resin in presence of NaCl solution, with methyl orange indicator [3]. The exchange capacity was determined under dynamic conditions, with a percolation layer 25 mm high, at a percolation rate of 5 m/hour, with the use of 0.014 N copper sulfate solution. The grain size of the resin (air-dry) was 0.5-1.0 mm.

**V. S. Matrosova took part in the experimental work.

***Original Russian pagination. See C. B. Translation.

REACTION OF ETHYLENE CHLOROHYDRIN WITH MAGNESIUM COMPOUNDS OF A BASIC CHARACTER

L. M. Kogan

Publications on the reaction of ethylene chlorohydrin with magnesium hydroxide are confined to two mutually contradictory patents. According to one of them [1], $Mg(OH)_2$ reacts similarly to $Ca(OH)_2$, ethylene oxide being formed in a high yield. According to the other [2], the main reaction product is acetaldehyde.

We showed [3] that CH_3CHO is formed in this reaction directly from $CH_2OH - CH_2Cl$, together with C_2H_4O, and not by secondary isomerization of C_2H_4O. It was also shown that ethylene glycol is formed as the result of hydration of C_2H_4O at the instant of its formation.

The aim of the present investigation was to determine the conditions which influence the yields of CH_3CHO and C_2H_4O.

EXPERIMENTAL

Ethylene chlorohydrin was prepared from C_2H_4O and HCl; after purification it had the following constants: b. p. $127 - 128^\circ$, d_4^{20} 1.1915, $n_D^{26.5}$ 1.4390. Magnesium hydroxide was prepared by the slaking of calcined magnesia under various conditions, and from $MgCl_2$ and NaOH. The reaction was carried out at the boil, by addition of $CH_2OH - CH_2Cl$ solution to the suspension, or vice versa. The reaction time was 1.5 hours. The vapor passed through a reflux condenser and then condensed at -5°. The residual gas was absorbed in a solution of common salt in hydrochloric acid. C_2H_4O was determined by the Lubatti method, CH_3CHO by means of hydroxylamine hydrochloride, $CH_2OH - CH_2Cl$ by means of caustic potash, and ethylene glycol by extraction from the reaction liquid, followed by distillation.

RESULTS OF THE EXPERIMENTS

The results obtained in the decomposition of $CH_2OH - CH_2Cl$ by magnesia suspension are given in Table 1 and in the graphs (Figs. 1-3).

Crotonaldehyde was not detected in the reaction products. It follows from the data in Table 1 that the same substances are formed in this reaction as in the reaction of $CH_2OH - CH_2Cl$ with caustic alkalies or milk of lime [3]. The difference lies in a sharp change in the ratio of the C_2H_4O and CH_3CHO yields. As in the reaction with $Ca(OH)_2$, the sequence in which the starting substances are added is of no significance; in this respect the reaction differs from the process with the use of caustic alkalies.

The graphs represent the results of experiments on the interaction of $CH_2OH - Cl$ with $Mg(OH)_2$ in aqueous solution, with different $CH_2OH - CH_2Cl$ concentrations, and also with different reaction times. The reason why the initial $CH_2OH - CH_2Cl$ concentration influences the relative yields of CH_3CHO and $C_2H_4O + C_2H_4(OH)_2$ is still unknown. This is probably because the mechanism of the process, which should account for the dual reactivity of $CH_2OH - CH_2Cl$ in this reaction, is not yet understood.

The formation of a higher yield of $CH_3CHO + C_2H_4O$ when $Mg(OH)_2$ is used, as compared with the yield of C_2H_4O in the decomposition of $CH_2OH - CH_2Cl$ by means of NaOH, can be explained as follows: the pH values of saturated $Mg(OH)_2$ and $Ca(OH)_2$ solutions are 10.5 and 12.5 respectively (the lower pH of $Mg(OH)_2$ means that the degree of hydration of C_2H_4O is correspondingly lower, as alkalinity favors formation of ethylene glycol

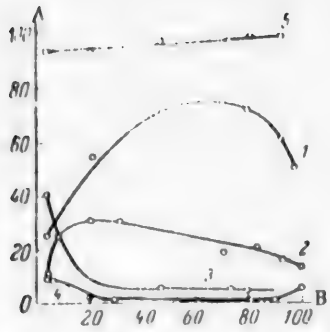

Fig. 1. Effect of initial content of ethylene chlorohydrin on the yields of the principal products of the reaction of ethylene chlorohydrin with magnesium hydroxide. $Mg(OH)_2$ concentration 10-20%.
A) Yields (%), B) concentration of $CH_2OH - CH_2Cl$ (%). Yields: 1 – CH_3CHO, 2 – C_2H_4O, 3 – $C_2H_4(OH)_2$ 4 – $CH_2OH - CH_2Cl$, 5 – total.

[3, 4]); 2) in the case of $Mg(OH)_2$ the principal reaction product is CH_3CHO, which, unlike C_2H_4O, does not undergo any further changes.

Comparison of data on the decomposition of $CH_2OH - CH_2Cl$ by magnesia suspensions, with different reaction times, with known data for the reactions with caustic alkali and milk of lime [5, 6] shows that the process in question is the slowest.

It is known that magnesium oxide reacts slowly with water, and that at room temperature the extent of this reaction is negligible [7]. Baikov [8] showed that this is because of the very low solubility of the resultant hydroxide in water ($1.5 \cdot 10^{-4}$ mole/liter, or about 1/200 of the solubility of $Ca(OH)_2$). The hydroxide coats the magnesium oxide particles and prevents further reaction.

We carried out experiments on the decomposition of $CH_2OH - CH_2Cl$ by magnesia suspension with different degrees of hydration of the magnesium oxide (Table 2).

It follows from these results that if the degree of hydration of MgO is low (MgO slaked by cold water), the main reaction product is C_2H_4O. Improvement of

TABLE 1

Decomposition of Ethylene Chlorohydrin by Magnesia Suspension. Concentration of $CH_2OH - CH_2Cl$ 20%, and of suspension, 10-15%•

Mixing sequence of the materials	Amount of $MG(OH)_2$ (% of stoichiometric)	Yield (%)				
		$CH_2OH - CH_2Cl$	C_2H_4O	CH_3CHO	$C_2H_4(OH)_2$	total
Solution added to suspension	300	2.8	30.3	47.5	16.5	97.9
	240	3.1	36.2	49.8	9.4	98.5
	240	1.9	32.8	51.5	12.2	98.4
	500	1.2	32.2	47.6	16.9	97.9
Suspension added to solution	190	—	33.3	40.2	—	—

the hydration conditions increases the CH_3CHO yield. Increase of the boiling time of the aqueous MgO suspension does not affect the results, probably because the saturation concentration of $Mg(OH)_2$ is quickly reached. In the experiment with $Mg(OH)_2$ prepared without the use of MgO, i. e., in the decomposition of $CH_2OH - CH_2Cl$ by means of what might be regarded as completely hydrated MgO, a high yield of CH_3CHO was obtained.

Experiments were carried out on the decomposition of $CH_2OH - CH_2Cl$ present in weakly acid solutions obtained in industry by the hypochlorination of ethylene (6-7% concentration). The $Mg(OH)_2$ used in these experiments was prepared from reactive $MgCl_2$ and NaOH, and subsequently by regeneration from the spent liquor, containing $MgCl_2$, by double decomposition with lime. In these experiments the CH_3CHO yield exceeded 50%, and the aggregate yield of CH_3CHO and C_2H_4O reached 80-85%, i. e., it was close to the C_2H_4O yield in the

•Here and subsequently the concentrations are given in terms of $Mg(OH)_2$, on the assumption of complete hydration of MgO.

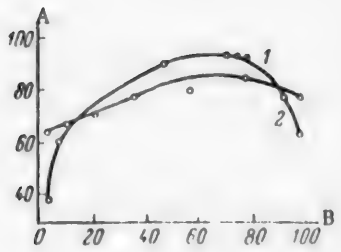

Fig. 2. Effect of ethylene chlorohydrin concentration on the yield of ethylene oxide in the alkaline decomposition of ethylene chlorohydrin, and on the combined yield of ethylene oxide and acetaldehyde in the reaction of ethylene chlorohydrin with magnesium hydroxide.
A) Yield (%), B) concentration of $CH_2OH - CH_2Cl$ (%). Yields: 1 – $C_2H_4O + CH_3CHO$, 2 – C_2H_4O.

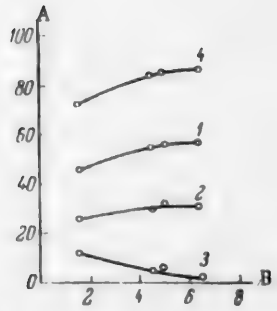

Fig. 3. Effect of the reaction time in the decomposition of ethylene chlorohydrin by magnesia suspension on the yields of ethylene oxide and acetaldehyde, and on the amount of unchanged ethylene chlorohydrin. Concentration of $CH_2OH - CH_2Cl$ 20%, $Mg(OH)_2$ 10%.
A) Yield (%), B) reaction time (hours). Yields: 1 – CH_3CHO, 2 – C_2H_4O, 3 – $CH_2OH - CH_2Cl$, 4 – $C_2H_4O + CH_3CHO$.

TABLE 2

Effect of the Method of Preparation of Magnesium Hydroxide on the Decomposition of Ethylene Chlorohydrin

Reaction time 4.5 hours at the boil; batch operation

Method of preparation of $Mg(OH)_2$	Concentration of $CH_2OH - CH_2Cl$ (wt. %)	Concentration of $Mg(OH)_2$ in suspension (wt. %)	Yield on the $CH_2OH - CH_2Cl$ (in %)		
			C_2H_4O	CH_3CHO	total
MgO slaked by cold water, cold suspension added to $CH_2OH - CH_2Cl$ solution	20.0	10.0	50.0	19.0	69.0
			49.0	21.6	70.6
MgO slaked by cold $CH_2OH - CH_2Cl$ solution when the solution is added in the reaction	6.7	—	47.7	17.1	65.4
			42.5	15.6	58.1
			45.8	19.7	65.5
MgO slaked by hot water immediately before the experiment	20.0	16.4	26.2	42.0	68.2
		10.2	28.4	42.5	71.1
		9.7	33.3	40.2	73.5
MgO slaked by 15-hour boiling of the suspension	20.0	9.7	45.9	32.9	78.8
		9.7	49.9	37.0	86.9
Reaction of NaOH with $MgCl_2$	20.0	3.8	18.6	56.5	75.1
		4.9	20.4	52.7	73.1

decomposition of $CH_2OH - CH_2Cl$ by alkalies or lime. This method for the production of CH_3CHO has a number of advantages over the known methods, and may be of practical importance under certain economic conditions.

SUMMARY

1. When aqueous ethylene chlorohydrin is decomposed by boiling magnesia suspension, the main reaction product is acetaldehyde (75% yield), and ethylene oxide and ethylene glycol are also formed in yields of 20% and 5% respectively.

2. The relative yields of acetaldehyde and ethylene oxide may be varied; the ratio depends on the degree of hydration of the magnesium oxide. Increased hydration favors acetaldehyde formation.

The author offers his gratitude to Professor P. V. Zimakov for help in this investigation.

LITERATURE CITED

[1] U. S. Patent 2,103,849 (1937).

[2] French Patent 850,752 (1939); Chem. Abs. 44, 1942 (1950).

[3] P. V. Zimakov and L. M. Kogan, J. Appl. Chem. 31, 4, 613 (1958). *

[4] H. I. Lichtenstein and G. H. Twigg, Trans. Farad. Soc. 49,11,905 (1948).

[5] L. M. Kogan, Candidates Dissertation (Moscow, 1951). [In Russian]

[6] L. M. Kogan, Production and Conversion of Ethylene Oxide in Germany (Moscow, Goskhimizdat, 1947). [In Russian]

[7] V. A. Klement'ev, Trans. State Inst. Appl. Chem. 25 (1934).

[8] A. A. Baikov, J. Russ. Metallurgical Soc. 1, 3, 846 (1913).

Received May 6, 1957.

* Original Russian pagination. See C. B. Translation.

REACTION OF SALICYLALDEHYDE WITH ACETIC ANHYDRIDE IN PRESENCE OF BF_3

K. A. Bogdanov

(Central Laboratory of the Kaluga Synthetic Perfume Combine)

Aromatic aldehydes, in presence of boron fluoride in etherate form, add on acetic ahydride at their carbonyl groups with formation of alkylidene diesters (diacetyl derivatives) [1].

For example, benzaldehyde reacts as follows:

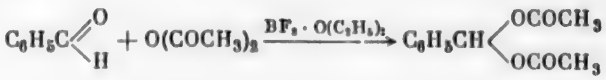

with formation of benzylidene diacetate in 80% yield.

We found no reports in the literature of an analogous reaction with salicylaldehyde, although this reaction was of practical interest to us in relation to the synthesis of coumarin by Briusova's method [2].

It was thought that the final products of the reaction of salicylaldehyde with acetic anhydride in presence of BF_3 should be the mono- or triacetate of salicylaldehyde:

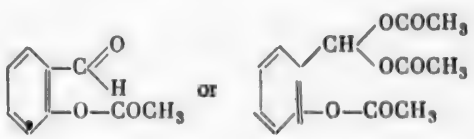

However, the action of the etherate $BF_3 \cdot C_6H_5OCH_3$ on a mixture of salicylaldehyde and acetic anhydride did not give the expected acetyl derivatives. The principal reaction product was disalicylic aldehyde (dibenzo-2, 6, 9-bisdioxane) of m. p. 128-129°

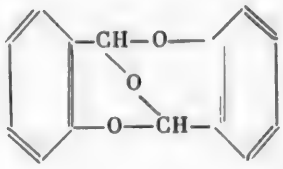

which was prepared by another method as long ago as 1922 [3].

It follows that BF_3 acts as an acid catalyst in this reaction, like H_2SO_4, forming an acetal by dehydration of two salicylaldehyde molecules. The function of acetic anhydride is to bind the water.

EXPERIMENTAL

61 g of 98% salicylaldehyde (~ 0.5 mole) were mixed in a 0.5 liter beaker with 100 g of 96% acetic anhydride (~ 1 mole), 5 ml of BF_3. $C_6H_5OCH_3$ was added, and the mixture was stirred. The temperature rose

spontaneously to 55°. The reaction mass was left overnight. On the next day the precipitated acicular crystals were filtered off by suction and washed twice with alcohol. The product was sufficiently pure and did not require further purification. The weight of the dry product was 21.8 g, m. p. 128°. The filtrate was treated with cold water. The oil which separated out crystallized rapidly. The water was decanted, and the residue was treated with alcohol, in which disalicylic aldehyde is very sparingly soluble, but the oily impurities are very soluble; the liquid was filtered, and the residue on the filter was washed twice with alcohol. Drying of the residue yielded a further 12.4 g of disalicylic aldehyde in the form of a fine crystalline powder of m. p. 128°. The total yield of disalicylic aldehyde was 34.2 g, or 60% of the theoretical.

LITERATURE CITED

[1] E. H. Man, J. J. Sanderson, and C. R. Hauser, J. Am. Chem. Soc. 72, 847 (1950).

[2] L. Ia. Briusova, Food Industry 1, 13 (1945).

[3] R. Adams, M. Fogler, and C. Kreger, J. Am. Chem. Soc. 44, 1126 (1922).

Received March 11, 1957.

BOOK REVIEW

N. N. NEKRASOV. ECONOMICS OF THE CHEMICAL INDUSTRY. Soviet Science Press, Moscow, 1957, 396 pp., 7500 copies.

Apart from individual articles and a few brochures, our national literature until recently contained only one book on the economics of chemical industry*. The book entitled "Economics of the Chemical Industry," published as a textbook for institutes and faculties of engineering economics at the end of 1957, is the most important publication in this field, and its significance extends far beyond teaching requirements. The author of the book is the eminent Soviet Scientist, Corresponding Member (AN SSSR) N. N. Nekrasov; he presents the economics of chemical industry in close association with general economic problems of socialist industry, and thereby demonstrates and substantiates, very forcibly and convincingly, the outstanding role of the chemical industries in the development of the national economy.

Although the book was published nearly half a year before the May Plenary Session of the Central Committee of the CPSU, when historic decisions concerning the accelerated development of the chemical industry were made, it may serve as a reliable aid in the fulfillment of these decisions.

The book consists of 14 chapters, totalling 396 pages. Each chapter contains distinctive sections with subheadings, which makes it easier to use both by students and by specialists working in industry and in research and planning institutions.

Chapter I (Subject and Tasks of the Course), which contains a classification of different branches of chemical industry in the socialist economy, is followed by a long chapter(II) devoted to the development of chemical industry. In this chapter (pp. 19-66), which commences with a survey of the history of chemical industry in prerevolutionary Russia, the author shows that after the Great October Socialist Revolution, during the periods of the early five-year plans, a mighty chemical industry was created in our country; this industry withstood with credit the heavy demands of the Patriotic War, and can now ensure the rapid development of the most advanced industries. Data on the chemical industries of the People's Democracies are given at the end of the chapter.

Chapter III (Introduction of Chemical Processes in the National Economy of the USSR) presents a vivid picture of the adoption of chemical processes and materials in all branches of the national economy. It is correctly stressed that new technological processes have immeasurably raised the importance of synthetic materials in the national economy (p. 75), and that these materials, which were once substitutes, are becoming new materials or new kinds of industrial raw materials**, of special value in modern technology. The chapter also indicates the trends of future applications of chemistry in industry, agriculture, forestry, and transport.

In Chapter IV (Technical Progress of Chemical Industry) the author indicates the main trends of technical progress in the chemical industry which follow from the accelerated technical progress of socialist industry as a whole. The economic significance of intensification of chemical industries, and the role of electric power in speeding the progress, are considered in detail. The section on economic analysis and planning of new technological processes will undoubtedly attract the attention of research workers and planners. It is noteworthy that actual analysis of acetylene production enabled the author to draw correct conclusions concerning the transition from the old process, based on calcium carbide, to new methods based on electrical and thermal cracking of

*N. N. Kalmykov and S. A. Vaisbein, Economics of the Socialist Chemical Industry [in Russian] (Moscow, Goskhimizdat, 1955), 303 pp.

**The underlined words are quoted from the book.

hydrocarbon gases. It is known that the management of the Ministry of Chemical Industry for a long time opposed the adoption of these new methods; this was condemned in the report presented by Comrade Khrushchev to the May Plenary Session of the Central Committee of the CPSU.

Chapter V (Raw Materials of the Chemical Industry) is a logical sequel to Chapter IV. In this chapter, Nekrasov presents an economic evaluation of sources of raw materials, considers the economics of utilization of industrial wastes, convincingly demonstrates the outstanding significance of the chemical conversion of gases as sources of cheap industrial raw materials, and concludes the chapter with a discussion of the economic basis for the selection of raw materials for chemical industry. Here ethyl alcohol and synthetic ammonia are considered as examples, and it is concluded that the most economic materials for the production of these substances are by-product gases from the petroleum industry in the first case, and methane from natural gas (by the conversion process) in the second. Both these conclusions are fully consistent with the decisions of the May Plenary Session of the Central Committee of the CPSU.

Chapter VI (Heat and Power Requirements) contains the economic principles for the selection of fuels for industrial undertakings, and efficiency data on heat and power sources in chemical industries.

Chapter VII, which is devoted to concentration, specialization, cooperation, and combined processes in the chemical industry, deals especially with the problem of multiple utilization of raw materials, auxiliary materials, and power under conditions of combined production. It is pointed out that solution of this problem is an urgent task important in relation to the further development, not only of chemical industry, but of all branches of industry. The methods proposed by Nekrasov for determination of the economic efficency of combined industrial processes are most valuable.

In Chapter VIII (Distribution of Chemical Industries) questions of distribution are considered in close association with technical progress; in particular, this is illustrated by changes in distribution conditions as the result of development of new forms of transport – the conveying of petroleum and gases over long distances by pipelines.

Chapter IX-XIII (Labor Productivity, Basic Stocks, Fluid Resources, Production Costs, Management Organization, and Planning Systems in the Chemical Industry) are based on extensive factual data, carefully selected and skilfully analyzed. These chapters will be very useful to industrial workers whose tasks are to achieve maximum economy of resources coupled with accelerated growth of production.

In the concluding chapter (Technical and Economic Planning of New Undertakings in the Chemical Industry) the author considers the project and planning stages of capital construction, the technical and economic principles of the construction of new chemical undertakings, and determination of the economic efficiency of new plants. This chapter (as, indeed, the book as a whole) is exceptionally topical at the present time, when, by the decision of the May Plenary Session of the Central Committee of the CPSU 257 chemical plants are being completed, rebuilt, or redesigned.

Nekrasov's purpose was to create a textbook for colleges. However, and this is as it should be, a textbook written creatively, which considers the future prospects of technological development, merits a life far beyond the confines of teaching institutions. This is the best evaluation of its merits.

Nekrasov's book was published in a very small edition (7,500 copies). Hardly had it been published when it became a rarity. A new edition should be published as soon as possible; this is in the interests of a very wide circle of users – scientific workers and industrial chemists.

V. Sominskii

LETTER TO THE EDITOR

Since January 1, 1958, the All-Union monthly "Journal of Engineering Physics" has been published in Minsk.

The journal publishes the results of physical investigations which are of significance in industry and technology, and deals with engineering and technical methods for solution of scientific and technical problems.

In addition to other problems of engineering physics, the journal deals with questions of heat and mass transfer, thermodynamics of irreversible processes, surface physics, soil mechanics, spectroscopy and spectrum analysis, metal physics, electronics, and the theory of filtration in disperse media.

Eminent scientists of our country are participating in the work of the journal. It is intended for wide circles of engineers and technologists, workers in design and planning organizations, factory laboratories, scientific workers, and professors and academic workers.

The subscriptions to the journal should be sent by money order to Minsk, Head Post Office, "Soiuzpechat" Office.

The subscription is 72 rubles for 1 year, 36 rubles for 6 months, and 18 rubles for 3 months.

Papers for publication should be sent to: Minsk, Stalin Prospekt, Editorial Office of the Journal of Engineering Physics.

SIGNIFICANCE OF ABBREVIATIONS MOST FREQUENTLY ENCOUNTERED IN SOVIET PERIODICALS

FIAN	Phys. Inst. Acad. Sci. USSR.
GDI	Water Power Inst.
GITI	State Sci.-Tech. Press
GITTL	State Tech. and Theor. Lit. Press
GONTI	State United Sci.-Tech. Press
Gosenergoizdat	State Power Press
Goskhimizdat	State Chem. Press
GOST	All-Union State Standard
GTTI	State Tech. and Theor. Lit. Press
IL	Foreign Lit. Press
ISN (Izd. Sov. Nauk)	Soviet Science Press
Izd. AN SSSR	Acad. Sci. USSR Press
Izd. MGU	Moscow State Univ. Press
LEIIZhT	Leningrad Power Inst. of Railroad Engineering
LET	Leningrad Elec. Engr. School
LETI	Leningrad Electrotechnical Inst.
LETIIZhT	Leningrad Electrical Engineering Research Inst. of Railroad Engr.
Mashgiz	State Sci.-Tech. Press for Machine Construction Lit.
MEP	Ministry of Electrical Industry
MES	Ministry of Electrical Power Plants
MESEP	Ministry of Electrical Power Plants and the Electrical Industry
MGU	Moscow State Univ.
MKhTI	Moscow Inst. Chem. Tech.
MOPI	Moscow Regional Pedagogical Inst.
MSP	Ministry of Industrial Construction
NII ZVUKSZAPIOI	Scientific Research Inst. of Sound Recording
NIKFI	Sci. Inst. of Modern Motion Picture Photography
ONTI	United Sci.-Tech. Press
OTI	Division of Technical Information
OTN	Div. Tech. Sci.
Stroiizdat	Construction Press
TOE	Association of Power Engineers
TsKTI	Central Research Inst. for Boilers and Turbines
TsNIEL	Central Scientific Research Elec. Engr. Lab.
TsNIEL-MES	Central Scientific Research Elec. Engr. Lab.—Ministry of Electric Power Plants
TsVTI	Central Office of Economic Information
UF	Ural Branch
VIESKh	All-Union Inst. of Rural Elec. Power Stations
VNIIM	All-Union Scientific Research Inst. of Meteorology
VNIIZhDT	All-Union Scientific Research Inst. of Railroad Engineering
VTI	All-Union Thermotech. Inst.
VZEI	All-Union Power Correspondence Inst.

Note: Abbreviations not on this list and not explained in the translation have been transliterated, no further information about their significance being available to us. – Publisher.

SCIENTIST - TRANSLATORS WANTED

For over a decade, Consultants Bureau, Inc. has provided Western scientists with high quality cover-to-cover translations of Soviet scientific journals. Our unique contracts with the Soviet government are constantly revised to include more extensive coverage of technical activity in the USSR. In order to produce these journals at the high standards set down by both the Soviet and American governments, it is of prime importance to maintain a large staff of scientist-translators who can translate with precision in their specific scientific field. It is our strict policy to assign a translator only that material which is within his scope.

As part of our current and future* expansion programs, we have openings for a limited number of scientist-translators who can translate in the fields covered by the following journals:

Journal of General Chemistry

Antibiotics
Biochemistry
Bulletin of Experimental Biology and Medicine
Entomological Review
Microbiology
Pharmacology and Toxicology
Plant Physiology

Automation and Remote Control
Industrial Laboratory
Instruments and Experimental Techniques
Measurement Techniques

Czechoslovak Journal of Physics
Soviet Journal of Atomic Energy
Soviet Physics - Acoustics
Soviet Physics - Crystallography
Soviet Physics - Technical Physics

Our basic requirements are that the scientist-translator have a native command of English, a minimum degree of B.S. in his specific field, and a thorough knowledge of the contemporary technical terminology of his scientific discipline.

Translation may be done at home on a full or part-time basis.

For further information, please contact:

Translation Editor
CONSULTANTS BUREAU, INC.
227 West 17th Street
New York 11, New York

*We expect, in the near future, to initiate a program of translation from the growing amount of important Chinese scientific literature available. In preparation, we are accepting applications from Chinese to English translators.